Toxicity Evaluation of Gallium- and Indium-Related Chemicals by Using Freshwater Amphipod (*Hyalella azteca*) and Human Cultured Cells

TAN SHIH WEI

2022

Abstract

Over the past few decades, the rapid development of emerging technologies has been relevant to technology-critical elements of concern. Among those elements, gallium (Ga) and indium (In) are important raw materials in semiconductors and optoelectronic industries, and the enhanced production of the two metals has increased the distribution of Ga and *In* in the environment through the industrial manufacturing processes, especially in discharging of sewage in water bodies. Also, the workers engaged in the indium tin oxide (ITO) production line and recycling progresses are potentially exposed to Ga- and *In*-containing dusts. Occupational inhalation exposure to *In*-containing dusts (e.g., ITO, $In_2O_{3(s)}$ or $InP_{(s)}$) have been demonstrated to cause indium lung disease.

In addition, since the chemical properties of Ga(III) and In(III) are similar to Fe(III), they could serve as Fe-mimicking agents, a Trojan horse strategy for the Fe-searching cancer cells and pathogens within inflammation tissues. Although there has been progress in investigating and understanding the interaction of Ga and *In* with biological systems, much remains to be learned about their interaction with other Fe-dependent and Fe-independent processes.

In chapter one, chemical transformation, bioavailability, short-term and long-term toxic effects of ion species and insoluble hydroxide/oxide chemicals of Ga and *In* in aquatic environment were introduced. In chapter two, we focused on exploring the interaction of Ga and *In* with biological systems, which was either Fe-dependent or Fe-independent processes. Moreover, the potential

biological factors or modes of action related to chronic human health such as indium lung disease, cellular senescence, and carcinogenicity were also investigated.

In the literature review of chapter one, the characteristics, environmental concentrations, transformation, transport, environmental fate and aquatic toxicity of Ga and *In* in the environment were introduced. Also, the worldwide environmental quality standards and waste management strategies were also summarized that correspond to the potential risk to aquatic organisms.

According to water chemistry features, Ga and In tend to form insoluble hydroxides (i.e., $Ga(OH)_{3(s)}$, $In(OH)_{3(s)}$) or anionic species (i.e., $Ga(OH)_4^-$) depending on the pH, and part of them appeared to be deposited and accumulated in bottom of water bodies. The bottom water and sediment acts as both source and reservoir. It is believed that the hydrolysis products such as $Ga(OH)_{3(s)}$, $In(OH)_{3(s)}$ may decrease the bioavailability of Ga and *In* to aquatic organisms. However, the interactions between chemical transformation, bioavailability and toxicity of these insoluble particles remain unclear. Thus, we hypothesized that the epibenthic or benthic organisms may be exposed to these particles via direct contact with overlying water column and feeding behaviors.

This research purpose of chapter one aims at investigating the effects of aqueous chemical transformation on the bioavailability, toxicity (acute and chronic) and potential impacts of Ga- and *In*-related chemicals, including In(III), citrate-In(III), Ga(III), citrate-Ga(III), $In(OH)_{3(s)}$, $In_2O_{3(s)}$ and $Ga_2O_{3(s)}$, by using freshwater amphipod (*Hyalella azteca*) *in vivo* bioassays. Citrate was used as a metal chelating agent to prevent hydrolysis of In(III) and Ga(III).

H. azteca neonates were dosed with the five salts standard artificial medium (SAM-5S) spiked with Ga- and *In*-related chemicals in a wide range of concentrations to evaluate the 7-day acute toxicity (LC_{50}). The sublethal doses were determined by considering the calculated LC_{50} values, current wastewater discharge standards and background concentrations of Ga and In in aquatic environment, and the long-term chronic toxicity test was further performed to assess the sublethal effects, including survival, growth (body length and body weight), reproduction (based on young per surviving female) and bioaccumulation. All spiked solutions were well characterized for their particle characterization, water-quality parameters, concentration of total metal and overlying water (ionic species and colloidal particles) during exposure period.

In particle characterization assays, Ga- and *In*-related hydroxide/oxide chemicals were prone to form aggregates in both ultrapure water and SAM-5S. The aggregates of $In(OH)_{3(s)}$ and $In_2O_{3(s)}$ were irregular in shape, whereas the colloidal particles and aggregates of $Ga_2O_{3(s)}$ were respectively rod-shaped structure and irregular in shape. The zeta potential of $In(OH)_{3(s)}$ (33.67 mV), $In_2O_{3(s)}$ (22.23 mV) and $Ga_2O_{3(s)}$ (17.07 mV) indicated that stable dispersal in ultrapure water was more prolonged for these chemicals than in SAM-5S, which was $In(OH)_{3(s)}$ (-18.30 mV), $In_2O_{3(s)}$ (-17.37 mV) and $Ga_2O_{3(s)}$ (-11.11 mV).

In 7-day acute toxicity tests, the measured concentration of Ga and *In* in overlying water (ionic species and colloidal particles) of exposure solutions indicated that Ga(III) treatments appeared to be relatively stable as ionic species (e.g., Ga^{3+}, $Ga(OH)_4^-$), whereas In(III) and citrate-In(III) tended to transform to $In(OH)_{3(s)}$ through hydrolysis and thereby precipitated and decreased the overall In(III)

contents; also, the measured Ga or *In* concentration of insoluble chemicals (i.e., $In(OH)_{3(s)}$, $In_2O_{3(s)}$, and $Ga_2O_{3(s)}$) in overlying water were similar to that of In(III) treatments, suggesting these particles tended to gradually aggregate and precipitate to the bottom of solution.

Although Ga- and *In*-related chemicals did not induce lethal effects on *H. azteca* neonates in a dose-dependent manner, some treatments (i.e., In(III), citrate-In(III), Ga(III), $In_2O_{3(s)}$, and $Ga_2O_{3(s)}$) inhibited the growth rate of surviving *H. azteca* neonates. It is proposed that pH adjustment in the highest concentration (100 mg/L) of four treatments (i.e., In(III), citrate-In(III), Ga(III), and citrate-Ga(III)) with NaOH may increase the concentration of hydroxide ion (OH^-) and thereby enhance the hydrolysis processes even in the presence of citrate. The major hydrolysis products of $In(OH)_{3(s)}$ and $Ga(OH)_4^-$ appeared to have effect on either the bioavailability or toxicity of In(III) and Ga(III) to *H. azteca* neonates.

According to the results of 7-day acute toxicity tests, the toxic effects of chronic exposure (28- and 35-day) to sublethal concentrations of Ga- and *In*-related chemicals on survival, growth, reproduction, and bioaccumulation of *H. azteca* were further evaluated. Treatments of In(III) (0.5 and 5 mg/L), citrate-In(III) (5 mg/L), Ga(III) (5 mg/L), and $Ga_2O_{3(s)}$ (5 mg/L) did not affect survival rate during exposure period. Surprisingly, the survival of citrate-In(III) (0.5 mg/L), Ga(III) (0.5 mg/L), citrate-Ga(III) (0.5 and 5 mg/L), $In(OH)_{3(s)}$ and $In_2O_{3(s)}$ were decreased from the first seven days of exposure. The measured *In* concentrations in overlying water of exposure solutions indicated that *In* contents in all In(III) and citrate-In(III) treatments were much higher as compared to that of acute toxicity test. However, since the major hydrolysis products of Ga(III) is the anionic species $Ga(OH)_4^-$,

the measured Ga concentrations in overlying water of exposure solutions were similar to that of acute toxicity test. These findings have confirmed our hypothesis that the addition of hydroxide ions may decrease the bioavailability and toxicity of In(III) and Ga(III) to *H. azteca*.

As for the decreased survival of $In(OH)_{3(s)}$ and $In_2O_{3(s)}$ treatments during chronic exposure period in comparison with acute toxicity test, we hypothesized that the difference of water temperature monitored in exposure solutions between acute and chronic toxicity tests may be one of the reasons for the alterations in survival rate of *H. azteca*. Previous studies have demonstrated the lower water temperature could have effect on locomotor and feeding behavior of fish and amphipods, which appeared to decrease the bioavailability of colloidal particles and aggregates to *H. azteca* and thus attenuate their toxic effects. In addition, the measured *In* concentrations in overlying water of exposure solutions indicated that *In* contents in both $In(OH)_{3(s)}$ and $In_2O_{3(s)}$ treatments were much higher as compared to that of acute toxicity test, which also provided another proof for the effect of water temperature on the locomotor behaviors of *H. azteca*.

In chronic exposure which adult survival was above 80 % at day-28 and/or day-35, the exposure of In(III), citrate-In(III), Ga(III) or $Ga_2O_{3(s)}$ were associated with the sublethal effects on growth rate, sexual ratio, reproduction, and bioaccumulation factor (BAF) values. The exposure of Ga- and *In*-related chemicals appeared to affect the respiration, locomotion activity, feeding rate, and moulting behavior of freshwater amphipods, which are positively related to heavy metal uptake, individual growth, reproductive success, the size of offspring and the abortion rate. Moreover, BAF values inferred that the bioaccumulation ability of *H. azteca*. to Ga and *In* is different. The amphipod could

uptake Ga and *In* via direct contacting with overlying water column and feeding behaviors, but only *In* gradually accumulated in the body.

In consequence, chapter 1 provides new insight into the aquatic toxicity of Ga- and *In*-related chemicals that have not previously been evaluated in epibenthic freshwater amphipod. Our results proposed that the lower levels of In(III) and Ga(III) exposure, the higher toxic effects would be induced due to hydrolysis process in higher concentrations. Additionally, the use of metal chelating agent such as citrate could not prevent hydrolysis of In(III) and/or Ga(III), but has effect on the bioavailability and toxicity to *H. azteca*. We also investigated that the hydrolysis products of In(III), Ga- and *In*-based hydroxide/oxide chemicals may have lethal or sublethal toxic effects on *H. azteca*, which appeared to be greatly affected by any environmental factors (e.g., water temperature, dissolved oxygen) relating to locomotor and feeding behavior.

Although this study clearly illustrated the potential adverse impact of waterborne Ga- and *In*-related chemicals exposure on individual growth and population dynamics of *H. azteca*, it also raises the questions about: (1) bioavailability of anionic species $Ga(OH)_4^-$, (2) bioaccumulation ability of *H. azteca* to *In*-related chemicals, and (3) lethal toxic effects of $In(OH)_{3(s)}$ and $In_2O_{3(s)}$.

Based on these conclusions, future studies could address on the sublethal toxic effects of Ga- and *In*-related chemicals in a more complex exposure system (i.e., sediment phase). Since the exposure pathways for epibenthic and benthic organisms such as *H. azteca* may include ingestion of sediment particles (containing metal hydroxide and oxide flocs) and water, they could get exposed and accumulated to heavy metals primarily from overlying water, feeding behavior, and pore water

as well. However, the toxicity caused by direct exposure to Ga- and *In*-related chemicals, or via sediment resuspension, and their potential ecological impact on individual and populations of aquatic organisms, need to be explored.

In the literature review of chapter 2, the human exposure routes, uptake and metabolism, modes of action, and current knowledge on the exposure and health risk of Ga and *In* were elucidated. Additionally, the worldwide occupational exposure limits and effective preventive strategies to Ga and/or *In*, which correspond to occupational hygiene were also summarized.

Since the workers engaged in *In* and Ga processing are potentially exposed to *In*- and Ga-containing aerosols through inhalation, which have known to increase serum indium levels and the risk of indium lung disease (interstitial pneumonia and pulmonary fibrosis) and lung cancer. The latency period (month to years) of indium lung disease is relatively shorter than other occupational lung disease such as silicosis and asbestosis. So far, the entire pathogenesis of indium lung disease and factors affecting the duration of latency period in indium lung disease remain elusive, the available evidence indicates that the pathogenesis is closely associated with dissolved and accumulated indium in the body.

The main modes of toxic action of Ga and *In* to humans and mammals could be categorized into two types, Fe-dependent and Fe-independent pathways. However, there is still a large gap in knowledge about the relationship between the exposure of Ga- and *In*-related chemicals, pathogenic mechanisms, and chronic health effects. Therefore, the research purpose of this study aims at investigating the biological factors or modes of action that potentially associated with chronic health

impacts of occupational exposure to Ga- and *In*-related chemicals and the progression of indium lung disease.

The human colon carcinoma cell line DLD-1 was used in most toxicity assays, the cell viability assay was firstly performed in a wide range of concentrations of *In*- and Ga-related chemicals (In(III), citrate-In(III), Ga(III), citrate-Ga(III), $In(OH)_{3(s)}$, $In_2O_{3(s)}$, and $Ga_2O_{3(s)}$) to evaluate the cytotoxicity (LC_{50}). Citrate was used as a metal chelating agent to prevent hydrolysis of Ga(III) and In(III). Secondly, the sublethal doses (0.022 mM and/or 0.215 mM of Ga; 0.044 mM and/or 0.435 mM of *In*) were then determined by considering the estimated workplace exposure level and 72 h-LC_{50} values, thereby performing the cytotoxicity (programmed cell death and cell cycle profile), cellular morphological alterations, mitochondrial dysfunction, heme homeostasis, cellular senescence, and other potential toxicity (proteasome inhibition and genotoxicity) in order to assess the biological factors that potentially associated with chronic effects of Ga and *In* exposure.

The calculated LC_{50} values (72 hours) from cell viability tests indicated that the cytotoxicity increased in the order, Ga(III) > citrate-Ga(III) > $In(OH)_{3(s)}$ > citrate-In(III) > $In_2O_{3(s)}$ > In(III) > $Ga_2O_{3(s)}$. (0.014-3.586 mM of Ga; 0.009-2.177 mM of *In*). DLD-1 cells appeared to be more sensitive to Ga(III) and citrate-Ga(III) exposure as compared to In(III), citrate-In(III) and other hydroxide/oxides treatments.

In the programmed cell death assay, Fe(III) chelator deferoxamine (DFO, 5 μM) and Ga- and *In*-related chemicals did not significantly enhance either apoptosis or necrosis of the DLD-1 cells after 72 hours of exposure. In contrast, the cell cycle progression was arrested at the G_2/M phase after 72

hours exposure with DFO and higher concentration of In(III), Ga(III) and $In_2O_{3(s)}$ treatment groups, accompanied by decreases in the cell populations at the G_0/G_1 phase.

In the programmed cell death assay, DFO, Ga- and *In*-related chemicals did not significantly induce programmed cell death of the DLD-1 cells after 72 hours of exposure. In contrast, the cell cycle progression was arrested at the G_2/M phase after 72 hours exposure with DFO and higher concentration of In(III), Ga(III) and $In_2O_{3(s)}$ treatment groups, accompanied by decreases in the cell populations at the G_0/G_1 phase.

In addition to the cell cycle arrest, we also investigated that DFO and higher concentration of In(III) and Ga(III) treatment groups increased the cellular and nuclear size, resulting in flattened and irregular morphology after 72 hours of exposure. Also, mitochondria tended to aggregate in the budding-like structure at one perinuclear locus, whereas mitochondria showed broad cytoplasmic distribution in control cells. However, these alterations on cell morphology could be attenuated by the addition of citrate-Fe(III) (4.48 mM).

It is proposed that Ga(III) and In(III) could serve as Fe-mimicking agents and cause disruption of the cellular iron homeostasis through Fe-dependent pathways. The Fe deprivation conditions may further affect the cell cycle regulation and induce cell cycle arrest at G_2/M phase. Furthermore, since a variety of environmental stresses have demonstrated to trigger polyploidy formation, by which cancer cells would have larger cellular size, multiple nuclei or a single giant nucleus, and abnormal DNA content, and these cells have been defined as polyploid giant cancer cells (PGCCs). It is believed

that cellular Fe deprivation induced by either DFO or Ga(III)/ In(III) could be another stressful factor to trigger PGCCs formation.

In order to observe the toxic mechanisms of Ga- and *In*-induced cellular morphology changes (i.e., PGCCs formation) and abnormal alteration of mitochondrial dynamics (i.e., mitochondrial aggregation), we further evaluated the mitochondrial functions, including mitochondrial membrane potential ($\Delta\Psi_m$), enzymatic activities of mitochondrial respiratory chain complexes, and the concentration of protoporphyrin IX (PPIX, a normal precursor of heme), heme, and Zn protoporphyrin IX (ZnPPIX, Zn is instead of Fe). Results indicated that DFO, Ga and *In* sublethal exposure not only affected $\Delta\Psi_m$, mitochondrial PPIX, heme, and ZnPPIX contents, but also had the inhibition effect on enzymatic activities of mitochondrial respiratory chain complex I, II, III, and IV, leading to mitochondrial dysfunction.

Cellular senescence is associated with multiple cellular, molecular alterations and distinct phenotypic changes including an irreversible cell cycle arrest, which has been considered as a hallmark of aging-related diseases, fibrosis, diabetes, and cancer formation. Cellular senescence could be triggered by various kinds of environmental stresses, such as hypoxia, oxidative stress, and mitochondrial dysfunction. Data suggested that the sublethal doses of Ga(III), In(III), $In(OH)_{3(s)}$ and DFO treatments increased the percentage of senescence-associated β-galactosidase activity positive cells, indicating that Ga- and *In*-induced cell cycle arrest (G_2/M phase), cellular morphological changes, mitochondrial dysfunction, dysregulation of heme homeostasis, and PGCCs formation were all related to cellular senescence.

Besides the Fe-dependent pathways, we also evaluated the Fe-independent pathways of Ga- and *In*-induced toxic effects by using proteasome inhibition assay and genotoxicity screening assay (EGFP-MDC1 foci). Ga(III) and In(III) treatments inhibited the chymotrypsin-like, trypsin-like, and caspase-like peptidase activity of purified proteasome, whereas $In(OH)_{3(s)}$, $In_2O_{3(s)}$, and $Ga_2O_{3(s)}$ treatments did not affect proteasome activity. It is proposed that the direct or indirect interaction between Ga(III), In(III) and proteasome could induce proteostatic dysfunction, which has been identified as another stress factor to trigger senescence. In addition, citrate-In(III), Ga(III), citrate-Ga(III), and $Ga_2O_{3(s)}$ treatments appeared to have the genotoxic potency to induce DNA damage.

To sum up, the present study provides new insight into the potential role of In-induced cellular senescence in the pathological progression of indium lung disease. In recent years, the aging-related lung diseases have been identified to be associated with alterations in lung function, increased susceptibility to acute and chronic lung diseases, such as obstructive and fibrotic lung disease. The hallmarks of cellular aging include genome-based failures (genomic instability, telomere attrition, epigenetic alterations), signaling dysfunction (deregulated nutrient sensing, altered intercellular communication), organelle compromise (mitochondrial dysfunction, loss of proteostasis), and cell phenotypic changes (stem cell exhaustion, cellular senescence). Our results demonstrated that In(III) and/or citrate-In(III) could induce mitochondrial abnormalities and cellular senescence based on iron deficiency stress. Other toxic outcomes regarding iron-independent pathways also indicated In(III) may disturb proteasome homeostasis and cause DNA damage. These hallmarks of cellular aging

appeared to accelerate cellular senescence processes, and eventually affect the rate of pathological progression of indium lung disease.

Although this study elucidated the potential relationship between cellular aging and indium lung disease, future studies could address on the questions of investigating the critical cellular players (epithelial cells, phagocytic macrophages, fibroblasts, immune cells) in *In*-induced cellular senescence, and the cellular and molecular mechanisms associated with senescence-associated secretory phenotype formation, by which these cells create subsets of senescent cells that are resistant to immune clearance and drive tissue degeneration, thereby contributing to the pathogenesis of indium lung disease.

Table of Contents

List of Tables

Chapter 1 Acute and Chronic Toxicity of Gallium- and Indium-Related Chemicals to Freshwater Amphipod (*Hyalella azteca*) in Water-Only Toxicity Tests

Chapter 2 Cellular Iron Homeostasis Disruption Capacity of Gallium- and Indium-Related Chemicals: A Cause of Mitochondrial Dysfunction in Relation to Indium Lung Disease?

List of Figures

Chapter 1 Acute and Chronic Toxicity of Gallium- and Indium-Related Chemicals to Freshwater Amphipod (*Hyalella azteca*) in Water-Only Toxicity Tests

Chapter 2 Cellular Iron Homeostasis Disruption Capacity of Gallium- and Indium-Related Chemicals: A Cause of Mitochondrial Dysfunction in Relation to Indium Lung Disease?

List of Abbreviation

Chapter 1 Acute and Chronic Toxicity of Gallium- and Indium-Related Chemicals to Freshwater Amphipod (*Hyalella azteca*) in Water-Only Toxicity Tests

BAF	Bioaccumulation factor
COST	European Cooperation in Science and Technology
DOC	Dissolved organic carbon
DOM	Dissolved organic matter
DO	Dissolved oxygen
EC	Electrical conductivity
ER	Endoplasmic reticulum
Ga	Gallium
In	Indium
ITO	Indium tin oxide
LCD	Liquid crystal display
LED	Light-emitting diodes
NOTICE	Network on Technology-Critical Elements
OLED	Organic light-emitting diode
TCEs	Technology-critical elements

Chapter 2 Cellular Iron Homeostasis Disruption Capacity of Gallium- and Indium-Related Chemicals: A Cause of Mitochondrial Dysfunction in Relation to Indium Lung Disease?

ACGIH	The American Conference of Governmental Industrial Hygienists
ATP	Adenosine triphosphate
AECL	Acceptable exposure concentration limit
ALA	5-aminolevulinic acid
ALAD	δ-aminolevulinic acid dehydratase

ALAS1	Aminolevulinic acid synthase
ALP	Alkaline phosphatase
CDKs	Cyclin-dependent kinases
CPO	Coproporphyrinogen-III
CS	Citrate synthase
DCPIP	2,6-dichlorophenol indophenol
DFO	Deferoxamine mesylate
DMSO	Dimethyl sulfoxide
DMT1	Divalent metal transporter 1
DSB	DNA double-strand breaks
DTT	Dithiothreitol
EGFP	Enhanced green fluorescent protein
EMMPRIN	Matrix metalloproteinase inducer
ERK	Extracellular-signal-regulated kinase
E-waste	Electronic waste
FA	Formic acid
FECH	Ferrochelatase
GM-CSF	Granulocyte-macrophage colony-stimulating factor
GADD45α	Growth arrest and DNA-damage inducible protein
GSH	Reduced glutathione
GSSG	Oxidized glutathione
HIF-1α	Hypoxia inducible factor-1α
HO-1	Heme oxygenase-1
HRCT	High-resolution computed tomography
IARC	International Agency for Research on Cancer

IFN-γ	Interferon-γ
IL-1β	Interleukin-1β
JNK	c-Jun N-terminal kinase
JSOH	Japan Society for Occupational Health
KL-6	Krebs von den Lungen-6
MDC1	Mediator of DNA damage checkpoint 1
MHLW	The Japanese Ministry of Health, Labor and Welfare
MIF	Macrophage migration inhibitory factor
MMP	Matrix metalloprotenase
MMP-9	Matrix metalloproteinase-9
MRM	Multiple reaction monitoring
MT2A	Metallothionein-2A
mTOR	Mammalian target of rapamycin
NDPs	Nucleoside diphosphates
Ndrg-1	Downstream regulatory gene-1
NIOSH	National Institute for Occupational Safety and Health
PAP	Pulmonary alveolar proteinosis
PBS	Phosphate buffered saline
PDGF-AA	Platelet-derived growth factor-AA
PET/CT	Positron emission tomography/Computed tomography
PGCCs	Polyploid giant cancer cells
PI3K	Phosphatidylinositol 3-kinase
PPIX	Protoporphyrin IX
pRb	Retinoblastoma protein
PSMA	Prostate-specific membrane antigen

PTP	Protein tyrosine phosphatase
REL	Recommended exposure limit
RNR	Ribonucleotide reductase
ROI	Regions of interests
ROS	Reactive oxygen species
RRM1	Ribonucleotide reductase homodimeric M1 subunit
RRM2	Ribonucleotide reductase homodimeric M2 subunit
SASP	Senescence-associated secretory phenotype
SA-β-Gal	Senescence-associated β-galactosidase
STAT3	Signal transducer and activator of transcription 3
SP-D	Surfactant protein-D
STEL	Short-term exposure limit
Tf	Transferrin
TfR	Transferrin receptor
TGF-β1	Transforming growth factor β-1
TLV-TWA	Threshold limit value-time weighted average
TNF-α	Tumor necrosis factor-α
TWA	Eight-hour time-weighted average
UPLC-MS/MS	Ultra-performance liquid chromatography tandem mass spectrometry
ZnPPIX	Zinc protoporphyrin IX

Chapter 1

Acute and Chronic Toxicity of Gallium- and Indium-Related Chemicals to Freshwater Amphipod (*Hyalella azteca*) in Water-Only Toxicity Tests

1. General Background Information

Over the past few decades, the development of emerging key technologies, such as semiconductors, optoelectronic, precision machinery, renewable energy, and energy efficiency industries, are relevant to emerging chemicals of concern. In fact, the European Cooperation in Science and Technology (COST) and the U.S. EPA become more aware of the potential risk of these emerging chemicals. From 2015 to 2019, COST disclosed the European COST Action TD1407: Network on Technology-Critical Elements (NOTICE) to regulate the increasing use of these trace elements, which are key components for the development of new technologies currently (Cobelo-García et al., 2015; Filella and Rodríguez-Murillo, 2017). These elements are defined as technology-critical elements (TCEs) (Figure 1.1), including Ge, Ga, *In*, Nb, Ta, Te, Tl, the platinum group elements (Ir, Os, Pd, Pt, Rh, Ru) and most of the rare earth elements (Ce, Dy, Er, Eu, Gd, Ho, La, Lu, Nd, Pr, Sm, Tb, Y, Yb) (Cobelo-García et al., 2015). Due to the rapid development of TCEs related industries, the presence of these chemicals has more commonly detected at ultra-trace concentrations in aquatic environment using highly sensitive and selective analytical techniques (e.g., inductively coupled plasma mass spectrometry, laser ablation inductively coupled plasma mass spectrometry).

In TCEs, gallium (Ga) and indium (*In*) are important commodities in semiconductors and optoelectronic industries, such as wafers, solar cells, photodetectors, light-emitting diodes, flat-panel display screens and touchscreens (Kabata-Pendias and Szteke, 2015; Nordberg et al., 2014). According to the historical statistics for mineral and material commodities in the U. S., the primary world production of the two elements has risen steadily over forty years (1973-2015) (Figure 1.2) (Kelly and Matos, 2016). The multiple industrial and technological applications have increased the distribution of Ga and *In* in the environment through the industrial manufacturing processes, discharging of sewage, fly ash or flue dust generated in the combustion of certain coals for electric power (Kabata-Pendias and Szteke, 2015; Løvik et al., 2015).

The main oxidation states of Ga and *In* in aqueous environment are Ga(III) and In(III). The metal ions tend to hydrolyze in water, such as $Ga(OH)_{3(s)}$, $Ga(OH)_4^-$ and $In(OH)_{3(s)}$, which are likely to be transported downstream or deposited at bottom of water bodies, and the bottom water and sediment act as both pollution source and reservoir (Brookins, 2012; Wood and Samson, 2006). In the aquatic environment, there may be only a small portion of the hydroxides could be taken away by water flows and a large quantity of them get deposited at the bottom of water bodies. However, the geochemical interactions, bioavailability and toxic effects of these chemicals remain unclear between the bottom water, sediment particles and pore-water. Also, the epibenthic and benthic organisms may be exposed to these chemicals by direct contacting with overlying water column, sediment pore-water and feeding behaviors.

In the literature review, the characteristics, environmental concentrations, transformation, transport, environmental fate and aquatic toxicity of Ga and *In* in the environment will be introduced. Also, the worldwide environmental quality standard and waste management strategy will be summarized that correspond to the potential risk to aquatic organisms in the near future.

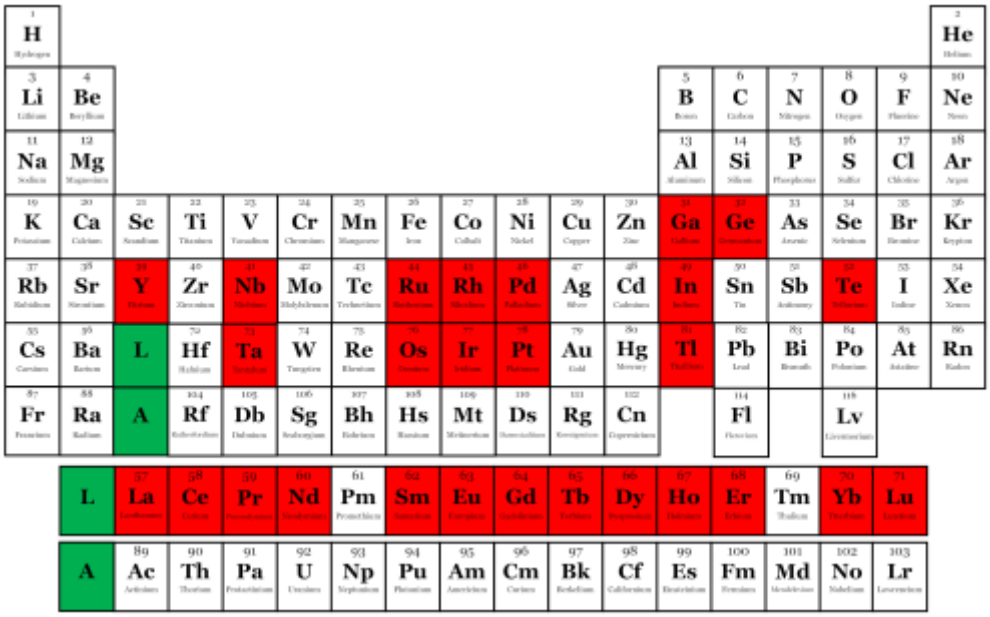

Figure 1.1 Technology-critical elements (TCEs) in red.

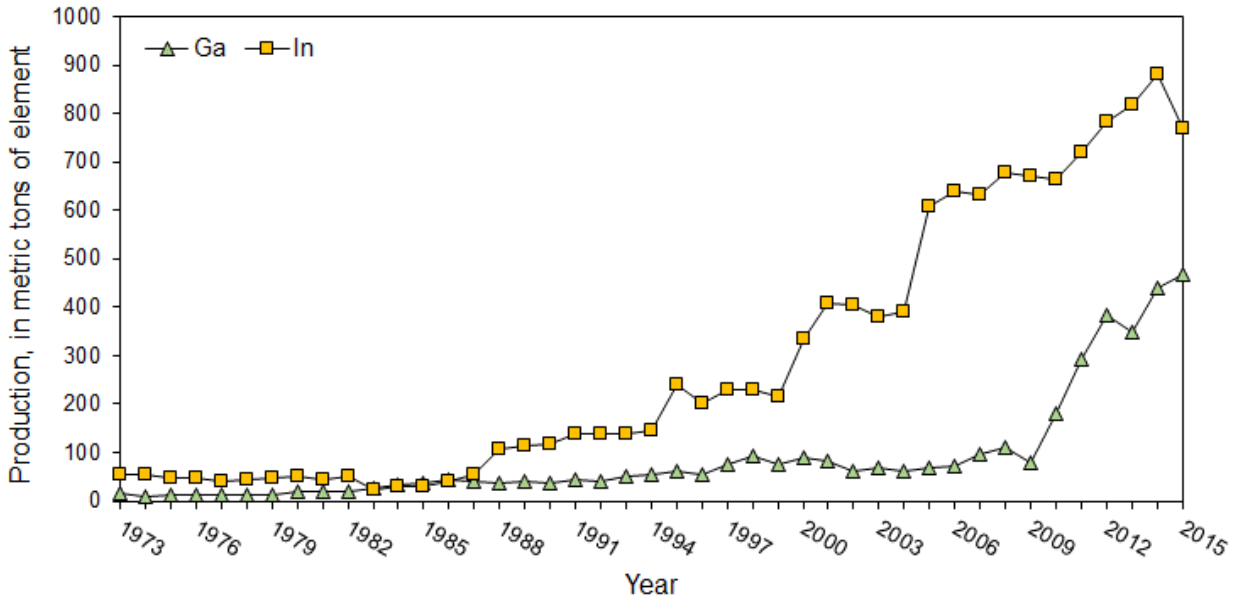

Figure 1.2 Graph showing worldwide production of gallium and indium from 1973 to 2015.

2. Literature Review

2.1 Physical and Chemical Properties

Both Ga and *In* are members of Group 13 of the periodic table of the elements, and the chemical characteristics are similar to other metals of the same group (Aluminum and thallium).

Ga was first predicted in the first periodic table of elements by Dmitri Mendeleev (Mendeleev, 1871), and Ga was further discovered in sphalerite ores by the French chemist Paul-Emile Lecoq de Boisbaudran. He named the element "gallia" for his native land of France (*Gallia*, or Gaul) (Schulz et al., 2017). Ga is a soft, silvery metallic element with an atomic number of 31, atomic weight of 69.723, ionic radius of 0.062 nm, main valence states of Ga(II) and Ga(III), melting point of 29.78°C, and density of 5.91 g/cm^3 at near room temperature. The major chemicals of Ga are: Ga metal, gallium nitrate ($Ga(NO_3)_3$), gallium trichloride ($GaCl_3$), gallium sulfate ($Ga_2(SO_4)_3$), gallium oxide (Ga_2O_3), gallium arsenide (GaAs), gallium nitride (GaN), gallium phosphide (GaP), gallium antimonide (GaSb), etc.

In was discovered in sphalerite ores by German chemists Fredinand and H. T. Richter, they named the element as "indium" after the distinctive indigo-blue line in its emission spectrum (Reich and Richter, 1863). Like Ga, *In* is also a soft, lustrous, silvery-white metal with an atomic number of 49, atomic weight of 114.818, ionic radius of 0.080 nm, major oxidation states of In(I), In(II) and In(III), melting point of 156.6°C, and density of 7.31 g/cm^3 at near room temperature. *In* chemicals include indium trichloride ($InCl_3$), indium hydroxide ($In(OH)_3$), indium oxide (In_2O_3), indium sulfate

($In_2(SO_4)_3$), indium sulfide (In_2S_3), trimethylindium (InC_3H_9), indium arsenide (InAs), indium nitride (InN), indium phosphide (InP), indium tin oxide (ITO), etc.

2.2 Water Chemistry

The main oxidation states of Ga and *In* in aqueous environment are Ga(III) and In(III), and may also be Ga(I), Ga(II), In(I) and In(II). In surface weathering and industrial wastewater environments, Ga and *In* tend to form metal complexes with chloride, fluoride, hydroxide, organic compounds, phosphate and sulfate. The pH and temperature of aqueous environment may largely affect the chemical form of Ga and *In*. They appeared to form hydroxide complexes ($Ga(OH)_3$ or $Ga(OH)_4^-$, $In(OH)_3$ or $In(OH)_4^-$) at pH values > 4, $Ga(OH)^{2+}$ or $Ga(OH)_2^+$ and $In(OH)^{2+}$ or $In(OH)_2^+$ at pH values < 4 at a temperature of 25 ºC (Benézéth et al., 1997; Diakonov et al., 1997; Wood and Samson, 2006). Therefore, Ga and *In* are expected to be transported in surface water and sediment in hydroxide anion or the insoluble chemical species because of the solubility of metal ions and/or minerals of Ga and *In* in natural water bodies.

2.3 Natural Sources

There are only a few minerals of Ga and *In* that served as an essential structural component in nature. They form several ores and minerals in low concentration, replacing by some elements with similar atomic radius and charge.

There are four Ga-rich minerals (sulfide gallite, gallobeudantite, sohngeite, tsumgallite) have been recognized by the International Mineralogical Association, Commission on New Minerals,

Nomenclature and Classification. The sulfide gallite ($CuGaS_2$) contains about 35 Wt % of Ga, and the hydroxide mineral sohngeite ($Ga(OH)_3$) and tsumgallite (GaO(OH)) contain about 60 Wt % of Ga (Schulz et al., 2017). However, these minerals may also be associated with several ores and rocks, such as feldspars, amphibolites, sphalerite, eyselite and micas.

In tends to co-precipitate with Fe and Mn oxyhydroxide minerals in weathering conditions, therefore, it is usually associated with Fe-containing minerals. *In* forms a few minerals in natural, sulfide minerals such as infite ($FeIn_2S_4$) and roquesite ($CuInS_2$), and the hydroxide of dzhalindite ($In(OH)_3$) (Kabata-Pendias and Szteke, 2015; Schulz et al., 2017). *In* also appears to be associated with other sulfide minerals such as sphaleryt (ZnS), galena (PbS) and chalcopyrite ($CuFeS_2$) (Kabata-Pendias and Szteke, 2015). *In* is very rarely found in native ores, and its primary sources are Zn ores. However, *In* could also be recovered from metal slags that generated from the Pb and Sn mining processes (Kabata-Pendias and Szteke, 2015).

2.4 Production and Uses

At the present time, primary Ga is produced as a by-product mainly from Al hydroxide minerals (boehmite, diaspore and gibbsite), and some amounts of Ga are also extracted from Zn sulfide deposits. In 2020, the world primary Ga production was estimated to be 300 metric tons, of which China produced 290, Russia produced 4, Japan and South Korea produced 3 respectively (USGS, 2021a); moreover, the world primary *In* production capacity was estimated to be 900 metric tons, the leader producer China produced 500, South Korea produced 200, Japan produced 65, Canada and

France produced 50 respectively, and the remaining were manufactured from Belgium, Peru and Russia (USGS, 2021b).

Ga has been used to produce low-melting alloys due to the low melting temperature, which is used instead of Hg for some thermometers. Nowadays, a wide variety of chemicals of Ga are used in the field of semiconductor and optoelectronic industries. Gallium arsenide (GaAs) and gallium nitride (GaN) are used in various microelectronic devices, including light-emitting diodes (LEDs), laser diodes, photodetectors, wafers and solar cells. GaAs is also used in the production of integrated circuits, semiconductors and transistors (Schulz et al., 2017; Ziegler et al., 2004). According to the major end uses of Ga of the U.S. consumption in 2012 (Schulz et al., 2017), the largest application (60 %) for Ga was the production of analog integrated circuits. Optoelectronic devices such as LEDs, laser diodes and solar cells accounted for 32 % of consumption, with the remaining 8 % used in digital integrated circuits, research and development.

The production of indium tin oxide (ITO) accounts for most of global *In* consumption (65 %), which has been used in liquid crystal display (LCD) devices, flat-panel display screen and touchscreen of optoelectronic industries due to its ductility, malleability, conductivity and transparency features (Madden et al., 2004; Schulz et al., 2017). ITO is typically coating as a thin-film on the display surface, and it could transform the electrical data into an optical form. Other end uses of *In* are alloys and solders (9 %) and semiconductor materials (9 %) (Schulz et al., 2017). In addition, *In*-based chemicals including indium antimonide (InSb), indium arsenide (InAs) and indium phosphide (InP) could be used as substrates to produce LEDs, laser diodes and optical fibers.

2.5 Waste Management

The demand of Ga and *In* is driven by emerging technology applications that require their unique chemical properties. The proceeding establishment of the fifth generation (5G) wireless technology results in more requirements for GsAs to maintain high data transfer rates and power amplifiers on particular devices, especially smartphones. Although the global smartphone market may become saturated in the near future, there will still be a need for GaAs due to the ongoing development of 5G technologies (Flerus et al., 2019).

In recent years, the recovery, refining and recycling of Ga and *In* metals and chemicals have been improved, and these have contributed to stabilize supply chains. Moreover, the impacts of the COVID-19 pandemic and the U.S. – China trade dispute in 2019-2020, which may also result in the shortages of materials and the rising prices, and further stimulate the innovative technologies for recycling these metals in the near future.

The global electronic products market continues to grow exponentially, while the lifespan of those products becomes shorter and shorter. Therefore, the waste management including recycling strategy, legislation, and mandatory policies for treatment of electronic waste has been focused on smartphones, tablet computers, LCD, LED, organic light-emitting diode (OLED) and other screen types. The average lifespans are approximately 2 years for smartphones, 7 years for tablet computers and 10-15 years for the screen types (LCD, LED, OLED). Consequently, the volume of electronic

waste appears to grow rapidly every year and is also need for waste management officials to develop the suitable and profitable techniques of Ga and *In* recycling (Bhutta et al., 2011; Ciacci et al., 2019).

In fact, recycling of Ga and *In* appears to occur mainly from pre-consumer products in manufacturing plants, utilized and recycled in the same or similar product types, which belongs to closed-loop recycling network. Furthermore, the end-of-life treatment of Ga and *In* is limited nowadays (Graedel et al., 2011; Ylä-Mella and Pongrácz, 2016). The material flows of Ga and *In* are currently unrecyclable because of technical limitations and economical barriers; moreover, the low technology maturity and economic incentives, or relatively high recycling costs constrain the development of electronic waste recycling (Ylä-Mella and Pongrácz, 2016). As a consequence, there is about 45 million metric tons of electronic waste produced annually in the world, a large amount of electronic waste may end up in incineration, landfills or improperly disposed in unprotected dump sites. Only a small portion (< 20 %) is being decontaminated recycled and reused (Chugainova and Rudakova, 2020; Uryu et al., 2003).

Electronic waste belongs to multi-component waste, which often consists of plastic, metal elements and other hazardous materials. Most smartphones, tablet computers, LCD, LED and OLED include a significant amount of TCEs (e.g., In, Ga, Ge, Y, La, Tb, Nd, Gd and Pr) and other elements (e.g., Ag, Au, Al, Cu, Co, Mn and Ni) (Chugainova and Rudakova, 2020; Zhang et al., 2015). These elements are contained in a variety part of electronic waste, making it much more difficult to separate and extract the valuable elements by simple recycling processes.

Some possible recycling processes for electronic waste that contained Ga and *In* have been reported in recent years. The possible recovery pathways are summarized and shown in Fig 2.1. Pretreatment methods include a variety of dismantling-crushing of electronic waste for specific components, followed by pre-processing methods, such as pyrolysis, physical-chemical methods and electrical disintegration have been taken into consideration to separate the raw materials (ITO-glasses, and GaAs scraps) (Flerus et al., 2019; Götze and Rotter, 2012; Swain et al., 2015; Zhang et al., 2015).

The acid leaching treatment is the main processes to dissolve *In* and Ga from raw materials, followed by a variety of purification methods to remove the impurity elements, including hydrometallurgical and hot immersion processes, solvent extraction, liquid membrane separation, vacuum chlorinated separation, vacuum carbonization reduction, chemical precipitation, anion exchange resin and homogeneous liquid–liquid extraction (Chen et al., 2012a; Cheng et al., 2019; Chugainova and Rudakova, 2020; Götze and Rotter, 2012; He et al., 2014; Hsieh et al., 2009; Inoue et al., 2008; Kato et al., 2013; Ma et al., 2012; Swain et al., 2015; Zeng et al., 2015; Zhan et al., 2018; Zhang et al., 2017; Zhang et al., 2015). In addition, some innovative techniques such as hydrothermal processes, pyrometallurgy, chloride induced vaporization and biosorption have also been reported (Chugainova and Rudakova, 2020; Flerus and Friedrich, 2020; Inoue et al., 2008; Park, 2011; Pennesi et al., 2019; Satoshi Itoh and Katsuya Maruyama, 2011).

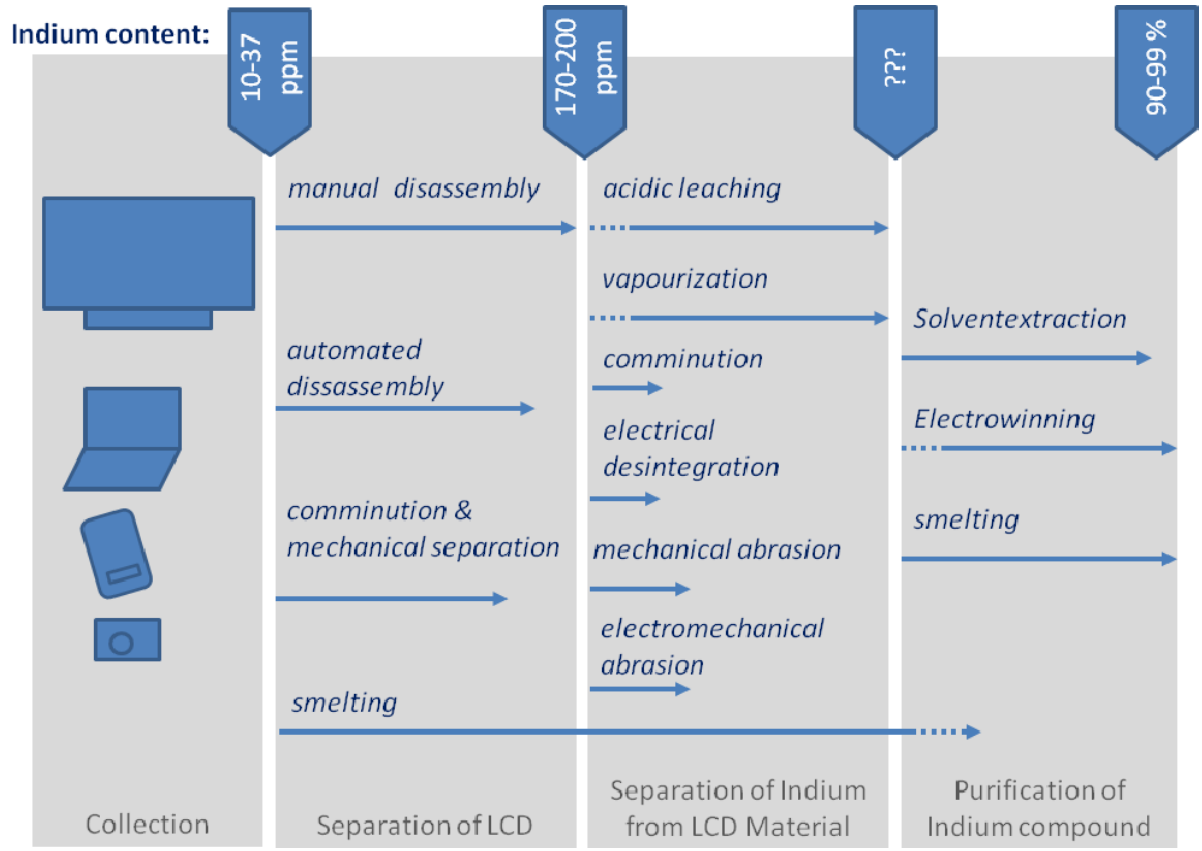

Figure 2.1 Possible pathways for indium recovery from electronic waste (Götze and Rotter, 2012).

2.6 Environmental Distribution, Fate and Pollution Sources

2.6.1 Soil

In weathering environments, Ga and *In* may dissolve to ion species and tend to co-precipitate with Fe and Mn hydroxides. Also, natural organic matters appear to have a large sorption capacity towards Ga and *In*, they likely to be more concentrated in surface soil horizons. The concentrations of Ga and *In* on the Earth's surface are within the range 1-25 mg/kg and 0.11-0.25 mg/kg, respectively (Kabata-Pendias and Szteke, 2015).

The abundance of Ga varies from 0.47 to 268 mg/kg, and the average background concentration of Ga in natural soils is estimated at 15.2 mg/kg (Table 2.1) (Asami et al., 1990; Eriksson, 2001; Kabata-Pendias, 2000; Kabata-Pendias and Mukherjee, 2007; Kabata-Pendias and Szteke, 2015; Koljonen and Elo, 1992; Liu et al., 2021; Połedniok et al., 2012; Shacklette and Boerngen, 1984; Smith et al., 2005; Su et al., 2018; Syu et al., 2020; Takeda et al., 2004; Tyler, 2004; You, 2014). The worldwide concentration of *In* in original soils has been reported from < 0.01 to 4.1 mg/kg, and the mean concentration is estimated at 0.06 mg/kg (Table 2.1) (Asami et al., 1990; Eriksson, 2001; Kabata-Pendias, 2000; Kabata-Pendias and Mukherjee, 2007; Kabata-Pendias and Szteke, 2015; Liu et al., 2021; Smith et al., 2005; Su et al., 2018; Syu et al., 2021; Takeda et al., 2004; You, 2014).

The chemical form of Ga and *In* in soil depends largely on the pH and temperature. It is estimated that the major form presents in soils as hydroxide complexes of $Ga(OH)_{3(s)}$ or $Ga(OH)_4^-$ at room temperature and pH > 4, and $Ga(OH)^{2+}$ and $Ga(OH)_2^+$ at pH < 4 (Kabata-Pendias, 2000; Kabata-

Pendias and Szteke, 2015; Wood and Samson, 2006); *In* ion species may be transformed into $In(OH)_2^+$, $In(OH)_2^+$, $InCl_2^+$ at room temperature and pH > 4, and the predominant chemical form may change into insoluble $In(OH)_{3(s)}$ at pH 5-9 (Kabata-Pendias, 2000; Kabata-Pendias and Szteke, 2015; Su et al., 2018; Wood and Samson, 2006).

The distribution of Ga and *In* in soils is positively associated with clay fractions, soluble organic matters, Fe and Mn hydroxides, and the use of biosolids (e.g., sewage sludge) in farmland soils may serve as another sources of pollution (Sharma et al., 2017). The chemical properties of Ga are much similar to Al than *In* and are usually associated with Al minerals, Al(III) also could be easily replaced by Ga(III) in acidic soils because the atomic radius of Ga (0.135 nm) is similar to Al (0.143 nm), leading to Al phytotoxicity (Su et al., 2018; Syu et al., 2021; Syu et al., 2020).

2.6.2 Water

The worldwide concentrations of dissolved Ga and *In* in freshwater ranges from 0.1 to 120 ng/L and 0.115 to 3.2 ng/L (Table 2.2), respectively. Seawater contains Ga and *In* within the range of 0.3 to 1.0 ng/L and 0.005 to 34.8 ng/L (Table 2.2) (Alibo et al., 1999; Amakawa et al., 1996; Chen, 2006; Gaillardet et al., 2003; Kabata-Pendias and Mukherjee, 2007; Miyazaki et al., 2012; Nozaki et al., 2000a; Nozaki et al., 2000b; Obata et al., 2007; Shiller, 1998; Shiller and Frilot, 1996; Viers et al., 2009; You, 2014). In addition, the dissolved and particulate forms of *In* in coastal seawater has been measured to be as high as 4.7 and 34.8 ng/L at Tokyo bay (Miyazaki et al., 2012).

In fact, Ga and *In* appear to present as small particulates rather than dissolved ion species, the major species of Ga and *In* are $Ga(OH)_{3(s)}$, $Ga(OH)_4^-$, $In(OH)_{3(s)}$ and $InCl_2^+$, depending upon pH and oxidation-reduction potential of water bodies (Kabata-Pendias and Szteke, 2015; Schulz et al., 2017). Therefore, it is estimated that the two metals could be highly concentrated in fine particles and finally transport into bottom sediments. For instance, the global average concentration of Ga is approximately 18.1 mg/kg in suspended sediment of world rivers (Viers et al., 2009).

Acid mine drainages (AMD), which associated with sulfide-bearing mine and sulfide minerals in nature that may release heavy metals and sulfuric acid into the environment. The acidic conditions of AMD may largely dissolve heavy metals and result in environmental problem. Ga and *In* dissolved in AMD may be removed through insoluble precipitation, sorption to hydroxide minerals or dilution with freshwater at circumneutral pH (Schulz et al., 2017). Those insoluble particles are expected to be transported into farmland soils and bottom sediments of water bodies, and the remaining ion species may be transported downstream and further pose threats to freshwater resources (Campanella et al., 2017; Połedniok et al., 2012; Schulz et al., 2017).

Over the past decade, the rapid development of high-technology such as semiconductor and optoelectronic industries, leading to the increasing use of Ga- and *In*-related chemicals. They have been used as key raw materials of wafer foundry, integrated circuit packaging and testing processes, which may become potential environmental pollution sources by electronic waste and Ga- and *In*-containing wastewater effluent (Liu et al., 2021; Su et al., 2018; Syu et al., 2020). In Taiwan, the concentrations of Ga and *In* in groundwater of science-focused industrial parks are much higher than

worldwide average background concentrations in freshwater (Table 2.2) (Chen, 2006). Therefore, the semiconductor and optoelectronic industries may also pose a risk to those non-industrial and residential nearby areas.

2.6.3 Air

The concentrations of Ga and *In* in the atmosphere of remote regions range from <0.14 ng/m^3 and 0.05 to 78 pg/m^3 (Table 2.3), respectively (Kabata-Pendias and Mukherjee, 2007; Kabata-Pendias and Szteke, 2015; Ragaini et al., 1977). The volcanic emission has been verified as the main nature source, and the anthropogenic sources include coal combustion, ore processing, semiconductor and optoelectronic manufacturing processes (Kabata-Pendias and Szteke, 2015; Matsumoto and Hinkley, 2001; Schulz et al., 2017). The content of Ga and *In* could be as high as 1 to 12 ng/m^3 and 20 to 1,200 ng/m^3 near urban/industrial regions, respectively (Chen, 2007a; Kabata-Pendias and Mukherjee, 2007). Also, atmospheric transport and deposition of Ga- and *In*-bearing particulates may pose a potential impact to surrounding environments (White et al., 2015).

Table 2.1 Gallium and indium concentrations in soils.

Environment and (or) location	Metal concentration (value or range)	Unit	Type	Notes	Reference(s)
			Gallium		
Earth's crust	15-19	mg/kg	-	-	Kabata-Pendias and Mukherjee (2007)
World	10-22	mg/kg	Light sandy	-	Kabata-Pendias and Mukherjee (2007)
World	15-35	mg/kg	Medium loamy and silty	-	Kabata-Pendias and Mukherjee (2007)
World	15-40	mg/kg	Heavy loamy	-	Kabata-Pendias and Mukherjee (2007)
World	10-100	mg/kg	Calcareous	-	Kabata-Pendias and Mukherjee (2007)
World	20-54	mg/kg	Organic	-	Kabata-Pendias and Mukherjee (2007)
The United States	<5-30	mg/kg	Sandy soils and lithosols on sandstones	-	Kabata-Pendias (2000)
The United States	5-50	mg/kg	Light loamy soils	-	Kabata-Pendias (2000)
The United States	5-30	mg/kg	Loess and soils on silty deposits	-	Kabata-Pendias (2000)
The United States	5-70	mg/kg	Clay and clay loamy soils	-	Kabata-Pendias (2000)
The United States	5-30	mg/kg	Alluvial soils	-	Kabata-Pendias (2000)
The United States	15-50	mg/kg	Soils over granites and gneisses	-	Kabata-Pendias (2000)
The United States	15-30	mg/kg	Soils over volcanic rocks	-	Kabata-Pendias (2000)
The United States	<5-30	mg/kg	Soils over limestones and calcareous rocks	-	Kabata-Pendias (2000)
The United States	7-30	mg/kg	Soils on glacial till and drift	-	Kabata-Pendias (2000)
The United States	7-30	mg/kg	Light desert soils	-	Kabata-Pendias (2000)
The United States	10-20	mg/kg	Silty prairie soils	-	Kabata-Pendias (2000)
The United States	7-30	mg/kg	Chernozems and dark prairie soils	-	Kabata-Pendias (2000)
The United States	<5-50	mg/kg	Organic light soils	-	Kabata-Pendias (2000)
The United States	<5-50	mg/kg	Forest soils	-	Kabata-Pendias (2000)
The United States	<5-50	mg/kg	Various soils	-	Kabata-Pendias (2000)
The United States (Alaska)	<4-32	mg/kg	Various soils	-	Kabata-Pendias (2000)

Note: b.d.l., below detection limit; mg, milligram; kg, kilogram; cm, centimeter.

Table 2.1 Gallium and indium concentrations in soils. - Continued

Environment and (or) location	Metal concentration (value or range)	Unit	Type	Notes	Reference(s)
			Gallium		
The United States	0.5-23.1	mg/kg	Soils	Surface soils (0-5 cm)	Smith and others (2005)
The United States	1.68-27.1	mg/kg	Soils	Soil profile (A-horizon)	Smith and others (2005)
The United States	0.29-34.6	mg/kg	Soils	Soil profile (C-horizon)	Smith and others (2005)
Western Unites States	16	mg/kg	Soil	Surface soils (Mean for 20 cm)	Shacklette and Boerngen (1984)
Eastern Unites States	9.3	mg/kg	Soil	Surface soils (Mean for 20 cm)	Shacklette and Boerngen (1984)
The United States	0.53-15.6	mg/kg	Soils	Soil profile (O-horizon)	Smith and others (2005)
World	17	mg/kg	Soil, bulk	-	Koljonen (1992)
Taiwan (Siaoli River basin)	1.186-3.422	mg/kg	Agricultural soils	Downstream of optoelectronic plants	You (2014)
Taiwan (Taoyuan)	22	mg/kg	Clay soils	Surface soils (0-30 cm); Pinchen series	Su and others (2018)
Taiwan (Tainan)	8	mg/kg	Slity clay loamy soils	Surface soils (0-30 cm); Chengchung series	Su and others (2018)
Western Taiwan	33	mg/kg	Clay soils	Surface soils (0-30 cm); Pinchen series	Syu and others (2021)
Western Taiwan	12	mg/kg	Sandy loamy soils	Surface soils (0-30 cm); Jente series	Syu and others (2021)

Note: b.d.l., below detection limit; mg, milligram; kg, kilogram; cm, centimeter.

Table 2.1 Gallium and indium concentrations in soils. - Continued

Environment and (or) location	Metal concentration (value or range)	Unit	Type	Notes	Reference(s)
			Gallium		
Western Taiwan	29	mg/kg	Clay soils	Surface soils (0-30 cm); Taikang series	Syu and others (2021)
Taiwan	9.47-23.4	mg/kg	Various soils	Soil profiles (0-130 cm)	Liu and others (2021)
Poland	38-219	mg/kg	Agricultural soils	-	Poledniok and others (2012)
Poland	93-268	mg/kg	Soils	Proximal to a former Zn-Pb and bauxite mine	Poledniok and others (2012)
Sweden	4.27-13.3	mg/kg	Soils	Soil profiles (0-110 cm)	Tyler (2004)
Sweden	3.4-16	mg/kg	Agricultural soils	Topsoil	Eriksson (2001)
Sweden	<1.2-17	mg/kg	Agricultural soils	Subsoil	Eriksson (2001)
Japan	0.47-41	mg/kg	Various soils (Andosols, Cambisols, Gleysols and Acrisols)	-	Takeda and others (2004)
Japan (Jinzu River basin)	13.1-16.3	mg/kg	Paddy soils	Nearby Zn-Pb smelting plants	Asami and others (1990)
Japan (Annaka)	12.9-15.7	mg/kg	Upland soils	Nearby Zn-Pb smelting plants	Asami and others (1990)
Japan (Annaka)	12.8-14.4	mg/kg	Paddy soils	Nearby Zn-Pb smelting plants	Asami and others (1990)

Note: b.d.l., below detection limit; mg, milligram; kg, kilogram; cm, centimeter.

Table 2.1 Gallium and indium concentrations in soils. - Continued

Environment and (or) location	Metal concentration (value or range)	Unit	Type	Notes	Reference(s)
			Indium		
World	0.01-0.5	mg/kg	Various soils	-	Kabata-Pendias (2000)
Earth's crust	0.25	mg/kg	-		Kabata-Pendias and Mukherjee (2007)
World	<0.2-0.5	mg/kg	Light sandy	-	Kabata-Pendias and Mukherjee (2007)
World	0.03-4.1	mg/kg	Medium loamy and silty	-	Kabata-Pendias and Mukherjee (2007)
World	-	mg/kg	Heavy loamy	-	Kabata-Pendias and Mukherjee (2007)
World	-	mg/kg	Calcareous	-	Kabata-Pendias and Mukherjee (2007)
World	<0.1-2.6	mg/kg	Organic	-	Kabata-Pendias and Mukherjee (2007)
The United States	<0.01-0.12	mg/kg	Soils	Surface soils (0-5 cm)	Smith and others (2005)
The United States	<0.02-0.12	mg/kg	Soils	Soil profile (A-horizon)	Smith and others (2005)
The United States	<0.02-0.1	mg/kg	Soils	Soil profile (C-horizon)	Smith and others (2005)
The United States	<0.01-0.04	mg/kg	Soils	Soil profile (O-horizon)	Smith and others (2005)
Sweden	<0.04-0.064	mg/kg	Agricultural soils	Topsoil	Eriksson (2001)
Sweden	<0.04-0.073	mg/kg	Agricultural soils	Subsoil	Eriksson (2001)
Taiwan (Siaoli River basin)	1.025-1.922	mg/kg	Agricultural soils	Downstream of optoelectronic plants	You (2014)
Taiwan (Taoyuan)	b.d.l	mg/kg	Clay soils	Surface soils (0-30 cm); Pinchen series	Su and others (2018)
Taiwan (Tainan)	b.d.l	mg/kg	Slity clay loamy soils	Surface soils (0-30 cm); Chengchung series	Su and others (2018)

Note: b.d.l., below detection limit; mg, milligram; kg, kilogram; cm, centimeter.

Table 2.1 Gallium and indium concentrations in soils. - Continued

Environment and (or) location	Metal concentration (value or range)	Unit	Type	Notes	Reference(s)
			Indium		
Western Taiwan	0.04	mg/kg	Clay soils	Surface soils (0-30 cm); Pinchen series	Syu and others (2021)
Western Taiwan	0.08	mg/kg	Sandy loamy soils	Surface soils (0-30 cm); Jente series	Syu and others (2021)
Western Taiwan	0.09	mg/kg	Clay soils	Surface soils (0-30 cm); Taikang series	Syu and others (2021)
Taiwan	0.00477-0.0371	mg/kg	Various soils	Soil profiles (0-130 cm)	Liu and others (2021)
Japan	0.008-0.25	mg/kg	Various soils (Andosols, Cambisols, Gleysols and Acrisols)	-	Takeda and others (2004)
Japan (Jinzu River basin)	0.016-0.103	mg/kg	Paddy soils	Nearby Zn-Pb smelting plants	Asami and others (1990)
Japan (Annaka)	0.041-1.66	mg/kg	Upland soils	Nearby Zn-Pb smelting plants	Asami and others (1990)
Japan (Annaka)	0.026-1.92	mg/kg	Paddy soils	Nearby Zn-Pb smelting plants	Asami and others (1990)

Note: b.d.l., below detection limit; mg, milligram; kg, kilogram; cm, centimeter.

Table 2.2 Gallium and indium concentrations in waters.

Environment and (or) location	Metal concentration (value or range)	Unit	Type	Note	Reference(s)
			Gallium		
River	0.03	μg/L	Freshwater	-	Kabata-Pendias and Mukherjee (2007)
Ocean	0.001	μg/L	Seawater	-	Kabata-Pendias and Mukherjee (2007)
Atlantic Ocean	0.0003-0.004	μg/L	Seawater	Dissolved and colloidal (<0.4 μm)	Shiller (1998)
California streams	0.0001-0.006	μg/L	Freshwater	Dissolved and colloidal (<0.4 μm)	Shiller and Frilot (1996)
African rivers	0.02-0.11	μg/L	Freshwater	Dissolved load (<0.2 μm)	Gaillardet and others (2003)
North American rivers	0.001-0.012	μg/L	Freshwater	Dissolved load (<0.2 μm)	Gaillardet and others (2003)
South American rivers	0.003-0.12	μg/L	Freshwater	Dissolved load (<0.2 μm)	Gaillardet and others (2003)
Idel River	0.009	μg/L	Freshwater	Dissolved load (<0.2 μm)	Gaillardet and others (2003)
Taiwan (Siaoli River basin)	b.d.l	μg/L	Freshwater (Downstream of optoelectronic plants)	-	You (2014)
Taiwan (Hsinchu)	7.91-41.39	μg/L	Groundwater (Science-based industrial park)	Dissolved and colloidal (<0.45 μm)	Chen (2006)
Taiwan (Hsinchu)	0.01-0.12	μg/L	Groundwater (North district)	Dissolved and colloidal (<0.45 μm)	Chen (2006)
Taiwan (Hsinchu)	0.01-0.05	μg/L	Groundwater (Hsiangshan district)	Dissolved and colloidal (<0.45 μm)	Chen (2006)
Taiwan (Siaoli River basin)	b.d.l	mg/kg	Sediments (Downstream of optoelectronic plants)	-	You (2014)
World rivers	18.1	mg/kg	Suspended sediments	-	Viers and others (2009)

Note: b.d.l., below detection limit; μg, microgram; L, liter; mg, microgram; kg, kilogram; μm, micrometer.

Table 2.2 Gallium and indium concentrations in waters. - Continued

Environment and (or) location	Metal concentration (value or range)	Unit	Type	Note	Reference(s)
			Indium		
River	-	μg/L	Freshwater	-	Kabata-Pendias and Mukherjee (2007)
Ocean	0.0001	μg/L	Seawater	-	Kabata-Pendias and Mukherjee (2007)
North Atlantic Ocean	0.07-0.19	ng/L	Seawater	Dissolved and colloidal (<0.45 μm)	Alibo and others (1999)
Mediterranean Sea	0.72-1.23	ng/L	Seawater	Dissolved and colloidal (<0.45 μm)	Alibo and others (1999)
Northwest Pacific Ocean	0.005-0.018	ng/L	Seawater	Unfitered	Amakawa and others (1996)
Japan (Tokyo Bay)	b.d.l-4.7	ng/L	Seawater	Particulate	Miyazaki and others (2012)
Japan (Tokyo Bay)	0.2-34.8	ng/L	Seawater	Dissolved and colloidal (<0.45 μm)	Miyazaki and others (2012)
Japan (Osaka)	1.2-4.1	ng/L	Seawater	Particulate	Miyazaki and others (2012)
Japan (Osaka)	3.6-4.3	ng/L	Seawater	Dissolved and colloidal (<0.45 μm)	Miyazaki and others (2012)
Japan (Okinawa)	0.6-0.8	ng/L	Seawater	Particulate	Miyazaki and others (2012)
Japan (Okinawa)	0.2-0.5	ng/L	Seawater	Dissolved and colloidal (<0.45 μm)	Miyazaki and others (2012)
Japan	0.8-4.1	ng/L	Seawater	Particulate	Miyazaki and others (2012)
Japan	0.8-19.4	ng/L	Seawater	Dissolved and colloidal (<0.45 μm)	Miyazaki and others (2012)
Japan (Japan Sea)	0.005-0.067	ng/L	Seawater	Dissolved (<0.04 μm)	Obata and others (2007)
Japan (Sea of Okhotsk)	0.007-0.067	ng/L	Seawater	Dissolved (<0.04 μm)	Obata and others (2007)
Japan (Rvier)	b.d.l-12.8	ng/L	Freshwater	Particulate	Miyazaki and others (2012)
Japan (Rvier)	b.d.l-3.2	ng/L	Freshwater	Dissolved and colloidal (<0.45 μm)	Miyazaki and others (2012)
Japan (Rvier)	0.115-1.687	ng/L	Freshwater	Dissolved (<0.04 μm)	Nozaki and others (2000a)

Note: b.d.l., below detection limit; μg, microgram; L, liter; ng, nanogram; μm, micrometer.

Table 2.2 Gallium and indium concentrations in waters. - Continued

Environment and (or) location	Metal concentration (value or range)	Unit	Type	Note	Reference(s)
			Indium		
Japan (Biwako Lake)	1.5-3.2	ng/L	Freshwater	Particulate	Miyazaki and others (2012)
Japan (Biwako Lake)	1.1-3.2	ng/L	Freshwater	Dissolved and colloidal (<0.45 μm)	Miyazaki and others (2012)
Thailand (Chao Phraya River estuary)	0.003-0.049	ng/L	Freshwater	Dissolved (<0.04 μm)	Nozaki and others (2000b)
Taiwan (Hsinchu)	0.95-20.05	μg/L	Groundwater (Science-based industrial park)	Dissolved and colloidal (<0.45 μm)	Chen (2006)
Taiwan (Hsinchu)	0.01-0.09	μg/L	Groundwater (North district)	Dissolved and colloidal (<0.45 μm)	Chen (2006)
Taiwan (Hsinchu)	b.d.l-0.05	μg/L	Groundwater (Hsiangshan district)	Dissolved and colloidal (<0.45 μm)	Chen (2006)
Taiwan (Siaoli River basin)	b.d.l	μg/L	Freshwater (Downstream of optoelectronic plants)	-	You (2014)
Taiwan (Siaoli River basin)	1.012-1.383	mg/kg	Sediments (Downstream of optoelectronic plants)	-	You (2014)

Note: b.d.l., below detection limit; μg, microgram; L, liter; ng, nanogram; μm, micrometer.

Table 2.3 Gallium and indium concentrations in air.

Environment and (or) location	Metal concentration (Value or range)	Unit	Reference(s)
		Gallium	
Urban/industrial	0.23-1	pg/m^3	Kabata-Pendias and Mukherjee (2007)
Remote regions	<0.001	pg/m^3	Kabata-Pendias and Mukherjee (2007)
South Pole	<0.14	pg/m^3	Kabata-Pendias and Mukherjee (2007)
Environment and (or) location	Metal concentration (Value or range)	Unit	Reference(s)
		Indium	
Urban/industrial	20-1,200	pg/m^3	Kabata-Pendias and Mukherjee (2007)
Antarctica	0.05	pg/m^3	Kabata-Pendias and Mukherjee (2007)
Remote regions	0.05-78	pg/m^3	Kabata-Pendias and Szteke (2015)
North America	20-140	pg/m^3	Schulz and others (2017) and references therein
The United States (Idaho)	5,800	pg/m^3	Ragaini and others (1977)
Japan	1,200	pg/m^3	Schulz and others (2017) and references therein
Shetland Islands	20	pg/m^3	Schulz and others (2017) and references therein
West Germany	30-360	pg/m^3	Schulz and others (2017) and references therein

Note: pg, picogram; m^3, cubic meter.

2.7 Aquatic Toxicity

The toxicity of Ga on marine organisms suggests that $GaCl_3$ exhibited very limited toxicity on the population growth of diatom (*Nitzschia closterium*) and golden-brown haptophyte (*Isochrysis galbana*), the fertilization and metamorphosis of coral (*Acropora tenuis*), the growth rate of marine snail (*Nassarius dorsatus*), and developmental inhibition of the Australian land hermit crab (*Coenobita variabilis*) (Table 2.4) (Harford et al., 2011; Negri et al., 2011; Trenfield et al., 2015; 2016; van Dam et al., 2018).

In freshwater systems, zebrafish (*Danio rerio*), rosy bitterling (*Rhodeus ocellatus*), common carp (*Cyprinus carpio*), tilapia (*Oreochromis mossambicus*), crustacean species (*Americamysis bahia* and *Artemia salina*), rotifer (*Brachionus plicatilis*), swamp shrimp (*Macrobrachium nipponense*) and amphipod (*Hyalella azteca*) were exposed to Ga chemicals (Table 2.4) (Betoulle et al., 2002; Borgmann et al., 2005a; Lin and Hwang, 1998; Olivares et al., 2016; Onikura et al., 2005; Yang, 2014; Yang and Chen, 2003; Yang and Chen, 2018), such as citrate-Ga(III), $Ga_2(SO_4)_3$ or $GaCl_3$, the results suggested that Ga(III) has been shown to display some inhibitory effects on some aquatic species at moderate concentrations. Furthermore, the longer the test duration, the lowest the Ga concentration needed to achieve the same toxic effect (LC_{50}), suggesting that the chronic effects of Ga may be more significant than its acute toxicity. The hardness of water appears to have no effect on modifying the toxicity of Ga chemicals (Borgmann et al., 2005a).

The acute toxicity tests of *In* and Tl in brackish-water and marine systems were conducted on four aquatic model organisms (*Americamysis bahia*, *Brachionus plicatilis*, *Artemia salina* and *Sillago japonica*) (Table 2.4), showing that the toxicity of Tl was higher than *In* toward all models. In addition, the toxicity of *In* and Tl was significantly affected by the salinity of the artificial medium, the toxicity decreased as the salinity of the medium decreased (Onikura et al., 2008).

In freshwater systems, microalga (*Chlorella vulgaris*), water flea (*Daphnia magna*), zebrafish (*Danio rerio*), rosy bitterling (*Rhodeus ocellatus*), swamp shrimp (*Macrobrachium nipponense*) and amphipod (*Hyalella azteca*) were exposed to In ion species (Table 2.4) (Borgmann et al., 2005a; Brun et al., 2019; Olivares et al., 2016; Yang, 2014; Yang and Chen, 2018; Zurita et al., 2007), such as In(III)-citrate, $InCl_3$ and $In(NO_3)_3$. The acute toxicity of In(III) appears to be similar to that of Ga chemicals described previously, and the toxic effects were much lower than other metals (e.g. Sb, Al, Cu, Cd); furthermore, the water hardness also may not affect the acute toxicity of In(III) to the larval stage of *Hyalella azteca* (Borgmann et al., 2005a).

In addition, the zebrafish (*Danio rerio*) embryos were exposed to citrate-In(III) and $In(NO)_3$, although exposure results revealed that In(III) and citrate-In(III) had no significant mortality, In(III) could cause oxidative stress, endoplasmic reticulum (ER) stress and associated unfolded protein response, and the induction of ER stress was associated with apoptotic and inflammatory reactions (Brun et al., 2014; Olivares et al., 2016). The developmental abnormalities in embryos were also observed over the citrate-In(III) concentrations (56-900 mM), specifically, citrate-In(III) could cause hypoactivity at the highest concentration (900 mM), suggesting that In(III) may have neurotoxic

effects by directly and indirectly interfering with normal trunk muscle, central nervous system and cardiovascular development in zebrafish (Olivares et al., 2016).

The acute toxicity of insoluble ITO and $In_2O_{3(s)}$ nanoparticles to hydra (*Hydra vulgaris*), crustacean (*Thamnocephalus platyurus*), microalga (*Pseudokirchneriella subcapitata*) and marine diatom (*Skeletonema costatum*) has also been reported (Table 2.4) (Blaise et al., 2008; Ng et al., 2015). ITO nanoparticles appear to be more toxic to these model organisms than $In_2O_{3(s)}$.

Although the aquatic toxicity of Ga and *In* chemicals has documented in a number of *in vivo* studies with freshwater and marine model organisms in water-phases, the general toxicity of these chemicals is relatively low in comparison with As, Al, Cd, Cu, Sb and Tl (Borgmann et al., 2005a; Brun et al., 2019; Olivares et al., 2016; Onikura et al., 2008; Trenfield et al., 2016; Yang, 2014; Yang and Chen, 2018). Thus, there is still a lack of studies reporting on the dose-toxicity relationship between ion species, hydroxide and oxide chemicals of Ga and *In* with epibenthic and benthic organisms in sediment and overlying-water phases.

Table 2.4 Published measures of aquatic toxicity for gallium and indium chemicals.

Compound	Model organism	End point		Exposure period	Value or result	Reference
$GaCl_3$	Tilapia (*Oreochromis mossambicus*)	Acute toxicity	Mortality	48 h-LC_{50}	204 μM	Lin and Hwang (1998)
$GaCl_3$	Tilapia (*Oreochromis mossambicus*)	Chronic toxicity	Growth inhibition	16-day	Total body length decreased Yolk diameters increased	Lin and Hwang (1998)
$Ga(NO_3)_3$	Common carp (*Cyprinus carpio*)	Acute toxicity	Mortality	96 h-LC_{50}	LC_{50} (96 h): 96.25 mg/L	Betoulle and others (2002)
$Ga_2(SO_4)_3$	Common carp (*Cyprinus carpio*)	Acute toxicity	Mortality	48 h-96 h-LC_{50}	LC_{50} (48 hr): 28.81 mg/L LC_{50} (72 hr): 22.11 mg/L LC_{50} (96 hr): 19.78 mg/L	Yang and Chen (2003)
$Ga_2(SO_4)_3$	Common carp (*Cyprinus carpio*)	Chronic toxicity	TP, GLU, BUN, CR, CHOL and TG	28-day	BUN, CR, CHOL and TG contents increased GLU contents decreased	Yang and Chen (2003)
$GaCl_3$	Crustacean (*Americamysis bahia*)	Acute toxicity	Mortality	96 h-LC_{50}	LC_{50} (24 hr): 22.47 mg/L LC_{50} (96 hr): 12.76 mg/L	Onikura and others (2005)
$GaCl_3$	Crustacean (*Artemia salina*)	Acute toxicity	Mortality	48 h-LC_{50}	LC_{50} (24 hr): 54.64 mg/L LC_{50} (48 hr): 52.78 mg/L	Onikura and others (2005)
$GaCl_3$	Rotifer (*Brachionus plicatilis*)	Acute toxicity	Mortality	24 h-LC_{50}	LC_{50} (24 hr): 11.48 mg/L	Onikura and others (2005)
Ga^{3+}	Freshwater amphipod (*Hyalella azteca*)	Acute toxicity	Mortality	7-day-LC_{50}	LC_{50} (7-day, soft water): > 1.00 mg/L LC_{50} (7-day, tap water): > 3.15 mg/L	Borgmann and others (2005)
$GaCl_3$	Diatom (*Nitzschia closterium*)	Acute toxicity	Mortality	72 h-LC_{50}	IC_{50} (72 hr): 19.64 mg/L	Harford and others (2011)
$GaCl_3$	Coral (*Acropora tenuis*)	Acute toxicity	Fertilization and Metamorphosis of larvae	Fertilization of sperm and eggs: 6 h Metamorphosis of larvae: 18 h	Fertilization of sperm and eggs: IC_{50} (6 h): 3.43 mg/L Metamorphosis of larvae: IC_{50} (18 h): 3.57 mg/L	Negri and others (2011)

Note: TP, total protein; GLU, glucose; BUN, blood urea nitrogen; CR, creatinine; CHOL, cholesterol; TG, triglyceride; μM, micromolar; mg, milligram; L, liter; LC_{50}, 50% lethal concentration; IC_{50}, 50% inhibition concentration.

Table 2.4 Published measures of aquatic toxicity for gallium and indium chemicals. - Continued

Compound	Model organism	End point		Exposure period	Value or result	Reference
Ga^{3+}	Freshwater swamp shrimp (*Macrobrachium nipponense*)	Acute toxicity	Mortality	96 h-LC_{50}	LC_{50} (24 h): 12.6871 mg/L LC_{50} (48 h): 6.1262 mg/L LC_{50} (96 h): 2.7742 mg/L	Yang (2014)
$GaCl_3$	Alga (*Isochrysis galbana*)	Acute toxicity	Mortality	72 h-LC_{50}	No measurable toxicity of Ga up to 6.0 mg/L	Trenfield and others (2015)
Ga^{3+}-citrate	Zebrafish (*Danio rerio*)	Acute toxicity	Mortality	LOEL: 24 and 120 hpf	LOEL (24 hpf): 113 μM LOEL (120 hpf): 24 μM	Olivares and others (2016)
$Ga_2(SO_4)_3$	Zebrafish (*Danio rerio*)	Acute toxicity	Mortality	48 h-96 h-LC_{50}	LC_{50} (48 h): 17.70 mg/L LC_{50} (72 h): 12.18 mg/L LC_{50} (96 h): 9.10 mg/L	Yang and Chen (2018)
$Ga_2(SO_4)_3$	Rosy bitterling (*Rhodeus ocellatus*)	Acute toxicity	Mortality	48 h-96 h-LC_{50}	LC_{50} (48 h): 18.02 mg/L LC_{50} (72 h): 14.54 mg/L LC_{50} (96 h): 10.71 mg/L	Yang and Chen (2018)
$GaCl_3$	Hermit crab (*Coenobita variabilis*)	Chronic toxicity	Developmental inhibition	6-day	No significant effects at the highest concentration (EC_{10} > 6 mg/L)	van Dam and others (2018)
In^{3+}	Freshwater amphipod (*Hyalella azteca*)	Acute toxicity	Mortality	7-day-LC_{50}	LC_{50} (7-day, soft water): > 1.00 mg/L LC_{50} (7-day, tap water): > 3.15 mg/L	Borgmann and others (2005)
$In(NO_3)_3$	Alga (*Chlorella vulgaris*)	Acute toxicity	Proliferation inhibition	24 h-EC_{50}	EC_{50} (24 h): 0.68 mM	Zurita and others (2007)
$In(NO_3)_3$	Water flea (*Daphnia magna*)	Acute toxicity	Immobilization	24 h-EC_{50}	EC_{50} (24 h): 0.28 mM	Zurita and others (2007)

Note: LOEL, lowest observed effect level; hpf, hours post fertilization; LC_{50}, 50% lethal concentration; EC_{50}, 50% effective concentration; EC_{10}, 10% effective concentration; μM, micromolar; mg, milligram; L, liter.

Table 2.4 Published measures of aquatic toxicity for gallium and indium chemicals. - Continued

Compound	Model organism	End point		Exposure period	Value or result	Reference
$InCl_3$	Crustacean (*Americamysis bahia*)	Acute toxicity	Mortality	96 h-LC_{50}	LC_{50} (96 h): 30.48 mg/L	Onikura and others (2008)
$InCl_3$	Rotifer (*Brachionus plicatilis*)	Acute toxicity	Mortality	24 h-LC_{50}	LC_{50} (24 h): 24.42 mg/L	Onikura and others (2008)
$InCl_3$	Crustacean (*Artemia salina*)	Acute toxicity	Mortality	48 h-LC_{50}	LC_{50} (48 h): 51 mg/L	Onikura and others (2008)
$InCl_3$	Japanese whiting (*Sillago japonica*)	Acute toxicity	Mortality	24 h-LC_{50}	No significant effects at the highest concentration (20 mg/L)	Onikura and others (2008)
In^{3+}	Freshwater swamp shrimp (*Macrobrachium nipponense*)	Acute toxicity	Mortality	96 h-LC_{50}	LC_{50} (24 h): 21.5464 mg/L LC_{50} (48 h): 14.8985 mg/L LC_{50} (96 h): 6.8938 mg/L	Yang (2014)
In^{3+}-citrate	Zebrafish (*Danio rerio*)	Acute toxicity	Mortality	LOEL: 24 and 120 hpf	No significant mortality over the tested range of 56-900 μM	Olivares and others (2016)
$InCl_3$	Zebrafish (*Danio rerio*)	Acute toxicity	Mortality	48 h-96 h-LC_{50}	LC_{50} (24 h): 21.84 mg/L LC_{50} (48 h): 18.28 mg/L LC_{50} (96 h): 15.35 mg/L	Yang and Chen (2018)
$InCl_3$	Rosy bitterling (*Rhodeus ocellatus*)	Acute toxicity	Mortality	48 h-96 h-LC_{50}	LC_{50} (48 h): 20.62 mg/L LC_{50} (72 h): 17.07 mg/L LC_{50} (96 h): 13.99 mg/L	Yang and Chen (2018)
$InCl_3$	Water flea (*Daphnia magna*)	Acute toxicity	Mortality	24 h-48 h-LC_{50}	LC_{50} (24 h): 58.93 mg/L LC_{50} (48 h): 54.49 mg/L	Brun and others (2019)
$InCl_3$	Water flea (*Daphnia magna*)	Chronic toxicity	Growth and reproduction inhibition	21-day	Growth rate and sexual maturity were reduced in a dose-response manner (2.29-9.17 mg/L)	Brun and others (2019)

Note: LOEL, lowest observed effect level; hpf, hours post fertilization; LC_{50}, 50% lethal concentration; μM, micromolar; mg, milligram; L, liter.

Table 2.4 Published measures of aquatic toxicity for gallium and indium chemicals. - Continued

Compound	Model organism	End point		Exposure period	Value or result	Reference
ITO	Cnidarian (*Hydra attenuata*)	Acute toxicity	Morphological changes	96 h-EC_{50}	EC_{50} (96 h): 0.1-1.0 mg/L (Very toxic)	Blaise and others (2008)
ITO	Crustacean (*Thamnocephalus platyurus*)	Acute toxicity	Mortality	24 h-LC_{50}	LC_{50} (24 h): 0.1-1.0 mg/L (Very toxic)	Blaise and others (2008)
ITO	Alga (*Pseudokirchneriella subcapitata*)	Chronic toxicity	Growth inhibition	72 h-IC_{25}	IC_{25} (72 h): 1.0-10 mg/L (Toxic)	Blaise and others (2008)
In_2O_3	Marine diatom (*Skeletonema costatum*)	Acute toxicity	Growth inhibition	72 h-IC_{50}	IC_{50} (72 h): 739.8 mg/L	Ng and others (2015)

Note: LC_{50}, 50% lethal concentration; EC_{50}, 50% effective concentration; IC_{50}, 50% inhibition concentration; IC_{25}, 25% inhibition concentration; μM, micromolar; mg, milligram; L, liter.

2.8 Environmental and Quality Standards

At the present time, although some aquatic toxicity data has been reported, toxicological data is still incomplete, Ga and *In* are not regulated in most countries, and the worldwide environmental quality standards for the two metals are currently non-existent.

In Taiwan, the wastewater effluent from semiconductor and optoelectronic industries are treated to meet the criteria of Water Pollution Control Act, and the treated wastewater will be further permitted to discharge into the aquatic environment. Nevertheless, Ga and *In* had not been regulated in any water bodies by Taiwan's EPA until 2010. The downstream and nearby areas of semiconductor and optoelectronic industries might be affected because the concentrations of Ga or *In* in groundwater, farmland soils and sediments were much higher than background concentration (Chen, 2006; You, 2014). To prevent environmental contamination, Taiwan's EPA has recommended that Ga and *In* levels in wastewater effluent of optoelectronic industry should not exceed 0.1 mg/L, and *In* levels in drinking water should not exceed 0.07 mg/L.

In the near future, there is still a need for more ecotoxicity data from subchronic and chronic studies to truly understand potential impacts of Ga- and In-related chemicals to the aquatic ecosystem, and the government could further enact new environmental regulations and/or environmental qualities to protect and control the environment.

3. Research Purpose

In aquatic environment, there may be only a small portion of the Ga and *In* could be taken away by water flows and a large quantity of them get deposited in the bottom of water bodies. The epibenthic and benthic organisms may be potentially exposed to either dissolved metal ions or insoluble hydroxide and oxide chemicals by direct interacting with aqueous- and sediment-phase as well as feeding behaviors. However, the chemical transformation, bioavailability and toxic effects of these chemicals remain unclear between the aqueous-, pore-water-, and sediment phases.

Although the effect of short-term exposure to Ga(III) and In(III) may have minimal toxic effects on aquatic organisms, there is still a large gap in knowledge about the potential impact on long-term exposure to ion species and insoluble hydroxide/oxide chemicals of Ga and *In*, and their relationship to other elements (e.g., Fe, Mn and Al) in aquatic environment.

Therefore, in this study, two questions are raised as follows.

Question 1: Are the physical or chemical properties of Ga- and *In*-related chemicals in water phase associated with the bioavailability and toxicity to aquatic organisms?

Question 2: Do exposure to Ga- and *In*-related chemicals induce TCEs-specific sublethal effects?

To answer the two questions, the following three aims come up:

Aim 1: To explore the environmental fate including chemical changes and bioavailability of Ga- and *In*-related chemicals in the exposure systems.

Aim 2: To investigate acute and chronic toxic effects of Ga- and *In*-related chemicals by *in vivo* (*Hyalella azteca*) bioassays.

Aim 3: To evaluate the potential ecological impacts of Ga- and *In*-related chemicals according to sublethal effects.

4. Model Organism

The epibenthic freshwater amphipod (*Hyalella azteca*) is used as a model organism for in *vivo* bioassays. *Hyalella azteca* is a freshwater crustacean (Malacostraca: Amphipoda) that lives at the bottom of water and sediment surface, burrowing in sediment and scavenging on leaf litter, algae and bacteria in aquatic environment (Wang et al., 2004a).

Hyalella azteca species complex is one of the most abundant and broadly distributed amphipods in Northern, Central and Southern America, and it has also been investigated that contributes to a significant component of the diet of many fish species, larger macroinvertebrates, wading birds, and waterfowl (Borgmann, 1996; Bousfield, 1958; FRANCE, 1993; Lawrence, 1981; March, 1977; Novak and Taylor, 2017; Ryder and Pesendorfer, 1992; Wellborn, 1994; Witt and Hebert, 2000).

In addition, *Hyalella azteca* has short generation time, high tolerance to temperature and salinity changes, sensitive to a variety of environmental pollutants and, importantly, is easy to culture in laboratory conditions and cheap to maintain, which has made this freshwater amphipod an ideal model organism for assessing aquatic toxicity, bioavailability and bioconcentration of sediment contaminants (ASTM, 2010; Besser et al., 2018; Borgmann et al., 1998; Borgmann et al., 2005a; Borgmann et al., 2001; Cooman et al., 2015; Dussault et al., 2008; Liber et al., 2011; Milani et al., 2003; Norberg-King et al., 2006; Poynton et al., 2018; Taylor et al., 2016; Walsh et al., 2019; Wu et al., 2014; You et al., 2008; Zubrod et al., 2019).

5. Materials and Methods

5.1 Research Design

In this study, firstly neonates of freshwater amphipod (*Hyalella azteca*) were dosed with the standard artificial medium spiked with Ga- and *In*-related chemicals in a wide range of concentrations to evaluate the short-term acute toxicity (LC_{50}). Secondly, the sublethal doses were determined by considering the calculated LC_{50} values, current wastewater discharge standards and background concentrations of Ga and *In* in aquatic environment, and the long-term chronic toxicity test was further performed to assess the sublethal effects (survival, growth, reproduction and bioaccumulation factor) of Ga- and *In*-related chemicals. All spiked solutions were well characterized for their particle characterization, water-quality parameters, concentration of total metal and overlying water (ionic species and colloidal particles) during exposure. Casual research scheme is illustrated in Figure 5.1.

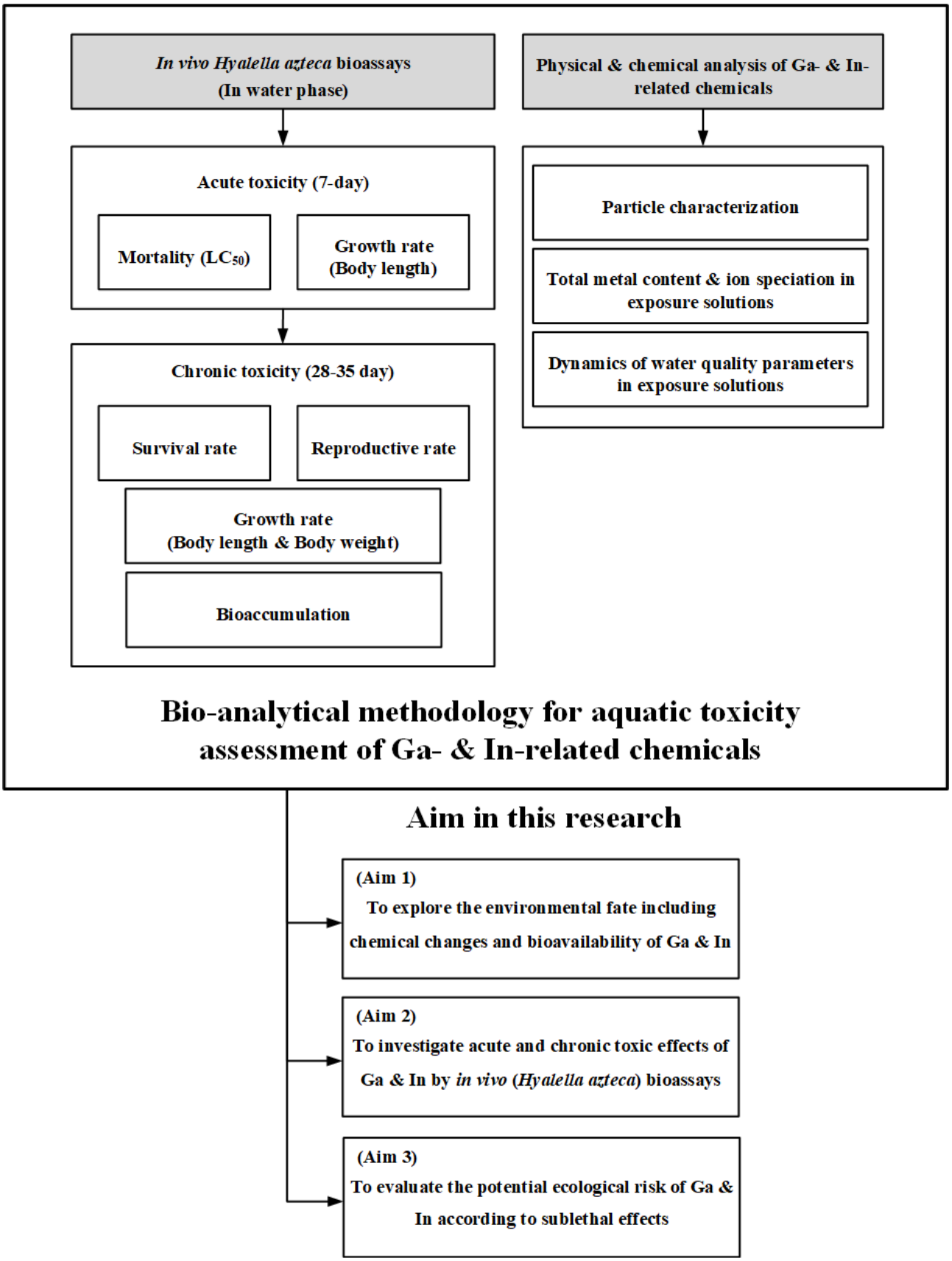

Figure 5.1 Scheme in casual aquatic toxicity assessment of Ga and *In* with bio-analytical strategy in freshwater amphipod (*Hyalella azteca*).

5.2 Preparation of Stock Solutions

The exposure experiments of different chemical forms of Ga and *In* were performed that may present in the aquatic environment, i.e., (1) ionic forms, (2) insoluble chemicals from hydrolysis process, and (3) insoluble chemicals discharged from manufacturing processes. Since both Ga(III) and In(III) have relatively low solubility near the pH of neutrality, and there would pose a risk of agglomeration and precipitation of hydrolysis products (i.e., $In(OH)_{3(s)}$ and $Ga(OH)_{3(s)}$) in the standard artificial medium. In addition, the ionic forms of Ga(III) and In(III) were also chelated with citrate (or citric acid) to prevent hydrolysis and evaluate the toxic effects of dissolved metal ions (Olivares et al., 2016; Zeng et al., 2017).

Indium hydroxide ($In(OH)_{3(s)}$), indium oxide ($In_2O_{3(s)}$) and gallium oxide ($Ga_2O_{3(s)}$) were used as insoluble chemicals, and the required amount was suspended in standard artificial medium for each exposure treatment. On the other hand, for the exposure experiments of ionic form, a stock solution of Gallium(III) chloride anhydrous ($GaCl_3$) and indium(III) chloride tetrahydrate ($InCl_3 \cdot 4H_2O$) were prepared and diluted with standard artificial medium for each treatment. In order to prepare metal ions chelated by citrate, sodium citrate dihydrate ($C_6H_5Na_3O_7 \cdot 2H_2O$) was added to the above stock solutions in a molar ratio of metal to citrate of 1:1 (Zeng et al., 2017).

5.3 Culture of *Hyalella azteca*

The *Hyalella azteca* culture was obtained in 2019 from National Institute for Environmental Studies (Ibaraki Prefecture, Japan) and was subsequently maintained in 3-L glass oven dish containing 500 g of small gravel stone (5-10 mm in size) (Figure 5.2) and 2.0 L of dechlorinated tap water at 23 ± 1 °C with 16:8 h light: dark photoperiod. Culture water was renewed three times a week and the culture chambers were fed with TetraMin® fish food (Tetra-Werke, Melle, Germany) twice a week. In order to increase the reproductive rate of *Hyalella azteca* population, each culture chamber also supplied with substrates of maple leaves and aquarium ceramic ring (10 mm×10 mm). Before use, fresh maple leaves litter was soaked in 30 ‰ salt water for about 30 days to reduce the occurrence of planaria, snails or other harmful organisms to *Hyalella azteca* (ASTM, 2010). The soaked leaves were then washed with tap water to remove the salt water and residuals of naturally occurring tannic acid before placing in culture chambers (ASTM, 2010).

5.4 Particle Characterization

In order to investigate how the water matrices in the standard five-salt artificial medium (SAM-5S) affect the physical and chemical properties of aqueous insoluble chemicals of Ga and *In* (i.e., $In(OH)_{3(s)}$, $In_2O_{3(s)}$ and $Ga_2O_{3(s)}$), resulting in the changes of bioavailability and toxicity to *Hyalella azteca*. Freshly prepared stocks of the three insoluble compounds were suspended in ultrapure water with 15 minutes of sonication, the hydro-diameter and zeta-potential of the particles in water suspensions were measured using a ZetaSizer Nano series (Malvern Panalytical, UK) instrument. The

shape and structure of particles and aggregates were observed by using inverted phase-contrast microscope (BZ-9000, Keyence, Osaka, Japan) and BZ-II viewer software (Keyence, Osaka, Japan), coupled with a 20x objective (Plan Fluor/0.45 numerical aperture; Nikon).

Figure 5.2 The culture condition of freshwater amphipod (*Hyalella azteca*).

5.5 Water-Only Exposure Tests

5.5.1 7-Day Acute Toxicity Test

Isolation of Hyalella azteca: In order to obtain the neonates, the amphipods in culture chambers were separated by sequentially passing them through different sieves: the U.S. Standard No. 18 sieve (1.00-mm mesh), the U.S. Standard No. 40 sieve (425-µm mesh), and the No. 45 sieve (355-µm mesh). The remaining neonates on the No. 45 sieve were collected. The size of sieved neonates was 1.54-2.0 mm in length, corresponding to the length of the neonates at 7-8 days of age.

Preparation of SAM-5S: The exposure solutions of toxicity tests were freshly prepared by the standard artificial medium, consisting of five salts (SAM-5S; $CaCl_2$, $NaHCO_3$, NaBr, KCl, and $MgSO_4$) (Table 5.1), which is representative of water qualities found near Lake Ontario, Northern America. The SAM-5S has been widely used as a standard artificial medium for culturing and conducting toxicity tests of *Hyalella azteca* (Baudy et al., 2017; Borgmann, 1996; Novak and Taylor, 2017; Walsh et al., 2019). Before preparing dosing solutions, the SAM-5S should be aerated for a minimum of 24 hours before use to adjust the dissolved oxygen, stabilize pH and water temperature.

Acclimation: The neonates were further acclimated gradually to their new conditions by holding them in 1.0-L glass beakers containing culture water, pieces of cotton gauze (5 cm×5 cm) and finely ground TetraMin® fish food (200 amphipods/beaker) with gentle aeration for two hours, then changed to 50:50 water mixture (culture water: SAM-5S) for two hours, and another two hours in a 25:75 water mixture (culture water: SAM-5S). After holding for a three-day acclimatization period

in the SAM-5S before testing to eliminate organisms injured during sieving, these neonates were about 9-days old at the start of acute toxicity test.

Exposure experiment: After three-day acclimation, the neonates (about 9-days old) were randomly assigned in 200-mL acid washed beakers (10 neonates per 200 mL solution) to undergo 7-day continuous exposure to seven freshly prepared exposure solutions of Ga- and *In*-related chemicals (1.0-100 mg/L, Ga- and/or *In*-equivalent concentration) (Table 5.2; Table 5.3). Furthermore, the pH values of the highest concentration (100 mg/L) of four exposure solutions (Ga(III), citrate-Ga(III), In(III) and citrate-In(III)) were adjusted with NaOH (10 M) to pH ranges of about 7.5-8.2. SAM-5S and citrate (421.8 mg/L, the maximum concentration used for citrate-Ga(III) and citrate-In(III)) served as blank controls. A piece of 2.5×2.5-cm cotton gauze (for amphipods to cling to) that presoaked with SAM-5S and a small amount of finely ground Tetra-Mint® fish food flasks were then added to each beaker. Dead neonates were removed daily, and the surviving neonates were sacrificed for Ga and/or *In* quantity measurement.

Ga and/or In quantification in water and Hyalella azteca: The surviving neonates were collected and rinse with SAM-5S, and then fixed with 8% sugar formalin solution in 2.0-mL glass vial for growth measurements (Figure 5.3). To determine Ga and *In* exposure levels in dosing solutions, the total metal concentration and metal contents in overlying water (ionic species and colloidal particles) were measured during exposure period. Water samples (5 mL, triplicate) were taken from the middle of the aqueous phase and acidified with 100 μL of concentrated nitric acid (60-

62 %). The concentrations of Ga and/or *In* in the water sample (5 mL) were quantified by use of ICP-MS (NexION 1000, PerkinElmer).

Measurement of water quality characteristics: Water temperature, conductivity (EC), hardness, pH, dissolved oxygen (DO), nitrate (NO_3^-) and nitrite (NO_2^-) were measured in all treatments during exposure period (Table 5.3).

Table 5.1 Standard recipe for preparing SAM-5S

Compound	Concentration (mg/L)
$CaCl_2$	110
$NaHCO_3$	84
$MgSO_4 \cdot 7H_2O$	61.4
KCl	3.7
NaBr	1.2

Note: The water quality should be approximately in the range of as follows: (1) hardness, 120-140 mg/L as $CaCO_3$;(2) alkalinity, 60-80 mg/L as $CaCO_3$; (3) conductivity, 300-500 μs/cm; (4) pH value, 6.5-8.5.

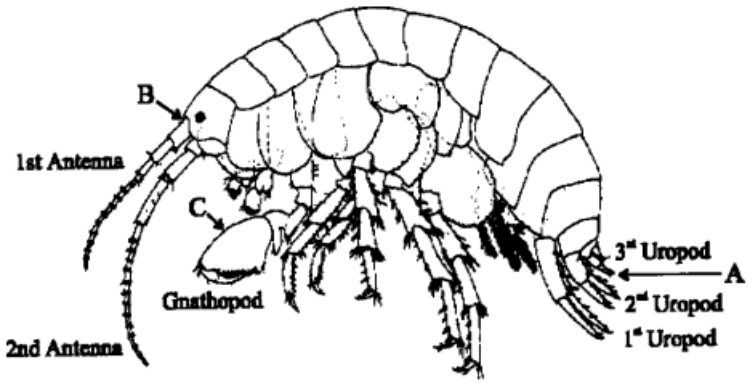

Figure 5.3 Freshwater amphipod (*Hyalella azteca*). Measurement of body-length is calculated from base of 3rd uropod (A) to (B). Females are recognized by the presence of egg cases or the absence of an enlarged gnathopod. (ASTM, 2010)

Table 5.2 Test conditions for conducting 7-day water phase toxicity test with *Hyalella azteca*

	Parameter	Conditions
1.	Test type:	7-day acute toxicity test in water phase
2.	Temperature:	23 ± 1 °C
3.	Light quality:	Wide-spectrum LED lights
4.	Illuminance:	About 100 to 1000 lux
5.	Photoperiod:	16 L:8 D
6.	Test chamber:	250-mL polypropylene beaker
7.	Water volume:	200-220 mL
8.	Renew of water:	None, unless DO in water drops below 2.5 mg/L
9.	Age of organisms:	7- to 14-day old (within 1- to 2-day range in age) at the start of the test
10.	Number of organism/ treatment:	10
11.	Number of replicate/ treatment:	4
12.	Feeding:	Finely ground Tetra-Min® fish food flasks. An additional food was provided midweek (Day-3)
13.	Aeration:	None, unless DO in water dropped below 2.5 mg/L
14.	Water source:	SAM-5S
15.	Water quality:	EC, pH, hardness, NO_3^- and NO_2^- at the beginning and end of a test. Temperature, pH and DO daily
16.	Test compounds:	Ga(III), In(III), citrate-Ga(III), citrate-In(III) $In(OH)_{3(s)}$, $In_2O_{3(s)}$, $Ga_2O_{3(s)}$
17.	Exposure concentration:	0, 1, 5, 10, 25, 50 and 100 mg/L (Ga- and/or *In*-equivalent concentration)
18.	Test duration:	7 days
19.	Endpoints:	Survival and growth
20.	Test acceptability:	Minimum mean control survival of 80 % and measurable growth of test organisms in the control

Table 5.3 General schedule for conducting 7-day water phase toxicity test with *Hyalella azteca*

Day	Activity
-4	Separate 7- to 14-day old amphipods and place in acclimation beakers (200 amphipods/1.0-L beaker). Begin preparing food for the test. There should be only a 1- to 2-day range in age of amphipods used to start the test.
-3 to-1	Feed and observe isolated amphipods, monitor water quality (temperature, pH, DO).
0	Measure total water qualities (pH, temperature, DO, hardness, EC, NO_3^- and NO_2^-). Transfer 10 neonates into each beaker. Add a small amount of finely ground Tetra-Min® fish food flasks. Exposure solutions are sampled for metal concentration analysis (day-0).
1-3	Add another finely ground Tetra-Min® fish food flasks to each beaker on day-3 and sampling dosing solutions for metal concentration analysis. Monitor water qualities daily (temperature, pH, EC, DO).
4-7	Exposure solutions are sampled for metal concentration analysis on day-7. Measure total water qualities (pH, temperature, DO, hardness, EC, NO_3^- and NO_2^-) on day-7. End the test by sampling the surviving amphipods. Count survivors and prepare for dry weight or length measurements.

5.5.2 28-35-day Chronic Toxicity Test

The isolation of *Hyalella azteca* neonates, preparation of SAM-5S and acclimation methods were performed as previously described in 5.5.1.

Exposure experiment: After three-day acclimation, the neonates (about 9-days old) were randomly assigned in 200-mL acid washed beakers (10 neonates per 200 mL solution) to undergo 28-35-day continuous exposure to seven freshly prepared exposure solutions of Ga- and *In*-related chemicals (0.5 or 5.0 mg/L, Ga- and/or *In*-equivalent concentration) (Table 5.4). SAM-5S served as a blank control and all dosing solutions were renewed every seven days. A piece of 2.5×2.5-cm cotton gauze (for amphipods to cling to) that presoaked with SAM-5S and a small amount of finely ground Tetra-Mint® fish food flasks were then added to each beaker. Dead amphipods were removed daily. Four replicates were used for 28-day growth and survival endpoints and the other four replicates were used for measurement of survival, growth, reproduction and bioaccumulation calculation on Day 35.

Ga and/or In quantification in water and Hyalella azteca: On day-28, offspring was removed and surviving amphipods of four replicates were counted and rinse with SAM-5S, then preserved in 8% sugar formalin solution in 2.0-mL glass vial for growth measurements (Figure 5.3). On day-35, the number of surviving adults and offspring of remaining four replicates were records. The surviving adult amphipods were preserved in 8% sugar formalin solution in 2.0-mL glass vial, and the number of adult males and females in each replicate was also determined (Figure 5.3). Reproduction was

calculated from the number of offspring produced per surviving young female per replicate from Day-28 to Day-35 (Table 5.5).

After growth measurements, the body weight of every sample was measured after drying at 60 °C for one week. The dry sample was digested in 125 µL of concentrated nitric acid (60-62 %, for analysis of poisonous metals, Fujifilm Wako) for one week at room temperature, followed by adding 100 µL of hydrogen peroxide (30 %, Fujifilm Wako) for one day. To determine Ga and *In* exposure levels in dosing solutions, the total metal concentration and metal contents in overlying water (ionic species and colloidal particles) were measured during exposure period. Water samples (5 mL, triplicate) were taken from the middle of the aqueous phase and acidified with 100 µL of concentrated nitric acid (60-62 %). The concentrations of Ga and/or *In* in the water sample and homogenate (5 mL) were quantified by use of ICP-MS (NexION 1000, PerkinElmer). Bioaccumulation factor (BAF) was calculated by using the following formula:

$$BAF\ (L/kg) = C_0/C_w$$

C_0: Concentration of metal in dry tissue (mg/kg); C_w: Concentration of substance in water (mg/L).

Measurement of water quality characteristics: Water temperature, EC, hardness, pH, DO, NO_3^- and NO_2^- were measured in all treatments during exposure period (Table 5.5).

Table 5.4 Test conditions for conducting 28-35-day water phase toxicity test with *Hyalella azteca*

	Parameter	Conditions
1.	Test type:	28-35-day chronic toxicity test in water phase
2.	Temperature:	23 ± 1°C
3.	Light quality:	Wide-spectrum fluorescent lights
4.	Illuminance:	About 100 to 1000 lux
5.	Photoperiod:	16 L:8 D
6.	Test chamber:	250-mL polypropylene beaker
7.	Water volume:	200-220 mL
8.	Renew of water:	Every seven days
9.	Age of organisms:	7- to 8-day old (within 1- to 2-day range in age) at the start of the test
10.	Number of organism/ treatment:	10
11.	Number of replicate/ treatment:	4 (28-day); 4 (35-day)
12.	Feeding:	Finely ground Tetra-Min® fish food flasks. An additional food was provided after water renewing
13.	Aeration:	None, unless DO in water drops below 2.5 mg/L
14.	Water source:	SAM-5S
15.	Water quality:	Temperature, pH, DO, EC, hardness, NO_3^- and NO_2^-
16.	Test compounds:	Ga(III), In(III), citrate-Ga(III), citrate-In(III) $In(OH)_{3(s)}$, $In_2O_{3(s)}$, $Ga_2O_{3(s)}$
17.	Exposure concentration:	Ionic groups: 0.5 and 5 mg/L Hydroxide/oxides groups: 5 mg/L
18.	Test duration:	28 and 35 days
19.	Endpoints:	28-day survival and growth; 35-day survival, growth, reproduction, and number of adult males and females on Day 35
20.	Test acceptability:	Minimum mean control survival of 80% on Day 28 and 35

Table 5.5 General schedule for conducting 28-35-day water phase toxicity test with *Hyalella azteca*

Day	Activity
-3	Separate 7- to 8-day old amphipods and place in acclimation beakers (200 amphipods/1.0-L beaker). Begin preparing food for the test. There should be only a 1- to 2-day range in age of amphipods used to start the test.
-2 to-1	Feed and observe isolated amphipods, monitor water qualities (temperature, pH, DO)
0	Measure total water qualities (pH, temperature, DO, hardness, EC, NO_3^- and NO_2^-). Transfer 10 amphipods into each beaker. Add a small amount of finely ground Tetra-Min® fish food flasks. Exposure solutions are sampled for metal concentration analysis (day-0). Observe behavior of test amphipods.
1-27	Renew exposure solutions every 7 days. Add a small amount of finely ground Tetra-Min® fish food flasks to each test beaker after water renewing and midweek. Measure temperature, EC, DO, and pH before/after water renewing. Observe behavior of test organisms.
28	Measure total water qualities (pH, temperature, DO, hardness, EC, NO_3^- and NO_2^-). Use four replicates for growth measurements: count survivors and preserve organisms in 8% sugar formalin solution for growth measurements. Renew exposure solutions and add a small amount of finely ground Tetra-Min® fish food flasks to each test beaker.
29-34	Measure temperature, EC, DO, and pH three times a week. Measure hardness, NO_3^- and NO_2^- weekly. Observe behavior of test organisms.
35	Count the number of surviving adults and offspring. Surviving adult amphipods on Day 35 are preserved in 8% sugar formalin solution. The number of adult males in each beaker is determined from this archived sample. This information is used to calculate the number of young produced per female per replicate from Day 28 to Day 35. Measure total water qualities (pH, temperature, DO, hardness, EC, NO_3^- and NO_2^-).

5.6 Statistical Analysis

Each experiment was performed at least in triplicate. All results were presented as mean ± standard deviation (SD). Prior to analysis, all results were tested for normality (Kolmogorov-Smirnov test) and for homogeneity of variances (Levene test). The acceptable data were then performed by Student's t test, two-proportions z-test or one-way analysis of variance (ANOVA) with post hoc tests to evaluate significant differences between treatments. The IBM SPSS statistics program (version 21) was used for all statistical analyses, and p values of <0.05 were considered significant.

6. Results

6.1 Particle Characterization

The colloidal particle shape and formation of aggregates of $In(OH)_{3(s)}$, $In_2O_{3(s)}$ and $Ga_2O_{3(s)}$ were observed by using phase-contrast microscope and BZ-II viewer software, coupled with a 20x objective (Plan Fluor/0.45 numerical aperture) (Figure 6.1). These three compounds were prone to form large aggregates in both ultrapure water and SAM-5S. The aggregates of $In(OH)_{3(s)}$ and $In_2O_{3(s)}$ were irregular in shape, whereas the colloidal particles and aggregates of $Ga_2O_{3(s)}$ were respectively rod-shaped structure and irregular in shape. The hydro-diameter of these three compounds was undetectable by ZetaSizer Nano series instrument because of the rapid agglomeration and precipitation in both ultrapure water and SAM-5S. However, the colloidal particles and aggregates of these three compounds were approximately a few micrometers in size under the phase-contrast microscope observation. The zeta potential of $In(OH)_{3(s)}$ (33.67 mV), $In_2O_{3(s)}$ (22.23 mV) and $Ga_2O_{3(s)}$ (17.07 mV) indicated that stable dispersal in ultrapure water was more prolonged for these three compounds than in SAM-5S, which was $In(OH)_{3(s)}$ (-18.30 mV), $In_2O_{3(s)}$ (-17.37 mV) and $Ga_2O_{3(s)}$ (-11.11 mV). The zeta potential of $In(OH)_{3(s)}$, $In_2O_{3(s)}$ and $Ga_2O_{3(s)}$ in SAM-5S suggested that instable dispersal in solution was prone to aggregate and precipitate gradually during exposure period.

6.2 Dynamic Behaviors of Dosing Solutions

7-day acute toxicity test: The water temperature of Ga- and *In*-ionic groups was consistently between 23.8 and 24.1 °C during the exposure period, whereas the temperature of Ga- and *In*-related hydroxide/oxides groups was between 17.9 and 18.3 °C (Table 6.1 and Table 6.2). Although the ambient temperature was controlled at 25 °C in 2021 winter, the average temperature of hydroxide/oxides groups was lower than those of ionic groups. However, the decrease in water temperature due to seasonal temperature variation should not affect the acute toxicity in *H. azteca* neonates but may have effect on both growth rate and reproduction in amphipod during chronic exposure (Panov and McQueen, 1998).

The pH values with all dosing solutions were consistently between 7.69 and 8.13 within one week exposure period, and the DO levels were between 6.58 and 8.00 mg/L (Table 6.1 and Table 6.2). The change in both pH and DO between would not significantly affect the physiologic features of *H. azteca* (ASTM, 2010; Borgmann, 1996). In addition, the EC values of Ga- and *In*-related hydroxide/oxides groups was between 448 and 469 μs/cm, similar to the EC level of untreated control group. In contrast, the EC values increased with the concentration of Ga(III) and In(III). The addition of Ga(III) and In(III) ions, and the adjustment of pH level with NaOH (10 M) in the highest concentration treatment (100 mg/L) would increase the EC levels in solutions. In the treatments with the highest concentration (100 mg/L), the EC values were approximately 1.7 to 2.6 times as compared to untreated control.

28-35-day chronic toxicity test: The water temperature of all treatments was between 24.2 and 24.7 °C before water renewing (day-3, day-6, day-10, day-13, day17, day-20, day-24, day-31, and day-35), and the temperature was between 23.9 to 24.4 °C after water renewing (day-0, day-7, day-14, day-21, and day-28) (Table 6.3). The pH values were consistently between 8.08 and 8.15 after water renewing and the similar pH levels (7.87 to 8.08) were observed before water renewing. After water renewing, the DO level among all treatments was between 8.04 and 8.12 mg/L, while the DO level gradually dropped to 6.95 to 7.64 mg/L before water renewing. The change in DO levels between 6 and 8 would not significantly affect the survival and growth of *H. azteca* (ASTM, 2010). Furthermore, the EC levels did not remarkably change as compared to SAM-5S control neither before nor after water renewing.

Table 6.1 Monitoring of water quality parameters during 7-day acute toxicity test. The exposure test of Ga- and *In*-ionic groups was performed from October 13th to October 20th, 2020.

Nominal concentration	(mg/L)	Temperature (°C)	pH	DO (mg/L)	EC (μs/cm)
Control	-	23.9±0.2	8.06±0.10	7.98±0.25	484±57
Citrate	421.8	24.0±0.3	8.13±0.11	7.61±0.20	698±66
In(III)	1	23.9±0.3	8.04±0.06	7.90±0.17	475±38
	5	23.8±0.2	8.00±0.07	7.85±0.13	481±33
	10	23.9±0.2	7.96±0.07	7.87±0.10	496±31
	25	24.0±0.2	7.94±0.06	7.78±0.15	546±37
	50	24.0±0.1	7.91±0.07	7.87±0.14	653±55
	100	23.9±0.2	7.87±0.08	7.81±0.11	800±60
Citrate-In(III)	1	24.0±0.2	7.91±0.07	7.72±0.16	472±32
	5	24.1±0.3	7.91±0.06	7.66±0.14	488±31
	10	24.0±0.2	7.90±0.06	7.59±0.15	507±37
	25	24.0±0.3	7.86±0.05	7.55±0.22	568±39
	50	23.9±0.2	7.97±0.11	7.83±0.20	698±59
	100	23.9±0.3	7.97±0.11	7.85±0.22	900±76
Ga(III)	1	23.9±0.2	7.91±0.08	7.54±0.21	475±28
	5	24.0±0.2	7.86±0.08	7.58±0.20	490±26
	10	24.1±0.2	7.81±0.10	7.61±0.24	516±25
	25	24.0±0.1	7.79±0.07	7.59±0.27	609±31
	50	24.0±0.2	7.79±0.09	7.09±0.37	744±35
	100	24.0±0.2	7.82±0.05	7.19±0.31	1,032±51
Citrate-Ga(III)	1	23.9±0.3	7.84±0.07	6.77±0.42	462±23
	5	23.9±0.2	7.74±0.04	6.58±0.34	495±30
	10	23.9±0.1	7.72±0.05	6.92±0.19	526±27
	25	24.0±0.1	7.72±0.04	7.08±0.38	637±34
	50	24.0±0.2	7.75±0.06	7.34±0.30	830±37
	100	24.1±0.2	7.80±0.07	7.01±0.43	1,237±54

Note: DO, dissolved oxygen; EC, electrical conductivity.

Table 6.2 Monitoring of water quality parameters during 7-day acute toxicity test. The exposure test of Ga- and *In*-related hydroxide/oxides groups was performed from January 18th to January 25th, 2021.

Nominal concentration (mg/L)		Temperature (°C)	pH	DO (mg/L)	EC (μs/cm)
Control	-	18.1±0.3	7.94±0.10	7.72±0.23	454±24
$In(OH)_{3(s)}$	1	18.1±0.2	7.93±0.10	7.73±0.32	453±23
	5	17.9±0.2	7.89±0.08	7.82±0.28	454±23
	10	17.9±0.2	7.87±0.07	7.93±0.15	454±24
	25	17.9±0.2	7.85±0.07	7.76±0.24	454±24
	50	17.9±0.2	7.82±0.08	7.69±0.38	453±22
	100	18.0±0.2	7.83±0.06	7.95±0.19	451±20
$In_2O_{3(s)}$	1	18.1±0.2	7.82±0.05	7.70±0.23	448±21
	5	18.0±0.2	7.79±0.05	7.70±0.27	451±22
	10	18.2±0.3	7.78±0.05	7.76±0.27	452±20
	25	18.3±0.3	7.77±0.05	7.83±0.34	453±20
	50	18.2±0.2	7.77±0.04	7.91±0.29	452±19
	100	18.0±0.3	7.77±0.04	8.00±0.22	451±21
$Ga_2O_{3(s)}$	1	17.9±0.2	7.77±0.04	7.64±0.22	451±20
	5	18.1±0.2	7.75±0.05	7.58±0.24	452±21
	10	18.1±0.2	7.74±0.04	7.28±0.35	452±22
	25	18.1±0.2	7.74±0.05	7.41±0.32	452±22
	50	18.1±0.2	7.71±0.03	7.26±0.44	452±21
	100	18.1±0.2	7.69±0.03	7.47±0.31	469±30

Note: DO, dissolved oxygen; EC, electrical conductivity.

Table 6.3 Monitoring of water quality parameters during 28-35-day chronic toxicity test.

Nominal concentration (mg/L)		Before water renewing [a]				After water renewing [b]			
		Temperature (°C)	pH	DO (mg/L)	EC (μs/cm)	Temperature (°C)	pH	DO (mg/L)	EC (μs/cm)
Control	-	24.5±0.4	8.08±0.08	6.95±0.98	447±16	24.4±0.6	8.15±0.03	8.09±0.31	423±10
In(III)	0.5	24.5±0.4	8.04±0.07	7.38±0.68	455±18	24.4±0.5	8.13±0.06	8.00±0.27	432±8
	5	24.5±0.4	7.99±0.07	7.42±0.74	456±16	24.1±0.4	8.12±0.06	8.08±0.25	434±8
Citrate-In(III)	0.5	24.6±0.4	7.96±0.07	7.60±0.64	457±19	24.2±0.5	8.12±0.07	8.05±0.33	429±6
	5	24.7±0.5	7.95±0.07	7.53±0.48	479±22	24.1±0.5	8.11±0.08	8.11±0.35	438±5
Ga(III)	0.5	24.6±0.5	7.93±0.07	7.41±0.69	448±19	24.1±0.5	8.11±0.07	8.12±0.37	435±6
	5	24.5±0.4	7.89±0.09	7.25±0.77	451±16	24.0±0.5	8.10±0.08	8.08±0.22	437±8
Citrate-Ga(III)	0.5	24.4±0.5	7.89±0.07	7.64±0.70	452±17	24.1±0.4	8.09±0.09	8.08±0.19	431±8
	5	24.3±0.4	7.90±0.06	7.57±0.62	468±21	24.1±0.4	8.08±0.09	8.06±0.23	443±8
$In(OH)_{3(s)}$	5	24.2±0.4	7.89±0.06	7.35±0.95	444±17	23.9±0.5	8.09±0.08	8.08±0.31	433±3
$In_2O_{3(s)}$	5	24.2±0.4	7.89±0.06	7.48±0.81	448±18	24.0±0.5	8.09±0.07	8.11±0.36	431±7
$Ga_2O_{3(s)}$	5	24.2±0.4	7.87±0.07	7.07±0.87	444±16	24.0±0.4	8.09±0.07	8.04±0.18	430±4

Note: DO, dissolved oxygen; EC, electrical conductivity.

[a] The water quality parameters were monitored at day-0, day-7, day-14, day-21, and day-28 of exposure.

[b] The water quality parameters were monitored at day-3, day-6, day-10, day-13, day-17, day-20, day-24, day-31, and day-35 of exposure.

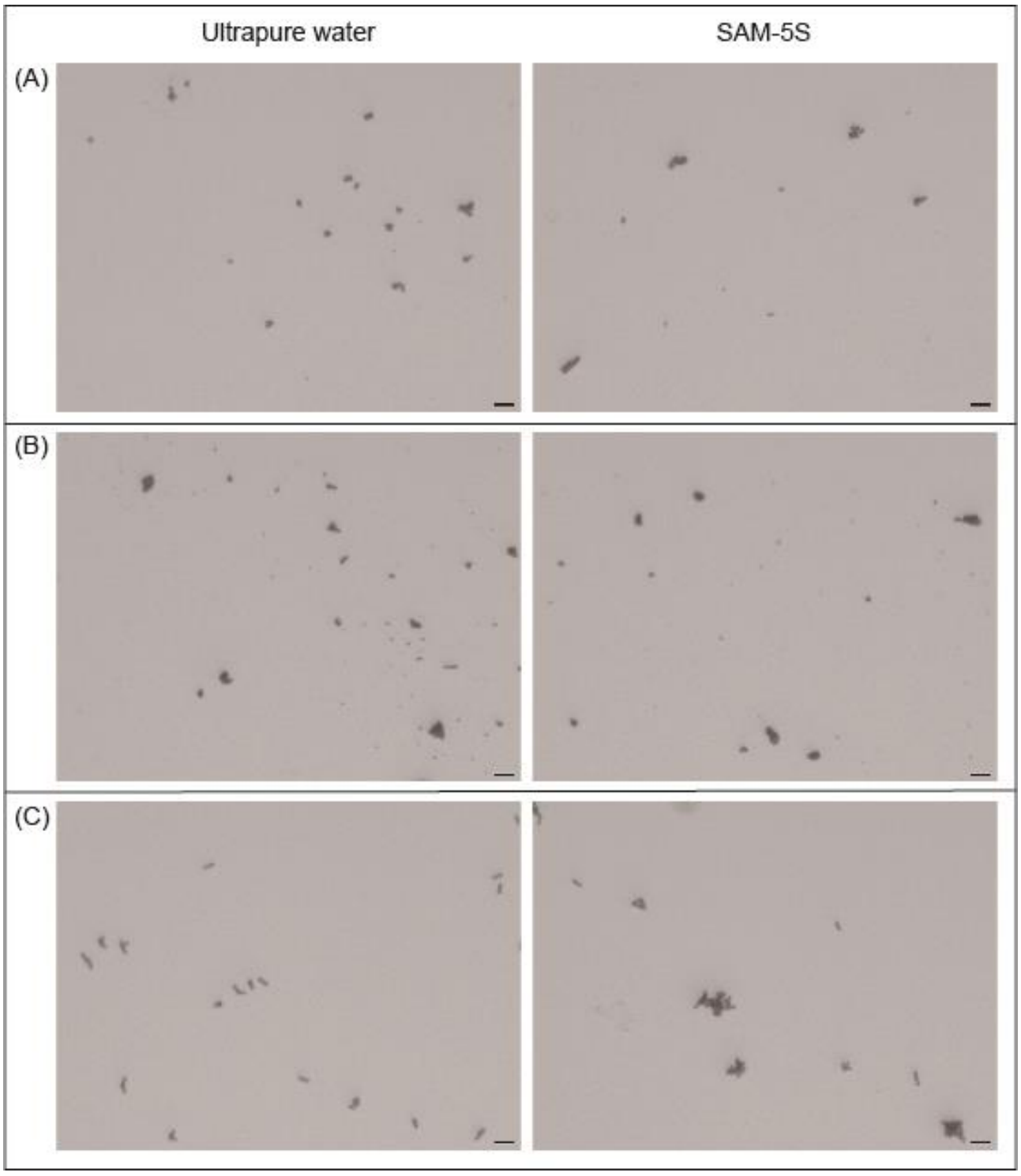

Figure 6.1 Phase-contrast microscopy observation of $In(OH)_{3(s)}$, $In_2O_{3(s)}$ (50 mg In/L) and $Ga_2O_{3(s)}$ (50 mg Ga/L) suspended in ultrapure water and SAM-5S medium. (A) $In(OH)_{3(s)}$; (B) $In_2O_{3(s)}$; (C) $Ga_2O_{3(s)}$. Images obtained from BZ-II viewer software confirm that the particle and aggregate sizes of these three compounds were approximately at 5-10 μm in diameter. Images were acquired using 60× magnification. Scale bar, 10 μm.

6.3 Neonatal Lethality of Ga- and *In*-Related Chemicals

The 7-day acute toxicity test of Ga- and *In*-ionic groups was performed from October 13th to October 20th, 2020; and the other test of Ga- and *In*-related hydroxide/oxides groups was performed from January 18th to January 25th, 2021. The measured total Ga/*In* concentrations in exposure solutions and remaining Ga/*In* (ionic species and colloidal particles) in overlying water were shown in Table 6.4. The solubility of In(III) and citrate-In(III) in SAM-5S was remarkably lower than Ga(III) and citrate-Ga(III), and $In(OH)_{3(s)}$, $In_2O_{3(s)}$, and $Ga_2O_{3(s)}$ were believed to be insoluble. The recovery of In(III) and citrate-In(III) in overlying water was < 5 % (in average), whereas the recovery of Ga(III) and citrate-Ga(III) was > 80 % (in average). In(III) tended to hydrolysis more $In(OH)_{3(s)}$ than citrate-In(III) in lower concentrations (1 and 5 mg/L), and citrate-Ga(III) was more stable in exposure solution than Ga(III) due to the variation of measured Ga concentrations in overlying water. In addition, the recovery of insoluble chemicals of $In(OH)_{3(s)}$, $In_2O_{3(s)}$, and $Ga_2O_{3(s)}$ in overlying water was < 1 % (in average), suggesting these particles tended to gradually aggregate and settled down.

The citrate control (421.8 mg/L) did not have significant acute toxicity or sublethal toxic effects in neonates as compared with the SAM-5S blank control. All the Ga- and *In*-related chemicals did not produce dose-dependent responses, the stabilized form of Ga and *In* ions did not induce a higher lethal effects to the neonates (Figure 6.2).

In addition to lethal effects, the body length of surviving neonates was also measured. The exposure of In(III) and citrate-In(III) (5-100 mg In/L) significantly decreased the body length at the

end of treatment despite the fact that citrate-In(III) (25 mg In/L) only had slightly adverse effects; the Ga(III) solutions (25-100 mg Ga/L) significantly decreased the body length, while the neonates had greater body length after exposed to citrate-Ga(III) (1, 10, 25 and 100 mg Ga/L) (Figure 6.3). Also, the exposure of $In_2O_{3(s)}$ (100 mg In/L) and $Ga_2O_{3(s)}$ (10 and 100 mg Ga/L) significantly decreased the body length of the neonates, whereas $In(OH)_{3(s)}$ solutions (1-100 mg In/L) did not affect the growth rate at the end of exposure (Figure 6.4).

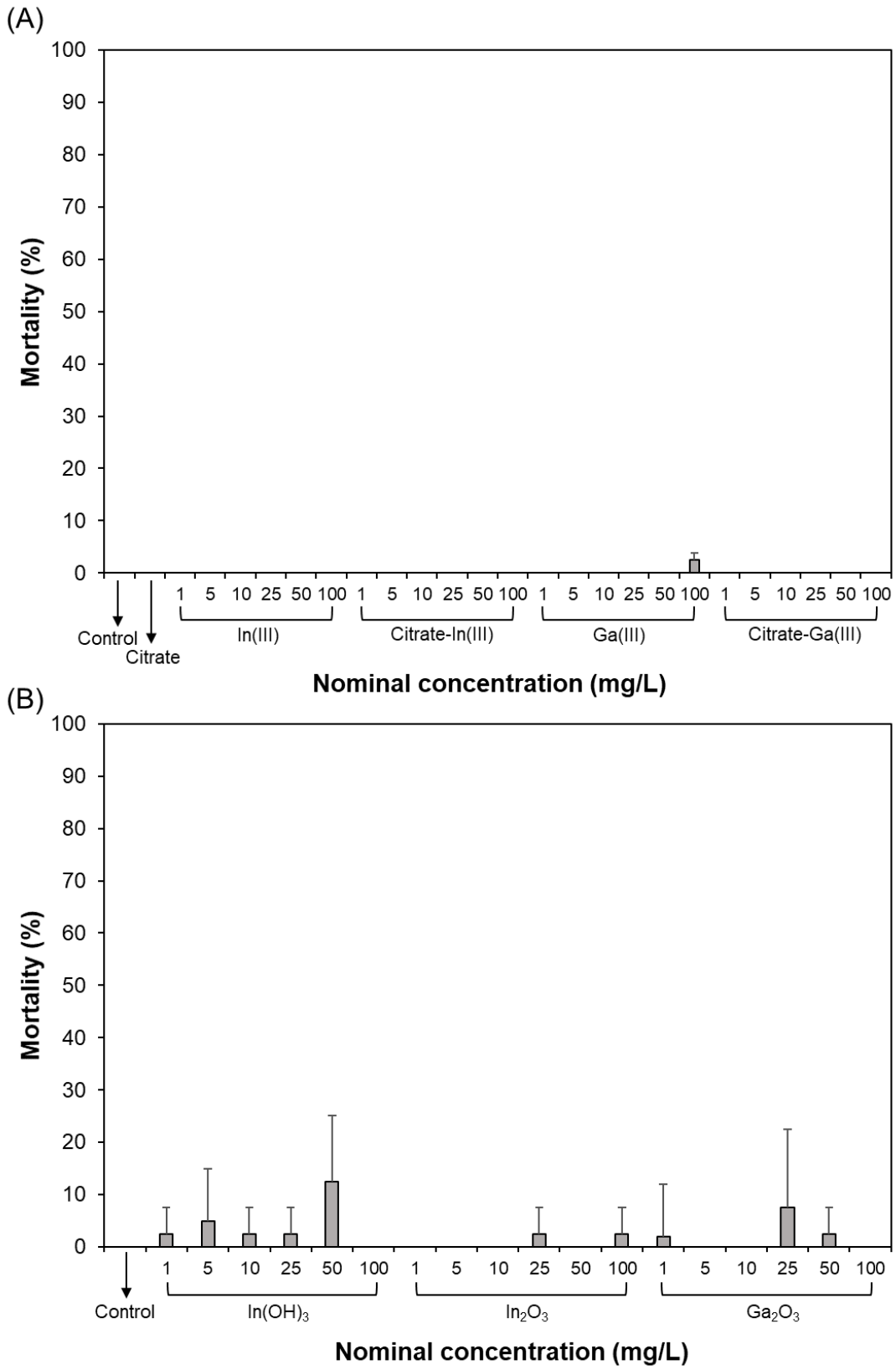

Figure 6.2 Mortality of *Hyalella azteca* neonates with 7-day aqueous exposure to (A) Ga- and *In*-ionic group, (B) Ga- and *In*-related hydroxide/oxides group. Independent sample t test; * $p<0.05$ versus control (n=4, 10 neonates in every replicate per treatment at the start of exposure).

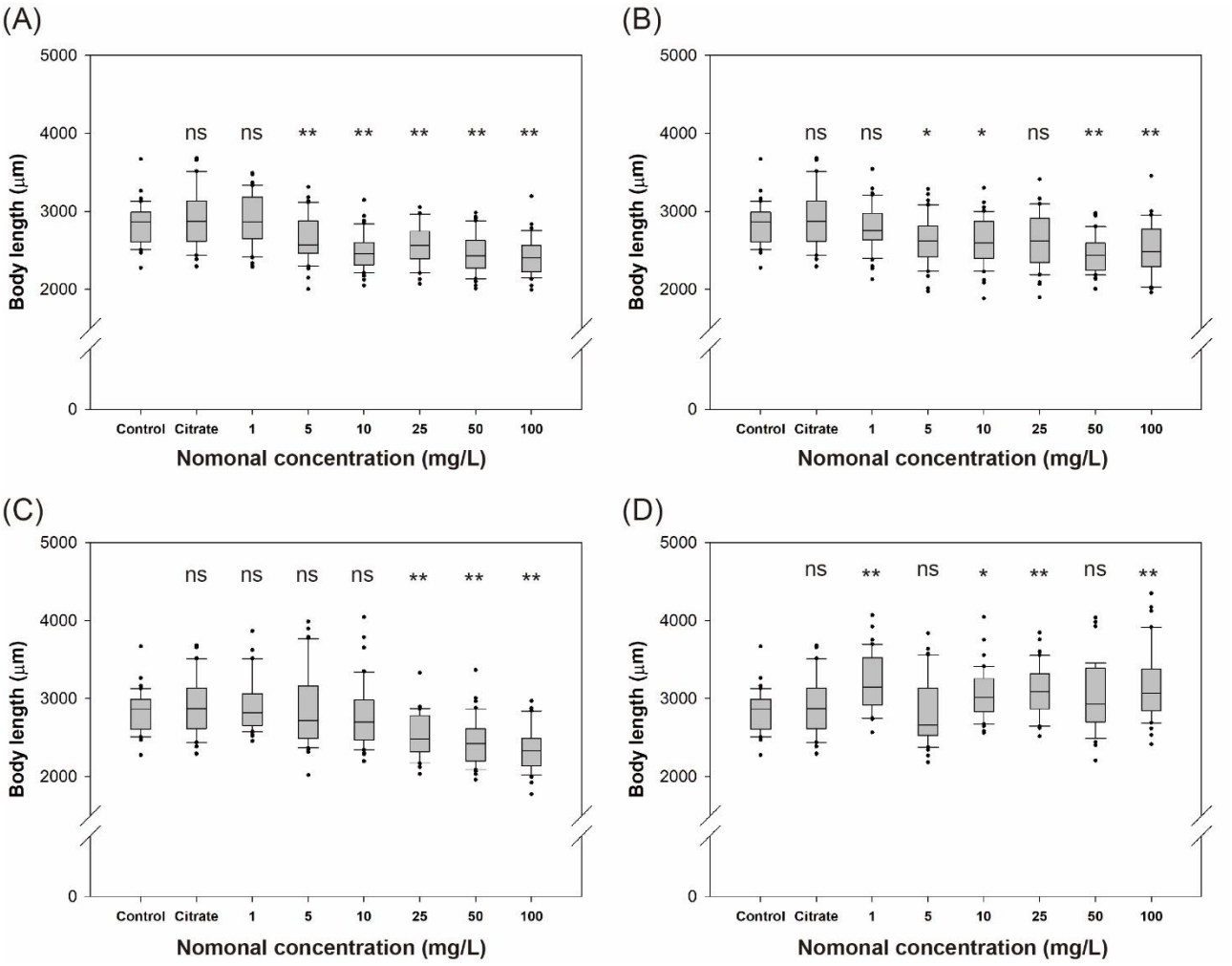

Figure 6.3 Body length of *Hyalella azteca* neonates after 7-day acute exposure to Ga- and *In*-ionic groups. (A) In(III), (B) Citrate-In(III), (C) Ga(III), (D) Citrate-Ga(III). * $p<0.05$ ** $p<0.01$ versus control, Kruskal–Wallis one-way analysis of variance followed by Dunnett T3 post-hoc test (n=40 neonates in 4 replicates per treatment at the start of exposure).

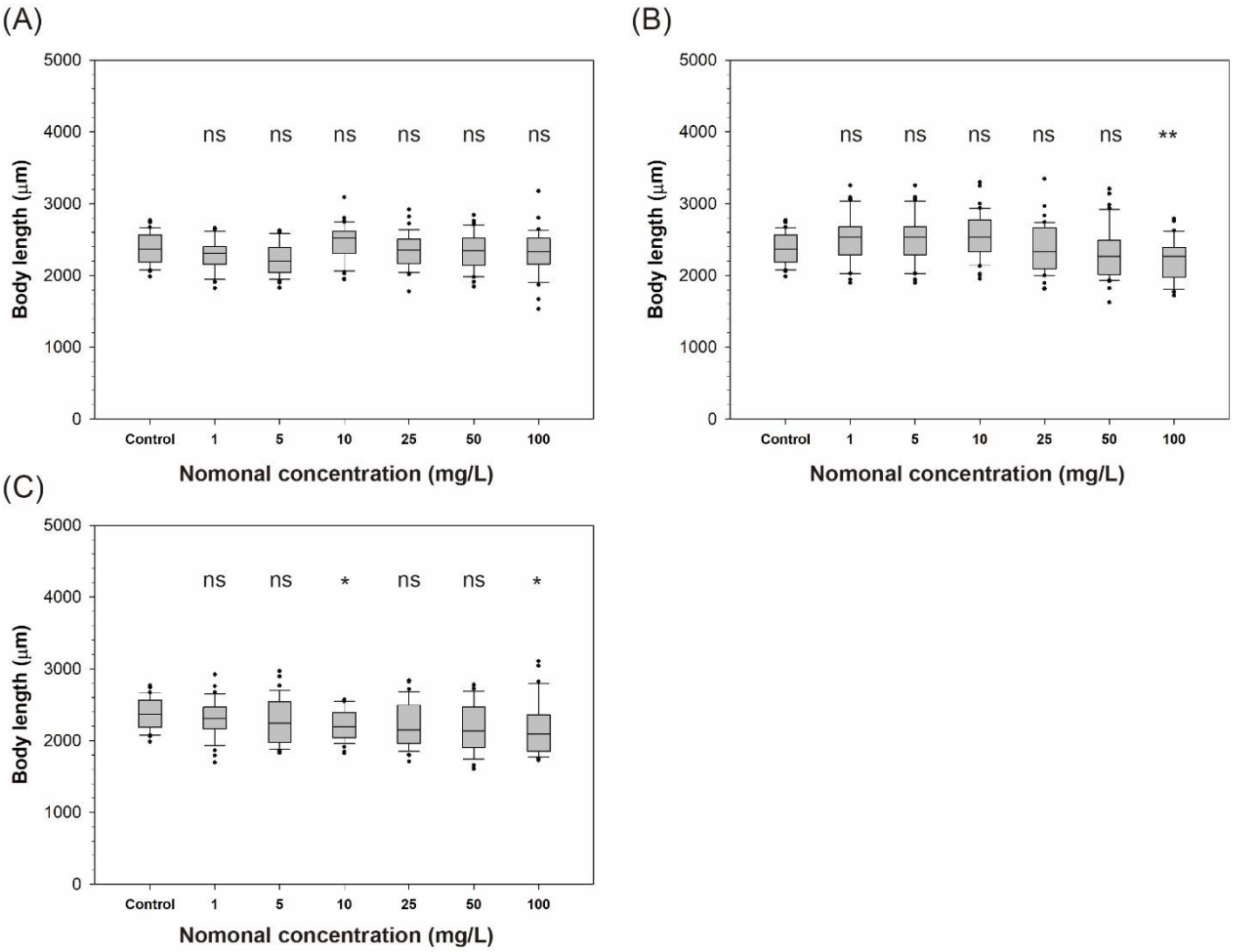

Figure 6.4 Body length of *Hyalella azteca* neonates after 7-day acute exposure to Ga- and *In*-related hydroxide/oxides groups. (A) $In(OH)_{3(s)}$, (B) $In_2O_{3(s)}$, (C) $Ga_2O_{3(s)}$. * $p<0.05$ ** $p<0.01$ versus control, Kruskal–Wallis one-way analysis of variance followed by Dunnett T3 post-hoc test (n=40 neonates in 4 replicates per treatment at the start of exposure).

Table 6.4 Metal concentrations in exposure solution during 7-day acute exposure period (n=3). Data are expressed as mean ± SD.

Treatment	Nominal concentration	Measured Ga/*In* (total content)	Measured Ga/*In* (overlying water)
	mg/L		μg/L
Control	-	ND	ND
Citrate	-	ND	ND
In(III)	1	1.03 ± 0.01	7.11 ± 10.02
	5	5.13 ± 0.04	15.20 ± 4.38
	10	10.04 ± 0.01	20.51 ± 13.65
	25	24.57 ± 0.37	12.12 ± 8.77
Citrate-In(III)	1	1.02 ± 0.01	16.03 ± 4.97
	5	5.17 ± 0.03	23.03 ± 1.24
	10	10.20 ± 0.14	72.93 ± 10.32
	25	25.89 ± 0.12	118.25 ± 77.60
Ga(III)	1	1.90 ± 0.02	465.30 ± 663.55
	5	4.66 ± 0.06	7,523.50 ± 4,195.26
	10	9.46 ± 0.02	6,540.00 ± 2,370.22
	25	23.27 ± 0.37	26,152.00 ± 14,538.12
Citrate-Ga(III)	1	0.96 ± 0.01	910.30 ± 250.74
	5	4.84 ± 0.05	5,485.00 ±319.61
	10	9.50 ± 0.05	10,825.00 ± 318.20
	25	23.93 ± 0.18	26,566.20 ± 1,587.03
$In(OH)_{3(s)}$	1	1.00 ± 0.01	2.14 ± 0.47
	5	4.83 ± 0.01	9.81 ± 2.51
	10	10.84 ± 0.07	20.28 ± 1.03
	25	25.32 ± 0.20	23.34 ± 8.93
$In_2O_{3(s)}$	1	0.82 ± 0.01	4.04 ± 1.99
	5	4.05 ± 0.03	14.43 ± 1.92
	10	8.61 ± 0.03	24.64 ± 2.92
	25	20.66 ± 0.09	53.83 ± 24.29
$Ga_2O_{3(s)}$	1	0.93 ± 0.01	3.82 ± 0.16
	5	5.00 ± 0.02	20.84 ± 1.67
	10	9.97 ± 0.15	45.74 ± 4.01
	25	25.60 ± 0.24	99.04 ± 29.40

Exposure solutions were collected immediately after water renewal.

Overlying water (without filtration) of exposure solutions were collected at day-1, day-3, and day-6 within 7-day exposure period.

6.4 Sublethal effects of Ga- and *In*-Related Chemicals

The measured total Ga/*In* concentrations in exposure solutions and remaining Ga/*In* (ionic species and colloidal particles) in overlying water were shown in Table 6.6. Results were similar to that of 7-day acute toxicity test, the solubility of In(III) and citrate-In(III) in SAM-5S was remarkably lower than Ga(III) and citrate-Ga(III), and $In(OH)_{3(s)}$, $In_2O_{3(s)}$, and $Ga_2O_{3(s)}$ were believed to be insoluble. The recovery of In(III) and citrate-In(III) (0.5 mg/L) in overlying water was 8.1 % (in average), whereas the recovery of In(III) and citrate-In(III) (5 mg/L) was 1.2 % (in average). The higher concentration (5 mg/L) of In(III) treatments tended to transform to $In(OH)_{3(s)}$ through hydrolysis and thereby precipitated and decreased the overall In(III) concentrations. The recovery of Ga(III) and citrate-Ga(III) (0.5 and 5 mg/L) in overlying water was > 90 % (in average), indicating that Ga(III) treatments were more stable in exposure solution than In(III) treatments. Also, the recovery of insoluble chemicals of $In(OH)_{3(s)}$, $In_2O_{3(s)}$, and $Ga_2O_{3(s)}$ in overlying water was 1.2 % (in average), suggesting these particles tended to gradually aggregate and precipitate to the bottom of exposure solutions.

Adult viability of >95 % in the control during the exposure, and the survival rate of *H. azteca* was significantly different from controls to citrate-In(III) (5 mg/L), Ga(III) (0.5 mg/L), citrate-Ga(III) (0.5 and 5 mg/L), $In(OH)_3$ (5 mg/L) and In_2O_3 (5 mg/L). Although the viability of Ga_2O_3 (5 mg/L) was decreased at day-21 and day-28, the overall adult survival was > 90 % (Figure 6.5; Table 6.5).

As the exposure groups which adult survival was > 85 % at day-28 and day-35, the growth rate (body length and body weight) was significantly declined at the higher concentration (5 mg/L) of In(III), citrate-In(III) and Ga(III), while In(III) (0.5 mg/L) and $G_2O_{3(s)}$ (5 mg/L) did not have effects on growth rate. Meanwhile, the treatments with adult survival < 50 % at day-28 and day-35 indicated that the body length and body weight of surviving *H. azteca* were not statistically significant compared to control values (Figure 6.6, Figure 6.7, Figure 6.8, Figure 6.9).

In the treatments that did not have significantly reduced survival at day-35, compared to the average male to female ratio in control was approximately 50:50, each treatment was approximately 20:80 (i.e., the percentage of females among survivors ranged from 78.3 % to 92.5 %) except for $Ga_2O_{3(s)}$ (5 mg/L) (Table 6.7). Total number of young across all treatments ranged from 0 to 5 per replicate. Reproduction (based on young per surviving female) was significantly reduced from the control to any of the Ga and *In* treatments which adult survival did not significantly decrease at day-35 (Figure 6.10).

The bioaccumulation factor (BAF) values in exposure groups at day-28 and day-35 of exposure were shown in Table 6.6. The BAF values in citrate-In(III) treatments revealed an opposite trend with increased concentration, and the BAF values did not change remarkably in In(III) treatments except for In(III) (0.5 mg/L) at day-28. BAF values of both Ga(III) and citrate-Ga(III) treatments were significantly lower than In(III) treatments, and the BAF values were apparently not related to their concentrations in exposure solution.

Treatments that survival rate did not significantly reduced at day-28 of exposure, BAF values increased in the order of In(III) (0.5 mg/L) > citrate-In(III) (5 mg/L) > In(III) (5 mg/L) > Ga(III) (5 mg/L) = $Ga_2O_{3(s)}$ (5 mg/L). In addition, at day-35 of exposure, BAF values increased in the order of In(III) (0.5 mg/L) = In(III) (5 mg/L) = citrate-In(III) (5 mg/L) > Ga(III) (5 mg/L) = $Ga_2O_{3(s)}$ (5 mg/L).

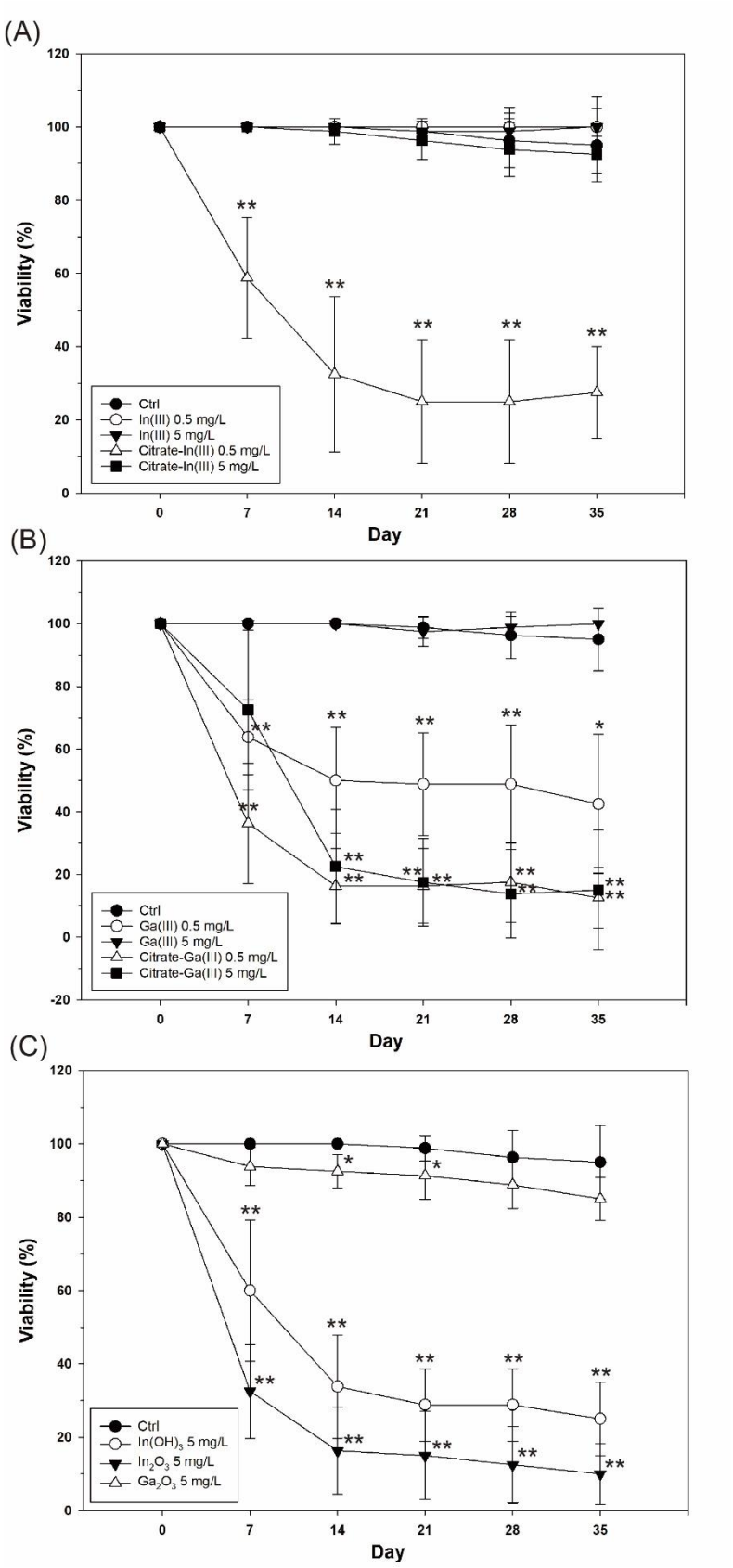

Figure 6.5 Survival rate of *Hyalella azteca* with 28-35-day aqueous exposure to (A) *In*-ionic group, (B) Ga-ionic group, (C) Ga- and *In*-related hydroxide/oxides group. Independent sample t test; * $p<0.05$ ** $p<0.01$ versus control (n=4, 10 neonates in every replicate per treatment at the start of exposure).

Table 6.5 Survival adult of *Hyalella azteca* after 28-d and 35-d exposure to Ga- and *In*-related chemicals (n=40-80 amphipods in 4-8 replicates per treatment at the start of exposure). Data are expressed as mean ± SD. Significance in difference between two groups were tested by independent sample t test. * $p<0.05$, ** $p<0.01$ versus control.

Treatment (mg/L)		Viability (%)					
		Day 0	Day 7	Day 14	Day 21	Day 28	Day 35
Control		100.0 ± 0.0	100.0 ± 0.0	100.0 ± 0.0	98.8 ± 3.5	96.3 ± 7.4	95.0 ± 10.0
In(III)	0.5	100.0 ± 0.0	100.0 ± 0.0	100.0 ± 0.0	100.0 ± 0.0	100.0 ± 5.3	100.0 ± 8.2
	5	100.0 ± 0.0	100.0 ± 0.0	100.0 ± 0.0	98.8 ± 3.5	98.8 ± 3.5	100.0 ± 0.0
Citrate-In(III)	0.5	100.0 ± 0.0	58.8* ± 16.4	32.5** ± 21.2	25.0** ± 16.9	25.0** ± 16.9	27.5** ± 12.6
	5	100.0 ± 0.0	100.0 ± 0.0	98.8 ± 3.5	96.3 ± 5.2	93.8 ± 7.4	92.5 ± 5.0
Ga(III)	0.5	100.0 ± 0.0	63.8** ± 11.9	50.0** ± 16.9	48.8** ± 16.4	48.8** ± 18.9	42.5* ± 22.2
	5	100.0 ± 0.0	100.0 ± 0.0	100.0 ± 0.0	97.5 ± 4.6	98.8 ± 3.5	100.0 ± 0.0
Citrate-Ga(III)	0.5	100.0 ± 0.0	36.3** ± 19.2	16.3** ± 11.9	16.3** ± 11.9	17.5** ± 12.8	12.5** ± 9.6
	5	100.0 ± 0.0	72.5 ± 25.5	22.5** ± 18.3	17.5** ± 13.9	13.8** ± 14.1	15.0** ± 19.1
$In(OH)_{3(s)}$	5	100.0 ± 0.0	60.0** ± 19.3	33.8** ± 14.1	28.8** ± 9.9	28.8** ± 9.9	25.0** ± 10.0
$In_2O_{3(s)}$	5	100.0 ± 0.0	32.5** ± 12.8	16.3** ± 11.9	15.0** ± 12.0	12.5** ± 10.4	10.0** ± 8.2
$Ga_2O_{3(s)}$	5	100.0 ± 0.0	93.8 ± 5.2	92.5* ± 4.6	91.3* ± 6.4	88.8 ± 6.4	85.0 ± 5.8

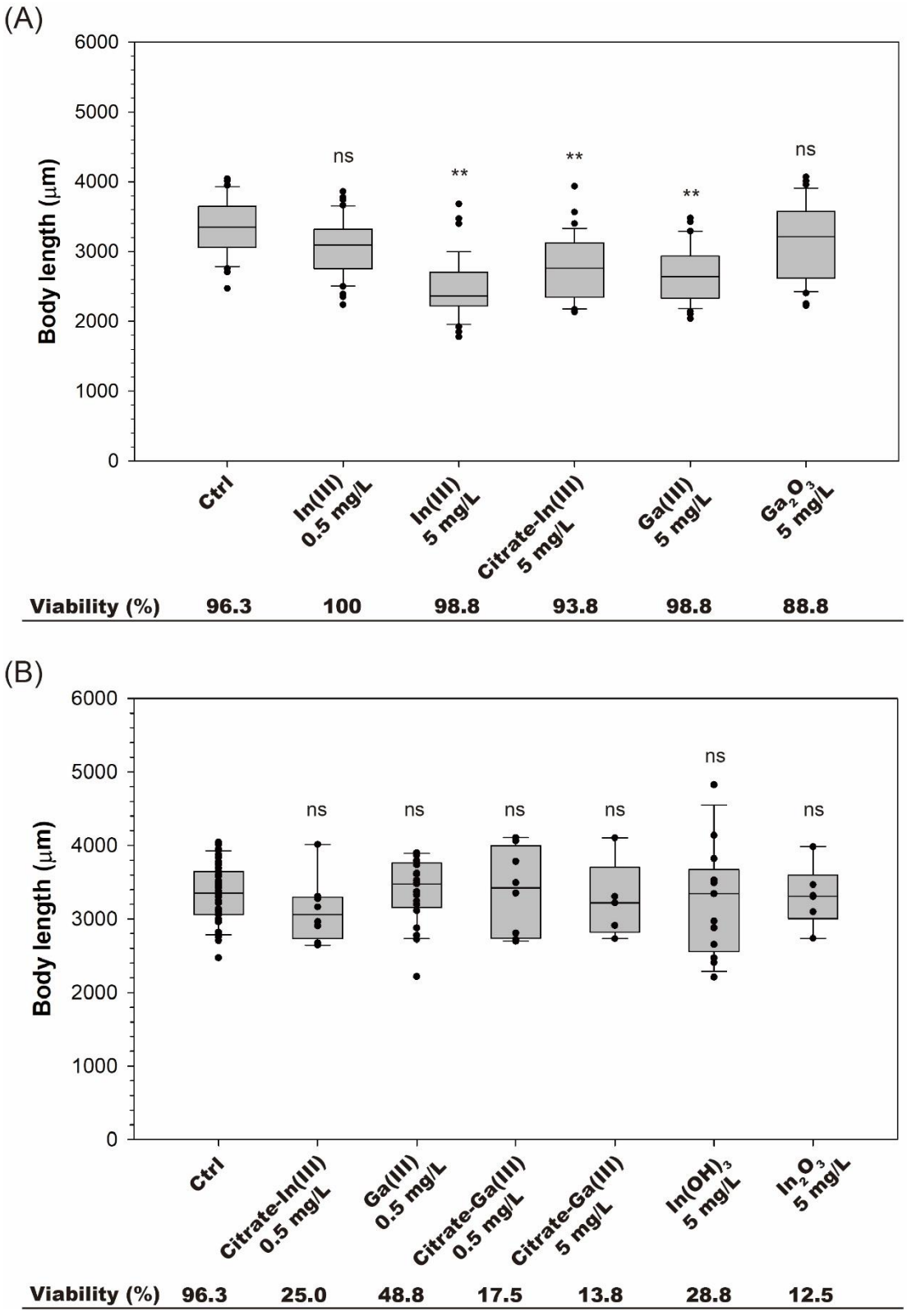

Figure 6.6 Body length of *Hyalella azteca* after 28-day chronic exposure period. * $p<0.05$, ** $p<0.01$ versus control, Kruskal–Wallis one-way analysis of variance followed by Dunnett T3 post-hoc test. (n=80 amphipods in 8 replicates per treatment at the start of exposure).

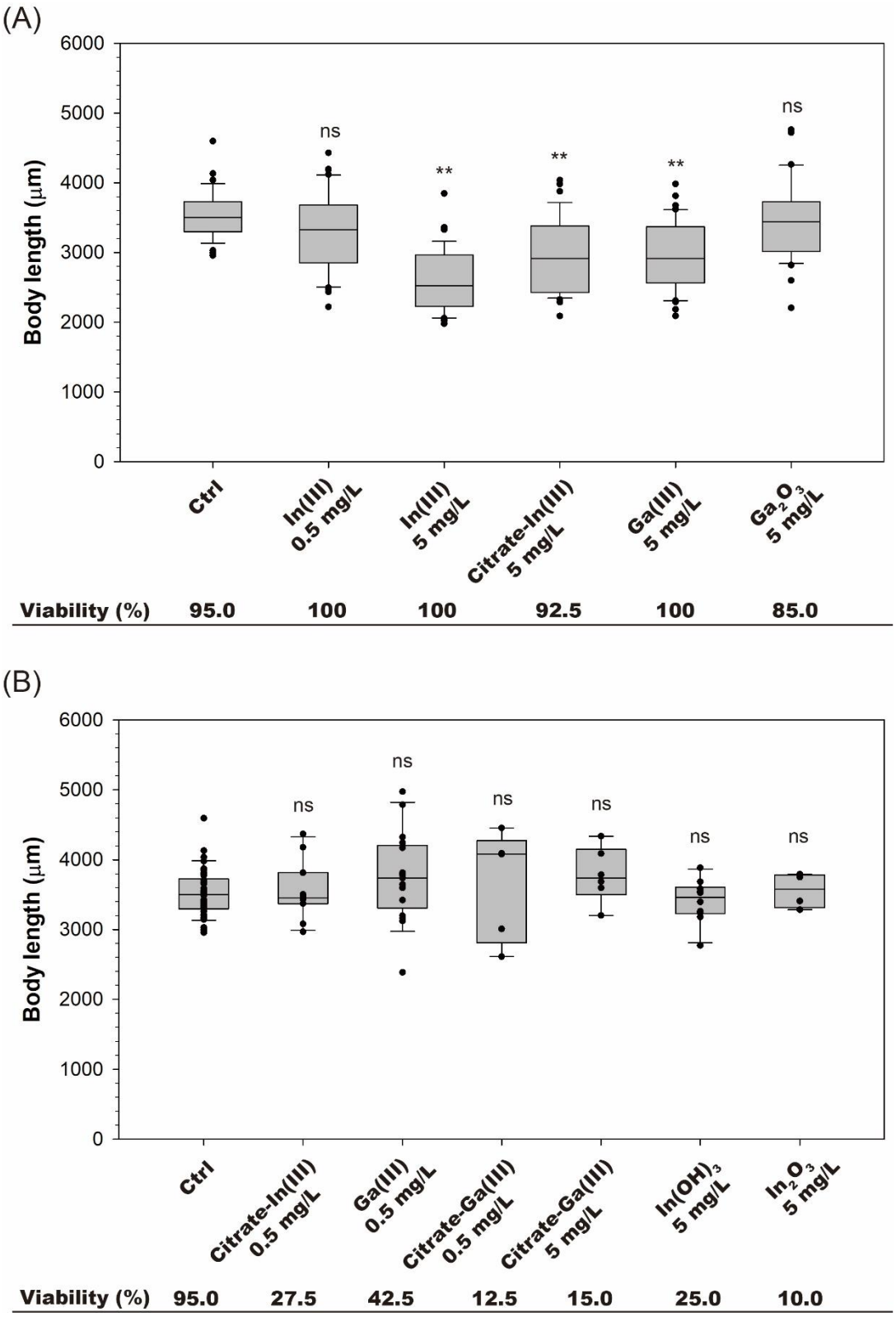

Figure 6.7 Body length of *Hyalella azteca* after 35-day chronic exposure period. * $p<0.05$, ** $p<0.01$ versus control, Kruskal–Wallis one-way analysis of variance followed by Dunnett T3 post-hoc test. (n=40 amphipods in 4 replicates per treatment at the start of exposure).

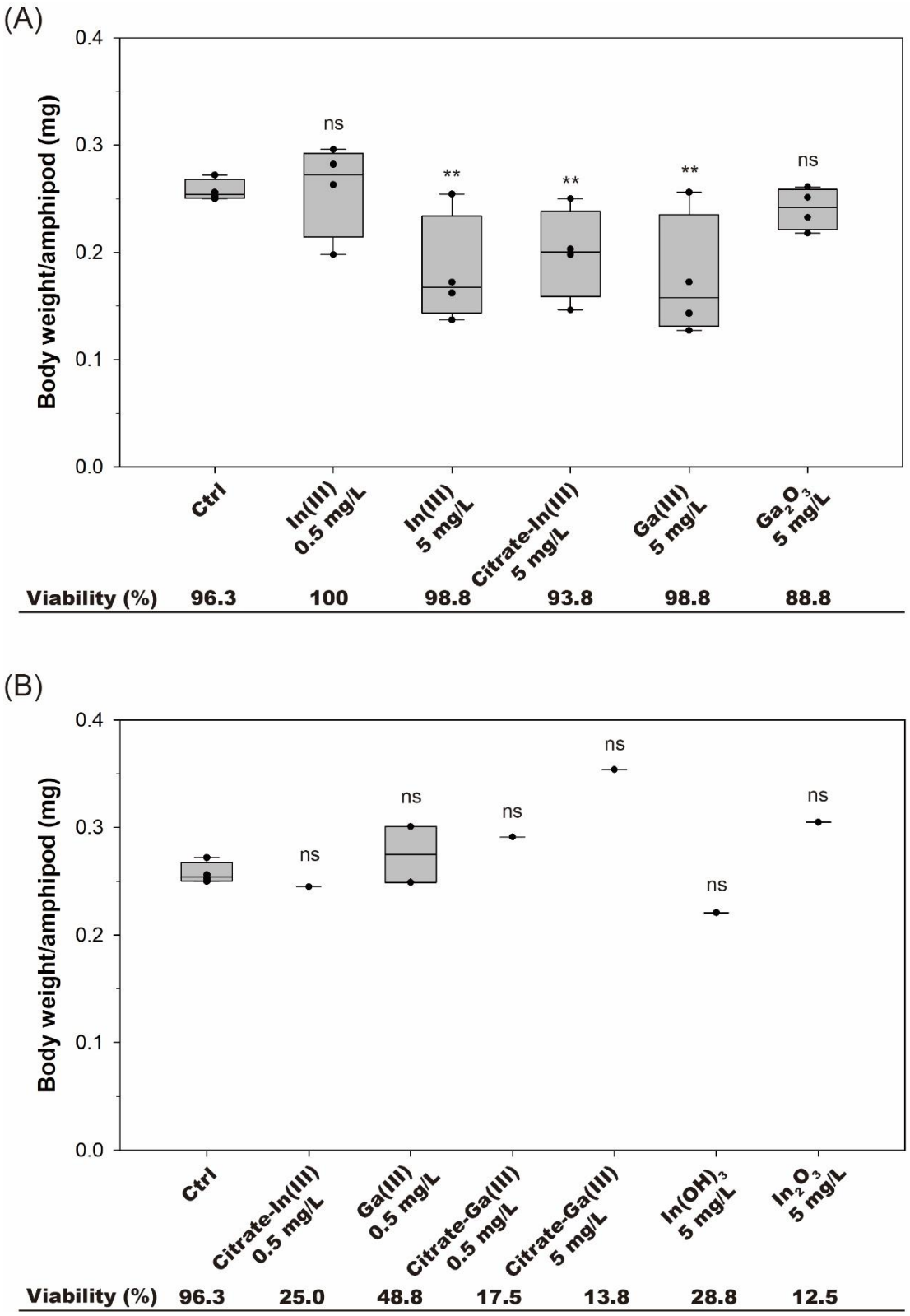

Figure 6.8 Body weight of *Hyalella azteca* after 28-day chronic exposure period. * $p<0.05$, ** $p<0.01$ versus control, Kruskal–Wallis one-way analysis of variance followed by Dunnett T3 post-hoc test. (n=80 amphipods in 8 replicates per treatment at the start of exposure).

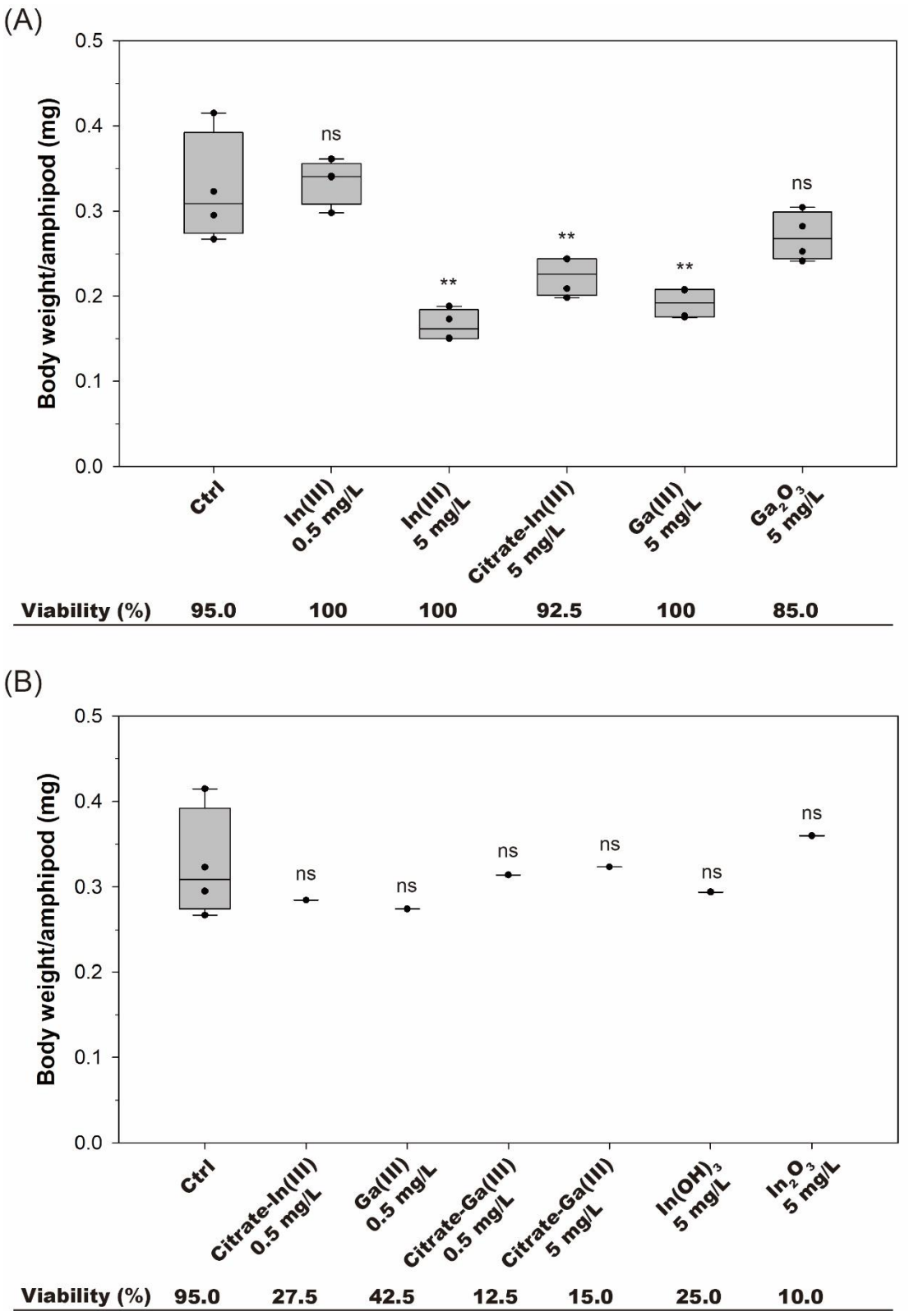

Figure 6.9 Body weight of *Hyalella azteca* after 35-day chronic exposure period. * $p<0.05$, ** $p<0.01$ versus control, Kruskal–Wallis one-way analysis of variance followed by Dunnett T3 post-hoc test. (n=40 amphipods in 4 replicates per treatment at the start of exposure).

Table 6.6 Bioaccumulation factor (BAF) in survival adult of *Hyalella azteca* after 28-d and 35-d exposure to Ga- and *In*-related chemicals (n=40 amphipods in 4 replicates per treatment at the start of exposure). Data are expressed as mean ± SD. Significance in difference between two groups were tested by independent sample t test ($p<0.05$).

Treatment	Nominal concentration	Measured Ga/*In* (total content)	Measured Ga/*In* (overlying water)	Measured BAF (Day-28)	Measured BAF (Day-35)
	mg/L		μg/L	L/kg	
Control	-	-	ND	-	-
In(III)	0.5	0.45 ± 0.06	40.30 ± 7.77	1,166 ± 137[a]	555 ± 135[a]
	5.0	4.88 ± 0.04	42.48 ± 0.27	305 ± 88[b]	413 ± 173[a]
Citrate-In(III)	0.5	0.50 ± 0.01	35.80 ± 0.27	1,420*	2,508*
	5.0	4.86 ± 0.11	73.80 ± 43.99	659 ± 199[c]	669 ± 183[a]
Ga(III)	0.5	0.46 ± 0.07	540.90 ± 36.46	145* ± 51	113*
	5.0	4.93 ± 0.12	5,049.33 ± 746.99	142 ± 58[d]	114 ± 33[b]
Citrate-Ga(III)	0.5	0.48 ± 0.00	613.77 ± 16.86	23*	5*
	5.0	4.35 ± 0.54	5,693.00 ± 133.09	27*	14*
$In(OH)_{3(s)}$	5.0	4.91 ± 0.40	64.69 ± 38.17	1,081*	1,062*
$In_2O_{3(s)}$	5.0	4.79 ± 0.62	84.15 ± 21.09	655*	1,184*
$Ga_2O_{3(s)}$	5.0	4.29 ± 0.18	21.03 ± 2.13	72 ± 16[d]	65 ± 59[b]

*: The adult survival of each treatment was below 50 %.

Exposure solutions were collected immediately after weekly water renewal.

Overlying water (without filtration) of exposure solutions were collected at day-6, day-13, and day-28 within 28-35-day exposure period.

Calculation of BAF (L/kg) = Concentration of metal in dry tissue (mg/kg)/ Concentration of the substance in water (mg/L).

Table 6.7 The ratio of males to females in survival adult of *Hyalella azteca* after 28-d and 35-d exposure to Ga- and *In*-related chemicals (n=40-80 amphipods in 4-8 replicates per treatment at the start of exposure). Data are expressed as mean ± SD. Significance in difference between two groups were tested by One proportion Z-test. * <0.05 ** p<0.01 versus control.

Treatment		Day-28 (n=80)			Day-35 (n=40)		
		Viability	Male	Female	Viability	Male	Female
mg/L		%			%		
Control		96.3 ± 7.4	33.3 ± 4.7	66.7 ± 4.7	95.0 ± 10.0	47.5 ± 5.0	52.5 ± 5.0
In(III)	0.5	100.0 ± 5.3	20.0 ± 18.3	80.0 ± 18.3	100.0 ± 8.2	20.3** ± 14.4	79.7** ± 14.4
	5	98.8 ± 3.5	15.8* ± 14.2	84.2* ± 14.2	100.0 ± 0.0	7.5** ± 5.0	92.5** ± 5.0
Citrate-In(III)	0.5	25.0 ± 16.9	41.7 ± 52.0	58.3 ± 52.0	27.5 ± 12.6	22.9 ± 15.8	77.1 ± 15.8
	5	93.8 ± 7.4	20.0 ± 21.6	80.0 ± 21.6	92.5 ± 5.0	21.7** ± 9.1	78.3** ± 9.1
Ga(III)	0.5	48.8 ± 18.9	35.8 ± 22.5	64.2 ± 22.5	42.5 ± 22.2	31.5 ± 22.1	68.5 ± 22.1
	5	98.8 ± 3.5	12.5** ± 5.0	87.5** ± 5.0	100.0 ± 0.0	20.0** ± 8.2	80.0** ± 8.2
Citrate-Ga(III)	0.5	17.5 ± 12.8	12.5 ± 25.0	87.5 ± 25.0	12.5 ± 9.6	33.3 ± 28.9	66.7 ± 28.9
	5	13.8 ± 14.1	16.7 ± 28.9	83.3 ± 28.9	15.0 ± 19.1	12.5 ±17.7	87.5 ± 17.7
$In(OH)_{3(s)}$	5	28.8 ± 9.9	41.7 ± 28.9	58.3 ± 28.9	25.0 ± 10.0	25.0 ±16.7	75.0 ± 16.7
$In_2O_{3(s)}$	5	12.5 ± 10.4	22.2 ± 38.5	77.8 ± 38.5	10.0 ± 8.2	66.7 ± 57.7	33.3 ± 57.7
$Ga_2O_{3(s)}$	5	88.8 ± 6.4	11.5* ± 10.3	88.5* ± 10.3	85.0 ± 5.8	40.6 ± 12.8	59.4 ± 12.8

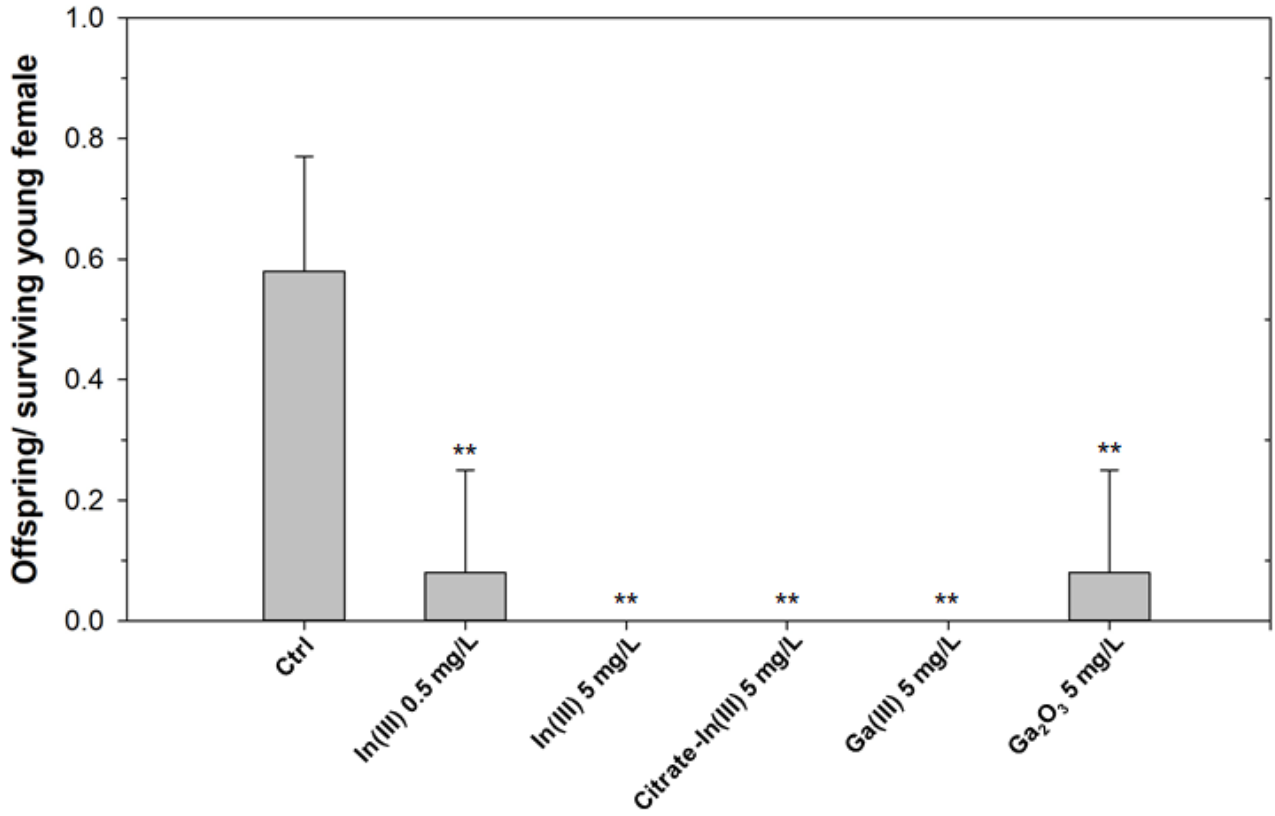

Figure 6.10 Offspring per surviving young female of *Hyalella azteca* after 35-d exposure to Ga- and *In*-related chemicals (n=40 amphipods in 4 replicates per treatment at the start of exposure). Data are expressed as mean ± SD. Significance in difference between two groups were tested by independent sample t test. ** $p<0.01$ versus control.

7. Discussion

By linking the observed toxic effects with acute to chronic exposure of exposure solutions containing In(III), citrate-In(III), Ga(III), citrate-Ga(III), $In_2O_{3(s)}$, $In_2O_{3(s)}$, or $Ga_2O_{3(s)}$, we revealed causal toxic effects of seven Ga- and *In*-related chemicals on survival, growth, reproduction and bioaccumulation of *H. azteca*. The differential acute mortality and chronic sublethal effects with the seven Ga- and *In*-related compounds in *H. azteca* neonates and adults could be ascribed to specific water chemistry characteristics of Ga(III) and In(III) ions that led to different aqueous behaviors, and further influenced the bioavailability and toxicity of Ga and *In* to the freshwater amphipod.

7.1 Effect of Reconstituted Water on Particle Characterization

The agglomeration and sedimentation of $In_2O_{3(s)}$, $In_2O_{3(s)}$, or $Ga_2O_{3(s)}$ increased the particle size, thereby diminishing reactivity and bioavailability of suspended colloidal particles. The ionic composition and strength in water matrices (e.g., SAM-5S used in the present study) changed the particle surface charge and decreased the zeta potential, which may further accelerate the agglomeration rate of colloidal particles and aggregates.

In addition, particle precipitation was also investigated in exposure solutions of 7-day acute toxicity test, the higher concentration groups (typically > 10 mg/L) of In(III), citrate-In(III), Ga(III), and citrate-Ga(III) gave rise to a large amount of hydroxide products sedimented in the bottom of test beakers. The addition of metal chelators (i.e., citrate) could form tight complexes with Ga(III) and In(III), then enhance the content of dissolved Ga(III) and In(III) ions by preventing the formation of

hydroxide products. However, the relatively higher water hardness of SAM-5S appeared to decrease the dissolved forms of Ga and *In* that may act as active toxic agents to aquatic organisms (Borgmann et al., 2005a; Rathore and Khangarot, 2003).

7.2 Effect of Ion Concentrations and Temperature on Survival and Growth Rate of *Hyalella azteca*

A variety of heavy metals are affected by major ion concentrations in the test water medium. The main components of water hardness, Ca and Mg could have effect on metal bioavailability and toxicity in many aquatic organisms, including *H. azteca* (Borgmann et al., 2005a; Ebrahimpour et al., 2010; Kiyani et al., 2018; Pascoe et al., 1986; Rathore and Khangarot, 2003; Stephenson and Mackie, 1989). The chloride forms complexes with metals such as Hg and Cd (Borgmann, 1983), and the reaction between cupric (CuO) and bicarbonate ions results in the formation of the soluble copper carbonate complex, which accounts for the different toxicity of Cu to aquatic biota (Stiff, 1971). Relative high K(I) ion and sulphate could reduce Tl(I) and Se(IV) toxicity, respectively (Borgmann et al., 1998; Brix et al., 2001; Forsythe and Klaine, 1994). Also, the dissolved organic carbon (DOC) presents in most natural waters could bind to both metal ions and their hydrolysis products, reducing their uptake and toxicity (Dahm, 1981; Nierop et al., 2002; Welsh et al., 1993).

As a standard medium for aquatic toxicity testing, dechlorinated water is not recommended for use as test water media, since its quality is not stable and it could contain unacceptably high concentrations of chloride, chloramines, fluoride, Cu, Pb, Zn, or other contaminants (ASTM, 2010;

Novak and Taylor, 2017). The reconstituted fresh water of SAM-5S has been developed for long-term exposure and culture of *H. azteca*, based on Burlington City tap water originating from Lake Ontario (hardness 130 mg/L, carbonate alkalinity 90 mg/L, pH 7.9-8.6), the SAM-5S provides a hardness of 120 to 140 mg/L, carbonate alkalinity 60 to 80 mg/L with a higher bromide concentration, which has been demonstrated to support adequate survival, growth, and reproduction of *H. azteca* in laboratories (Borgmann, 1996).

Borgmann et al. (2005) have reported the effect water hardness on the Ga(III) and In(III) concentrations in testing solutions after one week exposure period (Borgmann et al., 2005a). The authors used two levels of water hardness; the one with higher hardness was dechlorinated Burlington City tap water (hardness 124 mg/L, carbonate alkalinity 84 mg/L, pH 8.09-8.84) which originates from Lake Ontario, the other was soft water with lower hardness (10 % tap water; hardness 18 mg/L, carbonate alkalinity 14 mg/L, pH 6.79-7.84). The measured Ga concentrations suggesting that Ga was soluble in dosing solutions (> 75 % recovery at the end of the exposure), and the measured Ga concentrations in testing soft waters with initial concentration of 315 and 1,000 μg/L were respectively 326 and 750 μg/L. However, the measured *In* concentrations in exposure solutions indicating that *In* was sparingly soluble (< 10 % recovery at the end of the exposure), and the measured *In* concentrations in testing soft waters with initial concentration of 315 and 1,000 μg/L were undetectable and 10 μg/L, respectively.

Our results agreed with those reported in a previous study, the recovery of In(III) and citrate-In(III) in overlying water was < 5 % (in average), and the recovery of Ga(III) and citrate-Ga(III) was

> 80 % (in average) during the exposure. Both In(III) and citrate-In(III) were prone to form $In(OH)_{3(s)}$ at pH 5-9 despite the use of metal chelator citrate, and $Ga(OH)_4^-$ would be predominant at pH > 7 of Ga(III) (Wood and Samson, 2006). It remains to be determined that the predominance fields of citrate chelated Ga(III) and $Ga(OH)_4^-$ of citrate-Ga(III) at pH values greater than 7. It appeared that the predominant hydrolysis products (i.e., $In(OH)_{3(s)}$, $Ga(OH)_4^-$) of In(III) and Ga(III), as well as treatments of insoluble chemicals (i.e., $In(OH)_{3(s)}$, $In_2O_{3(s)}$, $Ga_2O_{3(s)}$) in exposure solutions have relatively lower bioavailability and/or acute toxicity to *H. azteca* neonates.

Vadim E. Panov and Donald J. McQueen (1998) reported that the growth parameters (survival, head length and body mass) of *H. azteca* were affected by water temperature (Panov and McQueen, 1998). The growth rates decreased with increasing size but increased with temperature, and both neonates and juveniles were more affected by temperature than adult individuals. In addition, filed observations indicated that a temperature of 20 °C is important for both the induction and termination of reproductive resting stages of *H. azteca*.

In our study, the water temperature monitored in exposure solutions during 7-day acute toxicity tests was relatively lower in Ga- and *In*-related hydroxide/oxides groups ($In_2O_{3(s)}$, $In_2O_{3(s)}$ and $Ga_2O_{3(s)}$) than Ga- and *In*-ionic groups. Although all treatments did not have significant acute toxicity in neonates in comparison with untreated control, the growth rate (body length) of control in Ga- and *In*-related hydroxide/oxides groups was significantly decreased approximately 1.2 times compared to that of Ga- and *In*-ionic groups. Volkoff, H. and Rønnestad, I. (2020) reported the temperature could have strong effect on feeding and digestive processes in fish (Volkoff and Rønnestad, 2020), it

supposed that water temperature may also affect the metabolic rate of *H. azteca* neonates and further change their energy balance and behavior, including locomotor and feeding behavior. Since we assumed that *H. azteca* can accidentally ingest colloidal particles and aggregates of Ga- and *In*-related hydroxide/oxides while feeding, the lower water temperature could indirectly decrease the bioavailability of those insoluble particles.

7.3 Comparison to Other Published LC_{50} Values for *Hyalella azteca*

Borgmann et al. (2005) have reported the effect water hardness on the toxicity of Ga(III) and In(III) to *H. azteca* in water phase (Borgmann et al., 2005a). The authors used two levels of water hardness as described previously. The 7-day acute toxicity test of *H. azteca* neonates (1 to 11 days of age) were performed by exposing to Ga(III) and In(III) at concentrations of up to 1,000 μg/L (soft water) or 3,150 (tap water) μg/L. After treatment, the percent survival of *H. azteca* at 315 μg/L and 1,000 μg/L of Ga(III) in soft water was 82 % and 48 %, and the survival at 1,000 μg/L of Ga(III) in tap water was 88 %; the percent survival of *H. azteca* at 315 μg/L (soft water) and 1,000 μg/L (soft water and tap water) of In(III) was respectively 89 %, 87 % and 90 %. The LC_{50} values could not be calculated for Ga and *In*, which were expected to be greater than 1,000 μg/L (soft water) and 3,150 (tap water) μg/L.

Similar results were obtained in the present study on the 7-day acute toxicity test of Ga- and *In*-related chemicals. All treatments (In(III), citrate-In(III), Ga(III), citrate-Ga(III), $In(OH)_{3(s)}$, $In_2O_{3(s)}$ and $Ga_2O_{3(s)}$) did not cause a dose-dependent increase in acute neonatal mortality. However, some

exposure groups including In(III), citrate-In(III), Ga(III), $In_2O_{3(s)}$ and $Ga_2O_{3(s)}$, which were observed to have adverse effect on the growth rate (body length) of surviving *H. azteca* neonates. Surprisingly, we also investigated the growth rates of neonates were statistically significant increase in several treatment groups of citrate-Ga(III), which could be roughly attributed to the greater variation of body length of treated neonates. However, there is still a need for investigating the contribution of citrate-Ga(III) exposure in the variation of growth rate.

The acute toxicity results reported here for Ga- and *In*-related chemicals are generally in agreement with the limited literature previously published for other aquatic species (Table 2.4). Recent studies evaluating the acute toxicity of In(III) and Ga(III) in fish (tilapia, *Oreochromis mossambicus*; common carp, *Cyprinus carpio*; zebrafish, *Danio rerio*; rosy bitterling, *Rhodeus ocellatus*; Japanese whiting, *Sillago japonica*) have shown that these metallic species are only inhibitory at moderate to high concentrations (96-h LC_{50} values for Ga(III) ranging from 9.10 to 96.25 mg/L, and 96-h LC_{50} values for In(III) ranging from 15.35 to >20 mg/L) (Betoulle et al., 2002; Lin and Hwang, 1998; Onikura et al., 2008; Yang and Chen, 2003; Yang and Chen, 2018). Toxic effects of In(III) and Ga(III) chelated with citrate were also recently evaluated by using the embryonic zebrafish (*Danio rerio*) model system (Olivares et al., 2016). The survival and developmental behavior of zebrafish embryos were not significantly changed by any of the metal ions at the highest exposure concentration (0.9 mM).

Moreover, previous studies also evaluating the acute toxicity of Ga- and *In*-related chemicals in either freshwater or marine invertebrates (crustacean, *Americamysis bahi*a, *Artemia salina*,

Thamnocephalus platyurus; rotifer, *Brachionus plicatilis*; swamp shrimp, *Macrobrachium nipponense*; water flea, *Daphnia magna*; Cnidarian, *Hydra attenuata*) (Blaise et al., 2008; Brun et al., 2019; Onikura et al., 2005; Onikura et al., 2008; Yang, 2014; Zurita et al., 2007).These studies have shown that In(III) and Ga(III) are only inhibitory at moderate to high concentrations (24-h LC_{50} values for Ga(III) ranging from 12.69 to 54.64 mg/L, and 96-h LC_{50} values for Ga(III) ranging from 2.77 to 12.76 mg/L; 24-h LC_{50} values for In(III) ranging from 21.55 to 58.93 mg/L, and 96-h LC_{50} values for In(III) ranging from 6.89 to 30.48 mg/L) while ITO nanoparticles were classified to very toxic (0.1 to 1.0 mg/L) to aquatic organisms based on European Union Commission Guideline 93/67/EEC classification and on measurement endpoint values (Blaise et al., 2008).

Wang N. et al. (2018) reported that both unionid mussel (*Lampsilis siliquoidea*) and *H. azteca* were insensitive to Al in 96-h acute exposures (pH of 6 and water hardness of 100 mg/L as $CaCO_3$) compared to the EC_{50} values in the U.S. EPA acute Al dataset (Wang et al., 2018). However, the results of chronic 28-day exposure tests (EC_{20}) indicated that the mussel and *H. azteca* were respectively the 4th and the 5th most sensitive species by comparing to the U.S. EPA chronic Al dataset for pH 5.0 to <6.5 (Cardwell et al., 2018; Wang et al., 2018). The chemical transformation of Ga and *In* is similar to Al due to water chemistry, our results of 7-day acute toxicity tests indicated that Ga- and *In*-related chemicals did not cause a dose-dependent increase in neonatal mortality despite the fact that some treatment groups had adverse effect on the growth rates. Therefore, it also suggested that *H. azteca* would be more sensitive to Ga and *In* in long-term exposure than short-term exposure.

Yang and Chen (2003) noted that the growth rates of younger larva of the common carp (*Cyprinus carpio*) were more affected by Ga(III) toxicity than older stages (Yang and Chen, 2003). Also, Onikura et al. (2005) reported that the longer the exposure duration, resulting in the lowest the Ga concentration needed to achieve the same acute toxic effect on the mysids (*Americamysis bahia*) (Onikura et al., 2005). Therefore, long-term effects of Ga- and *In*-related chemicals may be observed at much lower concentrations than acute toxicity for freshwater organisms such as *H. azteca*. These results suggested that the chronic toxic effects induced by Ga and *In* may be more significant than their acute toxicity.

7.4 Long-Term Exposure of Ga and *In* Affected the Survival, Growth and Reproduction of *Hyalella azteca*

In the light of the results of 7-day acute toxicity tests in this study, the effect of long-term exposure to sublethal concentration of Ga- and *In*-related chemicals on survival, growth, reproduction, and bioaccumulation of *H. azteca* was further evaluated. The following two concentrations (0.5 and 5 mg/L) were determined for chronic toxicity tests by considering the present Ga and *In* standards (< 0.1 mg/L) in wastewater effluent of optoelectronic industry in Taiwan and the minimal concentration of Ga- or *In*-related chemicals inhibiting growth of *H. azteca* neonates. The higher concentration (5 mg Ga or *In*/L) was used in hydroxide/oxides groups ($In(OH)_{3(s)}$, $In_2O_{3(s)}$ and $Ga_2O_{3(s)}$) due to the lower adverse effects on neonatal growth rate.

The treatments of In(III) (0.5 and 5 mg/L) did not have effect on survival of *H. azteca* during exposure period, whereas the lower concentration (0.5 mg/L) of citrate chelated In(III) significantly decreased the survival from the first seven days of exposure (Table 6.5). Similar results were observed in Ga treatment groups, Ga(III) (0.5 mg/L) and citrate-Ga(III) (0.5 and 5 mg/L) also declined the survival from the first seven to fourteen days of exposure.

According to the measured *In* concentrations in overlying water of testing solutions, citrate did not have greater effect on preventing hydrolysis of citrate-In(III) as mentioned earlier in acute toxicity tests; also, the measured Ga concentrations in overlying water appeared to be composed of Ga(III), $Ga(OH)_{3(s)}$, and $Ga(OH)_4^-$. The use of citrate may increase the proportion of Ga(III) by preventing Ga hydrolysis, and thereby contributing higher toxicity as compared to Ga(III) treatments (Borgmann et al., 2005a; Wood and Samson, 2006).

As a result, the solubility of In(III) was much lower than Ga(III) in exposure solutions, and *In* ions in both In(III) and citrate-In(III) treatments tended to settle out of the solution even at the lower concentration (0.5 mg/L). The lower concentration of Ga- and *In*-ionic treatments appeared to induce higher toxicity to *H. azteca* neonates and adults in comparison with the higher concentration (5 mg/L). We hypothesized that the hydrolysis of Ga and *In* may affect the bioavailability and toxicity from exposure to metal ions, and further increase the exposure risk of *H. azteca* to those insoluble colloidal particles (e.g., $In(OH)_{3(s)}$, $Ga(OH)_{3(s)}$) or $Ga(OH)_4^-$ anion (Benézéth et al., 1997; Diakonov et al., 1997; Wood and Samson, 2006).

Surprisingly, the survival rates of hydroxide/oxides treatments including $In(OH)_{3(s)}$ and $In_2O_{3(s)}$ were significantly decreased in the first seven days of exposure except for $Ga_2O_{3(s)}$) (Table 6.5), which were partially conflict with the result of 7-day acute toxicity tests (Figure 6.2). The difference of water temperature monitored in dosing solutions between acute and chronic toxicity tests appeared to be one of the reasons for the alterations in survival of *H. azteca* neonates (Table 6.2 and Table 6.3). As described previously, the lower water temperature could have effect on locomotor and feeding behavior of aquatic organisms such as fish and amphipods (Panov and McQueen, 1998; Volkoff and Rønnestad, 2020), which appeared to decrease the bioavailability of Ga- and *In*-related hydroxide/oxides particles and aggregates to *H. azteca* and thus attenuate the toxic effects.

In chronic exposure which adult survival was above 80 % at day-28 and day-35, In(III), citrate-In(III), Ga(III) and $Ga_2O_{3(s)}$ were associated with the toxic effects on growth rate, sexual ratio, reproduction and bioaccumulation. The body length and body weight were significantly decreased after exposure to the higher concentration of In(III), citrate-In(III) and Ga(III), suggesting that the retarded growth of *H. azteca* was caused by *In* and Ga. However, the adult growth did not significant change in other treatments which survival was below 50 % at day-28 and day-35. Results suggested the ability of surviving *H. azteca* to adapt and tolerant to the exposure conditions.

Heavy metal exposures are known to not only change the feeding patterns, energy intake (food consumption and food conversion) and growth hormone regulation in fish (e.g., *Perca fluviatilis*, *Cyprinus carpio*, *Catla catla*, *Labeo rohita*, *Cirrhina mrigala*, and *Mystus vittatus*) (Collvin, 1985; De Boeck et al., 1997; Deane and Woo, 2009; James et al., 2003; Javed, 2012; Moraes et al., 2003;

Subathra and Karuppasamy, 2007). Recent studies evaluating the chronic toxicity of Ga(III) in common carp (*C. carpio*) (2.0, 4.0 and 8.0 mg/L) and tilapia (*Oreochromis mossambicus*) (0.29 to 17.82 mg/L) have shown that the serum biochemistry parameters (i.e., glucose, blood urea nitrogen, creatinine, cholesterol, and triglyceride) and erythrocyte morphology were altered in common carp after 28-day exposure (Yang and Chen, 2003). The growth and body ion contents (i.e., K, Ca and Mg) were reduced in tilapia after 16-day exposure (Lin and Hwang, 1998). These results indicated that the treated fish were in an undernourished state or experiencing liver failure condition, and the deformation of erythrocytes also suggested the disturbance of respiration.

Furthermore, heavy metals also have reported to affect the respiration, locomotion activity, feeding rate, energy balance (between food intake and metabolic output) and moulting behavior of freshwater amphipods (*Gammarus fossarum* and *Gammarus pulex*) (Gerhardt, 1993; Lebrun and Gismondi, 2020; Maltby and Naylor, 1990; Maltby et al., 1990). These long-term toxic effects were found to be related to reduced growth rate and enhanced bioaccumulation of heavy metals, with possible adverse impact on individual growth, population dynamics and their associated ecological functions (i.e., litter decomposition and nutrient cycles) (Gerhardt, 1993; Lebrun and Gismondi, 2020; Maltby and Naylor, 1990).

Previous studies noted that Al exposure could cause respiratory disturbance in fish and freshwater amphipod (*Gammarus lacustris*), which appears to be predominant at pH above 5.5 (Gensemer and Playle, 1999; Gill, 2021; Neville, 1985; Playle et al., 1989; Poléo and Bjerkely, 2000). The production of $Al(OH)_{3(s)}$ precipitates could accumulate on gills, and the free-Al(III) could bind

to the negative charged gill surface, acting as polymerization nuclei forming clogging of interlamellar spaces by complexes of Al-polymers (e.g., Al_{13}^{7+}). The precipitation and accumulation of $Al(OH)_{3(s)}$ and/or Al-polymers appear to induce structural alterations of gill epithelia and mucus, thereby leading to hypoxia and ionoregulatory dysfunction (Gill, 2021; Oughton et al., 1992; Poléo and Bjerkely, 2000; Poléo, 1995; Poléo et al., 2017).

Reproduction (based on young per surviving female) was significant decreased in treatments (i.e., In(III), citrate-In(III), Ga(III) and $Ga_2O_{3(s)}$) which adult survival was above 80 % compared to untreated control at day-35 (Figure 6.10). Interestingly, the average male to female ratio in each treatment was in the range of 17.4 (7.5-21.7):82.6 (78.3-92.5) except for $Ga_2O_{3(s)}$, while the sexual ratio was approximately 50:50 in control group (Table 6.7). Concerning the method for sex identification in this study, the number of adult females was determined by simply counting the adult males (mature male *H. azteca* would have an enlarged second gnathopod; Figure 5.3) and assuming all other adults were females (ASTM, 2010). Therefore, the immature male without having an enlarged second gnathopod was identified as adult female and thus generates an increase in the percentage of female.

The sexual ratio in each treatment at day-28 was also determined (Table 6.7). Unlike the results at day-35, the average male to female ratio in untreated control was approximately 33:67, suggesting that about one-third of male sexual maturation occurred from day-28 to day-35 of exposure. In(III), Ga(III) and $Ga_2O_{3(s)}$ treatments appeared to either prevent or delay the sexual maturation process with delayed morphological changes of the male gnathopod, whereas results were varied between

$In(OH)_{3(s)}$ and $In_2O_{3(s)}$. Thus, the dramatic changes in sexual ratio would be a consequence of either changes in growth or less sensitive of adult females to the toxic effects of In(III) and Ga(III) (Taylor et al., 2016).

In addition to the reduced growth of freshwater amphipods caused by heavy metal (e.g., Cu, Pb, Zn, *In* and Ga) at the individual level (Lebrun and Gismondi, 2020; Maltby and Naylor, 1990; Maltby et al., 1990), Lebrun and Gismondi (2020) have reported the chronic exposure of Cu and Pb could induce gender-dependent alterations in biochemical responses of freshwater amphipod (*Gammarus fossarum*) (Lebrun and Gismondi, 2020), the inhibition on digestive enzyme activities (e.g., β-glucosidase and β-galactosidase) was observed to be more significant in males than females. The chronic toxic effects could be related to feeding rate inhibition, and these combined inhibitions could further affect energy acquisition essential for growth and the maintenance of vital functions of the amphipods (e.g., reproduction and moulting). However, the responses of biochemical parameters could be varied over model organism, exposure time and depended on the metal species and gender.

Our results appeared to be consistent with Lebrun and Gismondi (2020), the adverse effects caused by Ga(III) and In(III) exposure on many vital physiologic functions were likely to disturb individual growth. Retardation of growth has long-term effect on reproduction of *H. azteca*, it has reported that the reproductive success (through fecundity) is positively associated with body size in both genders (Wellborn, 1994). The male with enlarged gnathopod or larger gnathopod size would have the mating advantage of sexual selection in *Hyalella* species.

However, the precopula behavior and females carrying a brood are likely to be energetically costly (Maltby and Naylor, 1990; Othman and Pascoe, 2001). If the energy status of male and female is reduced, they may tend to increase the overall fitness by scarifying the broodings and reproducing later. Heavy metal (i.e., Zn) exposure to freshwater amphipod (*Gammarus fossarum*) has reported to cause the decrease in the size of offspring and the increase in abortion rate (Maltby and Naylor, 1990). The smaller individuals would take longer to maturity and may reproduce at a smaller size, which could further decline fecundity and disturb population renewing (Gerhardt, 1993; Maltby and Naylor, 1990). This hypothesis is also supported by our study that Ga(III) and In(III) caused the decrease in precopula pairs and number of offspring, while the $Ga_2O_{3(s)}$ treatment only resulted in reducing the number of offspring.

The calculated BAF values in treatments which adult survival was above 80 % at day-28 and day-35, BAF values of *In* treatments (i.e., In(III), citrate-In(III)) were significantly greater than Ga treatments (i.e., Ga(III), $Ga_2O_{3(s)}$). We also calculated BAF values in treatments which adult survival was below 50 % at day-28 and day-35, BAF values of *In* treatments (i.e., citrate-In(III), $In(OH)_{3(s)}$, $In_2O_{3(s)}$) were significantly larger than Ga treatments (i.e., Ga(III), citrate-Ga(III)). It is proposed that the predominant $Ga(OH)_4^-$ of Ga(III) treatment may decrease the bioavailability due to negative charge, whereas $In(OH)_{3(s)}$ and $In_2O_{3(s)}$ colloidal particles appear to increase the bioavailability through feeding behavior and/or respiratory disturbance. The relatively lower BAF of $Ga_2O_{3(s)}$ could be attributed to the particle characterization, which was prone to aggregate and precipitate at the bottom of testing solutions.

Burn et al. (2019) reported the chronic exposure of In(III) to water flea (*Daphnia magna*) could disrupt energy homeostasis, which is directly related to growth reduction, delayed age maturity, and reproductive impairment (Brun et al., 2019). *In* could accumulate on the carapace and in the midgut and thoracic appendages, possibly physically interfering with a constant flow of algae and thus reduce net energy and growth. Based on what is known from earlier investigations (Brun et al., 2019; Gill, 2021), it could be expected that predominant species $In(OH)_{3(s)}$ and/or remaining free-In(III), as well as *In*-related hydroxide/oxide chemicals (i.e., $In(OH)_{3(s)}$, $In_2O_{3(s)}$), could accumulate on the gill surfaces and/or gut of *H. azteca*. These toxic effects may further induce respiratory disturbance and disruption of energy balance, leading to mortality, growth retardation, and reproductive impairment.

Since there are no other studies investigating the chronic toxicity of Ga-related chemicals on *H. azteca*, and other invertebrates, our results appear to be the first evidence that Ga-related chemicals have little or no significance for the bioaccumulation effects but increase the chronic toxicity in Ga-ionic treatments. However, factors related to chronic toxic effects and bioaccumulation of Ga-related chemicals are needed to be further explored.

8 Future Recommendations

8.1 Evaluation the Toxic Effects of Ga and *In* in Sediment Phase

Ga and *In* are emerging contaminants in the environment and potentially toxic to living aquatic organisms. In natural water bodies, the pH and temperature of aqueous environment largely affect the chemical forms of Ga and *In*. They tend to form hydroxide complexes including $Ga(OH)_{3(s)}$ and $In(OH)_{3(s)}$ at pH 4-6 and 5-9, respectively (Wood and Samson, 2006). There appeared to be only a small portion of Ga(III) and In(III) ions could be taken away by water flows (e.g., river, irrigation canal) and a large quantity of them get deposited in either farmland soils (especially paddy soils) or sediments. In Taiwan, the downstream and nearby areas of semiconductor and optoelectronic industries were potentially contaminated by Ga and *In*, because the concentrations of Ga or *In* in groundwater, farmland soils and sediments were much higher than background concentrations (Chen, 2006; You, 2014).

In the present study, waterborne Ga- and *In*-related chemicals exposure did not induce an acute dose-dependent responses to freshwater amphipod (*H. azteca*) despite partial growth inhibition investigated in some treatments. However, in chronic toxicity test, Ga(III) and In(III) were shown to induce growth retardation, sexual ratio alteration and reproductive inhibition, and the citrate chelated complexes and hydroxide/oxide particles (i.e. $In(OH)_{3(s)}$ and $In_2O_{3(s)}$) had lethal effect to *H. azteca*. In addition, we also hypothesized that the water temperature could have effect on locomotor and

feeding behavior of *H. azteca*, which appeared to have effect on the bioavailability of Ga- and *In*-related hydroxide/oxides particles and aggregates to *H. azteca* and thus attenuate the toxic effects.

Still, relatively little information exists in the primary literature on the aquatic toxicity of Ga- and *In*-related chemicals to epibenthic and benthic organisms, especially via sediment exposures. The advective processes such as resuspension events arising from high flows, dredging, land preparation, or vessel propeller wash, anoxic depositional sediments and paddy soils may also be disturbed and released heavy metals into overlying oxygenated waters (Burton and Johnston, 2010; Wan et al., 2019; Zhang et al., 2019b; Zhou et al., 2014b). Changes in the physical and chemical environments, such as temperature, dissolved oxygen, redox, pH, and oxidation of sulfides may affect the chemical forms of metal and metalloid species by altering their mobility and bioavailability (Atkinson et al., 2007; Qi et al., 2014; Roberts, 2012; Zhou et al., 2014a).

Cervi et al. (2019) used the sediment flux exposure chambers to simulate sediment resuspension conditions and evaluate the bioavailability, transport, and toxicity of heavy metals (i.e., Fe, Mn, and Zn) (Cervi et al., 2019). The short-term (four hours) resuspension period rapidly deoxygenated the overlying water, decreased the pH and resulted in elevated dissolved Zn, Mn, and Fe. Zn and Fe were scavenged from solution after 20 hours, the initial release of Fe was associated with oxidation of acid-volatile sulfides, and the decrease was likely due to precipitation as oxyhydroxides. Additionally, there was no acute toxicity observed during resuspension by using water flea (*Daphnia magna*) and *H. azteca* models. However, lethal and sublethal effects of *D. magna* and *H. azteca* occurred during

the post-exposure period. The chronic toxicity of reduced neonate production in *D. magna* could have adverse effect on the zooplankton population growth.

The exposure pathways for epibenthic and benthic organisms such as *H. azteca* may include ingestion of sediment particles (containing metal hydroxide and oxide flocs) and water (Fetters et al., 2016; Kubitz et al., 1996). The amphipods appeared to expose and accumulate heavy metals primarily from overlying water and feeding behaviors, and they may also accumulate metals from pore water. Diffusion processes in static sediments probably cause metal bioavailability in the porewater near the sediment surface to be similar to that in overlying water (Borgmann et al., 2005b; Wang et al., 2004a). However, the potential toxicity caused by exposure to Ga- and *In*-related chemicals, or via either sediment or paddy soil resuspension, and their potential ecological impact on populations and communities of aquatic organisms, need to be explored.

8.2 Relationship Between Al, Ga and *In* in Soil and Sediment Phases

The toxicity of sediment-associated Ga and *In* to any aquatic species is sparse in the primary literature thus limiting comparison of results. However, previous studies have reported the chemical transformation, bioavailability and toxicity of Ga and *In* in soil-crop systems (Chang et al., 2017; Chang et al., 2020; Su et al., 2018; Syu et al., 2021; Syu et al., 2020), which could be used to evaluate the potential bioavailability and chemical forms Ga and *In* in sediment phases.

In general, the primary chemical forms of Ga and *In* in the most agricultural soils are similar to that of Al, $Ga(OH)_4^-$ and $In(OH)_{3(s)}$ due to soil pH ranged from 5.5 to 7.0 (Bojórquez-Quintal et al.,

2017; Jensen et al., 2018; Wood and Samson, 2006). Chang et al. (2020) have highlighted that In(III) reacts within the soil (even in acidic soils) could lead to the formation of *In*-associated Fe hydroxides, as well as $In(OH)_{3(s)}$ and phosphate, which determined *In* bioavailability (Chang et al., 2020). It is believed that the bioavailability and phytotoxicity of Ga and *In* are strongly controlled by a variety of soil properties (such as pH, redox potential, texture, organic matter, and Al availability) and the simultaneous tolerance of plants to Ga or *In* (Syu et al., 2020).

Under flooding conditions such as in paddy soils (pH 4-7), the mobility and concentration of Ga in soil solutions were greater than those of *In* with the same amount of spiked Ga and *In* because of the distribution of insoluble species (*In*-Fe hydroxides, $In(OH)_{3(s)}$, and *In*-phosphate) was much higher than $Ga(OH)_{3(s)}$, and the predominant Ga species ($Ga(OH)_4^-$) had lower affinity to silt and clay minerals (Chang et al., 2020; Jensen et al., 2018; Su et al., 2018; Syu et al., 2020; Wood and Samson, 2006). In addition, the concentration of Al in Ga-spiked acidic soils was greater than those in *In*-spiked acid soils, possibly because of the easier replacement of Al by Ga than by *In* due to the greater similarity of atomic radius of Ga (0.135 nm) to Al (0.143 nm) in comparison with *In* (0.167 nm) (Su et al., 2018). For acidic soils, the bioaccumulation of Ga and *In* in the shoots of rice plants was reduced by the concentrations of the bioavailable Al in soils (Syu et al., 2020). This leads to the competitive uptake by rice plants between Al and Ga or *In* in soil-rice systems, and the released Al in soil pore water may further result in Al toxicity to rice seedlings (Su et al., 2018).

Jensen et al. (2018) have reported that Ga and *In* were more strongly bound to soils than other heavy metals such as Cd, Cu, and Zn, and thus were likely to accumulate in soils (Jensen et al., 2018).

It is possible that the two metals also could accumulate and persist in sediments because sediments are usually in correlation with soils within watersheds or agricultural irrigation systems, thus increasing the risk of future exposure to aquatic organisms through overlying water, pore water, and feeding behaviors. Therefore, it is desirable to investigate the bioavailability and toxicity of Ga and *In* to epibenthic and benthic organisms in sediments, and the contribution of Al mobility to the bioavailability and toxic effects of Ga or *In*.

8. Conclusions

Recent decades, the rapid development of emerging technologies has been relevant to technology-critical elements of concern. Among those elements, Ga and *In* are important raw materials in semiconductors and optoelectronic industries, and the enhanced production of the two metals has increased the distribution of Ga and *In* in the environment through the industrial manufacturing processes, especially in discharging of sewage in water bodies. In the light of water chemistry features, Ga and *In* tend to form insoluble hydroxide (i.e., $Ga(OH)_{3(s)}$, $In(OH)_{3(s)}$) or anionic species (i.e., $Ga(OH)_4^-$) depending on the pH, which appeared to be transported downstream, or deposited at the bottom of water bodies. The bottom water and sediment would act as both source and reservoir of the two metals.

It is believed that the hydrolysis products may affect the bioavailability of Ga and *In* to aquatic organisms. However, the interactions between chemical transformation, bioavailability and toxicity of these chemicals remain unclear. Therefore, we hypothesized that the epibenthic or benthic organisms may be exposed to hydrolysis products via direct contacting with overlying water column and feeding behavior.

This study aims at investigating the effects of aqueous chemical transformation on the bioavailability, toxicity (acute and chronic) and potential ecological impacts of Ga- and *In*-related chemicals (i.e., In(III), citrate-In(III), Ga(III), citrate-Ga(III), $In(OH)_{3(s)}$, $In_2O_{3(s)}$ and $Ga_2O_{3(s)}$) by using freshwater amphipod (*Hyalella azteca*) *in vivo* bioassays.

In particle characterization assays, Ga- and *In*-related hydroxide/oxide chemicals were prone to form large aggregates in both ultrapure water and SAM-5S. The aggregates of $In(OH)_{3(s)}$ and $In_2O_{3(s)}$ were irregular in shape, whereas the colloidal particles and aggregates of $Ga_2O_{3(s)}$ were respectively rod-shaped structure and irregular in shape. The zeta potential of $In(OH)_{3(s)}$ (33.67 mV), $In_2O_{3(s)}$ (22.23 mV) and $Ga_2O_{3(s)}$ (17.07 mV) indicated that stable dispersal in ultrapure water was more prolonged for these compounds than in SAM-5S, which was $In(OH)_{3(s)}$ (-18.30 mV), $In_2O_{3(s)}$ (-17.37 mV) and $Ga_2O_{3(s)}$ (-11.11 mV). These results suggested that instable dispersal in dosing solution was prone to aggregate and precipitate gradually during exposure period.

In the acute toxicity exposure systems, the measured concentration of Ga and *In* in overlying water (ionic species and colloidal particles) of exposure solutions indicated that Ga(III) treatments appeared to be relatively stable as ionic species (e.g., Ga^{3+}, $Ga(OH)_4^-$), whereas In(III) and citrate-In(III) tended to transform to $In(OH)_{3(s)}$ through hydrolysis and thereby precipitated and decreased the overall In(III) contents; also, the measured Ga or *In* concentration of insoluble chemicals (i.e., $In(OH)_{3(s)}$, $In_2O_{3(s)}$, and $Ga_2O_{3(s)}$) in overlying water were similar to that of In(III) treatments, suggesting that they tended to gradually aggregate and precipitate to the bottom of solutions.

Although Ga- and *In*-related chemicals did not induce lethal effects on *H. azteca* neonates in a dose-dependent manner, some of the treatments (i.e., In(III), citrate-In(III), Ga(III), $In_2O_{3(s)}$, and $Ga_2O_{3(s)}$) significantly inhibited the growth rate (body length) of surviving *H. azteca* neonates. It is proposed that pH adjustment in the highest concentration stock (100 mg/L) of four treatments (i.e., In(III), citrate-In(III), Ga(III), and citrate-Ga(III)) with NaOH may increase the concentration of

hydroxide ion (OH^-) and thereby enhance the hydrolysis processes even in the presence of metal chelating agent, citrate. The major hydrolysis products of $In(OH)_{3(s)}$ and $Ga(OH)_4^-$ appeared to have effect on either the bioavailability or toxicity of In(III) and Ga(III) to *H. azteca* neonates.

According to the results of 7-day acute toxicity test, the effect of chronic exposure (28- and 35-day) to sublethal concentrations of Ga- and *In*-related chemicals on survival, growth, reproduction and bioaccumulation of *H. azteca* adults was further evaluated.

Treatments of In(III) (0.5 and 5 mg/L), citrate-In(III) (5 mg/L), Ga(III) (5 mg/L), and $Ga_2O_{3(s)}$ (5 mg/L) did not have effect on survival of *H. azteca* during exposure period. Surprisingly, the survival rate of citrate-In(III) (0.5 mg/L), Ga(III) (0.5 mg/L), citrate-Ga(III) (0.5 and 5 mg/L), $In(OH)_{3(s)}$ and $In_2O_{3(s)}$ were significantly decreased from the first seven days of exposure. The measured *In* concentrations in overlying water of exposure solutions indicated that *In* contents in all In(III) and citrate-In(III) treatments were much higher as compared to that of acute toxicity test. However, since the major hydrolysis products of Ga(III) is the anionic species $Ga(OH)_4^-$, the measured Ga concentrations in overlying water of exposure solutions were similar to that of acute toxicity test. These findings have confirmed our hypothesis that the addition of hydroxide ions (OH^-) may affect the bioavailability and toxic effects of In(III) and Ga(III) to *H. azteca*.

As for the decreased survival of $In(OH)_{3(s)}$ and $In_2O_{3(s)}$ treatments during chronic exposure period in comparison with acute toxicity test, we hypothesized that the difference of water temperature monitored in exposure solutions between acute and chronic toxicity tests may be one of the reasons for the alterations in survival of *H. azteca*. Previous studies have demonstrated the lower

water temperature could have effect on locomotor and feeding behavior of fish and amphipods (Panov and McQueen, 1998; Volkoff and Rønnestad, 2020), which appeared to decrease the bioavailability of colloidal particles and aggregates to *H. azteca* and thus attenuate their toxic effects. In addition, the measured *In* concentrations in overlying water of exposure solutions indicated that *In* contents in both $In(OH)_{3(s)}$ and $In_2O_{3(s)}$ treatments were much higher as compared to that of acute toxicity test, which also provided another proof for the effect of water temperature on the behaviors of *H. azteca*.

In chronic exposure which adult survival was above 80 % at day-28 and/or day-35, the exposure of In(III), citrate-In(III), Ga(III) or $Ga_2O_{3(s)}$ were associated with the sublethal effects on growth rate (decreased body length and body weight), sexual ratio, reproduction (based on young per surviving female), and BAF values. The exposure of Ga- and *In*-related chemicals appeared to affect the respiration, locomotion activity, feeding rate, energy balance, and moulting behavior of freshwater amphipods, which are positively related to heavy metal uptake, individual growth, reproductive success, the size of offspring and the abortion rate. Moreover, BAF values inferred that the bioaccumulation ability of *H. azteca*. to Ga and *In* is different. The amphipod could uptake Ga and *In* via direct contacting with overlying water column and feeding behavior, but only *In* gradually accumulated in the body.

Taken together, this study provides new insight into the aquatic toxicity of Ga- and *In*-related chemicals that have not previously been evaluated in epibenthic freshwater amphipod. Our results proposed that the lower levels of In(III) and Ga(III) exposure, the higher toxic effects would be induced due to hydrolysis process in higher concentrations. Additionally, the use of metal chelator

such as citrate could not prevent hydrolysis of In(III) and/or Ga(III), but has effect on the bioavailability and toxicity to *H. azteca*. We also demonstrated that the hydrolysis products of In(III), hydroxide/oxide chemicals may have lethal or sublethal toxic effects on *H. azteca*, which appeared to be greatly affected by environmental factors (e.g., water temperature, dissolved oxygen) relating to locomotor activity and feeding behavior.

Although this study clearly illustrated the potential adverse impact of waterborne Ga- and *In*-related chemicals exposure on individual growth and population dynamics of *H. azteca*, it also raises the questions about: (1) bioavailability of anionic species $Ga(OH)_4^-$, (2) bioconcentration ability of *H. azteca* to *In*-related chemicals, and (3) lethal toxic effects of $In(OH)_{3(s)}$ and $In_2O_{3(s)}$.

Based on these conclusions, future studies could address on the influence of hydrolysis & dissolved organic matters (e.g., citrate) on the aquatic toxicity of Ga and *In*, and sublethal toxic effects of Ga- and *In*-related chemicals in sediment phase. Since the exposure routes for epibenthic and benthic organisms such as *H. azteca* may include ingestion of sediment particles (containing metal hydroxide and oxide flocs) and water, they could expose and accumulate heavy metals primarily from overlying water, feeding behavior, and pore water as well. However, the toxicity caused by direct exposure to Ga- and *In*-related chemicals, or via sediment resuspension, and their potential ecological impact on individual and populations of aquatic organisms, need to be explored.

Chapter 2

Cellular Iron Homeostasis Disruption Capacity of Gallium- and Indium-Related Chemicals: A Cause of Mitochondrial Dysfunction in Relation to Indium Lung Disease?

1. General Background Information

In Chapter 1, the transformation, transport, environmental fate, and potential environmental problems caused by Ga- and *In*-related chemicals have been previously introduced. However, in this chapter, we will focus on how Ga- and *In*-based chemicals affect human health and safety. The two major exposure routes of Ga and *In* to humans are as follows: (1) medical applications, such as tumor imaging agents, anti-cancer/anti-microbial metallodrugs, and (2) occupational inhalation exposures (e.g., indium lung disease).

Since the chemical properties of Ga(III) and In(III) are similar to Fe(III), radioactive isotopes include ^{68}Ga-, ^{67}Ga- and ^{111}In-labelled compounds have been used as tumor, inflammation and infection imaging and therapeutic agents (Chitambar, 2010; Eychenne et al., 2020; Fani et al., 2017; Herron and Gossman, 2021; Kumar and Boddeti, 2013; Manyak, 2008; Xu and Chen, 2020). Unlike most antibiotics and traditional anticancer agents, which have a single target within the cell, Ga(III) and/or In(III) are typical multitarget agents that is predicted to impair several Fe-dependent and Fe-independent cellular functions (Minandri et al., 2014). Therefore, Ga and *In* compounds have been investigated for protection against microbial infection and several types of cancers, and further evaluated for human clinical trials (Chitambar, 2010; Chitambar, 2012; Merli et al., 2018).

Also, Ga- and *In*-related chemicals including GaAs, GaN, Ga_2O_3, ITO and InP also have been widely used in semiconductor and optoelectronic industrial manufacturing. *In* processing workers may potentially expose to these chemicals, which are known to increase both serum- and urine-*In* levels and the risk of indium lung disease (pulmonary fibrosis and interstitial pneumonia) and carcinogenesis in clinic cohort studies (Chonan et al., 2019; Cummings et al., 2012; Liao et al., 2004; Liu et al., 2012a; Mitsuhashi, 2020; Nakano et al., 2019).

In fact, the International Agency for Research on Cancer (IARC) have classified Ga- and *In*-based chemicals as carcinogens to humans, including GaAs (group 1, carcinogenic to humans), InP (group 2A, probably carcinogenic to humans) and ITO (group 2B, possibly carcinogenic to humans). Several studies have reported that the estimated biological half-life of *In* in serum or lung tissue appeared to be much longer than Ga (Amata et al., 2015; Jiang et al., 2017), leading to accumulate *In* in cells or tissues. Then, In(III) could be slowly released from *In*-based chemicals and causes oxidative stress, chronic inflammation and global DNA methylation (Gwinn et al., 2015; Jiang et al., 2017; Liou et al., 2017; Noguchi et al., 2016).

At the present time, the main modes of toxic action of Ga and *In* to humans and mammals could be divided into two groups, the one is disruption of cellular iron homeostasis, and the others are unrelated to iron homeostasis, such as inhibition of DNA polymerases, tyrosine phosphatase and proteasome activity (Chitambar, 2010; Chitambar, 2012). However, there is still a large gap in knowledge about the relationship between the exposure of Ga- and *In*-related chemicals, pathogenic mechanisms and long-term health effects.

In the Literature review, the main human exposure routes, uptake and metabolism, modes of action, and current knowledge on the exposure and health risk of Ga and *In* will be elucidated. Additionally, the worldwide occupational exposure limits and effective preventive strategies to Ga and/or *In*, which correspond to occupational hygiene will also be summarized.

2. Literature Review

2.1 Human Exposure of Ga- and *In*-Related Chemicals

In the light of environmental background concentrations of Ga and *In* described in Chapter 1 and their concentration measured in food products (Table 2.1) (Li et al., 2005; McHard et al., 1980; Millour et al., 2012; Rose et al., 2010), it appears to be much less significant for Ga- and *In*-related chemicals to transfer and adsorb through digestive system (Andersen et al., 2017). Although the concentrations of Ga and *In* in environmental matrices near semiconductor and optoelectronic manufacturing plants have been reported that are higher than background concentrations (Chen, 2006; You, 2014), local residents live in downstream areas and nearby manufacturing plants appear to have less health risk than workers in those electronic factories due to the chance of occurrence, exposure duration and routes. Consequently, in this chapter, human exposure to Ga- and *In*-related chemicals are focused on clinical applications and occupational exposure during the industrial manufacturing and recycling processes.

2.1.1 Medical Applications

Radionuclide imaging: From the late years of 20th century, the radioactive compounds of Ga and *In* have had been used as imaging agents for inflammation and infection lesions such as osteomyelitis, vascular graft infections, cellulitis, diabetic foot, Crohn's disease, inflammatory bowel disease, fever of unknown origin, etc. (Catane et al., 1977; Edwards and Hayes, 1969; Herron and Gossman, 2021; Parisi et al., 2018; Sayle et al., 1985; Sayle et al., 1982; Wheat, 1985; Xu and Chen, 2020). ^{67}Ga and ^{111}In salts such as ^{67}Ga-citrate, ^{67}Ga-nitrate, ^{111}In-chloride and ^{111}In-oxine could be directly injected into the body, or labelled with white blood cells which obtained from blood samples of a patient and re-injected intravenously (Catane et al., 1977; Edwards and Hayes, 1969; Herron and Gossman, 2021; Kabata-Pendias and Szteke, 2015; Lewis et al., 2014; Littenberg et al., 1973; Parisi et al., 2018; Sayle et al., 1985; Sayle et al., 1982; Wheat, 1985). Compared to ^{67}Ga radionucleotide scans, ^{111}In may have superior specificity in several infection diseases (Lewis et al., 2014).

With the improvements in the field of nuclear medicine, the increased availability of positron emission tomography/computed tomography (PET/CT) imaging devices has made ^{68}Ga and ^{111}In radiopharmaceuticals such as ^{68}Ga-citrate, ^{68}Ga-transferrin, ^{111}In-capromab pendetide and ^{111}In-pentetreotide, could be used in infectious diseases, inflammation and cancerous tumors imaging with higher spatial resolution and shorter biological half-life (Kumar and Boddeti, 2013; Manyak, 2008; Parisi et al., 2018; Xu and Chen, 2020; Zalom et al., 2009). Nevertheless, the use of ^{68}Ga and ^{111}In

still has some limitations, including lack of specificity and could not well distinguish between infectious, inflammatory and neoplastic processes (Parisi et al., 2018).

Fortunately, disease-specific markers have been developed as molecular targets to increase the specificity of ^{68}Ga and ^{111}In. For instance, the expression of prostate-specific membrane antigen (PSMA) and somatostatin receptors (SSTRs) are increased in prostate cancer and many solid tumors, respectively. The development of PSMA and SSTRs specific radiolabeled analogs (e.g., ^{111}In-capromab pendetide, ^{68}Ga-DOTATOC, ^{68}Ga-DOTATATE, ^{68}Ga-DOTANOC and ^{111}In- DOTATOC) have demonstrated to have better pharmacokinetic properties, imaging efficacy and safety (Eychenne et al., 2020; Fani et al., 2017; Manyak, 2008).

Anti-cancer agents: The first generation of Ga metallodrugs, gallium nitrate (Ganite®, Genta, NJ, USA) was approved by the U.S. Food and Drug Administration for the treatment of malignancy-associated hypercalcemia, which associated with cancer metastasis to bone tissues. In other clinical trials, gallium nitrate also has therapeutic efficacy to a variety of cancers, such as breast, prostate, lung, ovarian, bladder, renal, melanoma, sarcoma, chronic lymphocytic leukemia, Hodgkin's lymphoma and non-Hodgkin's lymphoma (Chitambar, 2004; Chitambar, 2012; Einhorn, 2003; Straus, 2003). In addition, gallium nitrate could be used safety in combination with other chemotherapeutic agents (e.g., vinblastine, ifosfamide, 5-fluorouracil, mitoguazone, etoposide and hydroxyurea) for treating bladder cancer or non-Hodgkin's lymphoma (Chitambar, 2004; Einhorn, 2003; Straus, 2003).

Table 2.1 Gallium and indium contents in food products

Product	Concentration	Unit	Reference(s)
Gallium			
Food of plant origin			
Wheat	0.118	mg/kg FW	Li and others (2005)
Wheat flour	0.148	mg/kg FW	Li and others (2005)
Rice	0.127	mg/kg FW	Li and others (2005)
Cereal and cereal products	0.001	mg/kg FW	Millour and others (2012)
Sweeteners, honey and confectionery	0.002	mg/kg FW	Millour and others (2012)
Orange juice (Florida)	0.030-0.040	mg/L	McHard and others (1980)
Orange juice (Brazil)	0.063-0.145	mg/L	McHard and others (1980)
Food of animal origin			
Fat and oil	0.016	mg/kg FW	Millour and others (2012)
Shrimps and mussels	0.008	mg/kg FW	Millour and others (2012)
Indium			
Food of plant origin			
Bread	<0.02	mg/kg FW	Rose and others (2010)
Miscellaneous cereals	<0.02	mg/kg FW	Rose and others (2010)
Vegetables	<0.004	mg/kg FW	Rose and others (2010)
Canned vegetables	0.096	mg/kg FW	Rose and others (2010)
Fresh fruits	<0.003	mg/kg FW	Rose and others (2010)
Fruit products	0.031	mg/kg FW	Rose and others (2010)
Orange juice (Florida)	0.001-0.002	mg/L	McHard and others (1980)
Orange juice (Brazil)	0-0.013	mg/L	McHard and others (1980)
Food of animal origin			
Carcass meat	<0.01	mg/kg FW	Rose and others (2010)
Offal	<0.01	mg/kg FW	Rose and others (2010)
Fish	<0.007	mg/kg FW	Rose and others (2010)
Milk	<0.003	mg/kg FW	Rose and others (2010)

Note: FW, fresh weight.

The newer generation of Ga-based compounds (e.g., gallium maltolate, tris(8-quinolinolato)gallium(III), gallium thiosemicarbazones, pyridine and phenolate ligand complexes of Ga) may have better specificity, bioavailability and antineoplastic activity for other cancers in the near future (Chitambar, 2012; Chitambar and Antholine, 2013). Furthermore, *In*-based compounds (i.e., indium maltolate) have developed as a counterpart of Ga metallodrugs, indicating greater *in vitro* protective effects than gallium maltolate on normal cells to mitoxantrone subsequent exposure (Merli et al., 2018). The difference of half-life period, tissue specificity and protective effects in Ga- and *In*-based drugs may offer the important advantage of providing a wider range of therapeutic options.

Antimicrobial agents: In light of antineoplastic activity of Ga- and *In*-based compounds, they also have been demonstrated to have antibacterial activity against a number of human pathogens due to the chemical similarity to Fe, such as ESKAPE pathogens with multidrug resistance and virulence (*Enterococcus faecium*, *Staphylococcus aureus*, *Klebsiella pneumoniae*, *Acinetobacter baumannii*, *Pseudomonas aeruginosa* and *Enterobacter* species) (Antunes et al., 2012; Baldoni et al., 2010; Hijazi et al., 2018; Kaneko et al., 2007; Kelson et al., 2013; Richter et al., 2017; Rogers et al., 1980; Thompson et al., 2015), *Francisella tularensis* (Olakanmi et al., 2010), several *Candida* species (Oliveira et al., 2017), pathogenic serotypes of *Escherichia coli* (Rogers et al., 1982), *Rhodococcus equi* (Coleman et al., 2010) and mycobacterial species (Olakanmi et al., 2000; Olakanmi et al., 2013).

Different from most antibiotics, Ga- and *In*-based compounds could target on multiple Fe(III)-dependent biofunctions in bacterial cells (Crunkhorn, 2018; Kelson et al., 2013; Minandri et al., 2014; Vinuesa and McConnell, 2021). Therefore, the development of drug resistance (e.g., target gene

mutation, enzymatic modification or alteration of metabolic pathways) is much difficult for bacteria to overcome the toxic mechanisms.

It has been investigated that the metabolic state of bacteria cells and culture conditions (e.g., oxygen levels, iron contents and pH values) could have impact on Ga and *In* susceptibility *in vitro* assays. In comparison with aerobic bacteria, facultative anaerobic bacteria, such as enterobacteria, enterococci, staphylococci and streptococci pathogens, are capable of switching to fermentation or anaerobic respiration in the absence of oxygen (Minandri et al., 2014), which could decrease the susceptibility of bacteria to Ga- and *In*-based compounds.

There are numbers of previous studies have reported that Ga-based compounds (e.g., gallium nitrate, gallium citrate, gallium-protoporphyrin, deferoxamine-gallium and EDTA-gallium) have antibiofilm activity or prevention of biofilm formation *in vitro* (Baldoni et al., 2010; Banin et al., 2008; Kaneko et al., 2007; Richter et al., 2017; Thompson et al., 2015; Zhu et al., 2013). Nevertheless, it should be taken into account that the development and ultrastructure of biofilm communities *in vivo* are more complex than *in vitro*. The metabolic states, nutrients and oxygen levels are not the same between cells growing on surface and deeper layers of a biofilm (Minandri et al., 2014); thus, the bacteria cells distributed in biofilm appears to have different susceptibility to Ga(III) treatment. In clinical trials, the use of higher dosages of Ga(III) than *in vitro* antimicrobial testing outcomes would be required for greater efficacy in biofilm-related infections therapy.

Still, a number of challenges to developing Ga- and *In*-based therapies have been reported in previous studies (Minandri et al., 2014; Vinuesa and McConnell, 2021). Firstly, Ga- and *In*-based

chemicals are likely to be used in combination with existing Fe chelators and/or antibiotics; however, there is still a large gap in knowledge on the interactions between these chemicals, Fe chelators and antibiotics, and to what extent could the disruption of bacterial iron homeostasis affect biofilm formation and antibiotic susceptibility. Secondly, Ga(III) but not In(III) has been demonstrated in preclinical studies to have immunosuppressive activity on macrophage and T-cell functions, and the long-term administration of Ga-based chemicals could weaken the host immune response (Chitambar, 2010; Drobyski et al., 1996; Huang et al., 1994; Matkovic et al., 1991). Therefore, the potential immunomodulatory properties of Ga(III) should be taken into account when Ga-based chemicals are being used for antibacterial therapies. Thirdly, the potential side effects or toxicity with the use of antibiotics, Fe chelators and Ga- and In-based chemicals should be kept in mind that the mechanisms of action are not fully understood at the present time. In the near future, a more detailed studies on assessing the potential toxicity, therapeutic efficacy and safety of these chemicals are required for the treatment of bacterial infections.

Antiviral agents: Compared to *In*-based chemicals appear to active the immune system (Zelicoff and Thomas, 1998), the immunosuppressive and anti-inflammatory properties have made Ga-based chemicals as potential candidates for the treatment of coronavirus disease 2019 (COVID-19) (Bernstein and Zhang, 2020). The severe acute respiratory syndrome coronavirus 2 (SARS-CoV-2) and the variant strains (B.1.1.7, alpha variant; B.1.351, beta variant and B.1.617.2, delta variant) have spread rapidly and caused a global pandemic within a short period of time. The SARS-CoV-2 virus could induce a variety of symptoms due to severe inflammatory responses of the body, and the new

delta variant has greater infectiousness and transmissibility, especially for children and younger people (Li et al., 2021; Tchidjou Kuekou et al., 2021).

Limited research studies have reported that Ga-based chemicals (gallium nitrate and gallium maltolate) could inhibit viral replication of RNA viruses, including influenza A virus, human immunodeficiency virus and SARS-CoV-2 virus *in vitro* (Bernstein and Zhang, 2020; Enkirch et al., 2019; Stapleton et al., 1993). Further antiviral activity of Ga(III) could be hypothesized due to cellular Zn metabolism alteration and Fe deprivation, which are essential factors for entry into the target cell and viral replication, respectively (Bernstein and Zhang, 2020). In addition, the viral replication inhibition abilities of Ga(III) appears to target on ribonucleotide reductase for reducing RNA synthesis and mitochondrial electron transport chain complexes for decreasing ATP synthesis, leading to elimination of infected cells (Bernstein and Zhang, 2020; Liu et al., 2020; Wang et al., 2021).

2.1.2 Indium Lung Disease

As previous summarized in Chapter 1 (2.4 Production and Uses), the production of indium tin oxide (ITO) accounts for most of global In consumption (65 %), which has been used in virtually every flat-panel display screen and touchscreen (Schulz et al., 2017). The ITO industry is mainly distributed in Japan, the U.S., Taiwan, China and South Korea. With the increasing demand for the production of ITO, the potential health risk of workers in ITO manufacturing plants has been reported in several studies (Amata et al., 2015; Cummings et al., 2012; Cummings et al., 2014; Hamaguchi et al., 2008; Hawley Blackley et al., 2019; Higashikubo et al., 2019; Higashikubo et al., 2018; Hsu et al., 2021; Liou et al., 2017; Nakano et al., 2019).

In a case of Japan, Hamaguchi et al. (2008) studied on *In*-exposed workers (*In*-exposure period was more than one year), indicating more than half of exposed workers had inhaled primary ITO aerosols, about 40 % of the raw material aerosols of ITO ($In_2O_{3(s)}$ and/or $In(OH)_{3(s)}$), and the remaining about 10 % mainly *In* metal (Hamaguchi et al., 2008). As a result, all the workers in ITO production line, including sintered/ unsintered ITO tile production, grinding and *In*-containing waste materials recycling, were potentially exposed to In compounds with different characteristics (Cummings et al., 2014; Hamaguchi et al., 2008; Hawley Blackley et al., 2019; Higashikubo et al., 2019; Hsu et al., 2021; Julander et al., 2014).

The first case of severe interstitial pneumonia consistent with the inhalation of ITO aerosols was reported in 2003, Japan; the exposed worker had been engaged in the metal processing manufacturing

plant as an operator of a wet surface grinder for three years (Homma et al., 2003). On histopathological examination, numerous fine ITO particles were investigated within the alveolar spaces, alveolar septum and bronchiolar lumens. In addition, the serum-*In* concentration of the worker was as high as 290 μg/L (Homma et al., 2003), while the existing biological exposure index of *In* in serum is 3 μg/L (Chonan et al., 2019; Nakano et al., 2009; Tsao et al., 2021).

Since then, there have been a number of case reports from Japan, the U.S., Taiwan and China (Chonan et al., 2007; Cummings et al., 2010; Homma et al., 2005; Taguchi and Chonan, 2006; Tsao et al., 2021; Xiao et al., 2010). The common features of these cases include: (1) occupational exposure history of handling *In*-related chemicals, (2) increase in serum-*In* concentration, (3) interstitial (and emphysematous) changes of the lung on high-resolution computed tomography (HRCT) images, (4) pathological confirmation of cholesterol (crystals-containing) granulomas and particles engulfed by alveolar macrophages and giant cells, (5) elevation of serum biomarkers of interstitial pneumonia including Krebs von den Lungen-6 (KL-6) and surfactant protein-D (SP-D), and (6) decrease in disusing capacity of the lung for carbon monoxide (Chonan et al., 2019).

Nevertheless, other pathological investigations have also been reported from the U.S. and China cases, which were pulmonary alveolar proteinosis (PAP) and increase in the levels of serum autoantibody against granulocyte-macrophage colony-stimulating factor (GM-CSF) (Cummings et al., 2010; Xiao et al., 2010). The authors proposed the inhalation of *In*-related chemicals aerosols might induce PAP through an autoimmune mechanism (Cummings et al., 2010).

Different from other pneumoconiosis, the latency period (month to years) of indium lung disease is relatively shorter than other occupational lung disease such as silicosis, asbestosis and coal workers' pneumoconiosis (Table 2.2) (Castranova and Vallyathan, 2000; Chonan et al., 2019; Chong et al., 2006; Leonard et al., 2020; Yuan et al., 2018; Zosky et al., 2016). Factors affecting the duration of the latency period in indium lung disease are not yet clear. However, the rate of pathological progression of indium lung disease appears to depend on not only the amount of inhaled *In*-related dust, but also the In(III) dissolved and accumulated in the patient's body.

At the present time, the modes of action of *In*-related chemicals and the pathogenesis of indium lung disease are still not fully understood. However, one hypothesis has been proposed by limited studies (Chonan et al., 2019; Cummings et al., 2012), the *In*-based particles engulfed by alveolar macrophages and the In(III) gradually released from those particles, leading to macrophages dysfunction and further accumulation of intraalveolar lipoproteinaceous material and development of cholesterol crystals. These cholesterol crystals may induce the formation of cholesterol granulomas and the eventual development of pulmonary fibrosis and emphysema. However, the investigation of fibrotic foci in areas without cholesterol crystals indicated that the pulmonary fibrosis induced by *In*-related chemicals may include multiple pathogenic mechanisms (Cummings et al., 2012). Moreover, it is believed that several case reports with PAP and elevated GM-CSF may play some role in the pathogenesis of indium lung disease, but their role is still unclear and remains to be investigated (Chonan et al., 2019).

Although the chemical properties of Ga are similar to *In*, there is still a key question about why occupational exposure disorders (i.e., pulmonary toxicity) related to Ga-based chemicals have rarely reported in the literature. The potential adverse effects of the group 1 carcinogen GaAs and the newer-generation semiconductor material of $Ga_2O_{3(s)}$ have been reviewed in several studies (Bomhard, 2020; Carter et al., 2003). The hypothesis of different pulmonary toxicity between GaAs, $Ga_2O_{3(s)}$ and *In*-related chemicals may be associated with (1) physical and chemical properties (solubility and surface activity of particles), (2) biological half-life (or biopersistence), (3) immune response (In(III) and Ga(III) appear to active and suppress immune system respectively) (Amata et al., 2015; Bomhard, 2020; Jiang et al., 2017; Minandri et al., 2014; Zelicoff and Thomas, 1998).

In light of several *in vivo* studies, compared to $Ga_2O_{3(s)}$, the inhalation exposure of GaAs could induce greater pulmonary toxicity due to its surface physical and chemical properties, the solubility and bioavailability are much higher in lung fluids (Bomhard, 2020; Carter et al., 2003). Subchronic inhalation studies in rats and mice indicated that both GaAs and $Ga_2O_{3(s)}$ could induce severe inflammatory response such as PAP and/or alveolar histiocytic infiltration, whereas Webb et al. (1986) reported that $Ga_2O_{3(s)}$ particles appear to deposit in the lung of rats without clear-out toxicity but no inflammatory response was investigated (Bomhard, 2020; Webb et al., 1986).

Consequently, the results from *in vitro* and *in vivo* studies on Ga-based chemicals are promising, but there is a need for more human studies such as case reports and cohort research for further risk evaluation. In addition, from human case studies of Al, *In*, quartz, titanium dioxide, and occupational health research with exposure to partly high levels, it could be assumed that rats and mice are more

sensitive to Ga- and *In*-related chemicals than humans. The species differences should be taken into account when assessing occupational health risk from *in vivo* mammalian models (Bomhard, 2020).

Table 2.2 Characteristics of indium lung disease as compared to other pneumoconiosis

	Indium lung	Silicosis	Asbestosis	Coal workers' pneumoconiosis (Black lung disease)
Latency	Month to years	Decades	Decades	Decades
Metal in blood	Indium detectable	Nothing specific	Nothing specific	Nothing specific
Serum biomarker (KL-6)	Increased	Rarely increased	Occasionally increased	Rarely increased
Distribution	No predilection	Upper zone dominant	Lower zone dominant	Upper zone dominant
Characteristic pathology	Cholesterol granuloma	Silicotic nodule	Asbestos body	Large conglomerate composed of multiple foci of central hyalinized collagen and a surrounding pigmented rim of macrophages
	Particles in giant cell			Focal necrosis, occasionally associated with granulomatous inflammation
	Alveolar proteinosis			
Interstitial pneumonia	++	+	+	+
Pulmonary fibrosis	+	++	+++	++
Pulmonary bullae	++	+	-	+
Emphysema	++	++	-	++

Note: KL-6, Krebs von den Lungen 6; -, no significant response; +, significant response; ++, greater response than +; +++, greater response than ++.

2.2 Uptake, Absorption, Distribution and Excretion

2.2.1 Medical Applications

Uptake and absorption: Generally, *In*- and Ga-based chemicals (e.g., gallium nitrate) used for radionuclide imaging and/or anti-cancer treatments are given by intravenous injection. It is reported that gallium chloride could be administrated orally as a single anti-cancer agent without major toxicity, whereas the bioavailability and antineoplastic activity might be decreased in some cancers (Collery et al., 1989). In contrast, the oral administration of gallium maltolate could be readily absorbed from the gastrointestinal tract, and the oral bioavailability is better than gallium chloride (Bernstein et al., 2000). Nevertheless, the uptake of Ga from oral administration appears to be more selective for tumor and even more so for metastatic cancers, compared to kidneys and intravenous injection (Collery et al., 2002; Collery et al., 1989).

Distribution: The distribution of Ga and *In* in body tissues are largely determined by the metal's chemical form. Both absorbed Ga(III) and In(III) are mainly bound to transferrin in the circulation and distributed to a number of organ systems; A large amount of Ga(III) is distributed in the liver, spleen, kidneys, brain, bone, bone marrow and pancreas (Belozerov, 1966; Nordberg et al., 2014), and In(III) is distributed in the bone marrow and kidneys (Catane et al., 1977; Nordberg et al., 2014; Sayle et al., 1982)

As an antibacterial, infection and inflammation scanning agent, Ga(III) and In(III) could further accumulate within inflammatory sites (Edwards and Hayes, 1969; Herron and Gossman, 2021;

Kumar and Boddeti, 2013; Lavender et al., 1971; Lewis et al., 2014; Littenberg et al., 1973; Parisi et al., 2018; Sayle et al., 1985; Xu and Chen, 2020). There are multiple factors contributed to the accumulation and retention of Ga(III) or In(III) in inflammatory lesions, many of which are attributable to the nonspecific response of injured tissues (Minandri et al., 2014).

Excretion: The main route of excretion for Ga and *In* from the body is through the urine, with lesser amounts excreted in the feces. In addition, the biological half-life of Ga and *In* depends somewhat on the chemical form administrated (Nordberg et al., 2014). For instance, in comparison with oral administration of gallium maltolate, intravenous injection of gallium nitrate could result in formation of considerable plasma gallate ($Ga(OH)_4^-$), which is rapidly excreted in the urine compared to the plasma bound Ga (Bernstein et al., 2000).

2.2.2 Occupational Exposure

Uptake, absorption and distribution: In semiconductor and optoelectronic manufacturing and recycling factories, workers are mainly exposed to Ga and *In* through inhaled particles (e.g., ITO, $In(OH)_3$, In_2O_3, GaAs and Ga_2O_3) suspended in the workplace, as well as ingested by hand-to-mouth pathway (Hsu et al., 2021). It is proposed that the inhaled dusts have a major size of micro- and/or nano-sized, and are likely to stay briefly in the upper respiratory tract or tracheobronchial tree; these particles are further deposited in the deep lung and are dissolved by the acidic lysosomes of alveolar macrophages during phagocytosis, and the remaining amount of particles transfer through the digestive system (Andersen et al., 2017; Hsu et al., 2021).

Excretion: Inhaled Ga and/or *In* particles are mainly deposited in the deep lung, then gradually dissolved in the blood, binding to plasma transferrin and excreted in the urine. Some part of the inhaled particles may also be expectorated by the mucociliary transport system of the airway (Chonan et al., 2019). Those ingested particles are primarily excreted in the feces.

Moreover, a nine-year cohort study of workers who had quit engaging in *In* processing for more than three years, indicating that the biological half-life of serum-*In* was 8.09 (5.91-13.79) years, and the half-life was longer for those with higher serum-*In* concentration initially (Amata et al., 2015). It would require considerable time to remove *In* from the lung tissues, the pulmonary vasculature might be more severely damaged and the blood flow to the lungs is limited, which subsequently prolongs the clearance of deposited *In*-related particles (Amata et al., 2015). However, data on the half-life of Ga-related chemicals in human body are not available at the present time.

2.3 Modes of Action

2.3.1 Action on Cellular Iron-Dependent Processes

Action on iron transport and cellular uptake: The chemical properties of Ga and *In* are similar to iron and permit them to bind with high avidity to certain Fe-binding proteins. The circulating Fe is bound to transferrin (Tf) and is taken up from the blood by a high-affinity specific transferrin receptor. There is approximately one third of circulating serum Tf is occupied by Fe(III), whereas the remaining two third of Tf is available to bind the incoming Ga(III) and/or In(III) (Chitambar, 2016). Hara (1974) reported that the binding affinity of Tf increases in the order of In(III)> Fe(III)> Ga(III) (Hara, 1974). Although Ga(III) could not outcompete and substitute for Fe(III), Tf remains the major carrier of Ga(III) in the blood (Chitambar, 2016; Collery et al., 2002). Nevertheless, it is reported that the binding affinity of Tf-Fe(III) to Tf receptor (TfR) in liver tissue is much higher than Tf-In(III) and Tf-Ga(III) (Sato et al., 2004). The uptake of Tf-Fe(III) appears to not depend on the binding affinity of Tf in some tissues (e.g., bone marrow, liver).

The presence of Tf-Ga(III) and Tf-In(III) could compete with Tf-Fe(III) for binding to TfR and further be taken up by cells via transferrin receptor (TfR) mediated endocytosis (Chitambar and Zivkovic, 1987; Harris and Sephton, 1977; Moran and Seligman, 1989; Nejmeddine et al., 1998). During the endocytic process, Tf-Ga(III) and Tf-In(III) could also have adverse effects on the intracellular Fe incorporation by interfering with acidification in the endosome, which affects the dissociation of Fe from Tf (Chitambar and Seligman, 1986). Note that, almost all Fe(III) remains

bound to Tf at pH values as low as 4.7, whereas Ga(III) and In(III) start to dissociate from Tf at pH <6.8 and pH <5.5, being already 50% dissociated at pH 6 and 4, respectively (Hultkvist et al., 1987; McGregor and Brock, 1992).

Compared to interfering with TfR-mediated cellular Fe uptake, Ga(III) and/or In(III) could increase the Tf-independent uptake of Fe(III) by a number of cell lines, and vice versa (Chitambar and Sax, 1992; Richardson, 2001; Sturm et al., 2006). The ability of Ga, *In* and Fe to stimulate each other's uptake indicated that they either use the same Tf-independent transport pathways for entering cells or induce a mechanism of transporter activation responsible for the uptake of either metal (Chitambar, 2016; Richardson, 2001).

Furthermore, several studies reported that a number of cell types could uptake Tf-independent Fe through the reduction of Fe(III) to Fe(II) at the cell membrane, which is then transported into the cells. The stimulation of glutamyltransferase- and/or ferrireductase (e.g., duodenal cytochrome b)-mediated Fe(III) reduction may participate in the process of Tf-independent Fe transport, and Fe(II) could be transported into cells by divalent metal transporter 1 (DMT1) on cell surface (Dominici et al., 2003; Jordan and Kaplan, 1994; Kovac et al., 2011; Shindo et al., 2006; Zhang, 2014).

The Tf-independent Fe transport systems could provide sufficient Fe to support cellular growth and proliferation (Dominici et al., 2003; Seligman et al., 1991; Shindo et al., 2006). Even if the presence of Ga(III) and In(III) could block the TfR-mediated Fe uptake, certain cells are still capable to activate TfR-independent Fe uptake pathways; therefore, the cells may be less sensitive to Ga(III)

and In(III), thereby providing a selective growth advantage. The relative contribution of TfR-dependent and TfR-independent Fe uptake systems may differ between cell types (Chitambar, 2016).

Ribonucleotide reductase (RNR): RNR is responsible for the formation of deoxyribonucleotides from ribonucleotides, which is the key enzyme in DNA synthesis and repair processes. RNR is a heterodimer comprising two homodimeric M1 and M2 subunits (RRM1 and RRM2) (Aye et al., 2015; Cory, 1983; L Thelander and Reichard, 1979; Yu et al., 2009; Zhan et al., 2021). Under physiological conditions, RRM1 and RRM2 are tightly regulated and expressed at different cell cycle phases. RRM1 is present during all phases of the cell cycle (G_0 to M phase) whereas RRM2 only appears during the period of late G_1 to S phase (Engström et al., 1985; Eriksson et al., 1984). In human, the large subunit of RRM1 could form an active enzyme with the small subunit RRM2. RRM1 contains the substrate (nucleoside diphosphate) and two effector-binding sites whereas RRM2 contains a binuclear Fe center and a tyrosyl free radical (Chitambar, 2016; Kircheva and Dudev, 2021).

The Fe center is essential for RRM2 function, which precipitates in the generation of tyrosyl free radical signal and thereby redox reaction of the nucleotide substrates. However, loss of Fe from RRM2 could result in missing of the tyrosyl radical and RRM2 function. When the cellular Fe level is low, the iron-free RRM2 (apoRRM2) would substitute for RRM2 that lacks of tyrosyl radical signal and is functionally inactive (Nyholm et al., 1993). It appears that the biological half-life of RRM2 protein is approximately three hours and therefore the cellular Fe homeostasis is essential for maintaining the activity of newly synthesized RRM2 protein during S phase (Eriksson et al., 1984).

A number of studies reported that Ga(III) and/or In(III) could disrupt RNR enzymatic activity through direct and indirect mechanisms (Chitambar et al., 2018; Chitambar et al., 1988; Chitambar and Narasimhan, 1991; Kircheva and Dudev, 2021; Narasimhan et al., 1992): (1) Ga(III) or In(III) does not block the biosynthesis of RRM2 protein but displaces the native metal cofactor from the active center of RRM2 and shrinks the protein structure of RNR; (2) substitution of redox-inactive Ga(III) or In(III) for redox-active Fe(III) results in inhibition of enzymatic reaction; and (3) Ga(III) or In(III) interferes with the availability of cellular Fe to maintain protein function of RRM2 subunit.

While the substitution of active center of RRM2 protein and the inhibition of cellular Fe availability by Ga(III) or In(III) should be sufficient to inhibit DNA synthesis, Ga(III) also could entrap the enzyme substrates (nucleoside diphosphates, NDPs) to form Ga(III)-NDP complexes (Chitambar et al., 1991; Kircheva and Dudev, 2019; Marzilli et al., 1980). These abnormal complexes (especially in Ga(III)-ADP and Ga(III)-CPD) could not serve as proper substrates for RNR due to significant structural alterations, and they could not fit properly to the substrates binding site of RRM1 subunit. Therefore, the concentration of the cellular free substrates decreased and further declines the enzymatic activity (Kircheva and Dudev, 2021).

Cell cycle regulation: In eukaryotes, the cell cycle is a strictly regulated event which take place in cells leading to their growth and division. Generally, the cell cycle is described by five phases: G_0, G_1, S, G_2 and M phase, and a number of major check points that control the progression of the cell growth through the cycle. These checkpoints are present at G_1/S, S, G_2/M and M phase (Matthews et al., 2021; Reed, 1997; Zetterberg et al., 1995). The key molecules that program the cell cycle are

cyclins and cyclin-dependent kinases (CDKs), play a crucial role in the regulation of the cell cycle at every checkpoint (Hydbring et al., 2016; Malumbres, 2014; Montalto and De Amicis, 2020; Nigg, 1995). Other molecules also participate in the cell cycle regulation, which include CDKs inhibitors (e.g., $p21^{Cip1/Waf1}$), tumor suppressors (e.g., p53, $p27^{kip1}$) and retinoblastoma protein (pRb) (Golias et al., 2004; Johnson and Walker, 1999; Kastan et al., 1995; Møller, 2000; Sherr, 1994; Sherr and Roberts, 1999; Zetterberg et al., 1995). Disruption of cell cycle regulation could lead to cell cycle arrest, cellular senescence, programmed cell death (e.g., apoptosis, ferroptosis) and tumor formation (Gorgoulis et al., 2019; Matthews et al., 2021).

Fe is an essential component of a variety of proteins and enzymes, such as RNR, iron-sulfur cluster, heme and cytochrome, which are involved in cell growth and replication. Considering the importance of Fe in vital cellular processes such as DNA synthesis and energy production, it is not surprising that the cell cycle is sensitive to Fe availability. For instance, the TfR1 expression is increased during the S phase of the cell cycle, which is associated with DNA synthesis due to the Fe requirement of RNR (Cory, 1983). However, it has been reported that decrease in TfR1 expression and cellular Fe deficiency could lead to cell cycle arrest (G_1) and alteration in the expression of genes that regulate the cell cycle (O'Donnell et al., 2006).

Compared to normal cells, a variety of cancer cells require greater amount of Fe to support the cell growth and proliferation. This is reflected by an increased levels of TfR1 and ferritin (the Fe storage protein), or decreased in the expression of the Fe efflux protein ferroportin in certain cancer

cells (Gatter et al., 1983; Habashy et al., 2009; Pinnix et al., 2010; Seymour et al., 1987; Shpyleva et al., 2011; Weinstein et al., 2005; Xue et al., 2015; Yang et al., 2001; Zhang et al., 2014b).

Moreover, overexpression of RRM2 subunit of RNR also has been demonstrated to be associated with malignant transformation, metastatic potential, and chemotherapy resistance in human cancer cells (Huang et al., 2014; Shah et al., 2015; Xu et al., 2008; Zhou et al., 1998). RRM2 functions as an oncogene and regulates multiple molecular mechanisms, which involved oncogenic signaling pathway, glycolysis and cell cycle-related genes (Mazzu et al., 2019). Present studies elucidated that abnormal RRM2 degradation could induce imbalance of the deoxynucleotides pool, dysregulated cell cycle and increase in genomic instability, and cells with increased expression of RRM2 is highly correlated with poor clinical outcomes in some cancers (Bedard et al., 2013; D'Angiolella et al., 2012; Mazzu et al., 2019; Mazzu et al., 2020).

Consequently, alteration in expression of Fe-regulated genes and atypical changes in intracellular Fe distribution and trafficking would be expected to increase intracellular Fe status to support aggressive cancer cells growth.

At the present time, some Fe-chelators have been demonstrated to be effective in inhibiting cancer cells proliferation. The mechanisms of Fe chelators appear to have effect on tumors by targeting molecules that are essential in regulating progression of the cell cycle (Chen et al., 2020; Corcé et al., 2016; Fryknäs et al., 2016; Gao and Richardson, 2001; Ibrahim and O'Sullivan, 2020; Le and Richardson, 2004; Lui et al., 2015a; Pahl and Horwitz, 2005; Yin et al., 2021). Some of these mechanisms include: (1) RNR (Dong et al., 2005; Green et al., 2001; Nyholm et al., 1993), (2) cyclins

(Golias et al., 2004; Kulp et al., 1996), (3) CDKs (Golias et al., 2004; Kulp et al., 1996), (4) p53 (Ashcroft et al., 2000; Fukuchi et al., 1995; Liang and Richardson, 2003), (5) $p21^{Cip1/Waf1}$ (Fu and Richardson, 2007; Kovacevic et al., 2011), (6) $p27^{Kip1}$ (Dong et al., 2005; Wang et al., 2000; 2004b), (7) GADD45α (growth arrest and DNA-damage inducible protein) (Gao and Richardson, 2001), (8) hypoxia inducible factor-1α (HIF-1α) (Yu et al., 2007), (9) N-myc and C-myc (Kyriakou et al., 1998; Wang et al., 2014; Wijesinghe et al., 2021), (10) downstream regulatory gene-1 (Ndrg-1) (Chen et al., 2012b; Dixon et al., 2013; Kovacevic et al., 2011; Liu et al., 2012b; Sun et al., 2013), (11) pRb (Gao and Richardson, 2001; Terada et al., 1991), (12) PI3K/AKT/mTOR (phosphatidylinositol 3-kinase/protein kinase B/mammalian target of rapamycin) signaling (Lui et al., 2015a; Ohyashiki et al., 2009; Shang et al., 2020), (13) Ras/Raf/Mitogen-activated protein kinase/ERK kinase (MEK)/extracellular-signal-regulated kinase (ERK) signaling (Dixon et al., 2013; Lui et al., 2015a), (14) JNK (c-Jun N-terminal kinase)/p38 (Kim and Chung, 2008; Kim et al., 2002; Lui et al., 2015a; Saitoh et al., 1998; Yu and Richardson, 2011), and (15) STAT3 (signal transducer and activator of transcription 3) signaling (Kuang et al., 2019; Lui et al., 2015a; Lui et al., 2015b; Wang et al., 2014).

Not surprisingly, Ga(III) and In(III) would be expected to have similar toxic mechanisms to Fe chelators due to cellular Fe deprivation, as well as induce further cytotoxicity through their chemical properties. In the present study, Ga maltolate could inhibit Fe uptake and upregulate TfR1 expression in glioblastoma cancer cell lines, and further decrease the activity of Fe-dependent RRM2, mitochondrial oxygen consumption and cell viability (Chitambar et al., 2018). In addition, tumors in Ga maltolate-treated animals also displayed an upregulation of TfR1 expression, retarded tumor

growth and reduced tumor mitotic figures in comparison with control animals, indicating Ga induced tumor Fe deprivation. These Fe-dependent mechanisms could result in further a block in DNA synthesis and energy production, which is expected to induce cell cycle arrest and programed cell death (Chitambar et al., 2018).

Mitochondria: Mitochondria are generally known as the "power plant" of the cells because they play an essential role in the production of ATP through the oxidative phosphorylation of electron transport chain. Furthermore, mitochondria are actively implicated in other processes, such as heme synthesis, cell differentiation, ROS generation, apoptosis, calcium signaling and Fe metabolism, etc. (Piomboni et al., 2012; Zhao et al., 2019)

It is proposed that iron-sulfur cluster and heme containing proteins in the citric acid cycle and the electron transport chain could be the potential target for Ga(III)- and In(III)-induced mitochondrial dysfunction in the cells. However, there are only a few studies of their action on the mitochondria (Chitambar et al., 2006; Yang and Chitambar, 2008; Yuan et al., 2017). The lymphoma cell lines exposed to Ga nitrate induced apoptosis through the mitochondrial pathway, which involved the activation of proapoptotic effector protein Bax in the cytosol. This pathway promotes mitochondrial outer membrane permeabilization, which allows the release of proapoptotic factors such as cytochrome *c* from the mitochondria to the cytosol to active the caspase-3 cascade, leading to programmed cell death (Chitambar et al., 2006).

Other mechanisms included Ga-induced mitochondrial oxidative stress which evidenced by a decrease in cellular reduced glutathione (GSH) and GSH/GSSG (oxidized glutathione) ratio (Yang

and Chitambar, 2008). It would be expected that the reactive oxygen species (ROS) originates from the mitochondria may be associated with Ga-induced apoptosis, but it remains to be determined where and how the increased mitochondrial ROS come from (Chitambar, 2016).

In order to investigate the effects of In(III) on mitochondria, Yuan et al. (2017) used rat liver mitochondria and treated with *In* chloride. In(III) could induce mitochondrial swelling, membrane depolarization and inhibits the protons transportation, eventually resulted in mitochondrial permeability transition, which primarily related to mitochondrial dysfunction and cell death. In addition, In(III) was able to accelerate mitochondrial ROS production and inhibit the electron transport chain, providing a possibility that the long-term exposure and accumulation of In(III) to the cells may cause mitochondrial dysfunction and a chronic cytotoxicity (Yuan et al., 2017).

Heme synthesis and zinc substitution: Heme is the major functional form of Fe, synthesized in mitochondria and plays a crucial role in respiratory phosphorylation, inhibiting oxidative stress, drug metabolism and oxygen transport (Dailey and Meissner, 2013). Biosynthesis of heme requires Vitamin B_6, riboflavin, biotin, pantothenic acid, lipoic acid, the metal ions of Zn, Fe and Cu, and succinyl-CoA produced by the citric acid cycle.

In mammals, plants, fungi, and α-proteobacteria cells, heme synthesis is accomplished in the mitochondria and cytosol over a series of eight enzymatic reactions, followed by modification of heme in a couple of sub-methylation steps (Dailey et al., 2017; Hamza and Dailey, 2012; Nilsson et al., 2009). The biosynthesis of heme is initiated by aminolevulinic acid synthase (ALAS1), the rate-limiting enzyme that catalyzes formation of 5-aminolevulinic acid (ALA) from succinyl-CoA and

glycine. ALA is then exported into the cytosol and converted through several intermediates into coproporphyrinogen-III (CPO) by coproporphyrinogen oxidase; The CPO is transported back into the mitochondrial matrix for the last two steps of the pathway. In the final step, ferrochelatase (FECH) incorporates Fe(II) into protoporphyrin IX (PPIX), synthesizing protoheme (Layer et al., 2010; Shetty and Corson, 2020). However, in plants, archaea and bacteria, there is an alternative course (C_5-pathway) for synthesizing ALA by using tRNA-bound glutamate (Layer et al., 2010).

Only a few studies have reported that Ga(III) may have effects on the second step enzyme of heme synthesis, delta-aminolevulinic acid dehydratase (ALAD), which is an octameric Zn-containing enzyme and catalyzes the synthesis of porphobilinogen from two molecules of ALA in cytosol. Goering and Rehm (1990) showed that rats received a single intraperitoneal injection of Ga sulfate (12.5-200 mg Ga/kg) produced a dose-dependent noncompetitive inhibition of ALAD in liver, kidney, and erythrocytes. Interestingly, Ga-induced hepatic and renal ALAD inhibition could be attenuated by the addition of Zn, indicating that toxic mechanisms of Ga on ALAD appeared to involve displacement of Zn from the sulfhydryl group of enzyme's active site (Goering and Rehm, 1990).

Ga(III) may also interfere with the Zn-dependent enzymatic activity, the alkaline phosphatase (ALP) and matrix metalloprotenase (MMP). It is expected that during the synthesis of the ALP protein, which requires Zn(II) and Mg(II) binding to active site for enzymatic activation, whereas Ga(III) becomes incorporated into the active site instead of Zn(II) or Mg(II) and further folded into its active confirmation. Also, once the ALP protein is folded, exchange with Zn(II) or Mg(II) by Ga(III) does not readily occur (Boskey et al., 1993). Panagakos et al. (1999) speculated that Ga may operate in the

same manner as ALP protein in regulating the activity of MMPs, and the ability of Ga to inhibit MMPs activity, such as MMP-2, MMP-9 and MMP-14, has been demonstrated *in vitro* (Bernstein, 2012; Mohsen et al., 2017; Panagakos et al., 2000).

Moreover, the human lymphoma cells treated with Ga nitrate could produce an expansion of an intracellular labile Zn pool, indicating a possible toxic mechanism of Ga on cellular Zn homeostasis. Ga nitrate also upregulated the expression of metallothionein-2A (MT2A) and heme oxygenase-1 (HO-1), which was partly associated with the increase in an intracellular Zn pool and Ga-induced ROS production (Yang and Chitambar, 2008).

Since Ga-related chemicals have been investigated to have effects on protoporphyrin IX/ heme synthesis, Zn-dependent enzymatic activity and cellular Zn homeostasis, it remains to be determined that what is the source of Zn contributing to the increased intracellular Zn pool and whether In(III) could induce the same toxicity as Ga(III). However, the possible toxic mechanisms of Ga on Zn homeostasis have been proposed, which may include: (1) Ga(III) increases the uptake of Zn(II) thereby expanding the intracellular Zn pool, and (2) Zn(II) is mobilized from endogenous intracellular Zn-metallothionein by Ga-induced ROS (Yang and Chitambar, 2008).

Microbial iron-uptake: Like eukaryotic cells, Fe also plays an important role in prokaryote cells for growth and proliferation. During the infection process, microorganisms such as bacterial pathogens need to sense, respond, and adapt rapidly to different environmental signals in hosts. The primary defense mechanism in those hosts against infection is Fe limitation, where the large amount of Fe(III) is existed in either iron-transport proteins (transferrin and lactoferrin), stored intracellular

by ferritin or bound in heme molecules, leading to a decrease in the bioavailability of free Fe(III) (Skaar, 2010).

In order to support the survival and growth, bacterial pathogens have developed sophisticated strategies to capture Fe from the host. There are three main uptake mechanisms used by bacteria to acquire Fe from the host, which include: (1) siderophore-based systems, (2) heme-acquisition systems and (3) transferrin/lactoferrin receptors (Kelson et al., 2013; Pattus and Abdallah, 2000).

Siderophores are low molecular weight peptide-based compounds, which produced under Fe-limited conditions and secreted by bacteria to capture Fe(III) from the environment. There have been more than 500 different identified siderophores and classified into four main types (hydroxamate, catecholate, carboxylate and mixed type) based on their chemical structure and properties (Khan et al., 2018; Kircheva and Dudev, 2021). Most siderophores typically exhibit hexa- or tetradentate structure comprising various types of ligating groups and chelate Fe(III) with high affinity, and further transport Fe(III) into gram-negative or gram-positive bacterial cells via different specialized ATP-dependent receptor systems (Ferguson and Deisenhofer, 2002; Kelson et al., 2013; Khan et al., 2018; Khasheii et al., 2021; Krewulak and Vogel, 2008).

The most abundant form of Fe in vertebrates is bound within a porphyrin ring as ferriprotoporphyrin IX (heme), which existed in hemoglobin, myoglobin and heme-containing proteins (Tong and Guo, 2009). Besides siderophore-based systems, bacteria have also developed mechanisms to scavenge and transport Fe from heme-based sources of Fe. The heme acquisition systems in bacteria have one or two general mechanisms: (1) direct contact between the bacterium

and the exogenous heme-based Fe sources, and (2) production of extracellular hemophores that bind to heme with high affinity and transport back to specific membrane receptors (Cescau et al., 2007; Khasheii et al., 2021; Wandersman and Delepelaire, 2004; Wilks and Burkhard, 2007). Furthermore, some bacteria could capture Fe from transferrin and lactoferrin via receptors that directly recognize these Fe transport proteins (Kelson et al., 2013; Khasheii et al., 2021).

Ga(III) has been demonstrated that could tightly bind to bacterial siderophores, decreasing the level of metal-free siderophores extracted to the environment to capture Fe(III) (Kelson et al., 2013; Nicolafrancesco et al., 2019; Porcaro et al., 2017). Ga(III) could effectively function as an Fe(III) mimic to escape from the bacteria defensive system, recognized by the ATP-dependent receptor systems and further enter the bacterial cell as a siderophore complex. Therefore, the Fe-siderophore complex is expected to be blocked by Ga due to the high binding affinity, and intracellular Ga(III) which transported by Ga-siderophore complex could disrupt the bacterial iron homeostasis and redox biological processes (Braud et al., 2009a; Braud et al., 2009b; Kircheva and Dudev, 2020; 2021).

Considering Fe dependency in bacterial survival and growth, several studies have proposed anti-infective strategies by using both the siderophore and heme-acquisition systems, to enhance uptake of Ga(III) into bacterial cells. In addition, these strategies also have been evaluated using structural mimics of complex siderophores and hemes to deliver toxic drug conjugates and Ga(III) to target key pathogens (Juárez-Hernández et al., 2012; Khasheii et al., 2021; Möllmann et al., 2009; Nagoba and Vedpathak, 2011; Rodriguez et al., 2008; Stojiljkovic et al., 2001; Stojiljkovic et al., 1999). However,

it remains to be determined whether In(III) is suitable for use as an anti-infective agent as Ga(III) but with different biological half-life.

2.3.2 Action on Cellular Iron-Independent Processes

DNA synthesis and protein tyrosine phosphatase (PTP): Ga nitrate was a weak inhibitor of DNA synthesis in Jurkat human T leukemia cells (IC_{50} 2.8 mM), whereas Ga-hydrogen peroxide complex strongly inhibited DNA synthesis with an IC_{50}< 10 μM. Moreover, both Ga nitrate and Ga-hydrogen peroxide complex have been demonstrated to be potent inhibitors of detergent-solubilized cellular membrane PTP in Jurkat cells and HT-29 human colon cancer cells (Berggren et al., 1993).

The PTP superfamily of signaling enzymes functions in a coordinated manner with protein tyrosine kinases to control tyrosine phosphorylation, which is essential for regulating a variety of cellular processes, such as normal cell growth, differentiation, metabolism, the cell cycle, cell-to-cell communications, cell migration, gene transcription, ion channels, immune response and survival (Hunter, 2000; Tonks, 2006; Zhang, 2002). However, the inhibition of detergent-solubilized cellular membrane PTP induced by Ga nitrate and Ga-hydrogen peroxide complex appeared to have no correlation with growth-inhibitory activity in the two cell lines (Berggren et al., 1993).

Proteasome: The ubiquitin-proteasome system is a large protein complex responsible for degradation of intracellular proteins in eukaryotic cells, a process that requires metabolic energy. The proteasome is made up of two subcomplexes, a catalytic core particle (20S proteasome) and one or two terminal 19S regulatory particle(s) (Bard et al., 2018; Tanaka, 2009). The 26S proteasome not

only participates in protein and amino acid homeostasis but also regulates a diverse array of basic cellular activities, including the cell cycle, DNA replication, transcription, and signal transduction (Bhattacharyya et al., 2014; Collins and Goldberg, 2017; Finley, 2009; Goldberg, 2007).

Previous studies reported that Ga maltolate and the pyridine and phenolate ligand complexes of Ga inhibited proteasome function and induced apoptosis in cancer cells *in vitro* and a prostate cancer xenograft in a mice model (Chen et al., 2007; Chitambar and Purpi, 2010). The inhibition of synthetic Ga complexes appeared to have effects on not only 26S proteasome but also the chymotrypsin-like activity of 20S proteasome. Additionally, the inhibition of proteasomal chymotrypsin-like activity in prostate cancer cells was associated with down-regulation of androgen receptor and induction of apoptosis (caspase-3/caspase-7 activation). However, the exact toxic mechanisms for these Ga-related chemicals to interact with the proteasome need to be further investigated (Chen et al., 2007).

2.4 Current Knowledge on the Exposure and Health Risk of Ga and *In*

Since the first case of indium lung disease initially reported in Japan, there have been several case reports from the U.S., Taiwan and China as described previously. Faced with the case report of the first human case of indium lung disease, the Japanese Ministry of Health, Labor and Welfare (MHLW) has enacted a technical guideline for preventing health impairment of workers engaged in ITO-handling processes, which contains two occupational standards: (1) target concentration of environmental *In* is set at 0.01 mg *In*/m^3 as the respirable fraction of *In* particulate matter, (2) acceptable exposure concentration limit (AECL) is set at 3×10^{-4} mg *In*/m^3 that based on the animal carcinogenicity studies (MHLW, 2010).

The American Conference of Governmental Industrial Hygienists (ACGIH) has recommended a threshold limit value-time weighted average (TLV-TWA) of 0.1 mg *In*/m^3 (ACGIH, 2017), and the same 0.1 mg *In*/m^3 for total dust has been recommended as the recommended exposure limit (REL) by the National Institute for Occupational Safety and Health (NIOSH) (NIOSH, 2021). Moreover, almost 20 countries have issued a standards of permissible exposure limits for workers engaged in the production line of In-related chemicals, the eight-hour time-weighted average (TWA) is set at 0.1 mg *In*/m^3 (Table 2.3) (GESTIS, 2021). Corresponding the short-term exposure limit (STEL) does exist in a few countries, including Austria, Denmark, Ireland, United Kingdom and China, the range of STEL from 0.2-0.3 mg *In*/m^3 (Table 2.3) (GESTIS, 2021).

In addition to occupational exposure limits, the Japanese MHLW and Taiwan's Institute of Labor Occupational Safety and Health have requested the manufacturing factories to install equipment to control the diffusion of *In* into the air and monitor the concentration of *In* dust in the air for a period of time since 2012 to 2013 (Iwasawa et al., 2017; MHLW, 2013). Furthermore, employers are also obligated to provide *In*-handling workers with personal protective equipment (e.g., powered air-purifying respirators), and a medical examination at the start of employment and for a period of time thereafter (MHLW, 2010; 2013). Medical examination includes a questionnaire on respiratory symptoms, measurement of serum-*In* and/or KL-6 concentration, and a computed CT scan of the lungs (Chonan et al., 2019; MHLW, 2013). In addition, The Japan Society for Occupational Health (JSOH) recommended an occupational exposure limit based on the biomarker of serum-*In* is 3 μg/L (Iwasawa et al., 2017).

The tightening regulations in Japan and Taiwan is expected to reduce the severe consequences of long-term and high concentration *In* exposure. Nevertheless, it has reported that some workers continue to present with subjective complaints of respiratory symptoms (e.g., dry cough, sputum production) (Mitsuhashi, 2020). The retrospective cohort studies in Japan workers using health examination data from 2013 to 2015 (Mitsuhashi, 2020), suggesting that there was a significant large risk of subjective respiratory symptoms in the *In*-handling workers despite strengthened regulations. The main explanations include: (1) the subjective respiratory symptoms may have been caused by cumulative exposure, (2) the long biological half-life (8.09 years in average) of *In* in human body

(Amata et al., 2015), and (3) inappropriate use of personal protective equipment and unhealthy working conditions in small companies (Aiba et al., 1995).

Furthermore, the same observation was also confirmed in follow-up studies on Taiwan *In*-handling workers (Hsu et al., 2021; Institute of Labor Occupational Safety and Health, 2015). The workers have requested to wear powered air-purifying respirators since 2011, the average serum-*In* and urine-*In* levels declined after intervention and further decreased with time. However, the serum-*In* levels were increased in *In*-handling workers engaged in the recycling-crushing, powdering and bonding processes who regularly wore personal protective equipment (Hsu et al., 2021). Also, the levels of antioxidant enzymes (i.e., superoxide dismutase, glutathione peroxidase and glutathione transferase) and oxidative stress biomarkers (i.e., malondialdehyde, olive tail moment and 8-OH-dG) were increased, indicating that the levels of oxidative stress biomarkers did not response to the intervention (Institute of Labor Occupational Safety and Health, 2015).

Other studies reported that semiconductor and optoelectronic industries, electrical and electronic waste (e-waste) recycling have increased the occupational exposure risks of workers to not only Ga and *In* but also Al, As, Sb, Cr, Co, Pb, Hg and V (Chen, 2007b; Julander et al., 2014; Liao et al., 2004; Liao et al., 2006). At the present time, *In*, Al, As, Sb, Cr, Co, Pb, Hg and V have their own occupational exposure limit values except for Ga; Furthermore, the existing exposure limits of GaAs are generally based on the carcinogen of inorganic As (GESTIS, 2021).

The serum-*In*, urine-Ga, urine-As and serum-malondialdehyde levels were increased in optoelectronic workers, and the urine-Ga and As levels were positively correlated with serum-

malondialdehyde (Liao et al., 2004; Liao et al., 2006). Different task types could pose a higher risk on workers exposed to dust and surface contaminants of optoelectronic manufacturing equipment, workers engaged in fabrication equipment preventative maintenance, fabrication supervisors and engineers had higher urine-As levels than dopants and thin film workers (Liao et al., 2004).

In addition, the recycling workers in e-waste recycling plants also had greater airborne exposure, and the exposure biomarkers indicated higher concentrations of Cr, Co, *In*, Pb and Hg in blood, urine and/or serum. Concentrations of Sb, *In*, Pb, Hg and V showed close to linear correlation between the inhalable particle fraction and blood, serum or urine (Julander et al., 2014). Comparing the urinary concentrations of multiple trace elements to other studies, the abnormal metal levels in urine appeared to be associated with work environment (formal or informal recycling), work practices and the types of goods for recycling (Asante et al., 2012; Decharat, 2018; Gerding et al., 2021; Kuntawee et al., 2020; Takyi et al., 2021; Wang et al., 2011).

Although the health risk is still present in semiconductor, optoelectronic industries and e-waste recycling workers, tightening of occupational regulations in Japan and Taiwan have proved to control the increase in biomarkers which related to *In* bioaccumulation. However, there is still a need for long-term follow-up and routine health examination for evaluating the health effects and possibility of *In*-related lung cancer risks (Gerding et al., 2021; Nakano et al., 2019); additionally, a series of on-the-job training may improve the hazard identification and appropriate use of personal protective equipment, advanced dust management strategies and exposure limits among different work practices are required for reducing the airborne dust and the exposure of workers (Hsu et al., 2021).

Table 2.3 Occupational exposure limits for *In* and *In*-related chemicals

Country or region	Concentration (mg/m^3)	Interpretation [a]
Australia	0.1	TWA
Austria	0.1 (inhalable aerosol)	TWA
	0.2 (inhalable aerosol)	STEL
Belgium	0.1	TWA
Canada – Ontario	0.1	TWA
Canada - Québec	0.1	TWA
Denmark	0.1	TWA
	0.2	STEL
Finland	0.1	TWA
Ireland	0.1	TWA
	0.3 (15 minutes reference period)	STEL
New Zealand	0.1	TWA
Norway	0.1	TWA
China	0.1	TWA
	0.3 (15 minutes average value)	STEL
Singapore	0.1	TWA
South Korea	0.1	TWA
Spain	0.1	TWA
Sweden	0.1	TWA
Switzerland	0.1 (inhalable aerosol)	TWA
USA – NIOSH [b]	0.1	TWA (REL)
United Kingdom	0.1	TWA
	0.3	STEL

Reference: GESTIS (GESTIS-Substance Database) 2021. IFA (Institut fur Arbeitsschutz). Available from: https://limitvalue.ifa.dguv.de/, accessed 10 November 2021.

Note: [a] TWA, time-weighted average; STEL, short-term exposure limit; REL, recommended exposure limit.

[b] NIOSH, National Institute for Occupational Safety and Health.

3. Research Purpose

In medical applications, Ga and *In* could serve as Fe-mimicking agents, a trojan horse strategy for the Fe-searching cancer cells and pathogens. Except for the Fe deprivation condition, intracellular Ga(III) and/or In(III) also could inhibit cellular Fe-dependent and -independent processes, including DNA synthesis, mitochondrial function, heme synthesis, Zn homeostasis, protein tyrosine phosphatase and proteasome activity. The effects of anticancer and antimicrobial therapies of Ga and/or *In* appeared to vary widely based on the bioavailability of chemicals, Fe requirement, Fe uptake and transport mechanisms.

Furthermore, the workers engaged in semiconductor, optoelectronic manufacturing and e-waste recycling progresses are potentially exposed to a variety of metals and metalloids such as Ga, *In*, As and Sb. Occupational inhalation exposure to *In*-related chemical dusts (e.g., ITO, $In_2O_{3(s)}$ and $In(OH)_{3(s)}$) have been demonstrated to cause indium lung disease. So far, the entire pathogenesis of the occupational disease remains elusive, the available evidence indicates that the disease progression is closely associated with dissolved and accumulated In(III) in the body.

Although there has been progress in investigating and understanding the interaction of Ga and *In* with biological systems, much remains to be learned about their interaction with other Fe-dependent and -independent processes. Additionally, the biological factors related to the relatively short latency period between indium lung disease and other pneumoconiosis also need to be

determined, which may be associated with long-term health risk such as chronic inflammation, cellular aging (senescence) and carcinogenicity.

Therefore, the research purpose of this study is to explore the biological factors or modes of action that potentially associated with the long-term health effects of Ga and *In* exposure and the progression of indium lung disease.

4. Model Organism

The human colon carcinoma cell line DLD-1 was used in this study, established from an adenocarcinoma of the sigmoid colon (Dexter et al., 1981). DLD-1 cells were moderately to poorly differentiated epithelial cells, and these cells generally have two distinct morphologies. One type of the cells (clone A) was larger, and the individual cells were easily identified, the others (clone D) were packed tightly, and the individual cell boundaries were difficult to recognize. The two clones appeared to responsible for the phenotypic heterogeneity and chemotherapeutic sensitivity of the cancer cells (Dexter et al., 1981).

The established human breast cancer cell line (MCF-7) expressing enhanced green fluorescent protein (EGFP)-fused mediator of DNA damage checkpoint 1 (MDC1) was also used for screening the genotoxicity of Ga- and In-related chemicals (Matsuda et al., 2014). The MCF-7 cell line was derived from a pleural effusion of a malignant breast cancer with metastatic mammary carcinoma (Soule et al., 1973). MCF-7 cells contain functional estrogen receptors and show a pleiotropic response to estrogen, which is widely studied model for hormone-dependent human breast cancer (Thompson et al., 1988). Furthermore, the biomarker of histone H2AX phosphorylated at Ser139 (γ-H2AX) in combination with MDC1 protein, are key DNA repair and DNA damage response (DDR) proteins. When DNA double-strand breaks (DSB) occur, γ-H2AX is phosphorylated and then recruits MDC1 proteins, thus forms nuclear foci in the same location as γ-H2AX in response to DNA damage (Matsuda et al., 2014; Salguero et al., 2019).

5. Materials and Methods

5.1 Research Design

In this study, firstly DLD-1 cells were exposed with Ga- and *In*-related chemicals in a wide range of concentrations to evaluate the cell viability (LC_{50}). Secondly, the sublethal doses were determined by considering calculated LC_{50} and the average workplace exposure of *In*-based chemicals (Badding et al., 2014; Olgun et al., 2017). Sublethal effects of cytotoxicity (programmed cell death and cell cycle), morphological alterations, mitochondrial dysfunction, cellular senescence, and other possible toxicity (proteasome inhibition and genotoxicity) were further performed to assess the biological factors and toxic mechanisms that potentially related to the long-term health effects of Ga and *In* occupational exposure and the progression of indium lung disease. The casual research scheme is illustrated in Figure 5.1.

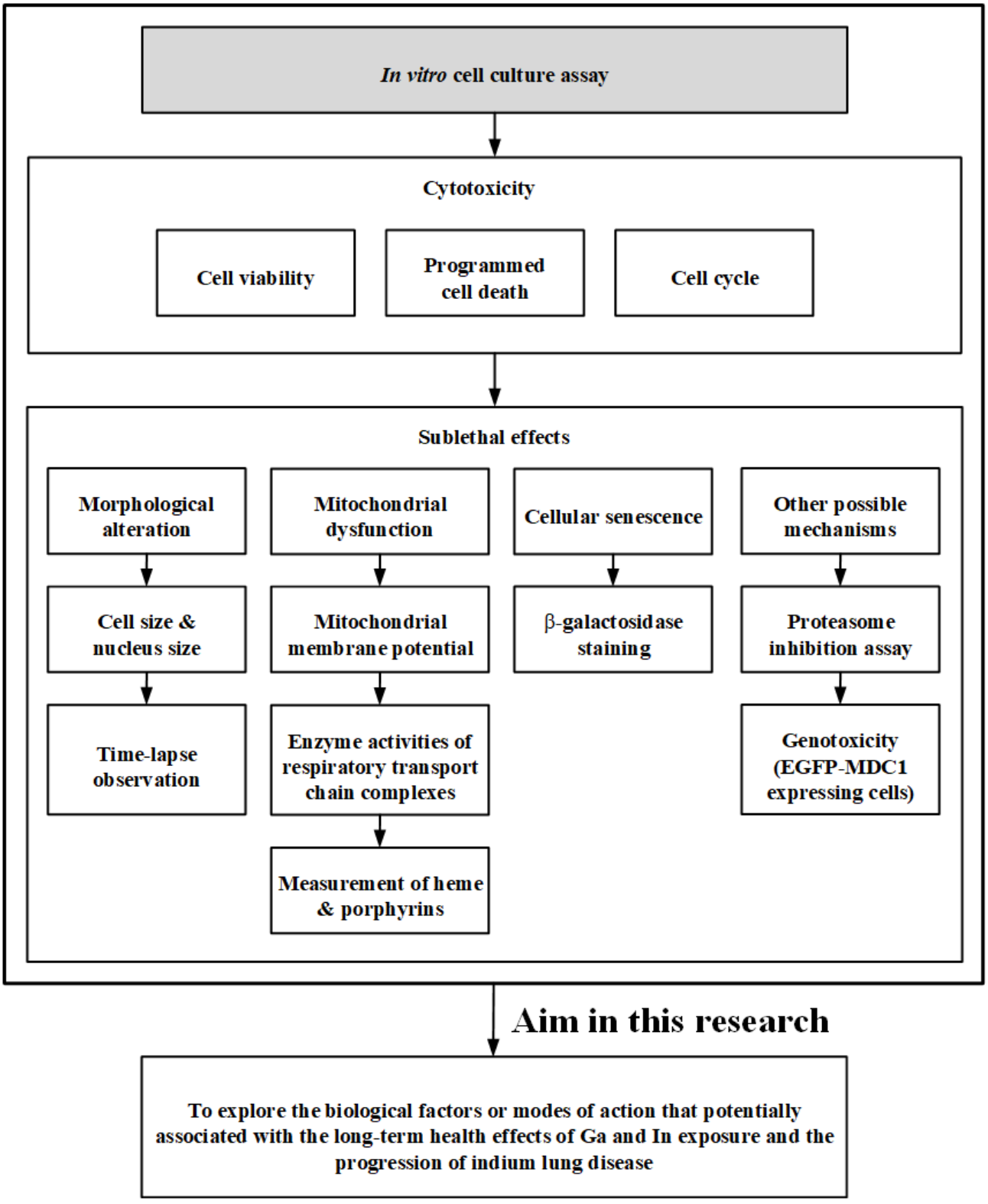

Figure 5.1 Scheme in *in vitro* toxicity assessment of Ga and *In* in human cell lines.

5.2 Cell line and Cell Culture

The human colon carcinoma cell line DLD-1 was maintained in high-glucose RPMI-1640 medium (Wako, Osaka, Japan) containing 10% fetal bovine serum (FBS, Invitrogen, Thermo Fisher Scientific, Inc., Waltham, MA, USA) at 37 °C under 5% CO_2.

The EGFP-MDC1 expressing MCF-7 cells were obtained as described in Matsuda et al. (2014). The EGFP-MDC1 MCF-7 cells were cultured in high-glucose RPMI-1640 medium containing 10% FBS at 37 °C and 5% CO_2 under moderate humidity.

5.3 Preparation of Exposure Solutions

Gallium(III) chloride anhydrous ($GaCl_3$), indium(III) chloride tetrahydrate ($InCl_3 \cdot 4H_2O$), indium hydroxide ($In(OH)_3$), indium oxide (In_2O_3), gallium oxide (Ga_2O_3) and sodium citrate dihydrate ($C_6H_5Na_3O_7 \cdot 2H_2O$) were used to prepare exposure solutions. $GaCl_3$ and $InCl_3 \cdot 4H_2O$ salts were used to prepare Ga(III), citrate-Ga(III), In(III) and citrate-In(III) stock solutions.

The stock solutions of aqueous insoluble chemicals including $In(OH)_3$ (8.71 mM of *In*), In_2O_3 (8.71 mM of *In*), and Ga_2O_3 (14.34 mM of Ga), which were freshly prepared by spiking the required amounts of compounds in ultrapure water and then sonicated for 30 minutes before preparing exposure solutions.

Ga(III) and In(III) stock solutions (8.71 mM of *In*, 14.34 mM of Ga) were freshly prepared by dissolving $GaCl_3$ and $InCl_3 \cdot 4H_2O$ salts in ultrapure water and filtered through 0.22-μm sterile syringe filters (Millex GV, hydrophilic PVDF membrane, 0.22-μm; Merck Millipore, Germany). Ga(III) and

In(III) are prone to hydrolysis in the circumneutral pH condition, citrate was also used as a metal chelating agent to prevent $In(OH)_{3(s)}$, $Ga(OH)_{3(s)}$ and $Ga(OH)_4^-$ formation in RPMI-1640 medium. The stock solutions of Ga and *In* were supplied with citrate at a molar ratio of 1:1 (metal: citrate) (Zeng et al., 2017), then filtered through 0.22-μm sterile syringe filters.

5.4 Cell Viability Assay (MTT Test)

DLD-1 cells were seeded at 1.0×10^4 cells per well in 96-well plates with 200 μL RPMI-1640 medium containing 10% FBS and incubated for 24 hours at 37 °C and 5% CO_2. After 24 hours, the medium was removed and the cells were treated with different exposure solutions (200 μL/well), incubated at 37 °C and 5% CO_2 for 72 hours. *In* concentrations of In(III), citrate-In(III), $In(OH)_{3(s)}$ and $In_2O_{3(s)}$ in solutions ranged from 8.71 μM to 2.18 mM, and the Ga concentrations of Ga(III), citrate-Ga(III) and $Ga_2O_{3(s)}$ ranged from 14.3 μM to 3.59 mM.

At two hours prior to the endpoint time, 20 μL of water-soluble yellow dye MTT [3-(4,5-dimethylthiazol-2-yl)-2,5-diphenyltetrazolium bromide] stock solution (5 mg/mL, dissolved in PBS) was added to each well, incubated the 96-well plates for two hours at 37 °C and 5% CO_2. A negative control was also prepared by adding 20 μL of the MTT stock solution to 200 μL of RPMI-1640 medium containing 10% FBS alone. After incubation, the exposure solutions were removed and 100 μL of dimethyl sulfoxide (DMSO) added to each well to solubilize formazan crystals, mix thoroughly with a pipette and incubated the 96-well plates for 30 minutes at 37 °C, protected from light. Mix

each sample again using a pipette and the absorbance was read in a spectrophotometer (FilterMax F5 Multi-Mode Microplate Reader, Molecular Devices, CA, USA) at 595 nm.

5.5 Flow Cytometry for Evaluation of Apoptosis

The apoptosis of DLD-1 cells, including the percentage of live, early apoptotic, late apoptotic and dead cells, were measured using the multifunctional Muse™ Annexin V and Dead Cell Kit (Merck Millipore, MA, USA) according to the user's guide and the manufacturer's instructions.

Briefly, DLD-1 cells (2.0×10^5 cells) were seeded in 60 mm petri dishes with 6 mL RPMI-1640 medium containing 10% FBS and incubated for 24 hours at 37 °C and 5% CO_2. After 24 hours, the medium was removed and the cells were washed two times in pre-warmed pH 7.4 phosphate buffered saline (PBS), then treated with different dosing solutions and incubated at 37 °C, 5% CO_2 for 72 hours. *In* concentrations of In(III), citrate-In(III), $In(OH)_{3(s)}$ and $In_2O_{3(s)}$ in exposure solutions were 0.0435 mM and 0.435 mM, Ga concentrations of Ga(III) and citrate-Ga(III) were 0.0215 mM and 0.215 mM, and 0.717 mM for $Ga_2O_{3(s)}$.

After exposure for 72 hours, the exposure solutions were removed, and the cells were washed twice in pre-warmed PBS. The cells were then harvested with TrypLE™ Express Enzyme (Gibco, Thermo Fisher Scientific, Inc., MA, USA). Fresh RPMI-1640 medium containing 10% FBS was added to each treatment to a final concentration of 2.0×10^5 cells/mL. Staining procedures included warming the Muse™ Annexin V and Dead Cell Reagent to room temperature, then 100 µL of cell suspension was added to each tube, further addition of 100 µL of the Muse™ Annexin V and Dead

Cell Reagent to each tube, and mixing thoroughly by vortexing at a medium speed for five seconds. Samples were incubated for 20 minutes at room temperature in the dark. The percentage of apoptotic cells was analyzed by flow cytometry using Muse™ Cell Analyzer (Merck Millipore, MA, USA) system and were expressed as percentage of apoptotic cells with standard deviation. The RPMI-1640 medium containing 10% FBS was used as a negative control.

5.6 Flow Cytometry for Cell Cycle Analysis

The cell cycle of DLD-1 cells, including the percentage of G_0/G_1, S, G_2/M phase and debris were measured using the multifunctional Muse™ Cell Cycle Kit (Merck Millipore, MA, USA) according to the user's guide and the manufacturer's instructions.

Briefly, DLD-1 cells (2.0×10^5 cells) were seeded in 60 mm petri dishes with 6 mL RPMI-1640 medium containing 10% FBS and incubated for 24 hours at 37 °C and 5% CO_2. After 24 hours, the medium was removed and the cells were washed two times in PBS, then treated with different dosing solutions and incubated at 37 °C, 5% CO_2 for 72 hours. *In* concentrations of In(III), citrate-In(III), $In(OH)_{3(s)}$ and $In_2O_{3(s)}$ in exposure solutions were 0.0435 mM and 0.435 mM, Ga concentrations of Ga(III) and citrate-Ga(III) were 0.0215 mM and 0.215 mM, and 0.717 mM for $Ga_2O_{3(s)}$. The RPMI-1640 medium containing 10% FBS was used as a negative control, and the 5 μM deferoxamine mesylate (DFO) was used as a positive control.

After exposure for 72 hours, the dosing solutions were removed, and the cells were washed twice in pre-warmed PBS. The cells were then harvested with TrypLE™ Express Enzyme. The minimum

number of cells for further fixation in a tube was 1.0×10^6 cells. Samples collected were gently centrifuged for five minutes at 300×g (KUBOTA 5200 Centrifuge, Kubota Corporation, Osaka, JAPAN) and washed with PBS. Leave approximately 50 μL of PBS per 1.0×10^6 cells, resuspended cell pellets and dropped-wise into the tube containing 1 mL of ice-cold 70% ethanol while vortexing at medium speed. The fixed samples were kept in -20°C for 24 hours until cell cycle was assayed.

The fixed samples were gently centrifuged for five minutes at 300×g at room temperature and washed with PBS. The cell pellets were resuspended in 0.25 mL PBS per 5.0×10^5 cells and centrifuged for five minutes at 300×g. The cell pellets were resuspended in 200 μL of Muse™ Cell Cycle Reagent, incubated for 30 minutes at room temperature in the dark. The cell suspensions were transferred to 1.5 mL microcentrifuge tubes prior to analysis. The cell cycle was assayed by fluorescence-activated cell sorting analysis using a flow cytometry of Muse™ Cell Analyzer system.

5.7 Cell Morphology

5.7.1 Measurement of Cell Size and Nucleus Size

DLD-1 cells (5.0×10^4 cells) were seeded in 35 mm petri dishes with 2 mL RPMI-1640 medium containing 10% FBS and incubated for 24 hours at 37 °C and 5% CO_2. After 24 hours, the medium was removed and the cells were washed two times in pre-warmed PBS, then treated with different dosing solutions and incubated at 37 °C, 5% CO_2 for 72 hours. *In* concentrations of In(III) and citrate-In(III) in exposure solutions were 0.0435 mM and 0.435 mM, and Ga concentrations of Ga(III) and

citrate-Ga(III) were 0.0215 mM and 0.215 mM. The RPMI-1640 medium containing 10% FBS was used as a negative control, and the 5 μM DFO was used as a positive control.

After exposure for 72 hours, the dosing solutions were removed, and the cells were washed twice in pre-warmed PBS. The cells were then fixed with pre-warmed 4% formaldehyde solution (in PBS) at 37 °C for ten minutes. The fixative solution was removed and washed the cells with pre-warmed PBS for three times. The pre-warmed 10 μg/mL Hoechst 33342 working solution (Dojindo Laboratories, Kumamoto, Japan) was added to each treatment and stained for one hour. After staining, the Hoechst 33342 solution was removed and the cells were washed with PBS, then 3 mL of PBS was added to each treatment. The cell size, morphology and nucleus were observed by using inverted fluorescence phase-contrast microscope (BZ-9000, Keyence, Osaka, Japan), coupled with BZ-II viewer software (Keyence, Osaka, Japan).

Both phase contrast and blue fluorescent (ex/em: 350/461 nm) images were acquired by fluorescence microscopy with a 20x objective (Plan Fluor/0.45 numerical aperture; Nikon). 20-30 field were randomly selected and imaged in each treatment, and the semiautomated image analysis was determined by using Fiji/ImageJ software (Hartig, 2013; Jensen, 2013). The “Set Scale” function was firstly used to calibrate image distance of pixels/μm. The cell area was manually drawn around cells using the “Polygon” selection tool and adding all regions of interests (ROI) to a list by choosing “Add to Manager” function. The cellular size and shape measurements were calculated by using the “Set Measurements” and “Measure” function in the “Analyze” menu, the Area was checked in the “Set Measurements” window.

The threshold of blue fluorescent images (cell nucleus) was adjusted by selecting “Default” as thresholding method and moving sliding bars in the “Threshold” window. The “Set Scale” function in the “Analyze” menu was used to calibrate image distance of pixels/μm. Nucleus area of each cell was further selected by the “Analyze Particles” function, the results were added to ROI Manager and saved their positions on the image. The nucleus area measurements were calculated by using the “Set Measurements” and “Measure” function in the “Analyze” menu, the Area, integrated density, mean grey value, limit to threshold, and display label were checked in the “Set Measurements” window.

5.7.2 Time-Lapse Life Cell Imaging Microscopy

DLD-1 cells (1.0×10^4 cells) were seeded in 35 mm petri dishes with 2 mL RPMI-1640 medium containing 10% FBS and placed on the stage of inverted fluorescence phase-contrast microscope with a 20x objective (Plan Fluor/0.45 numerical aperture), in a temperature- and CO_2-controlled humid incubation system (ToKai Hit, Shizuoka, Japan), incubated for 24 hours. After 24 hours, the medium was removed and the cells were washed two times in pre-warmed PBS, then treated with exposure solutions and incubated for 72 hours. The concentrations of Ga(III) and In(III) were 0.215 mM and 0.435 mM, respectively.

The real-time images were obtained with inverted fluorescence phase-contrast microscope and BZ-II viewer software, controlling a 1.5-million-pixel monochrome CCD (2/3 inch), electronic XY and Z stage, the Z-stack series consisted of 6 μm slice intervals. Two to three points were marked and

labeled with their coordinates, and the images (1360×1024 pixels) were acquired per 15 minutes, with a recording time of 72 hours.

5.8 Measurement of Mitochondrial Membrane Potential (ψ_m)

DLD-1 cells (2.0×10^5 cells) were seeded in 60 mm petri dishes with 6 mL RPMI-1640 medium containing 10% FBS and incubated for 24 hours at 37 °C and 5% CO_2. The medium was removed and the cells were washed two times in pre-warmed PBS, then treated with different dosing solutions and incubated at 37 °C, 5% CO_2 for 72 hours. *In* concentration of In(III), citrate-In(III), $In(OH)_{3(s)}$ and $In_2O_{3(s)}$ in exposure solutions was 0.435 mM, Ga concentrations of Ga(III) and citrate-Ga(III) were 0.0215 mM and 0.215 mM, and 0.717 mM for $Ga_2O_{3(s)}$. The RPMI-1640 medium containing 10% FBS was used as a negative control, and the 5 μM DFO was used as a positive control.

After exposure for 72 hours, the dosing solutions were removed, and the cells were washed twice in pre-warmed PBS. The cells were then treated with pre-warmed staining solution containing 100 nM MitoTracker™ Red CMXRos (Invitrogen, Thermo Fisher Scientific, Inc., MA, USA) for 30 minutes, washed two times with pre-warmed PBS. The cells were then fixed with pre-warmed 4% formaldehyde solution (in PBS) at 37 °C for ten minutes. The fixative solution was removed and washed the cells with pre-warmed PBS for three times. The pre-warmed Hoechst 33342 working solution (10 μg/mL in PBS) was added to each treatment and stained for one hour. After staining, the Hoechst 33342 working solution was removed and the cells were washed with pre-warmed PBS, then 3 mL of PBS was added to each treatment. The mitochondrial membrane potential in each treatment

was observed by using inverted fluorescence phase-contrast microscope, and the Hoechst 33342 staining was used in cell identification.

Both phase contrast, blue (ex/em: 350/461 nm) and red fluorescent (ex/em: 579/599 nm) images were acquired by inverted fluorescence phase-contrast microscope with a 20x objective (Plan Fluor/0.45 numerical aperture). 20-30 field were randomly selected and imaged in each treatment, and quantitative analysis were performed using Fiji/ImageJ software (Hartig, 2013; Jensen, 2013), expressed as percent (%) fluorescent intensity (red) compared to negative control.

The fluorescent images were firstly converted to monochrome image (16-bit) by using the "Type" function in the "Image" menu, and the "Set Scale" function in the "Analyze" menu was used to calibrate image distance of pixels/μm. The threshold of the images was adjusted by selecting "Li" as thresholding method (Li's Minimum Cross Entropy thresholding method). The fluorescent area of each cell was further selected by the "Analyze Particles" function, the results were added to ROI Manager and saved their positions on the image. The fluorescent intensity measurements were calculated by using the "Set Measurements" and "Measure" function in the "Analyze" menu, the Area, integrated density, mean grey value, limit to threshold, and display label were checked in the "Set Measurements" window.

5.9 Enzymatic Activities Assay of Mitochondrial Respiratory Chain Complexes I-IV

The measurement of the enzymatic activities of mitochondrial respiratory chain (RC) complexes I, II, III, IV, and citrate synthase (Table 5.1), a mitochondrial matrix enzyme that commonly used to normalize the results of the assays for the RC enzymes, have been published in detail elsewhere (Spinazzi et al., 2012).

DLD-1 cells were seeded in 150 mm (1.0×10^6 cells) petri dishes with 20 mL RPMI-1640 medium containing 10% FBS and incubated for 24 hours at 37 °C and 5% CO_2. After 24 hours, the medium was removed and the cells were washed two times in pre-warmed PBS, then treated with different exposure solutions and incubated at 37 °C, 5% CO_2 for 72 hours. *In* concentrations of In(III) and citrate-In(III) in exposure solutions were 0.0435 mM and 0.435 mM, and Ga concentrations of Ga(III) and citrate-Ga(III) were 0.0215 mM and 0.215 mM. The RPMI-1640 medium containing 10% FBS was used as a negative control, and the 5 μM DFO was used as a positive control. Sample preparation and spectrophotometric RC enzyme analysis are summarized below (Table 5.2).

Table 5.1 Spectrophotometric RC enzyme analysis

Complex(es) analyzed	Comment
Complex I	NADH: ubiquinone oxidoreductase
Complex II	Succinate dehydrogenase
Complex III	Decylubiquinol cytochrome *c* oxidoreductase
Complex IV	Cytochrome *c* oxidase
Citrate synthase	A mitochondrial matrix enzyme of citric acid cycle

Preparation of cell lysate: After exposure for 72 hours, the exposure solutions were removed and the cells in 150 mm petri dishes were washed twice in pre-warmed PBS. The cells were then harvested with TrypLE™ Express Enzyme. The minimum number of cells for further analysis in a tube was 5.0×10^6 cells. Samples collected were gently centrifuged for five minutes at 1,000×g at 4 °C (TOMY MX-301, Tokyo, Japan) and washed two times in ice-cold PBS. The supernatants were removed, and the cell pellets were flash-frozen in liquid nitrogen and stored at -80 °C until use (up to two weeks). The cell pellets were resuspended in 0.5 mL of ice-cold 20 mM hypotonic potassium phosphate buffer (pH 7.5) for ten minutes at 4 °C, and the cell suspensions were then homogenized with a 2-mL glass tissue grinder (DWK Life Science, Wheaton, Millville, NJ, USA) with a tight clearance kept on ice with 20 slow up-down strokes. The cell lysates were flash-frozen in liquid nitrogen and thawed at 37 °C for three times and kept on ice for the RC complexes (II, III and IV) and citrate synthase analysis. A 1.0-µL aliquot of cell lysate for total protein concentration measurements according to the Qubit™ Protein and Protein Broad Range (BR) Assay Kits (Invitrogen, Thermo Fisher Scientific, Inc., MA, USA) and the Qubit 2.0 fluorometer (Invitrogen, Thermo Fisher Scientific, Inc., MA, USA).

Preparation of mitochondrial-enriched fraction: After exposure for 72 hours, the dosing solutions were removed and the cells in 150 mm petri dishes were washed twice in PBS. The cells were then harvested with TrypLE™ Express Enzyme. The minimum number of cells for further analysis in a tube was 1.0×10^7 cells. Samples collected were gently centrifuged for five minutes at 1,000×g at 4 °C and washed two times in ice-cold PBS. The supernatants were removed, and the cell

pellets were flash-frozen in liquid nitrogen and stored at -80 °C until use (up to two weeks). The cell pellets were resuspended in 0.5 mL of ice-cold 10 mM hypotonic Tris buffer (pH 7.6) for ten minutes at 4 °C, and the cell suspensions were then homogenized with a 2-mL glass tissue grinder with a tight clearance kept on ice with 20 slow up-down strokes. The cell lysates were centrifuged for ten minutes at 2,500×g at 4 °C and washed in ice-cold PBS, transferred the cell supernatants to new centrifuge tubes and repeated the centrifugation step. The cell supernatants were further centrifuged for ten minutes at 15,000×g at 4 °C, discarded the supernatants and wash the mitochondrial-enriched pellets in 100 µL of ice-cold 250 mM sucrose and $T_{10}E_{20}$ (10 mM Tris-HCl, 20 mM EDTA) solution. The mitochondrial-enriched pellets were resuspended in 50 µL of ice-cold 250 mM sucrose and $T_{10}E_{20}$. The mitochondrial-enriched fractions were flash-frozen in liquid nitrogen and thawed at 37 °C for three times and kept on ice for the RC complex I analysis. A 1.0-µL aliquot of mitochondrial-enriched fraction for total protein concentration measurements according to the Qubit™ Protein and Protein Broad Range (BR) Assay Kits.

Complex I (NADH: ubiquinone oxidoreductase) activity: 25-µg of isolated mitochondrial-enriched fraction from DLD-1 cells were added to a 1-mL quartz cuvette (GL Sciences Inc., Tokyo, Japan) containing 700 µL of ultrapure water. 100 µL of potassium phosphate buffer (0.5 M, pH 7.5), 60 µL of fatty acid-free BSA (50 mg/mL), 30 µL of KCN (10 mM) and 10 µL of NADH (10 mM) were added to the cuvette. The total reaction volume was adjusted to 994 µL with ultrapure water. The reaction solution was mixed by inverting the cuvette using Parafilm and followed the decrease of absorbance at 340 nm for two minutes. The positive control was prepared by using a separate

cuvette containing the same quantity of reagents and sample (negative control) but with the addition of 10 µL of 1 mM rotenone solution. The reaction was started by adding 6 µL of ubiquinone$_1$ (10 mM), mixed by inverting the cuvette using Parafilm and followed the decrease of absorbance at 340 nm for two minutes inside the spectrophotometer (Aqualog, HORIBA, Kyoto, Japan). The enzymatic activity of complex I is calculated as nmol min^{-1} mg^{-1} of protein according to the following equation:

Enzymatic activity of complex I (nmol min^{-1} mg^{-1}) = (ΔAbsorbance/min × 1,000)/ [(extinction coefficient × volume of sample used in mL) × (sample protein concentration in mg mL^{-1})]. The extinction coefficient for NADH is 6.2 mM^{-1} cm^{-1}.

Complex II (succinate dehydrogenase) activity: 600 µL of ultrapure water, 50 µL of potassium phosphate buffer (0.5 M, pH 7.5), 20 µL of fatty acid–free BSA (50 mg/mL), 30 µL of KCN (10 mM), 50 µL of succinate (400 mM), 145 µL of 2,6-dichlorophenol indophenol (DCPIP, 0.015 % (wt/vol)) and 25 µg of cell lysate were added to a 1-mL quartz cuvette. The total reaction volume was adjusted to 996 µL with ultrapure water. The reaction solution was mixed by inverting the cuvette using Parafilm and incubated inside the spectrophotometer at 37 °C for ten minutes, the baseline activity was read at 600 nm for the last two minutes. The positive control was prepared by using a separate cuvette containing the same quantity of reagents and sample (negative control) but with the addition of 10 µL of 1 M malonate solution. The reaction was started by adding 4 µL of decylubiquinone (DUB, 12.5 mM), mixed by inverting the cuvette using Parafilm and followed the decrease of absorbance at 600 nm for three minutes. The enzymatic activity of complex II is calculated as nmol min^{-1} mg^{-1} of protein according to the following equation:

Enzymatic activity of complex II (nmol min^{-1} mg^{-1}) = (ΔAbsorbance/min × 1,000)/ [(extinction coefficient × volume of sample used in mL) × (sample protein concentration in mg mL^{-1})]. The extinction coefficient for DCPIP is 19.1 mM^{-1} cm^{-1}.

Table 5.2 Conditions for spectrophotometric assays of RC enzymes and citrate synthase activities in cultured cells

	Complex I	Complex II	Complex III	Complex IV	Citrate synthase
λ (nm)	340	600	550	550	412
ε ($mmol^{-1}$ cm^{-1})	6.2	19.1	18.5	18.5	13.6
Buffer	KP, 50 mM	KP, 25 mM	KP, 25 mM	KP, 25 mM	Tris, 100 mM
pH	7.5	7.5	7.5	7.0	8.0
Substrates/ electron acceptors	NADH, 100 μM Ub_1, 60 μM	Succinate, 20 mM DCPIP, 80 μM DUB, 50 μM	$DubH_2$, 100 μM Cyt c, 75 μM	Cyt c H_2, 50 μM	DTNB, 100 μM Ac CoA, 300 μM
Detergent	-	-	Tween-20 (0.025 % (vol/vol))	-	Triton X-100 (0.1 % (vol/vol))
Other reagent(s)	BSA, 3 mg mL^{-1} KCN, 300 μM	BSA, 1 mg mL^{-1} KCN, 300 μM	KCN, 500 μM EDTA, 100 μM	-	-
Specific inhibitor	Rotenone, 10 μM	Malonate, 10 mM	Antimycin A, 10 μg mL^{-1}	KCN, 300 μM	-

Note: λ, selected wavelength for the assay; ε, extinction coefficient; Ac CoA, acetyl coenzyme A; BSA, fatty acid–free bovine serum albumin; Cyt c, cytochrome *c*; Cyt c H_2, reduced cytochrome *c*; DCPIP, 2,6-dichlorophenolindophenol; DUB, decylubiquinone; $DubH_2$, decylubiquinol; DTNB, 5,5'-dithiobis(2-nitrobenzoic acid); KCN, potassium cyanide; KP, potassium phosphate buffer; Tris, Tris buffer; Ub_1, ubiquinone$_1$.

Complex III (decylubiquinol cytochrome *c* oxidoreductase) activity: 730 µL of ultrapure water, 50 µL of potassium phosphate buffer (0.5 M, pH 7.5), 75 µL of oxidized cytochrome *c* (1 mM), 50 µL of KCN (10 mM), 20 µL of EDTA (5 mM, pH 7.5), 10 µL of Tween-20 (2.5 % (vol/vol)) and 15 µg of cell lysate were added to a 1-mL quartz cuvette. The total reaction volume was adjusted to 990 µL with ultrapure water. The reaction solution was mixed by inverting the cuvette using Parafilm and read the baseline at 550 nm for two minutes. The positive control was prepared by using a separate cuvette containing the same quantity of reagents and sample (negative control) but with the addition of 10 µL of 1 mg/mL antimycin A solution. The reaction was started by adding 10 µL of decylubiquinol (10 mM), mixed rapidly by inverting the cuvette using Parafilm and then immediately observed the increase in absorbance at 550 nm for two minutes. The enzymatic activity of complex III is calculated as nmol min^{-1} mg^{-1} of protein according to the following equation:

Enzymatic activity of complex III (nmol min^{-1} mg^{-1}) = (ΔAbsorbance/min × 1,000)/ [(extinction coefficient × volume of sample used in mL) × (sample protein concentration in mg mL^{-1})]. The extinction coefficient for reduced cytochrome *c* is 18.5 mM^{-1} cm^{-1}.

Complex IV (cytochrome *c* oxidase) activity: 400 µL of ultrapure water, 250 µL of potassium phosphate buffer (100 mM, pH 7.0), and 50 µL of reduced cytochrome *c* (1 mM) were added to a 1-mL quartz cuvette and the baseline activity was read at 550 nm for two minutes. The total reaction volume was adjusted to 995 µL with ultrapure water. The positive control was prepared by using a separate cuvette containing the same quantity of reagents and sample (negative control) but with the addition of 30 µL of 10 mM KCN solution. The reaction was started by adding 5 µL of cell lysate (5-

40 µg), mixed by inverting the cuvette using Parafilm and read the decrease of absorbance at 550 nm for three minutes. The enzymatic activity of complex IV is calculated as nmol min^{-1} mg^{-1} of protein according to the following equation:

Enzymatic activity of complex IV (nmol min^{-1} mg^{-1}) = (ΔAbsorbance/min × 1,000)/ [(extinction coefficient × volume of sample used in mL) × (sample protein concentration in mg mL^{-1})]. The extinction coefficient for reduced cytochrome *c* is 18.5 mM^{-1} cm^{-1}.

Citrate synthase activity: 300 µL of ultrapure water, 500 µL of Tris (200 mM, pH 8.0) with Triton X-100 (0.2% (vol/vol)), 100 µL of 5,5'-dithiobis-(2-nitrobenzoic acid) (DTNB, 1 mM), 30 µL of acetyl coenzyme A (10 mM), and 25 µg cell lysate were added to a 1-mL quartz cuvette. The total reaction volume was adjusted to 950 µL with ultrapure water. The reaction solution was mixed by inverting the cuvette using Parafilm and read the baseline at 412 nm for two minutes. The reaction was started by adding 50 µL of oxaloacetic acid (10 mM), mixed by inverting the cuvette using Parafilm and read the increase in absorbance at 412 nm for three minutes. The enzymatic activity of citrate synthase is calculated as nmol min^{-1} mg^{-1} of protein according to the following equation:

Enzymatic activity of citrate synthase (nmol min^{-1} mg^{-1}) = (ΔAbsorbance/min × 1,000)/ [(extinction coefficient × volume of sample used in mL) × (sample protein concentration in mg mL^{-1})]. The extinction coefficient is 13.6 mM^{-1} cm^{-1}.

5.10 Measurement of Mitochondrial Heme, Protoporphyrin IX (PPIX) and Zinc Protoporphyrin IX (ZnPPIX)

5.10.1 Sample Preparation

DLD-1 cells (1.0×10^6 cells) were seeded in 150 mm petri dishes with 20 mL RPMI-1640 medium containing 10% FBS and incubated for 24 hours at 37 °C and 5% CO_2. After 24 hours, the medium was removed and the cells were washed two times in pre-warmed PBS, then treated with different dosing solutions and incubated at 37 °C, 5% CO_2 for 72 hours. *In* concentrations of citrate-In(III) in exposure solutions were 0.0435 mM and 0.435 mM, and the Ga concentrations of citrate-Ga(III) were 0.0215 mM and 0.215 mM. The RPMI-1640 medium containing 10% FBS was used as a negative control, and the 5 μM DFO was used as a positive control.

Preparation of mitochondrial-enriched fraction: After exposure for 72 hours, the exposure solutions were removed and the cells in two 150 mm petri dishes were washed twice in pre-warmed PBS. The cells were then harvested with TrypLE™ Express Enzyme. Samples collected were gently centrifuged for five minutes at 1,000×g at 4 °C and washed two times in ice-cold PBS. The supernatants were removed, and the cell pellets were flash-frozen in liquid nitrogen and stored at -80 °C until use. The cell pellets were resuspended in 0.5 mL of ice-cold 10 mM hypotonic Tris buffer (pH 7.6) for ten minutes at 4 °C, and the cell suspensions were then homogenized with a 2-mL glass tissue grinder with a tight clearance kept on ice with 20 slow up-down strokes. The cell lysates were centrifuged for ten minutes at 2,500×g at 4 °C and washed in ice-cold PBS, transferred the cell

supernatants to new centrifuge tubes and repeated the centrifugation step. The cell supernatants were further centrifuged for ten minutes at 15,000×g at 4 °C, discarded the supernatants and wash the mitochondrial-enriched pellets in 100 µL of ice-cold 250 mM sucrose and $T_{10}E_{20}$ (10 mM Tris-HCl, 20 mM EDTA) solution. The mitochondrial pellets were resuspended in 50 µL of ice-cold 250 mM sucrose and $T_{10}E_{20}$. The mitochondrial-enriched fractions were kept on ice for heme, PPIX and ZnPPIX analysis. A 1.0-µL aliquot of mitochondrial fraction for total protein concentration measurements according to the Qubit™ Protein and Protein Broad Range (BR) Assay Kits and the Qubit 2.0 fluorometer.

Preparation of heme, PPIX and ZnPPIX fraction: The sample preparation for the further ultra-performance liquid chromatography tandem mass spectrometry (UPLC-MS/MS) analysis was prepared as described previously with some adjustment (Fyrestam and Östman, 2017). Simply, 150 µL of acetonitrile was added to the microcentrifuge tube containing mitochondrial-enriched fraction and shake vigorously for five minutes by using a tube mixer (CM-1000 Cute Mixer, EYELA, Tokyo, Japan). The extraction solutions were centrifuged for five minutes at 15,000×g, and the supernatants (Porphyrin fraction containing PPIX and ZnPPIX) were transferred to new centrifuged tubes, protected from light. The pellets were resuspended in 200 µL of acetonitrile:1.7 M HCl (8:2, vol/vol) and shake vigorously for 20 minutes by using a tube mixer. After shaking, 50 µL of saturated $MgSO_{4(aq)}$ and 5 mg $NaCl_{(s)}$ were added to each tube, shake for five minutes by a tube mixer. The extraction solutions were centrifuged for five minutes at 15,000×g, and the supernatants (Hemin fraction) were transferred to new centrifuged tubes, protected from light. Both porphyrin and hemin

fractions were then concentrated for 5-10 minutes by using a centrifugal concentrator (TOMY CC-105, Tokyo, Japan) coupled with a low temperature trap (TOMY TU-055, Tokyo, Japan).

Preparation of standard curve: Stocks of hemin (0.2 mM), PPIX (0.25 mM) and ZnPPIX (0.2 mM) standards were prepared separately by dissolving 1.30 mg of hemin, 1.41 mg of PPIX and 1.25 mg of ZnPPIX in 10 mL DMSO. A seven-point calibration curve was made by hemin, PPIX and ZnPPIX standard solutions, the hemin concentrations in calibration curve were in the range of 2.5-25 μM, and the concentrations of PPIX and ZnPPIX were in the range of 0.25-2.5 μM.

5.10.2 UPLC-MS/MS Analysis

The analysis of hemin, PPIX and ZnPPIX were performed on a Xevo TQ-S tandem mass spectrometer coupled to an ultra-performance liquid chromatograph Acquity I-Class system (Waters Corporation, Milford, MA, USA). An Acquity UPLC CSH C18 column (2.1 × 150 mm, 1.7 μm), placed in a column oven (50 °C), was used for the separation with a gradient elution using acetonitrile and 0.1 % formic acid (FA) as mobile phases. Signals from all analytes were acquired in positive electrospray mode (ESI+) and multiple reaction monitoring (MRM) with three compound-specific transitions for each analyte, all transitions used as quantifier and qualifier ions. The dwell time for each transition was automatically set by the software to be 0.012 s in order to get approximate 12 data points over a peak with a width of 4 s. Liquid chromatography and mass spectrometry parameters are presented in Table 5.3.

Table 5.3 Conditions for the UPLC-MS/MS analysis

UPLC		ESI-MS/MS conditions			
Chromatographic conditions		Electrospray conditions			
Column dimensions	2.1 × 150 mm	Ionization mode		ESI (+)	
Stationary phase	C-18	Capillary voltage		3500 V	
Particle size	1.7 μm	Source temperature		150 °C	
Column temperature	50 °C	Desolvation temperature		650 °C	
Mobile phase A	Acetonitrile	Desolvation gas flow		650 L/h	
Mobile phase B	0.1 % FA				
Flow rate	0.5 mL/min	MS/MS conditions			
Injection volume	10 μL	Dwell time		0.012 s	
Autosampler temperature	20 °C	MS/MS		MRM	
Gradient		Compounds	Transition	CV	CE
Time (min)	B %	Hemin	616 > 482	64	120
Initial	20		616 >497	64	116
5.00	100		616 > 557	64	82
6.00	100	Protoporphyrin IX	563 > 444	20	110
10.00	20		563 > 489	20	96
			563 > 504	20	78
		Zinc protoporphyrin	626 > 492	64	120
			626 > 507	64	116
			626 > 567	64	82

Note: FA, formic acid; CV, cone voltage; CE, collision energy.

5.11 Senescence-Associated β-Galactosidase Staining

DLD-1 cells (2.0×10^5 cells) were seeded in 60 mm petri dishes with 6 mL RPMI-1640 medium containing 10% FBS and incubated for 24 hours at 37 °C and 5% CO_2. After 24 hours, the medium was removed and the cells were washed two times in pre-warmed PBS, then treated with different dosing solutions and incubated at 37 °C, 5% CO_2 for 72 hours. *In* concentrations of In(III), citrate-In(III), $In(OH)_{3(s)}$ and $In_2O_{3(s)}$ in exposure solutions were 0.0435 mM and 0.435 mM, Ga concentrations of Ga(III) and citrate-Ga(III) were 0.0215 mM and 0.215 mM, and 0.717 mM for $Ga_2O_{3(s)}$. The RPMI-1640 medium containing 10% FBS was used as a negative control, and the 5 μM DFO was used as a positive control.

After exposure for 72 hours, the dosing solutions were removed, and the cells were washed twice in pre-warmed PBS. The cells were then fixed with pre-warmed 4% formaldehyde solution (in PBS) at room temperature for ten minutes. The fixative solution was removed and washed the cells with pre-warmed PBS for three times. Staining solution containing 1 mg/mL X-gal, 5 mM potassium ferrocyanide, 5 mM potassium ferricyanide, 150 mM sodium chloride, 2 mM magnesium chloride in 40 mM citric acid/sodium phosphate solution (pH 6.0), was added to the fixed cells and an incubation period of 15 hours at 37°C in the dark. After staining, the cells were washed twice in PBS and 3 mL of PBS was added to each treatment. Blue-stained SA-β-gal positive cells were counted as a percentage (%) of the total cell number by using inverted fluorescence phase-contrast microscope with a 20x objective (Plan Fluor/0.45 numerical aperture) and BZ-II viewer software.

5.12 Other Possible Modes of Action

5.12.1 Proteasome Inhibition Assay

Preparation of proteasome fraction: DLD-1 cells (1.0×10^6 cells) were seeded in 150 mm petri dishes with 20 mL RPMI-1640 medium containing 10% FBS and incubated at 37 °C and 5% CO_2. After reaching 70-80% confluence, the cells of five petri dishes were washed twice in pre-warmed PBS. The cells were then harvested with TrypLE™ Express Enzyme. The cell pellets were resuspended with six volumes of 1 mM dithiothreitol (DTT) solution, and the suspensions were flash-frozen in liquid nitrogen and thawed at 37 °C for three times. The suspensions were centrifuged for 15 minutes at 10,000×g at 4 °C and the supernatants were collected, then the buffer B containing 250 mM of Tris-HCl (pH 7.4), 25 mM of $MgCl_2$,1.25 M of sucrose, and 10 mM of adenosine triphosphate (ATP) was added, and the ratio of the volume of supernatant and buffer B is 8:2. The mixtures were ultracentrifuged for one hour at 100,000×g at 4 °C (Himac CS 100GXII, Hitachi, Tokyo, Japan) and the supernatants were decanted to a new tube. These supernatants were further ultracentrifuged for five hours at 100,000×g at 4 °C, removed the supernatants and the pellets were dissolved in buffer C, which contained 50 mM of Tris-HCl (pH 7.4), 5 mM of $MgCl_2$, 10 % of glycerol, and 10 mM of ATP. This solution was centrifuged with Vivaspin® 6 centrifugal concentrators with a 100-kDa cutoff (Sartorius Stedim Biotech GmbH, Göttingen, Germany) for four minutes at 3,500×rpm at 4 °C, repeated three times. A 1.0-μL aliquot of proteasome fraction for total protein concentration

measurements according to the Qubit™ Protein and Protein Broad Range (BR) Assay Kits and the Qubit 2.0 fluorometer.

Proteasome inhibition assay: Purified proteasome fraction (10 μg/mL in final concentration) was incubated in a 50 μL of reaction solution, which contained proteasome assay buffer (50 mM Tris-HCl, 20 mM KCl, 0.5 mM MgOAc and 1 mM DTT, pH 7.8) with Ga- and *In*-related chemicals, and 10 μL of 10 μM fluorogenic peptide substrate (Suc-Leu-Leu-Val-Tyr-AMC for chymotrypsin-like peptidase activity, Boc-Leu-Arg-Arg-AMC for trypsin-like peptidase activity, and Z-Leu-Leu-Glu-AMC for caspase-like peptidase activity). The proteasome fraction and proteasome assay buffer with Ga- and *In*-related chemicals were gently mixed and incubated at 37 °C for ten minutes by using a Dry Thermo Unit (DTU-2C, Taitec Co. Ltd., Tokyo, Japan). *In* concentration of In(III), citrate-In(III), $In(OH)_{3(s)}$ and $In_2O_{3(s)}$ in reaction solutions was 0.435 mM, and the Ga concentration of Ga(III), citrate-Ga(III) and Ga_2O_3 was 0.717 mM. The proteasome assay buffer was used as a negative control, whereas the 1 μM of proteasome inhibitor (MG-132) was used as a positive control. After incubation, 10 μL of 10 μM fluorogenic peptide substrate was added into each treatment and further incubated at 37 °C in the dark for ten minutes by using a Dry Thermo Unit. The enzymatic reaction of proteasome was stopped by addition of 200 μL of methanol, mixed well and centrifuged at 15,000×rpm at room temperature. The supernatant (about 50 μL) was collected and transferred to a new centrifuge tube for further HPLC analysis.

The supernatant containing hydrolyzed 7-amido-4-methyl-coumarin (AMC) groups was measured by a Shimadzu VP HPLC System coupled with LC-10AT (liquid chromatography), SCL-

10A (system controller), SIL-10AD (auto injector), RF-10A (fluorescence detector) (Shimadzu, Kyoto, Japan) and a Shim-pack FC-ODS column (150 × 46 mm, 3 μm; Shimadzu, Kyoto, Japan). The excitation and emission wavelengths were set at 380 nm and 460 nm, respectively. Changes in fluorescence were calculated against negative controls.

5.12.2 Genotoxicity Assessment Using EGFP-MDC1-Expressing Human Cells

The established high-throughput genotoxicity screening assay was described previously (Matsuda et al., 2014). Briefly, EGFP-MDC1-expressing MCF7 cells (1.0×10^4 cells) were seeded in 35 mm glass-based petri dishes with 3 mL RPMI-1640 medium containing 10% FBS and incubated at 37 °C and 5% CO_2. After 24 hours, the medium was removed and the cells were washed two times in pre-warmed PBS, then treated with different exposure solutions and incubated at 37 °C, 5% CO_2 for 72 hours. *In* concentration of In(III), citrate-In(III), $In(OH)_{3(s)}$ and $In_2O_{3(s)}$ in exposure solutions was 0.435 mM, and the Ga concentration of Ga(III), citrate-Ga(III) and $Ga_2O_{3(s)}$ was 0.717 mM. The RPMI-1640 medium containing 10% FBS was used as a negative control.

After exposure for 72 hours, the exposure solutions were removed, and the cells were washed twice in pre-warmed PBS. The cells were then fixed with pre-warmed 4% formaldehyde solution (in PBS) at room temperature for ten minutes. The fixative solutions were removed and washed the cells for three times with PBS, then 3 mL of PBS was added to each treatment. In each treatment, a minimal of 10-15 different field were imaged by using inverted fluorescence phase-contrast microscope

coupled with BZ-II viewer software, the 20x objective (PlanApo/0.75 numerical aperture) and the quick full-focus function were used. The image-processing and calculation of foci area/nucleus were performed using *R* program. The outline of the procedure is shown in Figure 5.2.

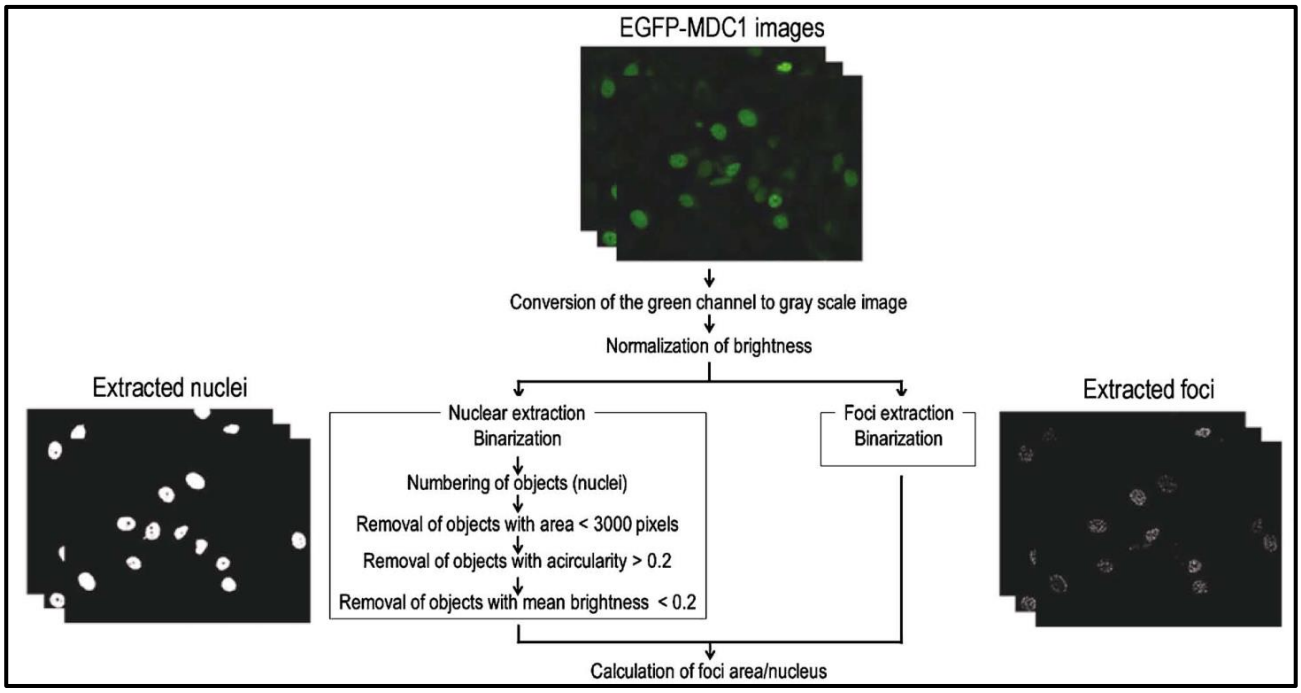

Figure 5.2 Workflow of image-processing using *R* program. After EGFP-MDC1 imaging, nuclei and foci were separately masked from the same EGFP-MDC1 image and then the masked foci area in each masked nucleus was calculated (Matsuda et al., 2014).

5.13 Statistical Analysis

Each experiment was performed at least in triplicate. All results were presented as mean ± standard deviation (SD). Prior to analysis, all results were tested for normality (Kolmogorov-Smirnov test) and for homogeneity of variances (Levene test). The acceptable data were then performed by Student's t test, or one-way analysis of variance (ANOVA) with post hoc tests to evaluate significant differences between treatments. The IBM SPSS statistics program (version 21) was used for all statistical analyses, and p values of <0.05 were considered significant.

6. Results

6.1 Cell Viability After Treatment

The MTT assay was used to assess cytotoxicity at the 72 hours timepoint. Ga- and *In*-related chemicals induced a dose-dependent manner decrease in cellular viability (Figure 6.1). In(III) and citrate-In(III) treated cells revealed dramatically decrease in viability when the nominal *In* concentration in exposure solution was above 0.435 mM, and the hydroxide/oxide groups decreased the viability when the nominal *In* concentration in solution was above 0.044 mM. Additionally, Ga(III) and citrate-Ga(III) treated cells decreased viability significantly when the nominal *Ga* concentration in exposure solution was above 0.359 mM, and the $Ga_2O_{3(s)}$ treatment (0.014 to 3.586 mM of Ga) also indicated a significant decrease in cell viability.

The calculated LC_{50} values (72 h) of In(III), citrate-In(III), $In(OH)_{3(s)}$ and $In_2O_{3(s)}$ were respectively 2.151 mM, 1.368 mM, 1.161 mM and 1.570 mM, indicating that the citrate stabilized In(III) and $In(OH)_{3(s)}$ particles could induce higher cytotoxicity to DLD-1 cells (Table 6.1). Furthermore, the LC_{50} values (72 h) of Ga(III), citrate-Ga(III) and $Ga_2O_{3(s)}$ were respectively 0.425 mM, 0.612 mM and 2.503 mM, the Ga(III) had the highest cytotoxicity among the three treatment groups (Table 6.1). The viability of DLD-1 cells appeared to be more sensitive to Ga(III) and citrate-Ga(III) exposure as compared to In(III), citrate-In(III) and other hydroxide/oxides groups.

To investigate the further sublethal effects of Ga- and *In*-related chemicals, the estimated workplace exposure level and 72 h-LC_{50} values were considered. The lower dose of 50 mg/L (0.435

mM) *In*-related chemicals containing equivalent amounts of *In* has previously been calculated to represent approximately three years of average workplace exposure, while the higher dose of 1 g/L (8.709 mM) is more representative of a career-long exposure (Badding et al., 2014). The following formula was used based on airborne particle concentrations of 0.1 mg/m^3 at the average inhaled air volume over an 8-h workday, according to 260 workday per year:

Lung burden = respirable dust concentration × inhaled air volume (breathing rate)/workday × alveolar deposition fraction × days.

As a result, the sublethal doses of Ga- (0.022 mM and/or 0.215 mM of Ga) and *In*- (0.044 mM and/or 0.435 mM of *In*) chemicals were determined to represented a range of occupational exposures calculated to be at maximum of three years and much less than 72 h-LC_{50} values.

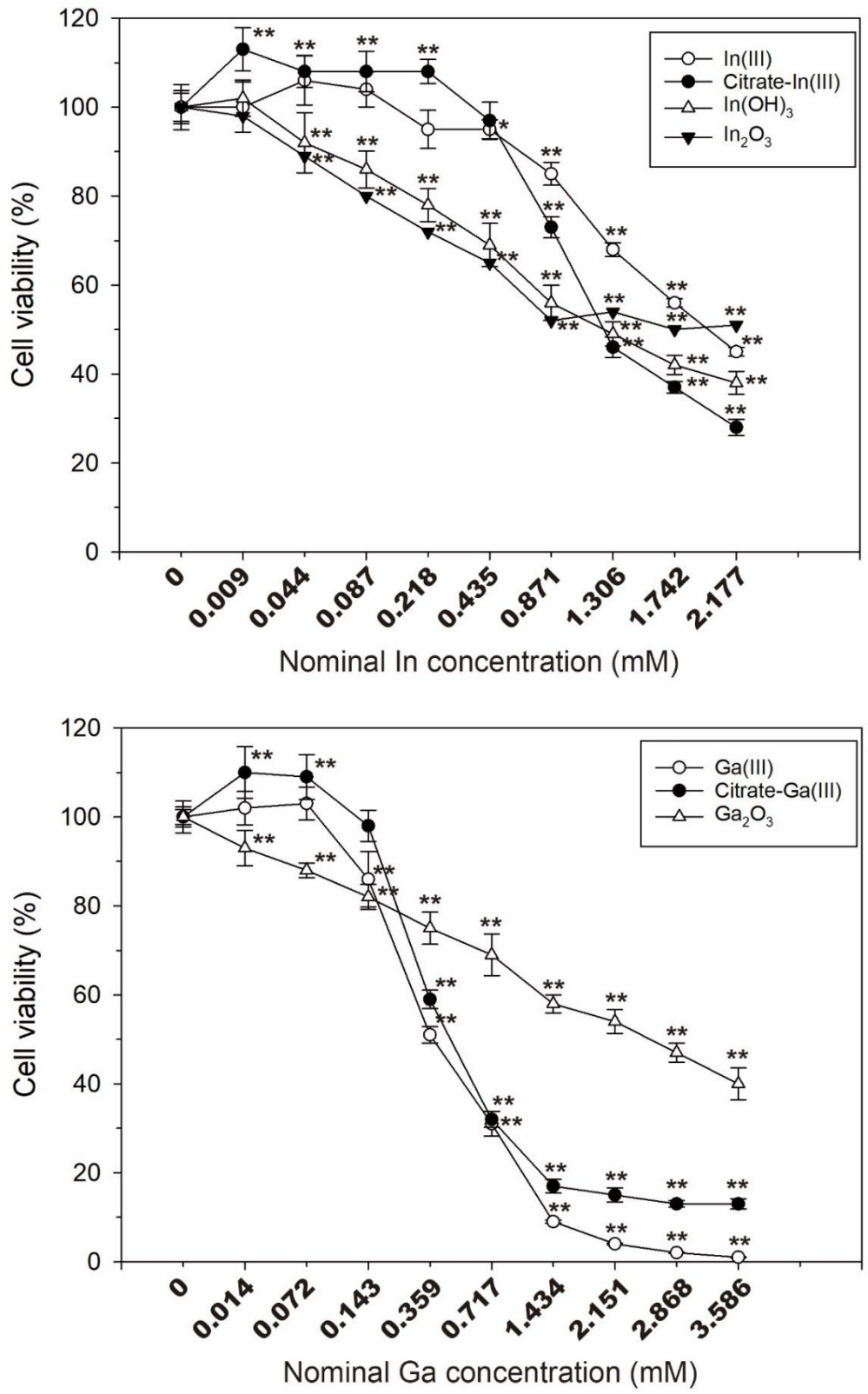

Figure 6.1 Cytotoxicity of Ga and *In*-related chemicals on DLD-1 cell growth. DLD-1 cells were treated with Ga and *In*-related compounds for 72 hours. Values are mean ± SD for each treatment group. Significance in difference between two groups were tested by independent sample t test. * $p<0.05$ ** $p<0.01$ versus control.

Table 6.1 LC_{50} values for Ga and *In*-related chemicals. DLD-1 cells were treated with Ga and *In*-related chemicals for 72 hours. The results were analyzed by probit analysis.

Treatment	LC_{50} (72 h)	95% lower confidence limit	95% upper confidence limit
	mM		
In(III)	2.151	N/A	N/A
Citrate-In(III)	1.368	1.273	1.474
Ga(III)	0.425	0.374	0.478
Citrate-Ga(III)	0.612	0.414	0.852
$In(OH)_{3(s)}$	1.161	1.004	1.362
$In_2O_{3(s)}$	1.570	1.111	2.460
$Ga_2O_{3(s)}$	2.503	1.830	4.052

Note: N/A, Not Applicable.

6.2 Apoptosis and Cell Cycle Profile After Treatment

Programmed cell death (apoptosis) is a crucial and active regulatory pathway of cell growth and proliferation. The Muse™ Annexin V & Dead Cell assay was performed in order to elucidate whether Ga and *In* would have adverse effect on DLD-1 cells through this pathway. The results indicated that Fe(III) chelator deferoxamine (DFO) and all Ga- and *In*-related chemicals did not significantly enhance apoptosis of the DLD-1 cells after 72 hours treatment period (Figure 6.2). The percentages of total apoptotic cells treated by Ga- and *In*-related chemicals were approximately in the range of 17.2 % to 29.3 %, the higher concentration of citrate-Ga(III) (0.215 mM) slightly increased the percentage of total apoptotic cells as compared with the untreated control, which was not statistically

significant. As a result, the percentage of live cells and dead cells among treated DLD-1 cells were in the range of 68.9 % to 81.5 % and 1.0 % to 1.9 %, respectively.

DFO-induced Fe deficiency could cause cell cycle arrest at the G_2/M phase in DLD-1 cells (Figure 6.3). The cell cycle progression was also arrested at the G_2/M phase in cells after 72 hours exposure with higher concentrations of In(III) and Ga(III) groups (i.e., In(III), citrate-In(III), Ga(III) and citrate-Ga(III)), accompanied by significant decreases in the cell populations at the G_0/G_1 phase (decrease in the range of 14.7 % to 21.2 %) in comparison to the untreated control; in addition, the lower concentration treatments had also slightly increased the cell populations at the G_2/M phase, which were not statistically significant. DLD-1 cells treated with $In_2O_{3(s)}$ (0.435 mM of *In*) also induced the cell cycle arrest at the G_2/M phase ($p<0.05$), whereas a decrease in the percentage of cells at the G_0/G_1 phase was not observed.

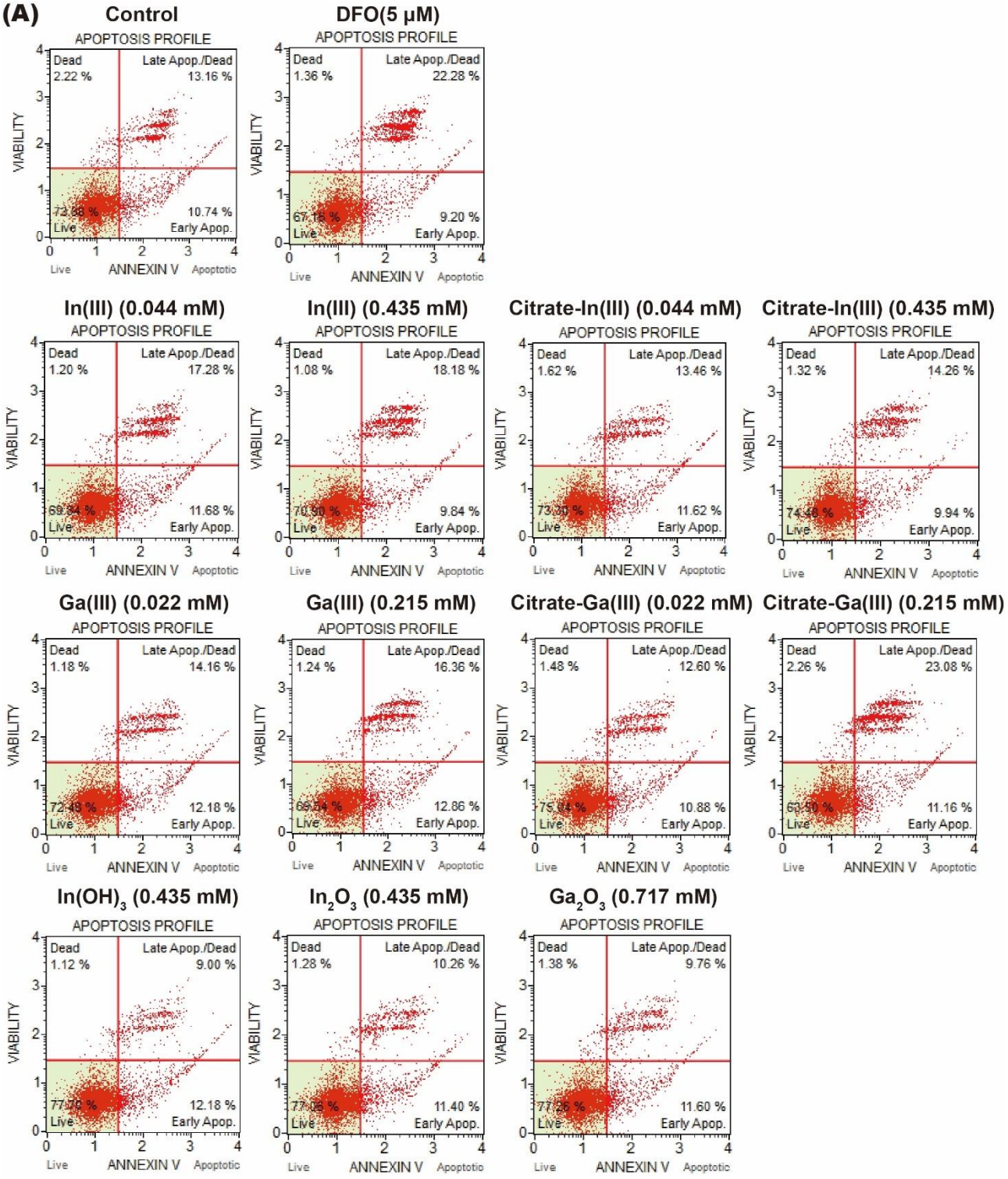

Figure 6.2 (A) Apoptosis profile of DLD-1 cells as studied by the Muse™ Annexin V & Dead Cell Kit after 72 hours of treatment.

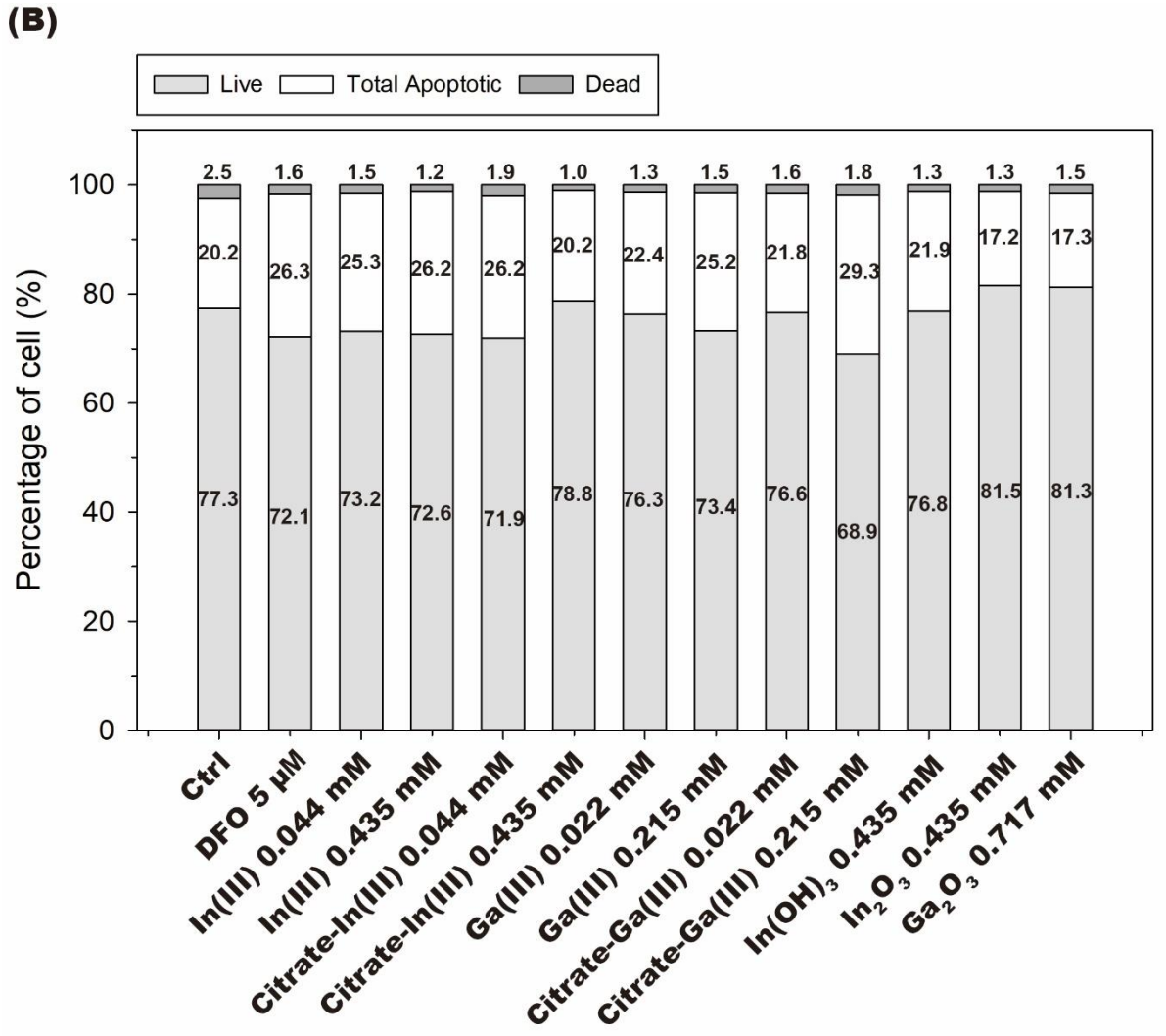

Figure 6.2 (B) The live, total apoptotic and dead cell percentages of control and treated DLD-1 cells. Significance in difference between two groups were tested by independent sample t test. * $p<0.05$ ** $p<0.01$ versus control.

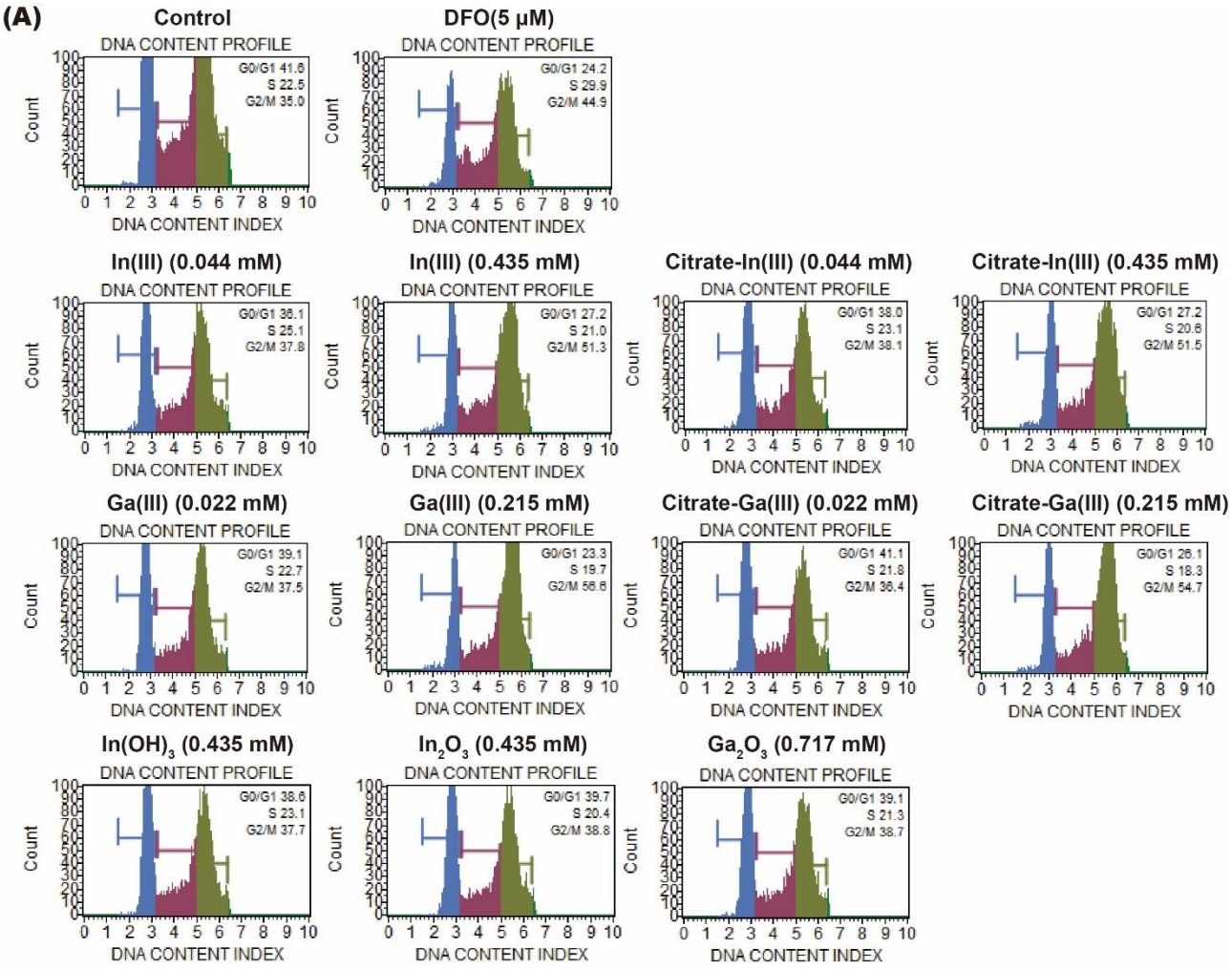

Figure 6.3 (A) Cell cycle analysis of DLD-1 cells using the Muse™ Cell Cycle Kit after 72 hours of treatment.

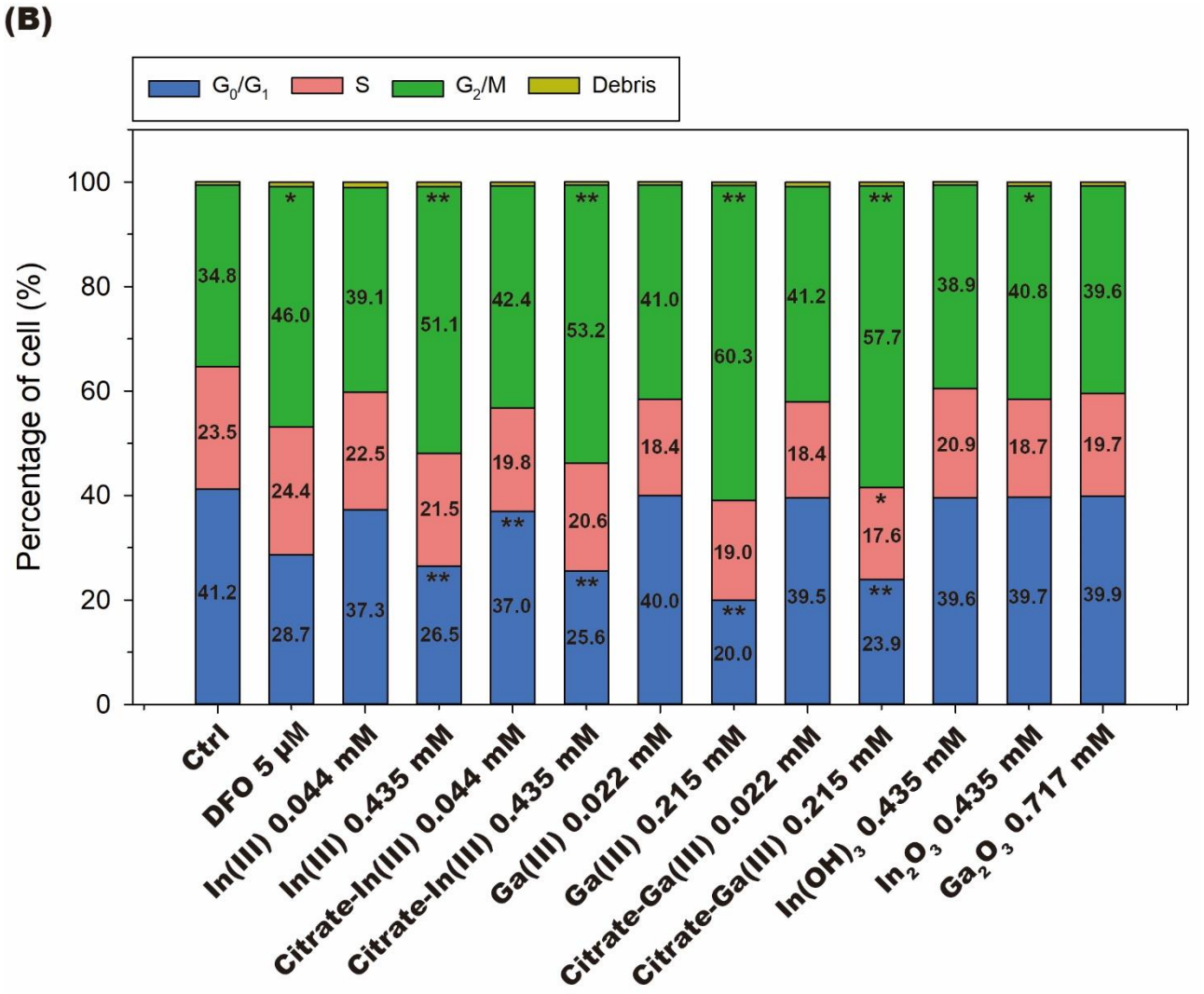

Figure 6.3 (B) The cell cycle percentages of control and treated DLD-1 cells. Significance in difference between two groups were tested by independent sample t test. * $p<0.05$ ** $p<0.01$ versus control.

6.3 Changes in Cell Size and Nucleus Size After Treatment

DLD-1 cells treated with Ga- and *In*-related chemicals showed typical temporal alterations of cell morphology associated with profound changes in cellular size, resulting in a flattened shape, senescent-like morphology after 72 hours of exposure. The population of attached untreated DLD-1 cells consisted of a mixture of cell types which were defined as small (<300 μm^2), medium (300-950 μm^2) or giant cells (> 950 μm^2) (Figure 6.4A). The results indicated that Fe(III) chelator DFO (5 μM) and the higher concentration of Ga(III) and In(III) treatments significantly increased the cell size than lower concentration. In those treatments that the cell populations were mainly composed of giant cells, it appeared to be difficult to identify the two distinct morphologies of DLD-1 cells (clone A and clone D). Since cell size not only depends on cell cycle phase and ploidy, the size of cell nucleus was also determined. As shown in Figure 6.4B, the changes in cell size were paralleled by similar changes in nuclear size, pointing to dynamic changes in ploidy during exposure period.

In addition, a reversibility in both cellular and nucleus sizes with either Ga(III) or In(III) in the co-presence of the citrate-Fe(III) concentrations (4.48 and 8.95 mM) was observed; however, the cells treated with citrate-Fe(III) (0.90 mM to 8.95 mM) did not induce an increase in both cell and nucleus sizes (Figure 6.4).

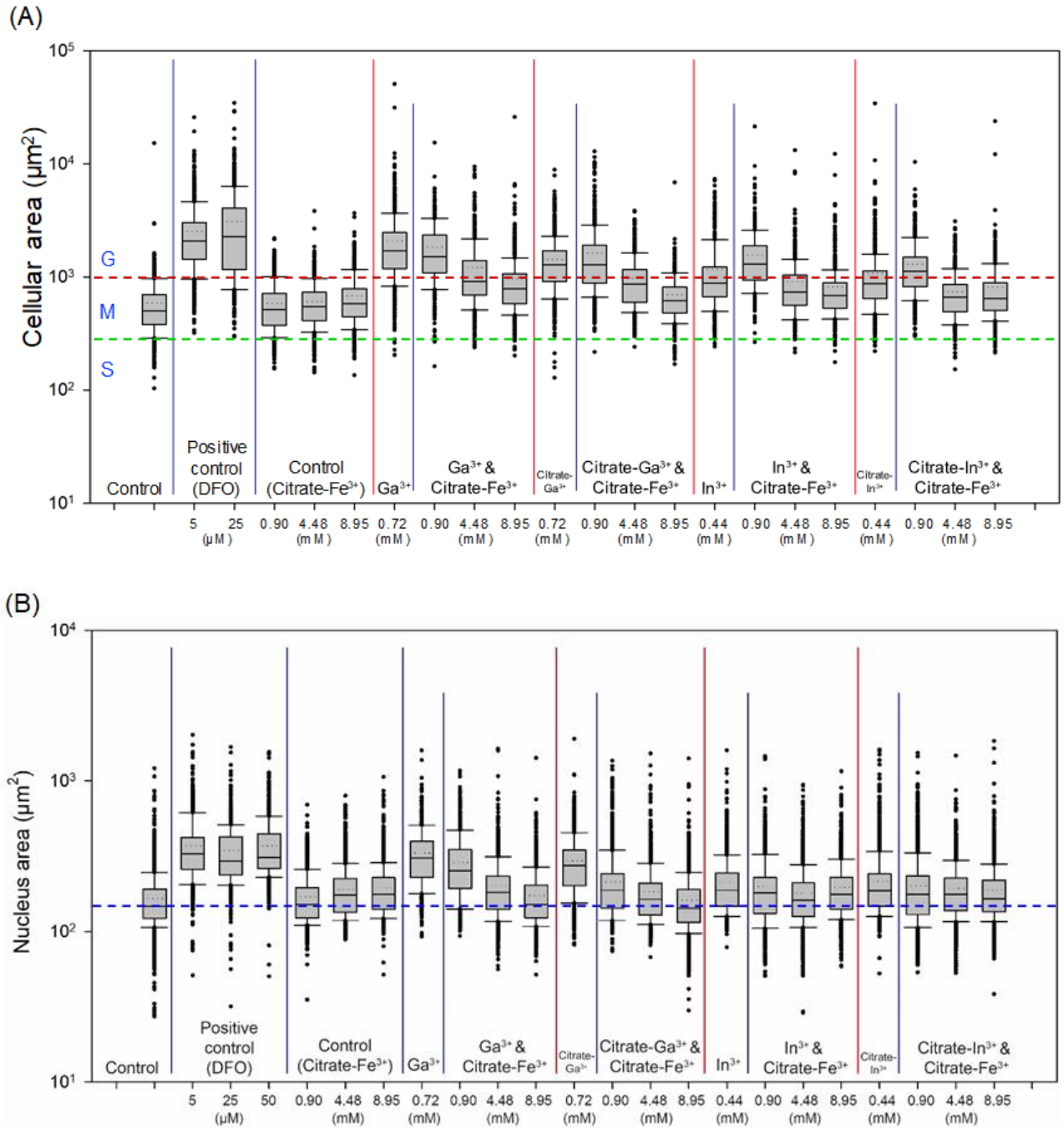

Figure 6.4 Cell and nucleus size of DLD-1 cells after Ga and *In*-ionic groups. DLD-1 cells were treated with Ga and *In*-ionic groups for 72 hours. (A) Boxplot of cell size (area) of DLD-1 cells, at least 250 cells were counted for each treatment. Dotted lines define three populations distinguished by size; small (S), 10th percentile of untreated cells; medium (M), the size of cells between 100th and 10th percentile of untreated cells; giant (G), >2-times the size of median cells. (B) Boxplot of nucleus area of DLD-1 cells, at least 250 cells were counted for each treatment.

6.4 Time-Lapse Cell Imaging of Ga- and *In*-Treated Cells

In order to analyze the fate of individual cells with regard to the induction of cell death, division and cell cycle arrest, we performed the time-lapse microscopy of DLD-1 cells for 72 hours of Ga(III) and In(III) sublethal exposure. Cell cycle arrest was the main fate of Ga(III)- and In(III)-treated cells, concomitantly with an decrease in cell divisions after approximately 40 hours of exposure (Figure 6.5 and Figure 6.6). Cell death was only clearly increased in Ga(III)-treated cells after 60 hours. Mitosis of mononuclear cells was usually followed by cytokinesis, and only rarely resulted in the formation of multinuclear cells. The formation of mononuclear giant cells appears to include cytokinesis failure and endoreplication, and the treated cells underwent cell fusion or cell-to-cell fusion immediately after cytokinesis failure, thereby forming multinuclear giant cells.

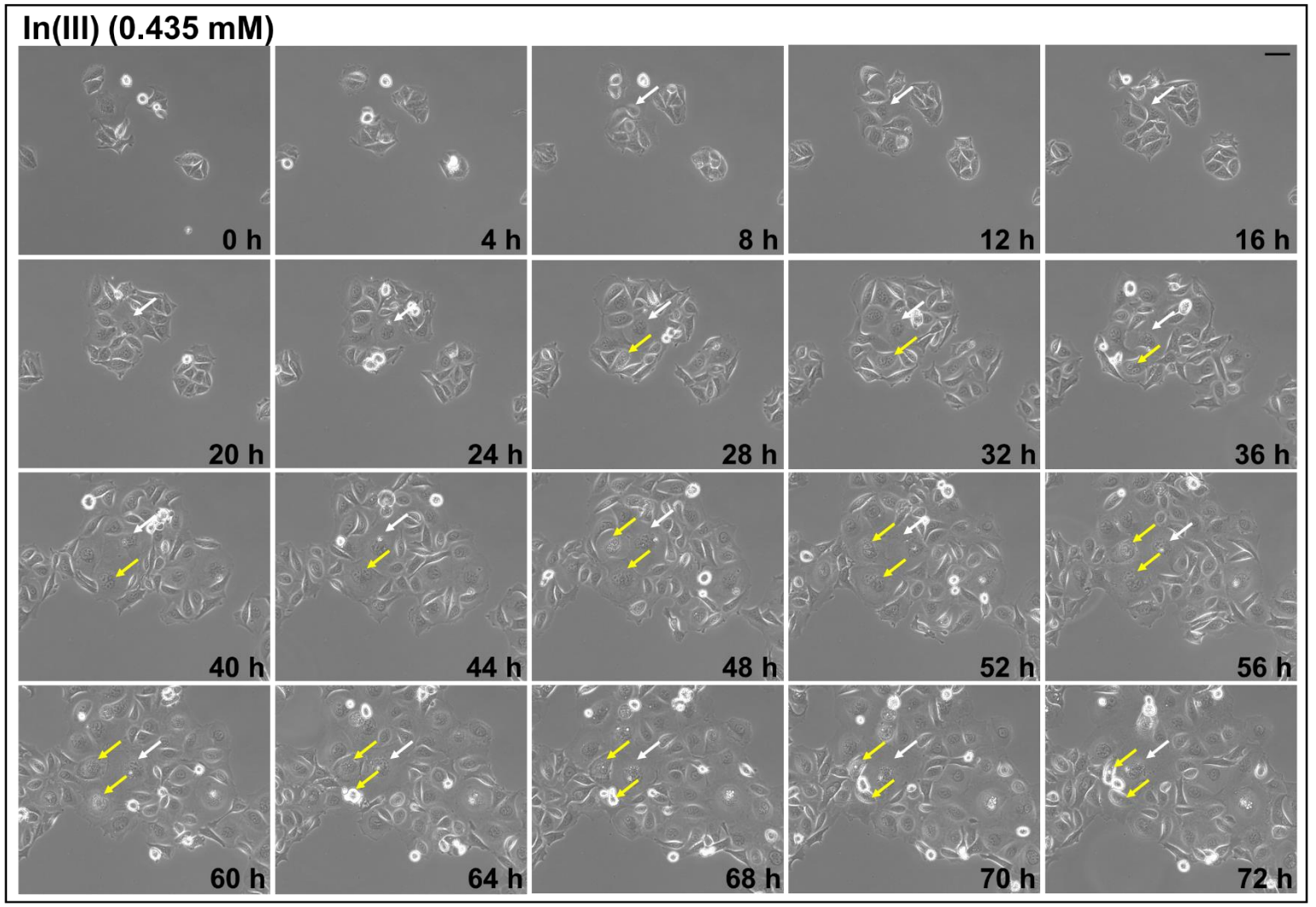

Figure 6.5 Time-lapse cell imaging of In(III)-treated DLD-1 cells. Images showed the giant cells undergoing cell cycle arrest with increasing cell volume and nucleus area (white arrow), and the formation of multinuclear giant cells by cell-to-cell fusion immediately after cytokinesis failure (yellow arrow). Scale bar, 50 μm.

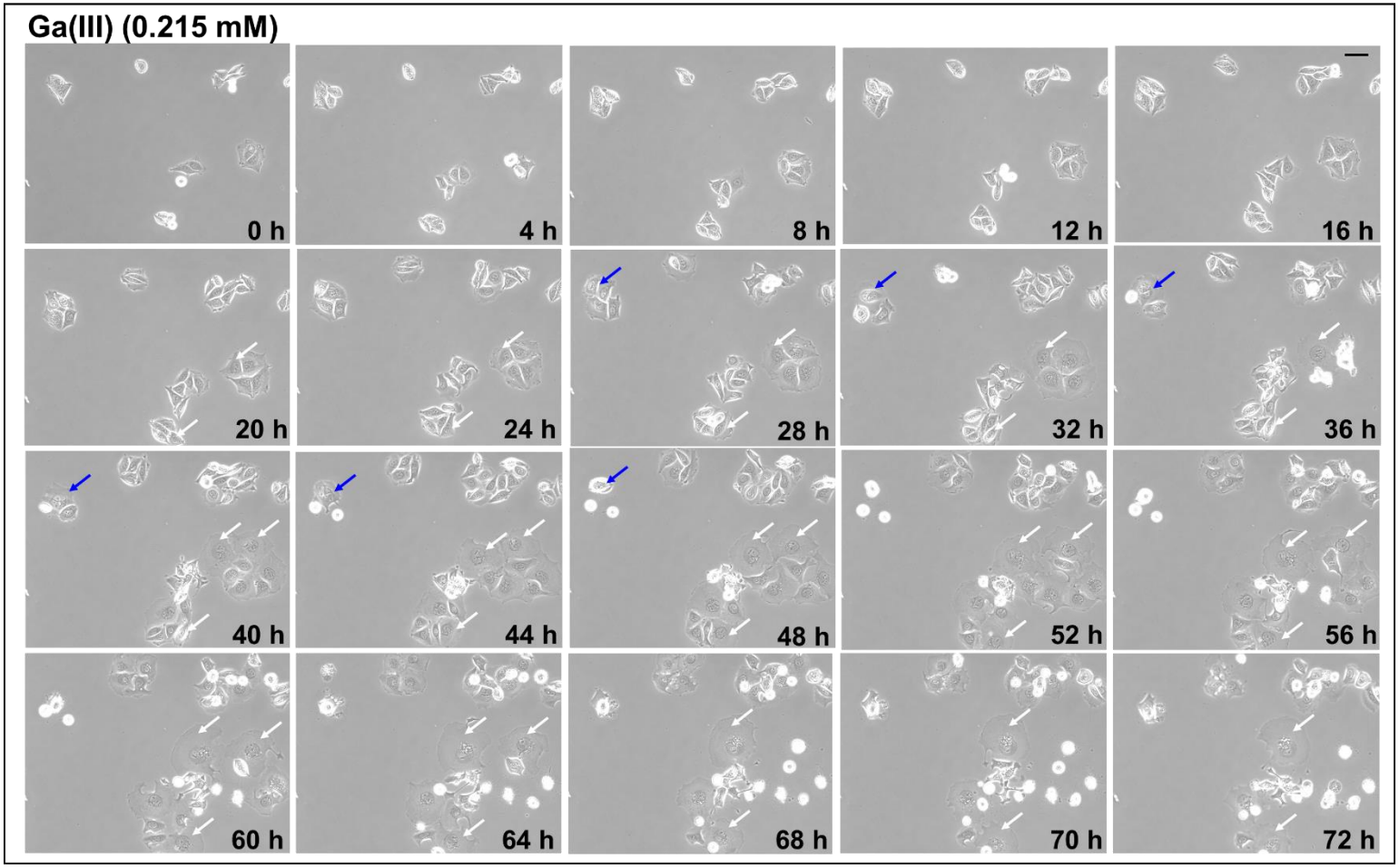

Figure 6.6 Time-lapse cell imaging of Ga(III)-treated DLD-1 cells. Images showed the giant cells undergoing cell cycle arrest with increasing cell volume and nucleus area (white arrow), and the formation of multinuclear cells by cell fusion of two cells (blue arrow). Scale bar, 50 μm.

6.4 Ga- and *In*-Induced Changes in Mitochondrial Membrane Potential ($\Delta\psi_m$)

DLD-1 cells were treated with Ga- and *In*-related chemicals for 72 hours, to examine the effect of these chemicals on mitochondrial function. At the conclusion of the treatment duration, mitochondrial function was determined by fluorescent microscopic examination of the $\Delta\psi_m$-dependent uptake and retention of MitoTracker Red (CMXRos) into mitochondria. Figure 6.7 demonstrated the effect of Ga- and *In*-related chemicals on the mitochondrial membrane potential ($\Delta\psi_m$) in cells. DFO (5 μM) remarkably increased (p<0.01) MitoTracker Red fluorescence, and there was also a significant increase (p<0.01) of red fluorescence following treatment with In(III) and citrate-In(III) (0.435 mM of *In*), Ga(III) and citrate-Ga(III) (0.215 mM of Ga). Similar results were obtained following treatment with $In(OH)_{3(s)}$ and $In_2O_{3(s)}$ (0.435 mM of *In*), and $Ga_2O_{3(s)}$ (0.717 mM of Ga). Additionally, both Ga(III) and citrate-Ga(III) (0.215 mM of Ga) treatments had a greater adverse effects on mitochondria, leading to the highest MitoTracker Red fluorescent per cell as compared with the untreated control as well as other treatments. It has been reported that the increase in MitoTracker Red fluorescence in mitochondria of treated cells could be attributed to: (1) the elevation of $\Delta\psi_m$, or (2) mitochondrial dysfunction by increasing the number of mitochondria and mitochondrial volume (Krohn et al., 1999).

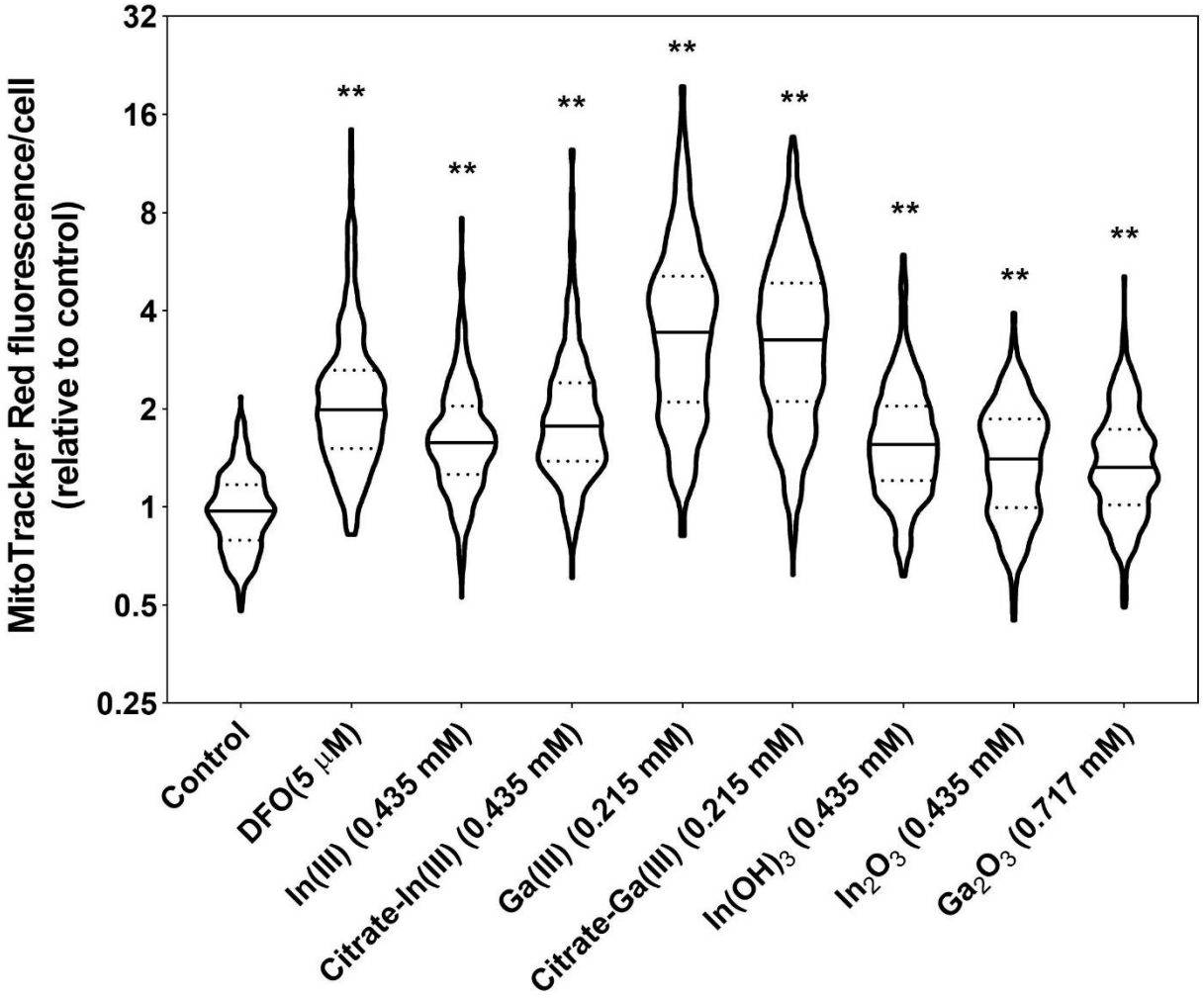

Figure 6.7 Violin plots reporting the mitochondrial membrane potential ($\Delta\psi_m$) of DLD-1 cells (MitoTracker Red CMXRos stain), at least 500 cells were counted for each treatment. DLD-1 cells treated to Ga- and *In*-related chemicals for 72 hours. The value on Y-axle represents the relative MitoTracker Red fluorescence in the binary logarithm (log2) value. Dotted and solid lines represent the quartile and median, respectively. ** $p<0.01$ versus control, Kruskal–Wallis one-way analysis of variance followed by Games-Howell post-hoc test.

6.5 Changes in Enzymatic Activities of Mitochondrial Respiratory Chain Complexes After Treatment

Citrate synthase (CS) is located in the mitochondrial matrix, which is one of the key regulatory enzymes in the energy-generating metabolic pathway. It has been extensively used as a metabolic marker in assessing oxidative and respiratory capacity of mitochondria (Siu et al., 2003; Spina et al., 1996). DLD-1 cells treated with In(III) (0.435 mM of *In*) and citrate-In(III) (0.044 mM and 0.435 mM of *In*), showed a significant decrease in CS activity as compared to control group after 72 hours of exposure. Similar results were obtained following treatment with higher concentration of citrate-Ga(III) (0.215 mM of Ga) (Figure 6.8).

A dose-dependent decrease in complex I (NADH: ubiquinone oxidoreductase) and complex II (succinate dehydrogenase) activity were observed after the treatment of cells with Ga- and *In*-ionic groups for 72 hours. Analysis of variance indicated that enzymatic activity of the complexes I was significantly inhibited with the treatment of the higher concentration of In(III) (0.435 mM of *In*), Ga(III) and citrate-Ga(III) (0.215 mM of Ga), as well as the positive control rotenone (10 μM) and DFO (5 μM) (Figure 6.9A). As for complex II activity, similar results were observed with treatments of the higher concentration of In(III) and citrate-In(III) (0.435 mM of *In*), Ga(III) and citrate-Ga(III) (0.215 mM of Ga), as well as the positive control malonate (10 mM) and DFO (5 μM) (Figure 6.9B).

Compared to complex I and II, complex III (decylubiquinol cytochrome *c* oxidoreductase) and complex IV (cytochrome *c* oxidase) are heme containing proteins. Each of the two complexes

contains two hemes, a cytochrome *b* and cytochrome *c1* for complex III and a cytochrome *a* and cytochrome *a3* for complex IV. A dose-dependent inhibition of complex III activity was observed after the cells treated with In(III) (0.044 mM and 0.435 mM of *In*), citrate-In(III) (0.435 mM of *In*), Ga(III) and citrate-Ga(III) (0.215 mM of Ga), as well as the positive control antimycin A (10 μg/mL) and DFO (5 μM) (Figure 6.10A). However, complex IV appeared to be more sensitive than complex I-III to Ga(III) and In(III). The enzymatic activity of complex IV was significantly inhibited ($p<0.01$) among all treatments, as well as the positive control KCN (300 μM) and DFO (5 μM) (Figure 6.10B).

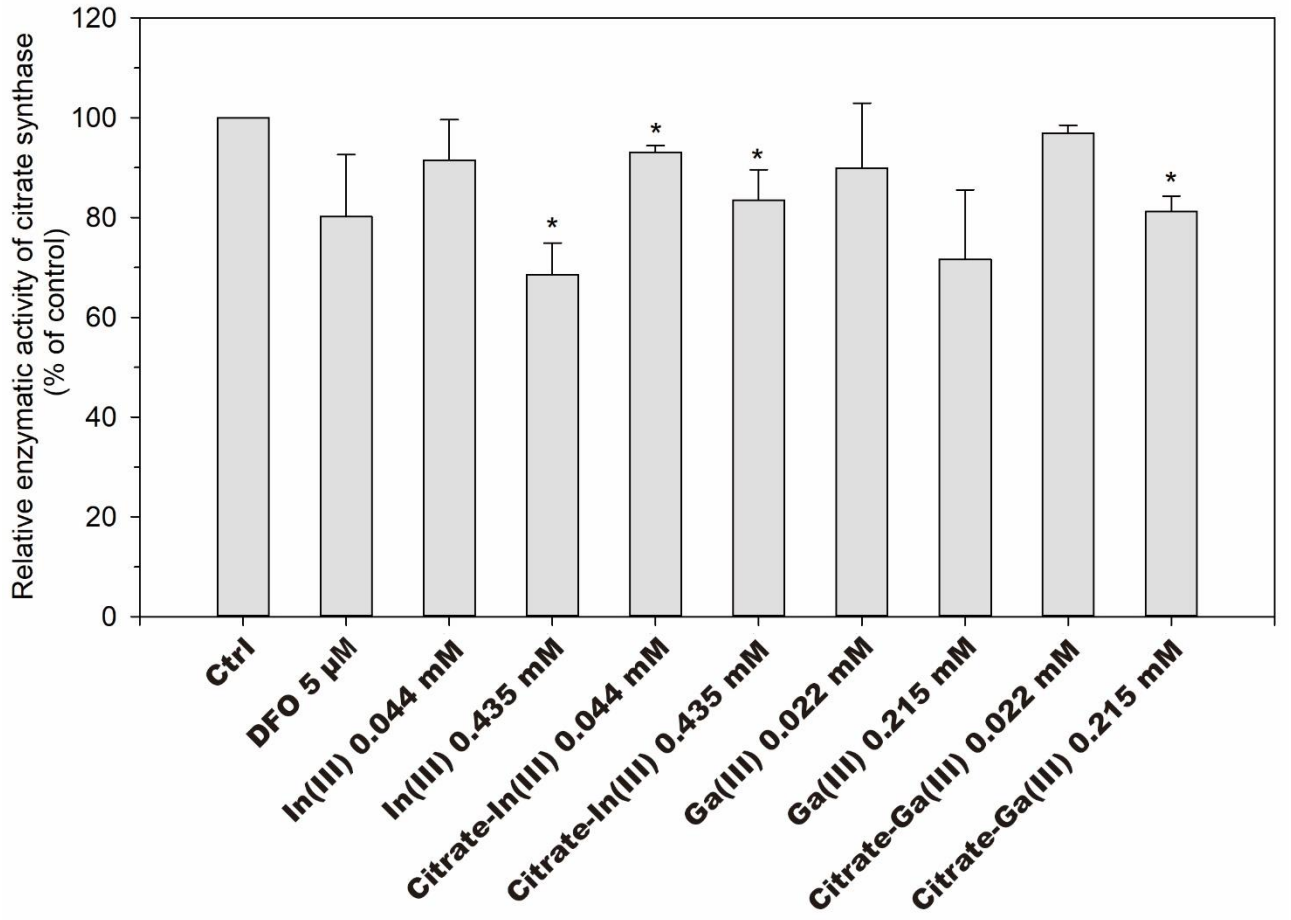

Figure 6.8 Enzymatic activities of citrate synthase. DLD-1 cells treated for 72 hours of Ga- and *In*-ionic groups. Data are expressed as mean ± SD. Significance in difference between two groups were tested by independent sample t test. * $p<0.05$ versus control.

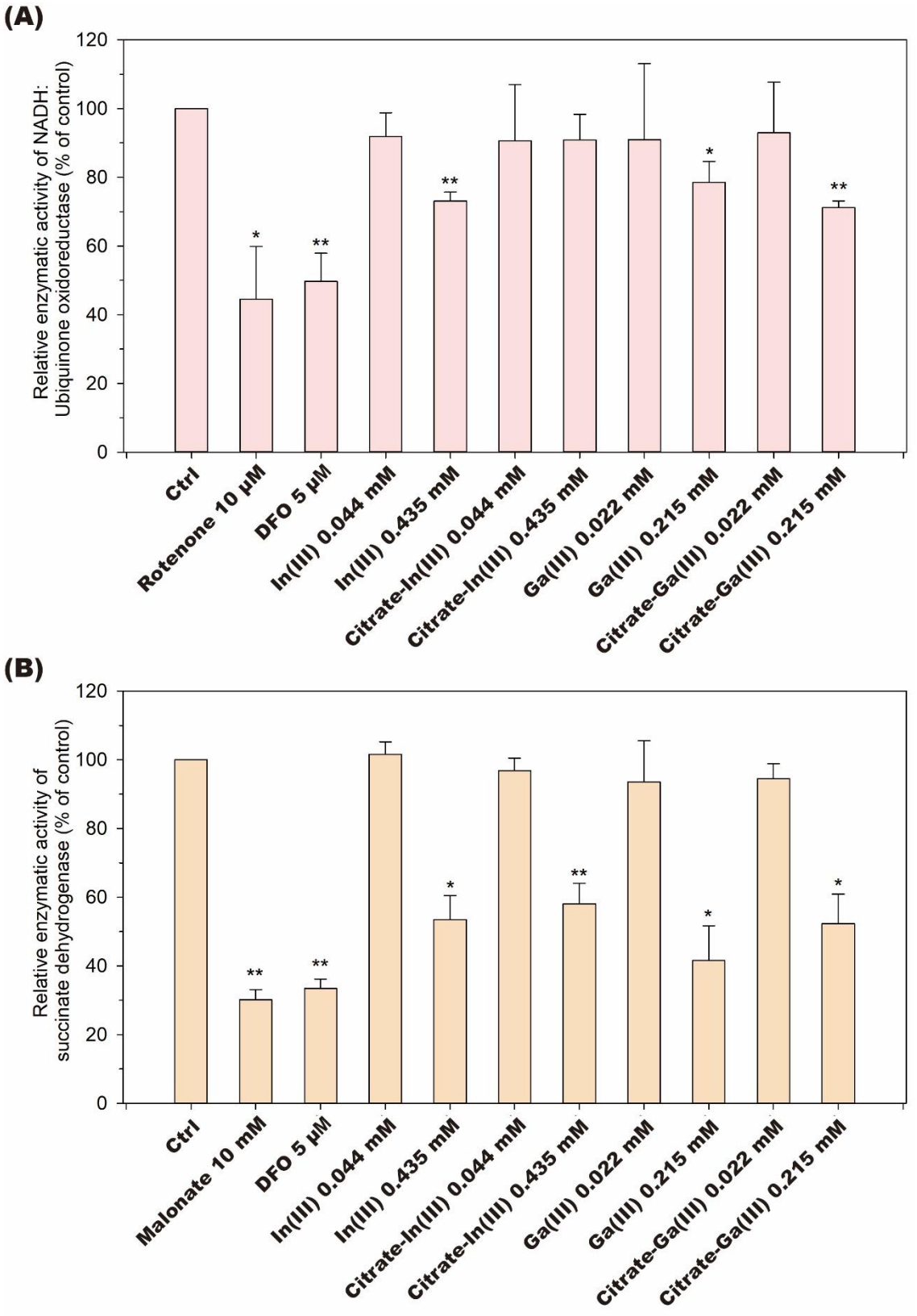

Figure 6.9 Results of mitochondrial respiratory transport chain enzymatic activities. DLD-1 cells were treated for 72 hours of Ga- and *In*-ionic groups. (A) Complex I (NADH: ubiquinone oxidoreductase) activity; (B) Complex II (succinate dehydrogenase) activity. Data are expressed as mean ± SD. Significance in difference between two groups were tested by independent sample t test. * $p<0.05$ ** $p<0.01$ versus control.

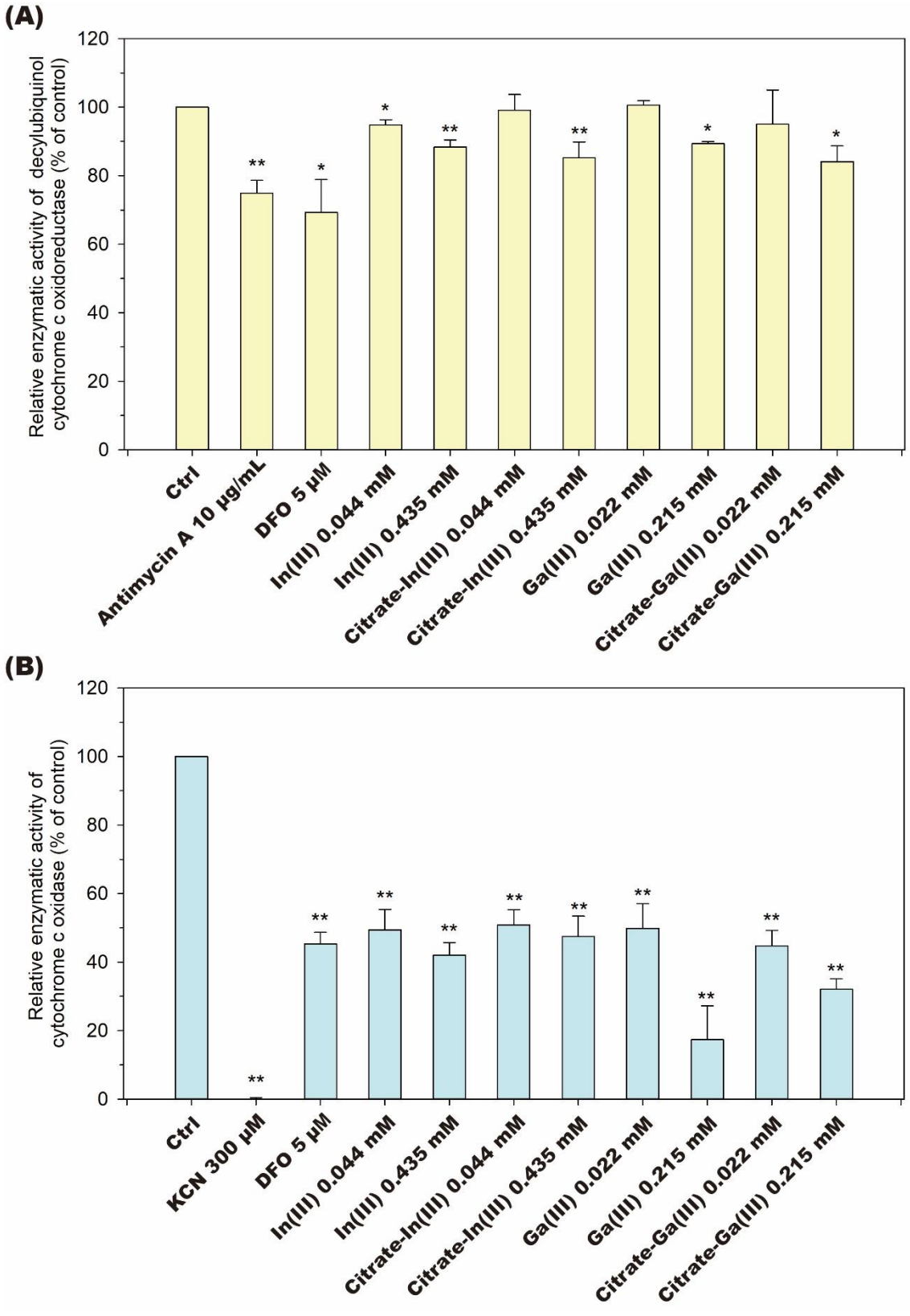

Figure 6.10 Results of mitochondrial respiratory transport chain enzymatic activities. DLD-1 cells were treated for 72 hours of Ga- and *In*-ionic groups. (A) Complex III (decylubiquinol cytochrome *c* oxidoreductase) activity; (B) Complex IV (cytochrome *c* oxidase) activity. Data are expressed as mean ± SD. Significance in difference between two groups were tested by independent sample t test. * $p<0.05$ ** $p<0.01$ versus control.

6.6 Alteration of Mitochondrial Heme and Porphyrins Contents After Treatment

Ga(III) and In(III) have been demonstrated to have adverse effects on mitochondrial function, including alteration in mitochondrial membrane potential and enzymatic activity of respiratory chain complexes. However, it remains unclear whether Ga(III) and In(III) could interfere with the biosynthesis processes of heme, which plays an important role in cellular iron homeostasis, gas exchange, mitochondrial energy production (e.g., cytochromes synthesis), antioxidant defense and signal transduction. An analytical method for the extraction, clean-up, and analysis of porphyrins and heme by UPLC-MS/MS was performed, to quantify the mitochondrial protoporphyrin IX (PPIX), heme and zinc protoporphyrin IX (ZnPPIX) in DLD-1 cells after 72 hours exposure with citrate-In(III) and citrate-Ga(III).

In Figure 6.11, a chromatogram was shown for the HPLC-MS/MS analysis of hemin, heme precursors (PPIX) and ZnPPIX (zinc is instead of iron). All compounds were baseline separated within six minutes. Total runtime for one sample, including pre- and pro-runs to clean and condition the column was ten minutes.

The calibration curve of hemin showed linear characteristics ($R^2 > 0.9934$) with a significant curvature in the concentration range 25 to 250 pmol; also, the standards of PPIX and ZnPPIX also showed linear calibration curves in the concentration range of 2.5 to 25 pmol ($R^2 > 0.9897$ for PPIX and $R^2 > 0.9911$ for ZnPPIX) (Figure 6.12).

Analysis of variance indicated that mitochondrial heme contents was significantly declined with the treatment of the citrate-In(III) (0.044 mM and 0.435 mM of *In*), citrate-Ga(III) (0.0215 mM and 0.215 mM of Ga), as well as DFO (5 μM) as compared to control group (Figure 6.13A). A similar result was obtained for the heme precursor PPIX and ZnPPIX, the concentration of mitochondrial PPIX and ZnPPIX were significantly decreased among all citrate-In(III) and citrate-Ga(III) treatments, whereas the cells treated with DFO (5 μM) only showed a decrease in mitochondrial PPIX to about half of control value (Figure 6.13B; Figure 6.13C).

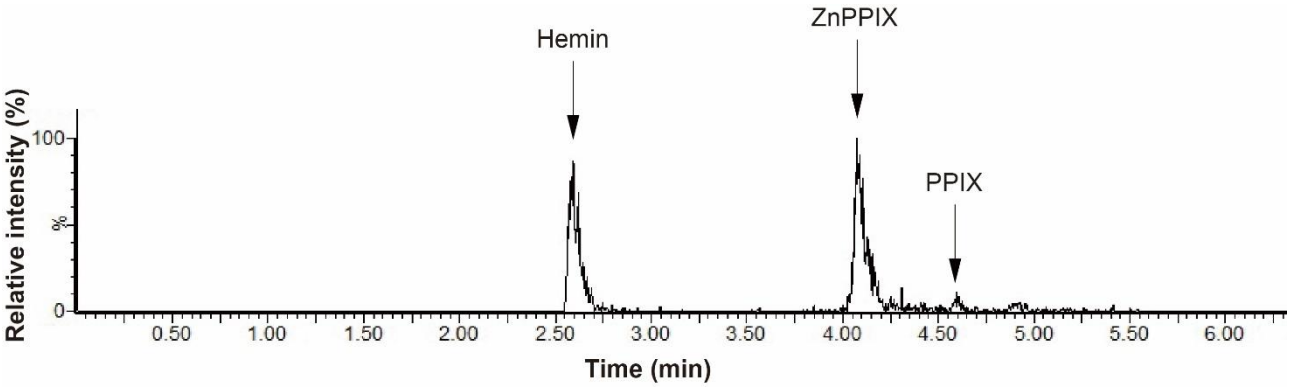

Figure 6.11 Total reconstructed ion chromatogram from the UPLC-MS/MS analysis of a standard mixture of protoporphyrin IX, hemin and zinc protoporphyrin IX. PPIX, protoporphyrin IX; Hemin; ZnPPIX, zinc protoporphyrin IX. Flow rate = 0.5 mL/min. Injection volume = 10 μL. Detection: MRM using three compounds-specific transitions for each analyte.

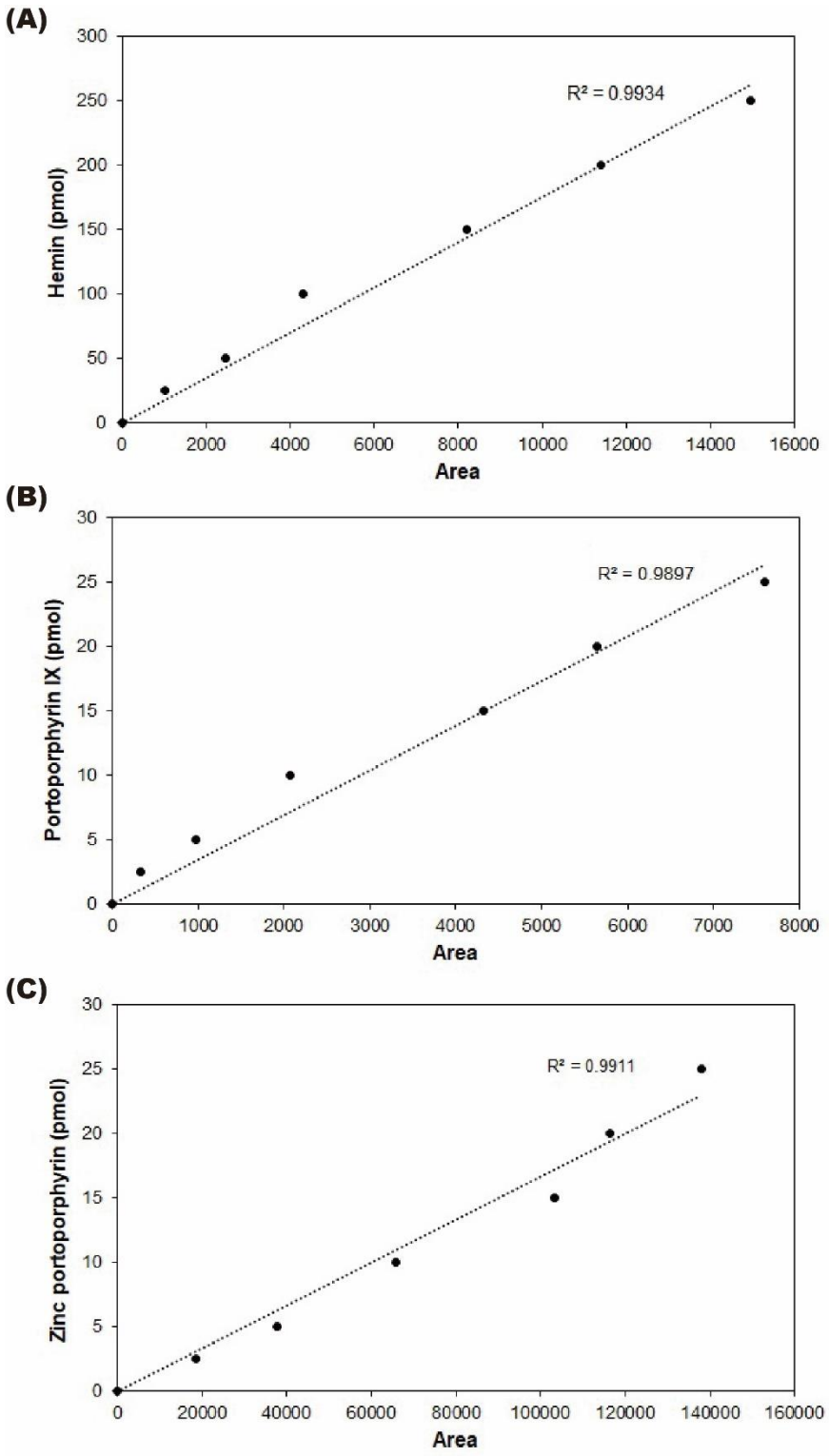

Figure 6.12 Calibration curve of hemin (5-250 pmol) and porphyrins (2.5-25 pmol) at 7 different levels. (A) Hemin; (B) Protoporphyrin IX; (C) Zinc protoporphyrin IX.

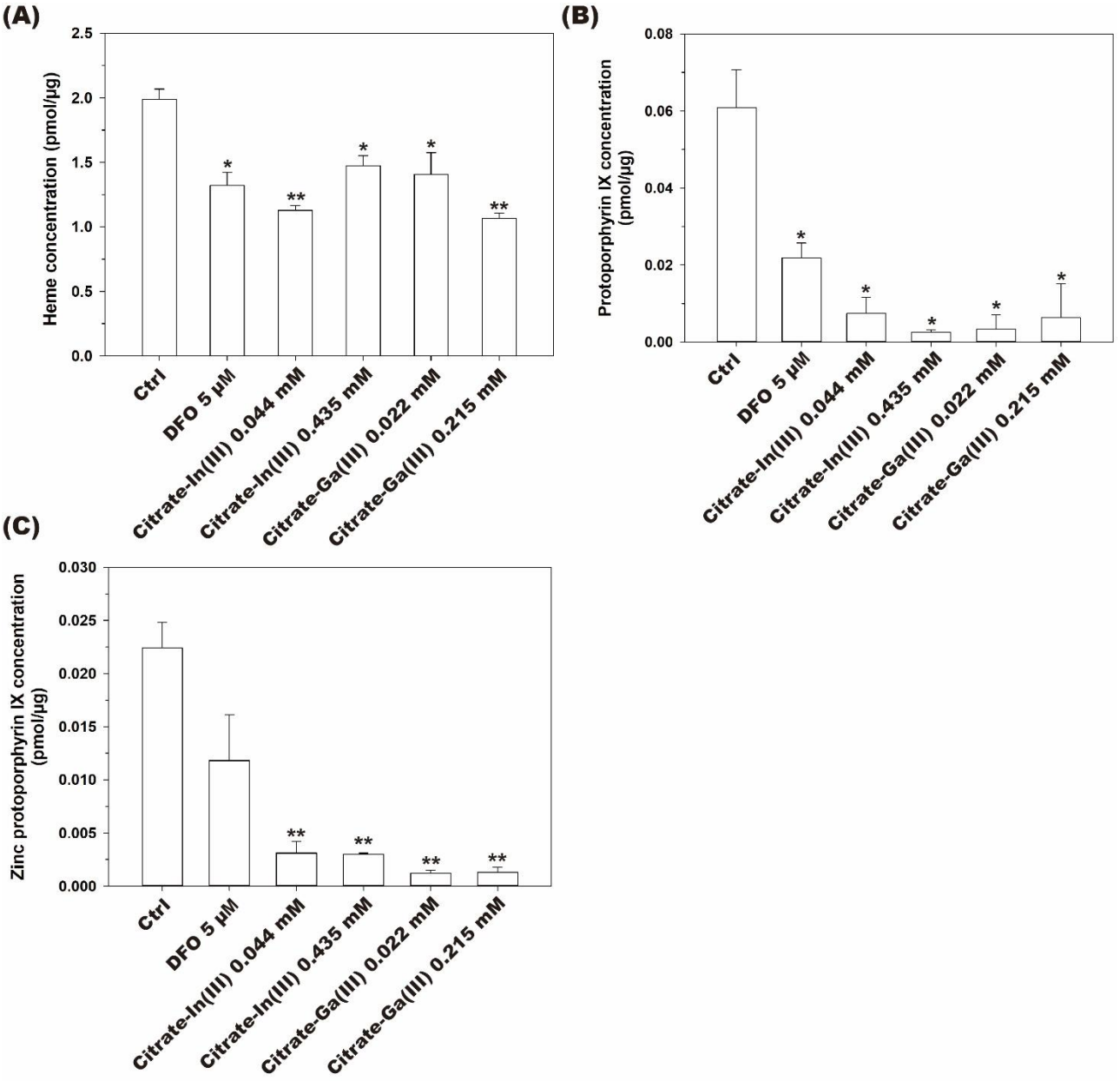

Figure 6.13 UPLC-MS/MS analysis of mitochondrial iron (II) protoporphyrin IX (heme), protoporphyrin IX and zinc protoporphyrin IX concentrations in DLD-1 cells. DLD-1 cells treated to Ga- and *In*-related chemicals for 72 hours. (A) Heme; (B) Protoporphyrin IX; (C) Zinc protoporphyrin IX. Data are expressed as mean ± SD. Significance in difference between two groups were tested by independent sample t test. * $p<0.05$ ** $p<0.01$ versus control.

6.7 Ga- and *In*-Induced Cellular Senescence

In addition to cytotoxicity (apoptosis and cell cycle), cellular and nucleus sizes, and mitochondrial function (mitochondrial membrane potential and enzymatic activity of respiratory chain complexes) measurements, staining for senescence-associated β-galactosidase (SA-β-Gal) activity was used to assess whether the Ga- and *In*-induced mitochondrial dysfunction could induce cellular senescence. Results indicated that there was a significant increase (p<0.01) of SA-β-Gal positive cells after 72 hours treatment with Ga- and *In*-related chemicals and DFO (5 μM) except for $In_2O_{3(s)}$ (0.435 mM of *In*) and $Ga_2O_{3(s)}$ (0.717 mM of Ga). (Figure 6.14).

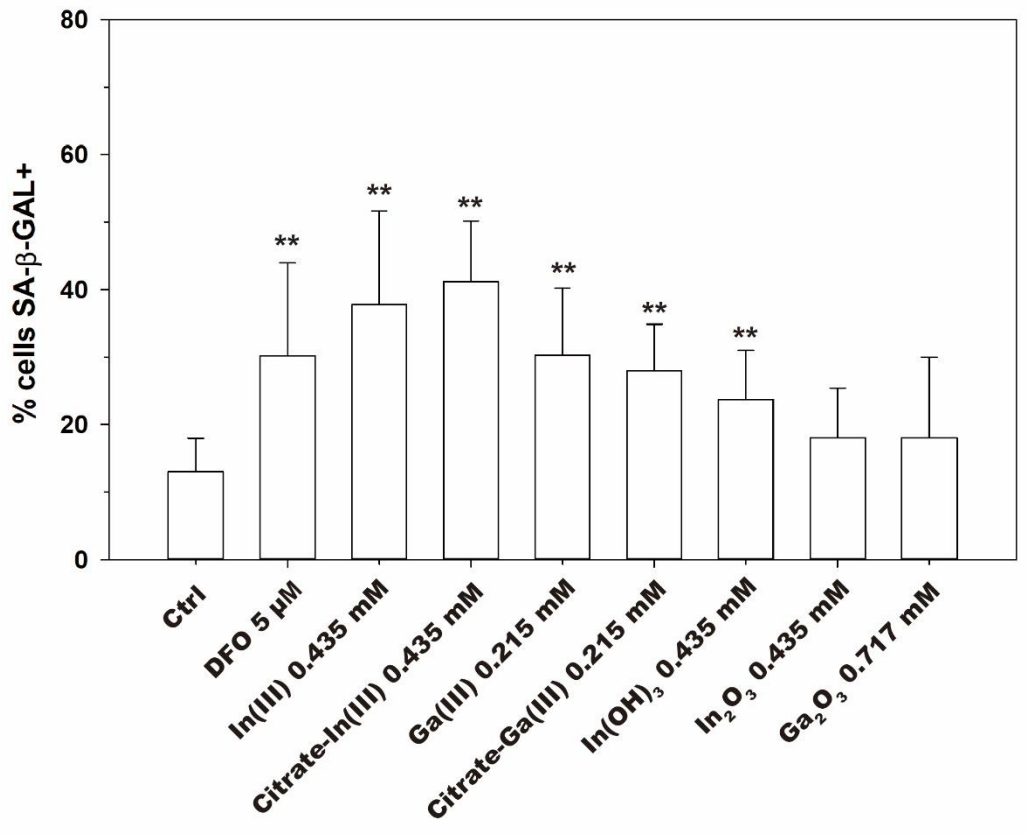

Figure 6.14 Senescence-associated beta-galactosidase (SA-β-gal) staining of DLD-1 cells, at least 500 cells were counted for each treatment. DLD-1 cells treated to Ga- and *In*-related chemicals for 72 hours. ** p<0.01 versus control, Kruskal–Wallis one-way analysis of variance followed by Games-Howell post-hoc test.

6.8 Ga- and *In*-Induced *in vitro* Proteasome Activity Inhibition

To explore the toxic mechanism by which Ga- and *In*-related chemicals may inhibit proteasome function, the *in vitro* assay of those compounds on 20S proteasome was performed. The 20S proteasome fraction was prepared from DLD-1 cell lysate. The proteasome activity was monitored by the fluorescently tagged substrates specific for the three main components of proteasome activity, including Suc-Leu-Leu-Val-Tyr-AMC for chymotrypsin-like peptidase activity, Boc-Leu-Arg-Arg-AMC for trypsin-like peptidase activity, and Z-Leu-Leu-Glu-AMC for caspase-like peptidase activity.

As expected, the proteasome inhibitor of MG132 significantly decreased overall activity of 20S proteasome, which was consistent with the established mechanism of this inhibitor acting on the proteasome (Figure 6.15). Furthermore, In(III) and citrate-In(III) (0.435 mM of *In*) also had shown proteasome inhibitory effects (chymotrypsin-like, trypsin-like and caspase-like activity) in the 20S proteasome, while Ga(III) and citrate-Ga(III) (0.717 mM of Ga) selectively inhibited the chymotrypsin-like and caspase-like activity of the 20S proteasome. However, $In(OH)_{3(s)}$ (0.435 mM of *In*) treatments only had inhibitory effect ($p<0.01$) on the chymotrypsin-like activity of 20S proteasome, and there were no significant differences in 20S proteasome activities between $In_2O_{3(s)}$ (0.435 mM of *In*), $Ga_2O_{3(s)}$ (0.717 mM of Ga) and control groups, indicating that the two compounds had no direct effect on 20S proteasome activity (Figure 6.15).

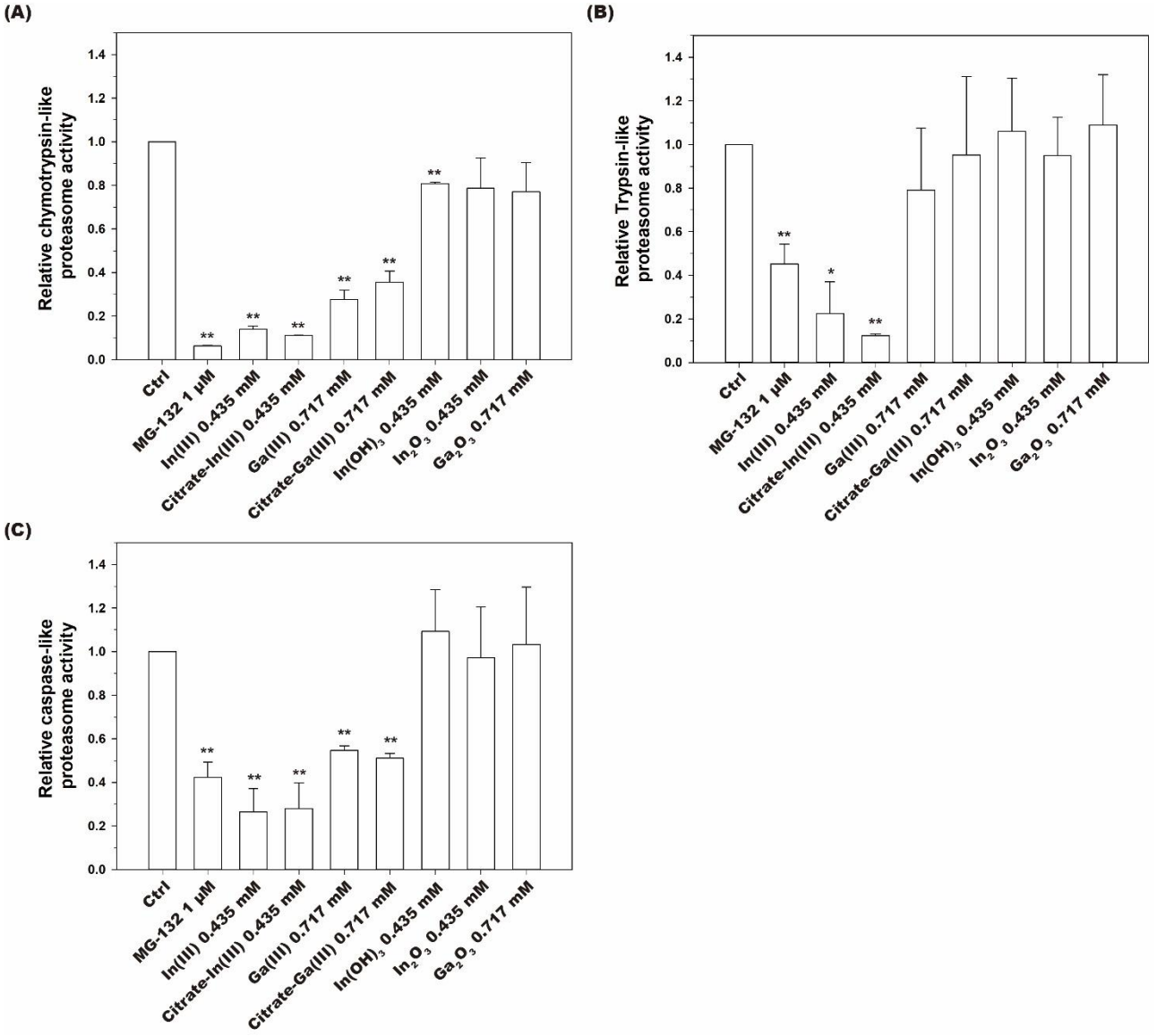

Figure 6.15 The inhibition effects of Ga- and *In*-related chemicals on the 20S proteasome activity. Purified 20S proteasome from DLD-1 cells treated to Ga- and *In*-related chemicals for 60 minutes. (A) Chymotrypsin-like activity; (B) Trypsin-like activity; (C) Caspase-like activity. Data are expressed as mean ± SD. Significance in difference between two groups were tested by independent sample t test. * $p<0.05$ ** $p<0.01$ versus control.

6.9 Possible Genotoxicity Induced by Ga- and *In*-Related Chemicals

The established high-throughput genotoxicity screening assay with EGFP-MDC1/MCF7 cells and the image-processing program was used to evaluate the potential of Ga- and *In*-related chemicals to induce genotoxicity. The results indicated that citrate-In(III) (0.435 mM of *In*), Ga(III), citrate-Ga(III) and $Ga_2O_{3(s)}$ (0.717 mM of Ga) significantly increased the EGFP-MDC1 foci area after 72 hours of exposure (Figure 6.16). On the other hand, In(III), $In(OH)_{3(s)}$ and $In_2O_{3(s)}$ (0.435 mM of *In*) did not increase the area of EGFP-MDC1 foci as compared to control groups.

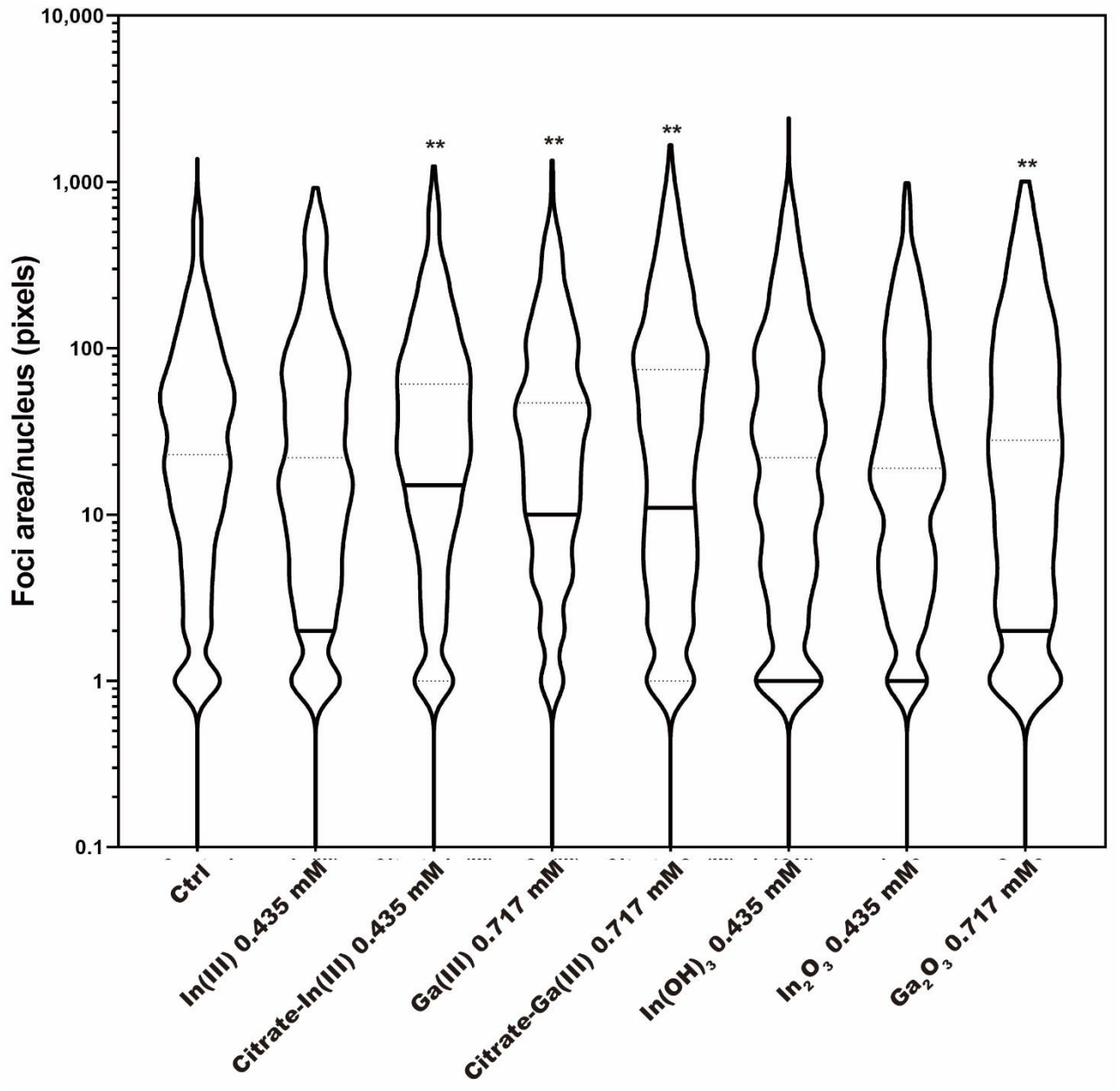

Figure 6.16 Result of mutagen test using the EGFP-MDC1 foci assay. Violin plots of foci area/ nucleus for each treatment. EGFP-MDC1/MCF7 cells treated to Ga- and *In*-related chemicals for 72 hours. 870-2,035 cells were counted for each treatment. The value on Y-axle represents the foci area/ nucleus in the common logarithm (log10) value. Dotted and solid lines represent the quartile and median, respectively. ** $p<0.01$ versus control, Kruskal–Wallis one-way analysis of variance followed by Games-Howell post-hoc test.

7. Discussion

7.1 Ga- and *In*-Induced Cytotoxicity is Associated with Cellular Iron Deficiency

7.1.1 Dose-Dependent of Ga- and *In*-Related Chemicals on Viability

According to previous studies, the cytotoxicity of Ga- and *In*-related chemicals was observed to be dependent on two factors, time, and dose (Ahamed et al., 2017; Badding et al., 2014; Gwinn et al., 2015; Merli et al., 2018; Olgun et al., 2017). In this study, we also investigated that the toxic effects become more pronounced to DLD-1 cells after approximately 24 hours to 72 hours of exposure (Figure 6.1). Therefore, 72 hours was chosen as endpoint for the analysis of lethal and sublethal toxic effects of Ga- and *In*-related chemicals to human cell lines (i.e., DLD-1 and EGFP-MDC1/MCF7).

The 72 h-LC_{50} values indicated that the cytotoxicity of Ga(III) treatments but not $Ga_2O_{3(s)}$, were greater than other *In* treatments (Table 6.1). It could be proposed that the ionic radius of Ga(III) (0.062 nm) was more similar to Fe(III) (0.0645 nm) than In(III) (0.080 nm), permitting it to bind with high affinity to certain iron-binding proteins and thus contribute to the cytotoxicity (Chitambar, 2016). The epithelial cells were more sensitive to the cytotoxic effects of *In*-related particle exposures as compared to the macrophage cells (Badding et al., 2014; Olgun et al., 2017), whereas the exposure of solubilized In(III) could remarkably increase the cytotoxicity to macrophage cells compared with the epithelial cells due to the increased expression of transferrin receptor on macrophage cell surface (Gwinn et al., 2015). In addition, it has been investigated that the decrease in viability as seen which

macrophage cells may be due to phagocytosis of Ga- or *In*-related particles in which these particles were solubilized within the cell through the phagolysosomal acidification pathway, resulting in cell death and the subsequent release of In(III) or Ga(III) extracellularly by the dying cells (Badding et al., 2014; Gwinn et al., 2015; Gwinn et al., 2013).

The direct exposure of In(III) or Ga(III) to both macrophage cells and epithelial cells could dramatically increase the susceptibility and toxicity as compared to the particulate chemicals (Gwinn et al., 2015), although we observed that 72 h-LC_{50} values of $In(OH)_{3(s)}$ and $In_2O_{3(s)}$ were much higher than In(III). It suggested that the higher concentration of In(III) treatments (e.g., 0.871 mM to 2.177 mM) tended to form hydroxide precipitates and thus decreased the solubilized form of *In* (Wood and Samson, 2006), and the use of citrate could prevent In(III) hydrolysis by forming a stable complex with In(III). Therefore, Ga(III) and In(III) appeared to be the main cytotoxic constituent of Ga- and *In*-based particles, although there was only a small part of particles solubilized by the macrophage cells. Those chemicals exhibited better water solubility could enhance their bioavailability to cells, and the release of solubilized metal ions from either phagolysosomal acidification or the dying cells appeared to increase the cytotoxicity (Bomhard, 2020; Gwinn et al., 2015).

7.1.2 Dose-Dependent Effect of Ga- and *In*-Related Chemicals on Cell Cycle Regulation but not Apoptosis

The sublethal dosesof Ga- and *In*-related chemicals did not induce apoptotic responses in DLD-1 cells (Figure 6.2), whereas these chemicals and DFO could induce cell cycle arrest at G_2/M phase

(Figure 6.3). DFO and the higher concentrations of Ga(III) and In(III) treatments appeared to slightly increase the proportion of total apoptotic cells, but the elevations did not reach statistical significance.

Because the chemical properties of Ga and *In* are similar to Fe and permit them to bind with high avidity to certain iron-binding proteins, they could serve as Fe-mimicking agents and result in disruption of the cellular iron homeostasis through cellular Fe-dependent pathways (Chitambar, 2012; Chitambar, 2016; Collery et al., 2002). Previous studies have reported that Ga(III) exposure inhibited the cell proliferation and increased the percentage of cells in either the G_0/G_1 phase or S phase (Chang et al., 2003; Collery et al., 2002). Also, the deprivation of Fe caused by Fe(III) chelators (e.g., DFO and ADR-529) could have effect on the cell cycle regulation and further induce cell cycle arrest at the G_1/S phase or G_2/M phase (Brodie et al., 1993; Lucas et al., 1995; Renton and Jeitner, 1996), and apoptosis (Hileti et al., 1995).

In previous reports, the exposure of *In*-based particles induced caspase-related apoptosis in macrophage cells, whereas the cytotoxicity in epithelial cells appeared to be necrosis (Badding et al., 2014; Gwinn et al., 2015). Tanaka et al. (2010) also indicated that intratracheal instillation of ITO and $In_2O_{3(s)}$ particles in hamsters resulted in significant necrotic debris within alveolar macrophages, which appeared to be a result of necrotic epithelial cell death (Tanaka et al., 2010).

Furthermore, the low concentrations (0.014 mM to 0.143 mM) of Ga(III) promoted the cultured human peripheral blood mononuclear cells to enter the S phase and further resulted in a cell cycle arrest at the S phase. In contrast, the high concentrations (0.717 mM to 1.434 mM) of Ga(III) could induce apoptotic responses, which were associated with increased cellular release of inflammatory

cytokines, including tumor necrosis factor-α (TNF-α), interleukin-1β (IL-1β), and interferon-γ (IFN-γ). However, the Ga-induced cytokine release and apoptosis could be inhibited by Fe(III)-saturated transferrin, indicating that these toxic effects of Ga were related to Fe metabolism (Chang et al., 2003).

Our results noted similar findings, the sublethal concentrations of Ga(III), In(III), and $In_2O_{3(s)}$ induced DLD-1 cells an increase in the G_2/M phase and a decrease in the G_0/G_1 phase, which were similar to that of DFO treated cells. It is proposed that if cellular damage and error are difficult to repair during cell division, the cells would enter the cell cycle arrest to inhibit cell proliferation (Hustedt and Durocher, 2017; Lezaja and Altmeyer, 2018). Other studies have demonstrated that DFO arrested cell proliferation at different stages of the cell cycle depending on the concentration and duration of exposure. The lower concentration of DFO and a longer exposure period (72 hours) could slow the passage of glioma cells through the cell cycle, eventually accumulating in the G_2/M phase (Renton and Jeitner, 1996). Consequently, the sublethal doses of the present study appeared to be not high enough to serve as a trigger to induce programmed cell death (apoptosis or necrosis), and the exposure time (72 hours) may accumulate the cell cycle in the G_2/M phase.

7.1.3 Ga-and *In*-Induced Polyploid Giant Cancer Cells Formation

Despite the programmed cell death and cell cycle, the sublethal toxic effects Ga(III) and In(III) on cell growth and division were also confirmed by direct time-lapse observation (Figure 6.5 and Figure 6.6). The sublethal concentrations of Ga(III) and In(III) showed typical temporal alterations of cell morphology associated with profound changes in cellular size, resulting in a enlarged, flattened

and irregular shape, senescent-like morphology after 72 hours of exposure. In addition, mitochondria of treated cells tended to aggregate in the budding-like structure at one perinuclear locus, whereas mitochondria showed broad cytoplasmic distribution in untreated control cells. Haga et al. (2003) have highlighted the changes in the localization of mitochondria participate in the regulation of mitochondrial-dependent apoptosis through cytochrome *c* release (Haga et al., 2003). However, DLD-1 cells treated with sublethal concentrations of Ga- and *In*-related chemicals did not induce either apoptosis or necrosis as described previously. The relationship between the cell morphology and abnormal alteration of mitochondrial dynamics is causal as well as the toxic mechanisms involved remain to be determined.

The cancer cells with relatively large cellular size, multiple nuclei or a single giant nucleus, and abnormal DNA content have been defined as polyploid giant cancer cells (PGCCs). In comparison with most solid tumors and cancer cell lines are aneuploid (i.e., chromosome number that is not a multiple of the diploid complement) (Weaver and Cleveland, 2008), PGCCs contain multiple sets of chromosomes that does not have an upper limit (e.g., 4N, 6N, or 16N) (Amend et al., 2019; Lv et al., 2014). Typically, the PGCCs have been defined as a cancer cell that is at least three times larger than the parental cancer cells (Fei et al., 2020; Zhang et al., 2014c).

Our study observed that not only DFO but also Ga(III) and In(III) sublethal exposures resulted in increasing the cell size and nuclear size, as well as the two distinct morphologies of DLD-1 cells (clone A and clone D) had become difficult to identify. Furthermore, these effects could be inhibited by the addition of citrate-Fe(III) (Figure 6.4), which indicated that the Ga- and *In*-induced PGCCs

formation were positively associated with cellular iron homeostasis. Polyploidy formation has been demonstrated to be triggered in response to cellular aging, abortive cell cycle, and a variety of genotoxic stresses including chemotherapeutics, radiation, hypoxia, oxidative stress, or environmental factors (e.g., air pollution, UV light or hyperthermia) (Walen, 2006; Was et al., 2021). The molecular basis of these phenomenon may be also related to increased chronic inflammation and damage response mechanism leading to the formation of PGCCs (Erenpreisa et al., 2008; Illidge et al., 2000). These findings suggested that disruption of iron homeostasis by either Fe(III) chelators or Ga(III) and In(III) could be another stressful factor to trigger polyploidy formation in cancer cells.

The general mechanism leading to formation of PGCCs may originate from endoreplication, mitotic slippage, cell fusion, cytokinesis failure, or cell cannibalism (Krajcovic and Overholtzer, 2012; Niu et al., 2016; Song et al., 2021; Was et al., 2021). By using time-lapse microscopy monitoring of the cell growth and division, we investigated that both Ga(III)- and In(III)-treated DLD-1 cells stimulated PGCCs formation within 72 hours of exposure, and the possible mechanisms may include endoreplication, cytokinesis failure, or cell-to-cell fusion due to morphological dynamic changes (Figure 6.5 and Figure 6.6). The cell cycle of Ga(III)- and In(III)-treated cells arrested at the G_2/M phase with increased DNA contents also confirmed our findings.

Also, DFO is the first Fe chelator to be used as an anticancer agent to prevent tumor progression in various types of cancer (Corcé et al., 2016; Hann et al., 1990; Lan et al., 2018; Salis et al., 2014; Yu et al., 2012), but some studies have shown that DFO promotes the invasion and migration of some aggressive cancer cells, such as colorectal cancer cells, glioblastoma cells, and breast cancer cells

(Chen et al., 2019a; Elstner et al., 2007; Liu et al., 2014; Zhang et al., 2014d). These results indicate that DFO has different effects on the different cell phenotypes, especially in those mechanisms that are associated with iron metabolism. Recent studies have noted that the number of PGCCs is more in high-grade malignant tumors than those low-grade counterparts, more in recurrence after chemotherapy, and more in the metastatic foci than in the primary sites (Fei et al., 2020; Fei et al., 2015; Zhang et al., 2014a). PGCCs may play some roles in DFO-induced cancer malignancy, however, the underlying mechanisms need to be explored between Fe deprivation and PGCCs formation.

The genomically unstable PGCCs have been found in various types of cancer with a relatively small (5-20 %) content of these cells within solid tumors (Alharbi et al., 2018; Coward and Harding, 2014; Fei et al., 2020), and are considered the seed cells fueling the proliferation, metastasis, chemoresistance, recurrence, and patients' prognosis in human cancers (Chen et al., 2019b; Fei et al., 2020; Fei et al., 2015; Lv et al., 2014; Niu et al., 2017; Zhang et al., 2014c; Zhang et al., 2016). The development of polyploidy has been demonstrated to favor escape from cellular senescence or mitotic catastrophe in systemic radiation-, hormone therapy-, immunotherapy-, or chemotherapy-treated cancer cells (Amend et al., 2019; Bharadwaj and Mandal, 2020; Mosieniak et al., 2015; Wang et al., 2013), and PGCCs have many properties of cancer stem cells and contribute to tumor heterogeneity (Chen et al., 2019b; Niu et al., 2016; Zhang et al., 2014c).

In response to acute stress (e.g., Fe deprivation, hypoxia), massive cancer cell death occurs in mitotic catastrophe and subsequent apoptosis whereas a small part of cancer cells could enter the giant cell cycle, which involves a multistep programmed processes (initiation, self-renewal,

termination, and stability) for the growth and division of PGCCs (Niu et al., 2016). PGCCs-derived daughter cells (i.e., nuclear budding or fragmentation) are capable of long-term proliferation and acquired numerous new genome/chromosome alterations, which play an important role in tumorigenesis and chemoresistance (Niu et al., 2017; Niu et al., 2016; Zhang et al., 2014c).

7.2 Ga and *In* Exposure Resulted in Mitochondrial Dysfunction and Dysregulation of Heme Homeostasis

To investigate the toxic mechanisms of Ga- and *In*-induced cell morphology changes (i.e., PGCCs formation) and abnormal alteration of mitochondrial dynamics (i.e., mitochondrial aggregation), we further evaluated the mitochondrial functions in DLD-1 cells, including mitochondrial membrane potential ($\Delta\Psi_m$) and enzymatic activities of mitochondrial respiratory chain complexes, following 72 hours exposure to sublethal concentrations of Ga- and *In*-related chemicals. The results indicated that these chemicals not only affected $\Delta\Psi_m$ (Figure 6.7), but also had the inhibition effect on enzymatic activities of mitochondrial respiratory chain complex I, II, III, and IV (Figure 6.9 and Figure 6.10), leading to mitochondrial dysfunction.

Previous studies also have reported that the higher concentration of In(III) (up to 1 mM) is able to impair isolated mitochondria by accelerating the ROS production, inhibiting mitochondrial respiratory chain functions and the protons transportation, resulting in isolated mitochondrial structure changes such as swelling and membrane depolarization (Yuan et al., 2017). The mechanism of In(III) on mitochondria appeared to be associated with the dysregulation of Ca(II), which also has

been observed in Ga(III) exposure (Gogvadze et al., 1996). Ga(III) could induce an efflux of Ca(II) from mitochondria in a dose-dependent manner, and the modes of action of Ga(III) may be located at the level of the mitochondrial membrane pore or involve pyridine nucleotide hydrolysis.

Mitochondria are generally known as the “power plant” of the cells because they play an essential role in the production of ATP through the oxidative phosphorylation of electron transport chain. Moreover, mitochondria are actively implicated in other processes, such as heme synthesis, cell differentiation, cell cycle regulation, ROS generation, apoptosis, calcium signaling, and iron metabolism, etc (Piomboni et al., 2012; Zhao et al., 2019). Since mitochondria are major sites of cellular Fe utilization and accumulation, Fe in the mitochondria functions as a cofactor in iron-sulfur cluster-containing proteins, and iron-containing proteins. It is proposed that iron-sulfur cluster and heme containing proteins in the citric acid cycle and the respiratory chain could be the potential target for Ga(III)- and In(III)-induced mitochondrial dysfunction in the cells (Chitambar et al., 2006; Yang and Chitambar, 2008; Yuan et al., 2017).

The mitochondrial respiratory chain is composed of transmembrane protein complexes (I-V) and the freely mobile electron transfer carriers ubiquinone and cytochrome *c*, and these complexes must be assembled into a specifically configured supercomplex to function properly (Guo et al., 2017; Iwata et al., 1998). The important mitochondrial iron sulfur cluster-containing protein in electron-transport chain include electron-transfer flavoproteins, NADH: ubiquinone oxidoreductase (complex I), Rieske iron-sulfur proteins (components of complex III), and subunits of succinate dehydrogenase (complex II). The heme-containing proteins include heme *b* of succinate dehydrogenase (complex II),

cytochrome *b* and cytochrome c_1 of cytochrome *c* reductase (complex III), heme *a* and heme a_3 of cytochrome *c* oxidase (complex IV) (Paul et al., 2017; Zhao et al., 2019). Besides the mitochondrial respiratory chain, iron-sulfur cluster containing proteins also involved in other processes, such as ferrochelatase, aconitase, lipoic acid synthase, biotin synthase, and radical S-adenosylmethionine enzymes (Dailey et al., 1994; Paul et al., 2017).

Iron deficiency is a major cause of heme deficiency, and the deficiency of heme synthesis in non-erythroid tissues could cause loss of complex IV, complex II and cytochrome *c*, increased ROS production, and decreased mitochondrial efficiency (Atamna, 2004; Atamna et al., 2001).

It has been reported that Fe(III) chelators (e.g., deferoxamine, deferiprone, and mitochondrially targeted deferoxamine) could affect cancer cell growth and metastasis, and Fe overload-induced osteoporosis. The underlying molecular mechanisms may include: (1) impairment of iron sulfur cluster and heme synthesis, leading to destabilization and dysfunction of iron-containing proteins/enzymes (Sandoval-Acuña et al., 2021), (2) Inhibition of mitochondrial respiratory chain complexes leading to mitochondrial ROS production, resulting in dysfunctional mitochondria with reduced supercomplexes and promoting apoptosis (Chen et al., 2019a; Fiorillo et al., 2020; Lan et al., 2018; Sandoval-Acuña et al., 2021; Zhang et al., 2019a), (3) fragmentation of the mitochondrial network and induction of mitophagy (Sandoval-Acuña et al., 2021), and (4) Regulation of genes related to iron metabolism (e.g., decreased expression of ferritin, increased expression of transferrin receptor 1, ferroportin or divalent metal transporter 1) (Chen et al., 2019a; Zhang et al., 2019a).

Our data showed that DFO significantly inhibited mitochondrial respiratory chain enzymatic activities from complex I to complex IV (Figure 6.10), these findings were similar to that of previous study (Zhang et al., 2019a). It was also revealed that Ga(III) and In(III) sublethal exposure demonstrated the inhibitory effects on the enzymatic activities of mitochondrial electron transport chain complexes (I-IV) as well as citrate synthase in citric acid cycle, in a dose-dependent manner. In addition, the severe inhibition effects of complex IV were also observed in lower concentrations of Ga(III) and In(III) as compared to those of complex I, II, and III, which indicated cells were iron/heme deficient (Atamna, 2004) (Figure 6.10).

To investigate whether the Ga- and *In*-induced Fe deficiency affect cellular heme biosynthesis, we further measured mitochondrial protoporphyrin IX (PPIX, a normal precursor of heme), heme, and zinc protoporphyrin IX (ZnPPIX, zinc is instead of iron) in DLD-1 cells, following 72 hours exposure to sublethal concentrations of Ga- and *In*-ionic groups. Data suggested that Ga(III), In(III) as well as DFO decreased not only heme contents but the concentrations of PPIX and ZnPPIX, whereas the decrease in ZnPPIX contents of DFO did not reach statistical significance (Figure 6.13).

Biosynthesis of porphyrins requires vitamins and minerals involved in heme biosynthesis mechanism, including pyridoxine (vitamin B_6), Zn, and riboflavin (Ponka, 1999). Also, heme biosynthesis depends on micronutrients such as biotin, lipoic acid, and pantothenic acid for producing succinyl-CoA from citric acid cycle. Fe and Zn are unique in their role in heme biosynthesis. Fe(II) is inserted into PPIX by ferrochelatase to form heme and is also essential for heme biosynthesis in a different way. The structure of ferrochelatase contains an iron-sulfur cluster, which is essential for its

enzymatic activity (Dailey et al., 2000). Under Fe deficiency or impaired iron utilization condition, Zn(II) becomes an alternative metal substrate for ferrochelatase, leading to increased ZnPPIX formation (Labbh et al., 1999). ZnPPIX may further regulate cellular heme catabolism through competitive inhibition of heme oxygenase, which is the rate-limiting enzyme in the heme degradation.

Ga- and *In*-induced Fe deficiency may further suppress heme biosynthesis, and the two metals appeared to have effect on either porphyrin synthesis or Zn metabolism (for ZnPPIX biosynthesis), which ultimately promoted dysregulation of heme homeostasis (Boskey et al., 1993; Goering and Rehm, 1990; Yang and Chitambar, 2008).

7.3 Ga- and *In*-Induced Mitochondrial Dysfunction is Associated with Cellular Senescence

Cellular senescence was first described as the irreversible cell cycle arrest resulting from prolonged replication of cultured cells *in vitro* (Hayflick and Moorhead, 1961), which could be considered a hallmark of aging-related diseases, wound healing, fibrosis, diabetes and carcinogenesis (Bharadwaj and Mandal, 2020; López-Otín et al., 2013). Senescence is triggered by development signals or a variety of environmental stress. According to the cell type and intensity of the stress, cells may respond by inducing repair, programmed cell death or senescence (Galluzzi et al., 2018; Sapieha and Mallette, 2018; Surova and Zhivotovsky, 2013). Cells could undergo senescence in response to various intrinsic and extrinsic stimuli, such as oncogenic activation (Di Micco et al., 2006), oxidative and genotoxic stress (Passos et al., 2010), mitochondrial dysfunction (García-Prat et al., 2016), inflammation, radiation or chemotherapeutic agents (Kumari and Jat, 2021; Mikuła-Pietrasik et al., 2020), and nutrient deprivation (Atamna, 2004).

Senescence is associated with multiple cellular, molecular alterations and distinct phenotypic changes including a stable and generally irreversible cell cycle arrest. Senescent cells remain viable with alterations in metabolic activity and are usually resistant to apoptosis (Childs et al., 2014; Hampel et al., 2004; Marcotte et al., 2004; Ryu et al., 2007; Sanders et al., 2013; Wang, 1995), and they could also develop morphological and structural changes, including an enlarged, flattened, multinucleated morphology with enlarged vacuoles (Campisi and d'Adda di Fagagna, 2007), altered

composition of the cell membrane and a significant nuclear enlargement (Hernandez-Segura et al., 2018; Kuilman et al., 2010; Ogrodnik et al., 2019; Salama et al., 2014).

Recent studies have demonstrated that treatment with chemotherapeutic agents or irradiation could provoke "therapy-induced senescence" in cancer cells. The "pseudo-senescence" or "senescence-like arrest" could be one avenue for tumor cells to evade the direct cytotoxic impact of anticancer therapy, thereby allowing for prolonged survival in a dormant state, with the potential to recover self-renewal capacity and contribute to cancer recurrence (Dörr et al., 2013; Dabrowska et al., 2018; Di Micco et al., 2006; Ewald et al., 2010; Mikuła-Pietrasik et al., 2020; Petrova et al., 2016; Saleh et al., 2018; Saleh et al., 2019; Toso et al., 2014). Nowadays, part of these senescent cancer cells has been defined as polyploid giant cancer cells (PGCCs) as mentioned earlier. They are formed by endoreplication, mitotic slippage, cell fusion, cytokinesis failure, or cell cannibalism (Krajcovic and Overholtzer, 2012; Niu et al., 2016; Song et al., 2021; Was et al., 2021). The genotoxic stress induced by anticancer therapies could result in cancer cells get arrested at G_2/M phase checkpoint for several days after which they undergo mitosis in the aberrant manner (Illidge et al., 2000). These cells then enter the giant cell cycle to initiate genomic reorganization, generating new tumor-initiating cells in response to anticancer therapy-induced stress and contributes to disease relapse (Niu et al., 2016).

In our study, the senescence-associated β-galactosidase activity (SA-β-Gal) of Ga- and *In*-related chemical treated DLD-1 cells was detected at pH 6.0. The sublethal concentration of Ga(III), In(III), $In(OH)_{3(s)}$ and DFO treatments significantly increased the percentage of SA-β-Gal positive cells (Figure 6.14), indicating that Ga- and *In*-induced cell cycle arrest (G_2/M phase), morphological

changes, mitochondrial dysfunction, dysregulation of heme homeostasis, and PGCCs formation were all related to cellular senescence (Bharadwaj and Mandal, 2020; Correia-Melo and Passos, 2015; Debacq-Chainiaux et al., 2016; Ogrodnik et al., 2019; Vasileiou et al., 2019).

Mitochondrial dysfunction-associated senescence has been identified to one of the different types of cellular senescence (Correia-Melo and Passos, 2015). Disruption of the mitochondrial respiratory chain complexes (e.g., dysregulation of iron homeostasis) and the electron transport chain have been associated to senescence (Atamna, 2004; Atamna et al., 2002; Miwa et al., 2014; Moiseeva et al., 2009; Stöckl et al., 2006; Yoon et al., 2003). It has proposed that the elevated mitochondrial ROS resulting from the disruption of the respiratory chain complexes and increased electron leakage could further decrease the electron transport chain efficiency contributing to additional ROS production, decreased ATP generation and oxidative damage in a positive feedback loop (Balaban et al., 2005; Wang et al., 2003; Zwerschke et al., 2003).

Yoon et al. (2003) reported that DFO-treated Chang cells induced cellular senescent process through the decrease of intracellular ATP level, $\Delta\Psi_m$ and complex II activity (Yoon et al., 2003). The declined activity of complex II was mainly due to down-regulation of protein expression of the iron-sulfur cluster containing subunit, which was associated with the irreversibility of the senescent arrest. Taken together, our results suggested that the decreased in activities of complex II and complex IV, mitochondrial PPIX, heme and ZnPPIX contents could be considered as the primary factors to regulate mitochondrial respiratory function by responding to Ga- and *In*-induced Fe deprivation, thereby triggering cellular senescence.

In consequence, Ga- and *In*-induced either cellular iron/heme deficiency or impairment of heme synthesis mechanisms was part of the major causes of Fe-dependent mitochondrial dysfunction, including decreased biosynthesis of PPIX, heme and ZnPPIX, enzymatic activity inhibition of citrate synthase (citric acid cycle) and mitochondrial respiratory chain complexes (I-IV). The alteration of $\Delta\Psi_m$ appeared to be due to the disruption of heme homeostasis and mitochondrial respiratory chain complexes, which eventually could drive cells into senescence and the formation of PGCCs.

7.4 Potential Modes of Action Related to Iron-Independent Pathways

In addition to the Fe-dependent pathways, we also evaluated the Fe-independent pathways of Ga- and *In*-induced toxic effect by using proteasome inhibition assay and genotoxicity screening assay (EGFP-MDC1 foci). Ga(III) and In(III) treatments significantly inhibited the chymotrypsin-like, trypsin-like, and caspase-like peptidase activity of purified proteasome, whereas $In(OH)_{3(s)}$, $In_2O_{3(s)}$, and $Ga_2O_{3(s)}$ particles did not affect proteasome activity (Figure 6.15). Previous studies have reported the synthetic Ga complexes could inhibit proteasomal chymotrypsin-like activity in prostate cancer cells, which appeared to be associated with down-regulation of androgen receptor and induction of apoptosis (caspase-3/caspase-7 activation) (Chen et al., 2007). However, the exact toxic mechanisms for Ga(III) and In(III) to interact with the proteasome need to be further investigated.

Moreover, proteasome inhibition has been demonstrated to be one of the factors to induce cellular senescence in human fibroblasts, and the senescent cells may have reduced proteolytic activities and less proteasome content (Chondrogianni and Gonos, 2004; Chondrogianni et al., 2003).

The prolonged disturbance of proteasome homeostasis could result in mitochondrial dysfunction, generation of mitochondrial ROS, and oxidative stress. The additional intracellular ROS may further impair proteasomal function and cause oxidative damage in a positive feedback loop, leading to nuclear DNA damage, cell cycle arrest, and eventual cellular senescence (Takenaka et al., 2020; Torres and Perez, 2008). Apart from Fe-dependent pathways, it appeared that the direct or indirect interaction between Ga(III)/In(III) and proteasome could be another factor to trigger mitochondrial dysfunction, ROS production, cellular senescence and PGCCs formation.

The International Agency for Research on Cancer (IARC) have classified Ga- and *In*-based compounds as carcinogens to humans, including GaAs (group 1, carcinogenic to humans), InP (group 2A, probably carcinogenic to humans) and ITO (group 2B, possibly carcinogenic to humans). Recent studies have demonstrated that DNA damage induced by either Ga- or *In*-related chemicals could occur through several key mechanisms, including oxidative stress induction (Ahamed et al., 2017; Badding et al., 2014; Flora et al., 2002; Olgun et al., 2017; Tabei et al., 2016; Takagi et al., 2011; Yang and Chitambar, 2008), Fe deprivation, and DNA replication stress accompanied by deregulation of cell proliferation (Chitambar, 2012; Chitambar, 2016; Merli et al., 2018). The phosphorylation of the histone H2AX is an early and sensitive biomarker of genotoxicity and is a consequence of different DNA lesions induced directly or indirectly by heavy metals (Kopp et al., 2018; Kuo and Yang, 2008). Using the EGFP-MDC1/MCF7 screening assay, similar results were obtained for both Ga- and *In*-related chemicals. We confirmed that average occupational exposure doses

(approximately three years) of citrate-In(III), Ga(III), citrate-Ga(III), and $Ga_2O_{3(s)}$ may have the genotoxic potency to induce DNA damage and produce oxidative stress (Figure 6.16).

7.5 The Potential Role of Cellular Senescence in Indium Lung Disease

As mentioned earlier, the latency period (month to years) of indium lung disease is relatively shorter than other occupational lung disease such as silicosis, asbestosis and coal workers' pneumoconiosis (Table 2.2) (Castranova and Vallyathan, 2000; Chonan et al., 2019; Chong et al., 2006; Leonard et al., 2020; Yuan et al., 2018; Zosky et al., 2016). Factors affecting the duration of the latency period in indium lung disease is not yet clear. However, the rate of pathological progression of indium lung disease appears to depend on not only the amount of inhaled In-related dust, but also the In(III) dissolved and accumulated in the patient's body.

As compared to occupational lung diseases with known etiology, natural lung aging has been demonstrated to be associated with molecular and physiological changes that alterations in lung function, declined pulmonary remodeling and regenerative capacity, and increased susceptibility to acute and chronic lung diseases, such as obstructive and fibrotic lung disease, fatal respiratory infection, and primary lung cancer (Cho and Stout-Delgado, 2020; Schneider et al., 2021) .

A variety of cellular stressors increase the development risk of aging-related lung diseases in a single or coordinated manner (Raghu et al., 2011; Schneider et al., 2021). The endogenous cellular stressors include genetic background, aging, gender, and pulmonary microbiology, whereas the

exogenous cellular stressors include cigarette smoking, hypoxia, infectious agents, environmental exposure, and air pollution.

The profound age-related processes impair the static and dynamic balance of lungs, resulting in abnormal cellular alteration in alveolar epithelial cells, alveolar macrophages, endothelial cells, immune cells, and fibroblasts (Schneider et al., 2021; Selman and Pardo, 2014). The hallmarks of cellular aging are proposed as major mechanisms for inducing aging lung, including genome-based failures (genomic instability, telomere attrition, epigenetic alterations), signaling dysfunction (deregulated nutrient sensing, altered intercellular communication), organelle compromise (mitochondrial dysfunction, loss of proteostasis), and cell phenotypic changes (stem cell exhaustion, cellular senescence) (López-Otín et al., 2013; Schneider et al., 2021).

A growing body of evidence suggested that cellular senescence and the senescence-associated secretory phenotype (SASP) may be a key potential pathogenic phenotype, which secrets pro-inflammatory cytokines, matrix remodeling proteases, and growth factors is particularly hazardous to the cells in the lung niche that require tight regulation of extracellular matrix remodeling and inflammatory responses to prevent abnormal tissue repair (Pardo and Selman, 2016; Schneider et al., 2021). The senescent cells could fuel the hallmarks of many aging phenotypes and age-related diseases, largely through the cell paracrine effects of SASP (Childs et al., 2017), which may further reinforce the growth arrest of the exposed adjacent cells, leading to secondary or paracrine senescence. A variety of the cell perturbations (e.g., telomere shortening, senescence, stem cell exhaustion, and

mitochondrial dysfunction) reported in age-related diseases have been shown to be present in epithelial and mesenchymal lung cells from patients with lung fibrosis (Mora et al., 2017).

Indeed, case studies of indium lung disease have shown aging-associated features, such as the increase in serum biomarker of chronic lung inflammation Krebs von den Lungen 6 (KL-6) and surfactant protein (SP-D), and alveolar macrophage dysfunction (forming cholesterol granulomas and alveolar proteinosis) (Chonan et al., 2019; Cummings et al., 2012; Tsao et al., 2021). Also, the follow-up studies on Taiwan In-handling workers have shown the increase in levels of global DNA methylation, antioxidant enzymes (i.e., superoxide dismutase, glutathione peroxidase and glutathione transferase) and oxidative stress biomarkers (i.e., malondialdehyde, olive tail moment and 8-OH-dG) (Institute of Labor Occupational Safety and Health, 2015; Liou et al., 2017). Recent studies indicated that *In*-containing particulates could have pro-inflammatory and pro-fibrogenic effects in the murine lungs, which were associated with the increased matrix metalloproteinase inducer (EMMPRIN), pro-inflammatory mediators of macrophage migration inhibitory factor (MIF) and transforming growth factor beta-1 (TGF-β1), and pro-fibrogenic mediators of platelet-derived growth factor-AA (PDGF-AA) and matrix metalloproteinase-9 (MMP-9) levels (Jiang et al., 2017).

In consequence, although exposure to air pollutants, silica, asbestos, and black carbon dusts promote the development of chronic pulmonary conditions, the age-related cellular changes still take several decades for disease progression and manifestation. In contrast, indium lung disease appeared to be a progressive decline in injury resolution processes stemming from various exogenous stress factors. The occupational exposure of *In*-containing dusts and released In(III) by phagocytic

macrophages may accelerate the pathogenesis of a senescent phenotype, which includes several hallmarks of cellular aging such as epigenetic dysregulation (Liou et al., 2017), oxidative stress, genomic instability (Afroz et al., 2018; Ahamed et al., 2017; Badding et al., 2014; Institute of Labor Occupational Safety and Health, 2015; Olgun et al., 2017; Tabei et al., 2016), as well as the increased pro-inflammatory and pro-fibrogenic effects (Huaux et al., 2018; Jeong et al., 2016; Jiang et al., 2017; Noguchi et al., 2016; Tanaka et al., 2010).

Our data demonstrated that In(III) and/or citrate-In(III) could induce cellular senescence (cell cycle arrest, PGCCs formation, senescence-associated β-galactosidase activity) based on Fe deficiency stress. In(III)-induced Fe deprivation condition resulted in mitochondrial abnormalities, including mitochondrial respiratory chain complexes impairment, heme homeostasis dysregulation, and alteration of mitochondrial membrane potential. Other toxic outcomes (proteasome inhibition, genotoxicity assay) regarding Fe-independent pathways also indicated In(III) may disturb proteasome homeostasis and cause DNA damage, and trigger cellular senescence.

However, it remains unclear who are the critical cellular players (epithelial cells, phagocytic macrophages, fibroblasts, immune cells) in *In*-induced cellular senescence, and the cellular and molecular mechanisms associated with multi-faceted SASP formation, by which these cells create subsets of senescent cells that are resistant to immune clearance and drive tissue degeneration, thereby contributing to the pathogenesis of indium lung disease.

8. Conclusions

Since the chemical properties of Ga(III) and In(III) are similar to Fe(III), the Ga-and/or *In*-based chemicals have been developed and further used as tumor, inflammation and infection imaging, and therapeutic agents. In addition, Ga- and *In*-related chemicals such as GaAs and ITO also have been widely used in semiconductor and optoelectronic industrial manufacturing. The workers engaged in Ga and *In* processing may potentially expose to these chemicals, which have known to increase serum-*In* levels and the risk of indium lung disease (interstitial pneumonia and pulmonary fibrosis) and lung cancer. The latency period (month to years) of indium lung disease is relatively shorter than other occupational lung disease such as silicosis and asbestosis. However, factors affecting the duration of the latency period in indium lung disease is not yet clear.

At the present time, the main modes of toxic action of Ga and *In* to humans and mammals could be divided into two groups, Fe-dependent and Fe-independent pathways. However, there is still a large gap in knowledge about the relationship between the exposure of Ga- and *In*-related chemicals, pathogenic mechanisms, and chronic health effects. Therefore, this study aims at investigating the biological factors or modes of action that potentially associated with the long-term health effects of Ga and *In* occupational exposure and the progression of indium lung disease.

The human colon carcinoma cell line DLD-1 was used in this study, firstly the viability assay was performed in a wide range of concentrations of Ga- and *In*-related chemicals (In(III), citrate-In(III), Ga(III), citrate-Ga(III), $In(OH)_{3(s)}$, $In_2O_{3(s)}$, and $Ga_2O_{3(s)}$) to evaluate the cytotoxicity (LC_{50}).

Secondly, the sublethal doses (Ga ionic groups: 0.022 mM and/or 0.215 mM of Ga; $Ga_2O_{3(s)}$: 0.717 mM of Ga; *In* treatments: 0.044 mM and/or 0.435 mM of In) were then determined by considering the calculated 72h-LC_{50} vales and estimated average workplace exposure level, the cytotoxicity (programmed cell death and cell cycle), cellular morphological alterations, mitochondrial dysfunction, heme homeostasis, cellular senescence, and other possible toxicity (proteasome inhibition and genotoxicity) were further performed to assess the biological factors that potentially related to sublethal effects of Ga and *In* exposure.

The calculated LC_{50} values (72 hours) from cell viability tests (MTT assay) indicated that the cytotoxicity increased in the order, Ga(III) > citrate-Ga(III) > $In(OH)_{3(s)}$ > citrate-In(III) > $In_2O_{3(s)}$ > In(III) > $Ga_2O_{3(s)}$. (0.014-3.586 mM of Ga; 0.009-2.177 mM of In). DLD-1 cells appeared to be more sensitive to Ga(III) and citrate-Ga(III) exposure as compared to In(III), citrate-In(III) and other hydroxide/oxides groups.

In the programmed cell death assay, Fe(III) chelator deferoxamine (DFO, 5 μM) and Ga- and *In*-related chemicals did not significantly enhance either apoptosis or necrosis of the DLD-1 cells after 72 hours of exposure. In contrast, the cell cycle progression was arrested at the G_2/M phase after 72 hours exposure with DFO and higher concentration of In(III), Ga(III) and $In_2O_{3(s)}$ treatment groups, accompanied by decreasing in the cell populations at the G_0/G_1 phase.

In addition to the cell cycle arrest, we also investigated that DFO and higher concentration of In(III) and Ga(III) treatments increased the cellular volume and nuclear size, resulting in enlarged flattened and irregular shape after 72 hours of exposure. Also, mitochondria tended to aggregate in

the budding-like structure at one perinuclear locus, whereas mitochondria showed broad cytoplasmic distribution in control cells. However, these alterations on cell morphology could be attenuated by the addition of citrate-Fe(III) (4.48 mM).

Ga(III) and In(III) could serve as Fe-mimicking agents and cause disruption of the cellular iron homeostasis through Fe-dependent pathways. The Fe deprivation conditions may further affect the cell cycle regulation and induce cell cycle arrest at G_2/M phase. Furthermore, since a variety of environmental stresses have demonstrated to trigger polyploidy formation, by which cancer cells would have larger cellular size, multiple nuclei or a single giant nucleus, and abnormal DNA content, and these cells have been defined as polyploid giant cancer cells (PGCCs). It is believed that cellular Fe deprivation induced by either DFO or Ga(III)/ In(III) could be another stressful factor to trigger PGCCs formation.

To investigate the toxic mechanisms of Ga- and *In*-induced cell morphology changes (i.e., PGCCs formation) and abnormal alteration of mitochondrial dynamics (i.e., mitochondrial aggregation), we further evaluated the mitochondrial functions, including mitochondrial membrane potential ($\Delta\Psi_m$), enzymatic activities of mitochondrial respiratory chain complexes, and the concentration of protoporphyrin IX (PPIX, a normal precursor of heme), heme, and zinc protoporphyrin IX (ZnPPIX, zinc is instead of iron). Results indicated that DFO, Ga and *In* sublethal exposure not only affected $\Delta\Psi_m$, mitochondrial PPIX, heme, and ZnPPIX contents, but also had the inhibition effects on enzymatic activities of mitochondrial respiratory chain complex I, II, III, and IV, leading to mitochondrial dysfunction.

Cellular senescence is associated with multiple cellular, molecular alterations and distinct phenotypic changes including a stable and irreversible cell cycle arrest, which has been considered as a hallmark of aging-related diseases, fibrosis, diabetes, and carcinogenesis. Senescence could be triggered by development signals or a variety of environmental stress, such as oxidative and genotoxic stress, and mitochondrial dysfunction. In our study, the sublethal exposure of Ga(III), In(III), $In(OH)_{3(s)}$ and DFO increased the percentage of senescence-associated β-galactosidase activity (SA-β-Gal) positive cells, indicating that Ga- and *In*-induced cell cycle arrest (G_2/M phase), morphological changes, mitochondrial dysfunction, dysregulation of heme homeostasis, and PGCCs formation were all related to cellular senescence.

In addition to the Fe-dependent pathways, we also evaluated the Fe-independent pathways of Ga- and *In*-induced toxic effects by using proteasome inhibition assay and genotoxicity screening assay (EGFP-MDC1 foci). Data suggested that Ga(III) and In(III) treatments inhibited the chymotrypsin-like, trypsin-like, and caspase-like peptidase activity of purified proteasome, whereas $In(OH)_{3(s)}$, $In_2O_{3(s)}$, and $Ga_2O_{3(s)}$ treatments did not affect proteasome activity. It is proposed that the direct or indirect interaction between Ga(III), In(III) and proteasome could induce proteostatic dysfunction, which has been identified as another stress factor to trigger cellular senescence. Furthermore, citrate-In(III), Ga(III), citrate-Ga(III), and $Ga_2O_{3(s)}$ treatments appeared to have the genotoxic potency to induce DNA damage.

Taken together, this study provides new insight into the potential role of *In*-induced cellular senescence in the pathological progression of indium lung disease. In recent years, the aging-related

lung diseases have been demonstrated to be associated with alterations in lung function, increased susceptibility to acute and chronic lung diseases, such as obstructive and fibrotic lung disease. The hallmarks of cellular aging include genome-based failures, signaling dysfunction, organelle compromise, and cell phynotypic changes.

Our results demonstrated that In(III) and/or citrate-In(III) could induce mitochondrial abnormalities and cellular senescence mainly based on Fe deficiency stress. Other toxic outcomes regarding to Fe-independent pathways also indicated In(III) may disturb proteostasis and cause DNA damage. These hallmarks of cellular aging appeared to accelerate cellular senescence process, and eventually affect the rate of pathological progression of indium lung disease.

Although this study elucidated the potential relationship between cellular aging and indium lung disease, future studies could address on the questions of investigating the critical cellular players (epithelial cells, phagocytic macrophages, fibroblasts, immune cells) in *In*-induced cellular senescence, and the cellular and molecular mechanisms associated with senescence-associated secretory phenotype (SASP) formation, by which these cells create subsets of senescent cells that are resistant to immune clearance and drive tissue degeneration, thereby contributing to the pathogenesis of indium lung disease.

References

American Conference of Governmental Industrial Hygienists (ACGIH). 2017. TLVs and BEIs: Based on the documentation of the threshold limit values for chemical substances and physical agents and biological exposure indices, Cincinnati, OH, USA.

Afroz, T., Hiraku, Y., Ma, N., Ahmed, S., Oikawa, S., Kawanishi, S. and Murata, M. 2018. Nitrative DNA damage in cultured macrophages exposed to indium oxide. Journal of Occupational Health 60(2), 148-155.

Ahamed, M., Akhtar, M.J., Khan, M.A.M., Alhadlaq, H.A. and Aldalbahi, A. 2017. Nanocubes of indium oxide induce cytotoxicity and apoptosis through oxidative stress in human lung epithelial cells. Colloids and Surfaces B: Biointerfaces 156, 157-164.

Aiba, Y., Kobayashi, K., Suzuki, J., Shimizu, Y., Nishimura, M., Sasaki, N., Makino, S. and Utsunomiya, T. 1995. A questionnaire survey on the use of dust respirators among lead workers in small scale companies. Industrial Health 33(1), 35-41.

Alharbi, A.M., De Marzo, A.M., Hicks, J.L., Lotan, T.L. and Epstein, J.I. 2018. Prostatic adenocarcinoma with focal pleomorphic giant cell features: A series of 30 cases. The American Journal of Surgical Pathology 42(10), 1286-1296.

Alibo, D.S., Nozaki, Y. and Jeandel, C. 1999. Indium and yttrium in North Atlantic and Mediterranean waters: Comparison to the Pacific data. Geochimica et Cosmochimica Acta 63(13), 1991-1999.

Amakawa, H., Alibo, D.S. and Nozaki, Y. 1996. Indium concentration in Pacific seawater. Geophysical Research Letters 23(18), 2473-2476.

Amata, A., Chonan, T., Omae, K., Nodera, H., Terada, J. and Tatsumi, K. 2015. High levels of indium exposure relate to progressive emphysematous changes: A 9-year longitudinal surveillance of indium workers. Thorax 70(11), 1040-1046.

Amend, S.R., Torga, G., Lin, K.-C., Kostecka, L.G., de Marzo, A., Austin, R.H. and Pienta, K.J. 2019. Polyploid giant cancer cells: Unrecognized actuators of tumorigenesis, metastasis, and

resistance. The Prostate 79(13), 1489-1497.

Andersen, J.C.Ø., Cropp, A. and Paradise, D.C. 2017. Solubility of indium-tin oxide in simulated lung and gastric fluids: Pathways for human intake. Science of The Total Environment 579, 628-636.

Antunes, L.C.S., Imperi, F., Minandri, F. and Visca, P. 2012. *In Vitro* and *in Vivo* antimicrobial activities of gallium nitrate against multidrug-resistant *Acinetobacter baumannii*. Antimicrobial Agents and Chemotherapy 56(11), 5961-5970.

Asami, T., Yoshino, A., Kubota, M. and Gotoh, S. 1990. Background level of indium and gallium in soil with special reference to the pollution of the soils from zinc and lead smelters. Zeitschrift für Pflanzenernährung und Bodenkunde 153(4), 257-259.

Asante, K.A., Agusa, T., Biney, C.A., Agyekum, W.A., Bello, M., Otsuka, M., Itai, T., Takahashi, S. and Tanabe, S. 2012. Multi-trace element levels and arsenic speciation in urine of e-waste recycling workers from Agbogbloshie, Accra in Ghana. Science of The Total Environment 424, 63-73.

Ashcroft, M., Taya, Y. and Vousden, K.H. 2000. Stress signals utilize multiple pathways to stabilize p53. Molecular and Cellular Biology 20(9), 3224-3233.

American Society for Testing and Materials (ASTM). 2010. Standard test method for measuring the toxicity of sediment-associated contaminants with freshwater invertebrates. ASTM International, West Conshohocken, PA, 2010.

Atamna, H. 2004. Heme, iron, and the mitochondrial decay of ageing. Ageing Research Reviews 3(3), 303-318.

Atamna, H., Liu, J. and Ames, B.N. 2001. Heme deficiency selectively interrupts assembly of mitochondrial complex IV in human fibroblasts: RELEVANCE TO AGING *. Journal of Biological Chemistry 276(51), 48410-48416.

Atamna, H., Walter, P.B. and Ames, B.N. 2002. The role of heme and iron-sulfur clusters in

mitochondrial biogenesis, maintenance, and decay with age. Archives of Biochemistry and Biophysics 397(2), 345-353.

Atkinson, C.A., Jolley, D.F. and Simpson, S.L. 2007. Effect of overlying water pH, dissolved oxygen, salinity and sediment disturbances on metal release and sequestration from metal contaminated marine sediments. Chemosphere 69(9), 1428-1437.

Aye, Y., Li, M., Long, M.J.C. and Weiss, R.S. 2015. Ribonucleotide reductase and cancer: Biological mechanisms and targeted therapies. Oncogene 34(16), 2011-2021.

Badding, M.A., Stefaniak, A.B., Fix, N.R., Cummings, K.J. and Leonard, S.S. 2014. Cytotoxicity and characterization of particles collected from an indium–tin oxide production facility. Journal of Toxicology and Environmental Health, Part A 77(20), 1193-1209.

Balaban, R.S., Nemoto, S. and Finkel, T. 2005. Mitochondria, oxidants, and aging. Cell 120(4), 483-495.

Baldoni, D., Steinhuber, A., Zimmerli, W. and Trampuz, A. 2010. *In vitro* activity of gallium maltolate against Staphylococci in logarithmic, stationary, and biofilm growth phases: comparison of conventional and calorimetric susceptibility testing methods. Antimicrobial Agents and Chemotherapy 54(1), 157-163.

Banin, E., Lozinski, A., Brady, K.M., Berenshtein, E., Butterfield, P.W., Moshe, M., Chevion, M., Greenberg, E.P. and Banin, E. 2008. The potential of desferrioxamine-gallium as an anti-Pseudomonas therapeutic agent. Proceedings of the National Academy of Sciences of the United States of America 105(43), 16761-16766.

Bard, J.A.M., Goodall, E.A., Greene, E.R., Jonsson, E., Dong, K.C. and Martin, A. 2018. Structure and Function of the 26S Proteasome. Annual review of biochemistry 87, 697-724.

Baudy, P., Zubrod, J.P., Konschak, M., Weil, M., Schulz, R. and Bundschuh, M. 2017. Does long-term fungicide exposure affect the reproductive performance of leaf-shredders? A partial life-cycle study using *Hyalella azteca*. Environmental Pollution 222, 458-464.

Bedard, P.L., Hansen, A.R., Ratain, M.J. and Siu, L.L. 2013. Tumour heterogeneity in the clinic. Nature 501(7467), 355-364.

Belozerov, E.S. 1966. The topography of gallium in the healthy human body. Bulletin of Experimental Biology and Medicine 62(4), 1141-1142.

Benézéth, P., Diakonov, I.I., Pokrovski, G.S., Dandurand, J.-L., Schott, J. and Khodakovsky, I.L. 1997. Gallium speciation in aqueous solution. Experimental study and modelling: Part 2. Solubility of α-GaOOH in acidic solutions from 150 to 250°C and hydrolysis constants of gallium (III) to 300°C. Geochimica et Cosmochimica Acta 61(7), 1345-1357.

Berggren, M.M., Burns, L.A., Abraham, R.T. and Powis, G. 1993. Inhibition of protein tyrosine phosphatase by the antitumor agent gallium nitrate. Cancer Research 53(8), 1862-1866.

Bernstein, L.R. 2012. Successful treatment of refractory postherpetic neuralgia with topical gallium maltolate: Case report. Pain Medicine 13(7), 915-918.

Bernstein, L.R., Tanner, T., Godfrey, C. and Noll, B. 2000. Chemistry and pharmacokinetics of gallium maltolate, a compound with high oral gallium bioavailability. Met Based Drugs 7(1), 33-47.

Bernstein, L.R. and Zhang, L. 2020. Gallium maltolate has *in vitro* antiviral activity against SARS-CoV-2 and is a potential treatment for COVID-19. Antiviral Chemistry and Chemotherapy 28, 2040206620983780-2040206620983780.

Besser, J.M., Steevens, J., Kunz, J.L., Brumbaugh, W.G., Ingersoll, C.G., Cox, S., Mebane, C., Balistrieri, L., Sinclair, J. and MacDonald, D. 2018. Characterizing toxicity of metal-contaminated sediments from the Upper Columbia River, Washington, USA, to benthic invertebrates. Environmental Toxicology and Chemistry 37(12), 3102-3114.

Betoulle, S., Etienne, J.C. and Vernet, G. 2002. *In vivo* and *in vitro* modulation of carp (*Cyprinus carpio* L.) phagocyte oxidative burst activity by gallium. Journal of Toxicology and Environmental Health, Part A 65(8), 603-615.

Bharadwaj, D. and Mandal, M. 2020. Senescence in polyploid giant cancer cells: A road that leads to chemoresistance. Cytokine & Growth Factor Reviews 52, 68-75.

Bhattacharyya, S., Yu, H., Mim, C. and Matouschek, A. 2014. Regulated protein turnover: Snapshots of the proteasome in action. Nature Reviews Molecular Cell Biology 15(2), 122-133.

Bhutta, M.K.S., Omar, A. and Yang, X. 2011. Electronic waste: A growing concern in today's environment. Economics Research International 2011, 1-8.

Blaise, C., Gagné, F., Férard, J.F. and Eullaffroy, P. 2008. Ecotoxicity of selected nano-materials to aquatic organisms. Environmental Toxicology 23(5), 591-598.

Bojórquez-Quintal, E., Escalante-Magaña, C., Echevarría-Machado, I. and Martínez-Estévez, M. 2017. Aluminum, a friend or foe of higher plants in acid soils. Frontiers in Plant Science 8(1767).

Bomhard, E.M. 2020. The toxicology of gallium oxide in comparison with gallium arsenide and indium oxide. Environmental Toxicology and Pharmacology 80, 103437.

Borgmann, U. 1983. Metal speciation and toxicity of free metal ions to aquatic biota. Advances in Environmental Technology 13, 47-72.

Borgmann, U. 1996. Systematic analysis of aqueous ion requirements of *Hyalella azteca*: A standard artificial medium including the essential bromide ion. Archives of Environmental Contamination and Toxicology 30(3), 356-363.

Borgmann, U., Cheam, V., Norwood, W.P. and Lechner, J. 1998. Toxicity and bioaccumulation of thallium in *Hyalella azteca*, with comparison to other metals and prediction of environmental impact. Environmental Pollution 99(1), 105-114.

Borgmann, U., Couillard, Y., Doyle, P. and Dixon, D.G. 2005a. Toxicity of sixty-three metals and metalloids to *Hyalella azteca* at two levels of water hardness. Environmental Toxicology and Chemistry 24(3), 641-652.

Borgmann, U., Grapentine, L., Norwood, W.P., Bird, G., Dixon, D.G. and Lindeman, D. 2005b.

Sediment toxicity testing with the freshwater amphipod *Hyalella azteca*: Relevance and application. Chemosphere 61(11), 1740-1743.

Borgmann, U., Néron, R. and Norwood, W.P. 2001. Quantification of bioavailable nickel in sediments and toxic thresholds to *Hyalella azteca*. Environmental Pollution 111(2), 189-198.

Boskey, A.L., Ziecheck, W., Guidon, P. and Doty, S.B. 1993. Gallium nitrate inhibits alkaline phosphatase activity in a differentiating mesenchymal cell culture. Bone and Mineral 20(2), 179-192.

Bousfield, E.L. 1958. Freshwater amphipod crustaceans of glaciated North America. Canadian Field-Naturalist 72, 55-113.

Braud, A., Hannauer, M., Mislin, G.L.A. and Schalk, I.J. 2009a. The *Pseudomonas aeruginosa* pyochelin-iron uptake pathway and its metal specificity. Journal of Bacteriology 191(11), 3517-3525.

Braud, A., Hoegy, F., Jezequel, K., Lebeau, T. and Schalk, I.J. 2009b. New insights into the metal specificity of the *Pseudomonas aeruginosa* pyoverdine–iron uptake pathway. Environmental Microbiology 11(5), 1079-1091.

Brix, K.V., Volosin, J.S., Adams, W.J., Reash, R.J., Carlton, R.G. and McIntyre, D.O. 2001. Effects of sulfate on the acute toxicity of selenate to freshwater organisms. Environmental Toxicology and Chemistry 20(5), 1037-1045.

Brodie, C., Siriwardana, G., Lucas, J., Schleicher, R., Terada, N., Szepesi, A., Gelfand, E. and Seligman, P. 1993. Neuroblastoma sensitivity to growth inhibition by deferrioxamine: Evidence for a block in G1 phase of the cell cycle. Cancer Research 53(17), 3968-3975.

Brookins, D.G. 2012. Eh-pH diagrams for geochemistry, Springer Berlin Heidelberg.

Brun, N.R., Christen, V., Furrer, G. and Fent, K. 2014. Indium and indium tin oxide induce endoplasmic reticulum stress and oxidative stress in zebrafish (*Danio rerio*). Environmental Science & Technology 48(19), 11679-11687.

Brun, N.R., Fields, P.D., Horsfield, S., Mirbahai, L., Ebert, D., Colbourne, J.K. and Fent, K. 2019. Mixtures of aluminum and indium induce more than additive phenotypic and toxicogenomic responses in *Daphnia magna*. Environmental Science & Technology 53(3), 1639-1649.

Burton, G.A. and Johnston, E.L. 2010. Assessing contaminated sediments in the context of multiple stressors. Environmental Toxicology and Chemistry 29(12), 2625-2643.

Campanella, B., Casiot, C., Onor, M., Perotti, M., Petrini, R. and Bramanti, E. 2017. Thallium release from acid mine drainages: Speciation in river and tap water from Valdicastello mining district (northwest Tuscany). Talanta 171, 255-261.

Campisi, J. and d'Adda di Fagagna, F. 2007. Cellular senescence: When bad things happen to good cells. Nature Reviews Molecular Cell Biology 8(9), 729-740.

Cardwell, A.S., Adams, W.J., Gensemer, R.W., Nordheim, E., Santore, R.C., Ryan, A.C. and Stubblefield, W.A. 2018. Chronic toxicity of aluminum, at a pH of 6, to freshwater organisms: Empirical data for the development of international regulatory standards/criteria. Environmental Toxicology and Chemistry 37(1), 36-48.

Carter, D.E., Aposhian, H.V. and Gandolfi, A.J. 2003. The metabolism of inorganic arsenic oxides, gallium arsenide, and arsine: A toxicochemical review. Toxicology and Applied Pharmacology 193(3), 309-334.

Castranova, V. and Vallyathan, V. 2000. Silicosis and coal workers' pneumoconiosis. Environmental Health Perspectives 108(suppl 4), 675-684.

Catane, R., Kaufman, J.H., Bakshi, S., Parthasarathy, K.L., Mittelman, A. and Murphy, G.P. 1977. Indium chloride bone-marrow scanning in advanced prostatic carcinoma. New York State Journal of Medicine 77(9), 1413-1416.

Cervi, E.C., Hudson, M., Rentschler, A. and Burton Jr., G.A. 2019. Metal toxicity during short-term sediment resuspension and redeposition in a tropical reservoir. Environmental Toxicology and Chemistry 38(7), 1476-1485.

Cescau, S., Cwerman, H., Létoffé, S., Delepelaire, P., Wandersman, C. and Biville, F. 2007. Heme acquisition by hemophores. BioMetals 20(3), 603.

Chang, H.-F., Wang, S.-L. and Yeh, K.-C. 2017. Effect of gallium exposure in *Arabidopsis thaliana* is similar to aluminum stress. Environmental Science & Technology 51(3), 1241-1248.

Chang, H.-F., Yang, P.-T., Lin, H.-W., Yeh, K.-C., Chen, M.-N. and Wang, S.-L. 2020. Indium uptake and accumulation by rice and wheat and health risk associated with their consumption. Environmental Science & Technology 54(23), 14946-14954.

Chang, K.L., Liao, W.T., Yu, C.L., Lan, C.C.E., Chang, L.W. and Yu, H.S. 2003. Effects of gallium on immune stimulation and apoptosis induction in human peripheral blood mononuclear cells. Toxicology and Applied Pharmacology 193(2), 209-217.

Chen, C., Wang, S. and Liu, P. 2019a. Deferoxamine enhanced mitochondrial iron accumulation and promoted cell migration in triple-negative MDA-MB-231 breast cancer cells via a ROS-dependent mechanism. International Journal of Molecular Sciences 20(19), 4952.

Chen, D., Frezza, M., Shakya, R., Cui, Q.C., Milacic, V., Verani, C.N. and Dou, Q.P. 2007. Inhibition of the proteasome activity by gallium(III) complexes contributes to their anti–prostate tumor effects. Cancer Research 67(19), 9258-9265.

Chen, H.W. 2006. Gallium, indium, and arsenic pollution of groundwater from a semiconductor manufacturing area of Taiwan. Bulletin of Environmental Contamination and Toxicology 77(2), 289-296.

Chen, H.W. 2007a. Characteristics and risk assessment of trace metals in airborne particulates from a semiconductor industrial area of Northern Taiwan. Fresenius Environmental Bulletin 16, 1288-1294.

Chen, H.W. 2007b. Exposure and health risk of gallium, indium, and arsenic from semiconductor manufacturing industry workers. Bulletin of Environmental Contamination and Toxicology 78(1), 5-9.

Chen, J., Niu, N., Zhang, J., Qi, L., Shen, W., Donkena, V.K., Feng, Z. and Liu, J. 2019b. Polyploid giant cancer cells (PGCCs): The evil roots of cancer. Current Cancer Drug Targets 19(5), 360-367.

Chen, W.-T., Tsai, L.-C., Tsai, F.-C. and Shu, C.-M. 2012a. Recovery of gallium and arsenic from gallium arsenide waste in the electronics industry. CLEAN – Soil, Air, Water 40(5), 531-537.

Chen, Y., Ohara, T., Xing, B., Qi, J., Noma, K. and Matsukawa, A. 2020. A promising new anti-cancer strategy: Iron chelators targeting CSCs. Acta Medica Okayama 74(1), 1-6.

Chen, Z., Zhang, D., Yue, F., Zheng, M., Kovacevic, Z. and Richardson, D.R. 2012b. The iron chelators Dp44mT and DFO inhibit TGF-β-induced epithelial-mesenchymal transition via up-regulation of N-Myc downstream-regulated gene 1 (NDRG1). Journal of Biological Chemistry 287(21), 17016-17028.

Cheng, T.-H., Liu, C.-J., Tsai, T.-Y. and Shen, Y.-H. 2019. A process for the recovery of gallium from gallium arsenide scrap. Processes 7(12), 921.

Childs, B.G., Baker, D.J., Kirkland, J.L., Campisi, J. and van Deursen, J.M. 2014. Senescence and apoptosis: Dueling or complementary cell fates? EMBO Reports 15(11), 1139-1153.

Childs, B.G., Gluscevic, M., Baker, D.J., Laberge, R.M., Marquess, D., Dananberg, J. and van Deursen, J.M. 2017. Senescent cells: An emerging target for diseases of ageing. Nature Reviews Drug Discovery 16(10), 718-735.

Chitambar, C.R. 2004. Gallium nitrate for the treatment of non-Hodgkin's lymphoma. Expert Opinion on Investigational Drugs 13(5), 531-541.

Chitambar, C.R. 2010. Medical applications and toxicities of gallium compounds. International Journal of Environmental Research and Public Health 7(5), 2337.

Chitambar, C.R. 2012. Gallium-containing anticancer compounds. Future Medicinal Chemistry 4(10), 1257-1272.

Chitambar, C.R. 2016. Gallium and its competing roles with iron in biological systems. Biochimica

et Biophysica Acta (BBA) - Molecular Cell Research 1863(8), 2044-2053.

Chitambar, C.R., Al-Gizawiy, M.M., Alhajala, H.S., Pechman, K.R., Wereley, J.P., Wujek, R., Clark, P.A., Kuo, J.S., Antholine, W.E. and Schmainda, K.M. 2018. Gallium maltolate disrupts tumor iron metabolism and retards the growth of glioblastoma by inhibiting mitochondrial function and ribonucleotide reductase. Molecular Cancer Therapeutics 17(6), 1240-1250.

Chitambar, C.R. and Antholine, W.E. 2013. Iron-targeting antitumor activity of gallium compounds and novel insights into triapine(®)-metal complexes. Antioxidants and Redox Signaling 18(8), 956-972.

Chitambar, C.R., Matthaeus, W.G., Antholine, W.E., Graff, K. and O'Brien, W.J. 1988. Inhibition of leukemic HL60 cell growth by transferrin-gallium: Effects on ribonucleotide reductase and demonstration of drug synergy with hydroxyurea. Blood 72(6), 1930-1936.

Chitambar, C.R. and Narasimhan, J. 1991. Targeting iron-dependent DNA synthesis with gallium and transferrin-gallium. Pathobiology 59(1), 3-10.

Chitambar, C.R., Narasimhan, J., Guy, J., Sem, D.S. and O'Brien, W.J. 1991. Inhibition of ribonucleotide reductase by gallium in murine leukemic L1210 cells. Cancer Research 51(22), 6199-6201.

Chitambar, C.R. and Purpi, D.P. 2010. A novel gallium compound synergistically enhances bortezomib-induced apoptosis in mantle cell lymphoma cells. Leukemia Research 34(7), 950-953.

Chitambar, C.R. and Sax, D. 1992. Regulatory effects of gallium on transferrin-independent iron uptake by human leukemic HL60 cells. Blood 80(2), 505-511.

Chitambar, C.R. and Seligman, P.A. 1986. Effects of different transferrin forms on transferrin receptor expression, iron uptake, and cellular proliferation of human leukemic HL60 cells. Mechanisms responsible for the specific cytotoxicity of transferrin-gallium. Journal of Clinical Investigation 78(6), 1538-1546.

Chitambar, C.R., Wereley, J.P. and Matsuyama, S. 2006. Gallium-induced cell death in lymphoma: Role of transferrin receptor cycling, involvement of Bax and the mitochondria, and effects of proteasome inhibition. Molecular Cancer Therapeutics 5(11), 2834-2843.

Chitambar, C.R. and Zivkovic, Z. 1987. Uptake of gallium-67 by human leukemic cells: Demonstration of transferrin receptor-dependent and transferrin-independent mechanisms. Cancer Research 47(15), 3929-3934.

Cho, S.J. and Stout-Delgado, H.W. 2020. Aging and lung disease. Annual Review of Physiology 82, 433-459.

Chonan, T., Amata, A., Kawabata, Y. and Omae, K. 2019. Indium lung: Discovery, pathophysiology and prevention. The Tohoku Journal of Experimental Medicine 248(3), 143-150.

Chonan, T., Taguchi, O. and Omae, K. 2007. Interstitial pulmonary disorders in indium-processing workers. European Respiratory Journal 29(2), 317-324.

Chondrogianni, N. and Gonos, E.S. 2004. Proteasome inhibition induces a senescence-like phenotype in primary human fibroblasts cultures. Biogerontology 5(1), 55-61.

Chondrogianni, N., Stratford, F.L.L., Trougakos, I.P., Friguet, B., Rivett, A.J. and Gonos, E.S. 2003. Central role of the proteasome in senescence and survival of human fibroblasts: Induction of a senescence-like phenotype upon its inhibition and resistance to stress upon its activation*. Journal of Biological Chemistry 278(30), 28026-28037.

Chong, S., Lee, K.S., Chung, M.J., Han, J., Kwon, O.J. and Kim, T.S. 2006. Pneumoconiosis: Comparison of imaging and pathologic findings. RadioGraphics 26(1), 59-77.

Chugainova, A. and Rudakova, L. 2020. Effectiveness assessment of different methods of indium leaching from mobile phone screens. E3S Web of Conferences 161, 01077.

Ciacci, L., Werner, T.T., Vassura, I. and Passarini, F. 2019. Backlighting the European indium recycling potentials. Journal of Industrial Ecology 23(2), 426-437.

Cobelo-García, A., Filella, M., Croot, P., Frazzoli, C., Du Laing, G., Ospina-Alvarez, N., Rauch, S.,

Salaun, P., Schäfer, J. and Zimmermann, S. 2015. COST action TD1407: Network on technology-critical elements (NOTICE)—from environmental processes to human health threats. Environmental Science and Pollution Research 22(19), 15188-15194.

Coleman, M., Kuskie, K., Liu, M., Chaffin, K., Libal, M., Giguère, S., Bernstein, L. and Cohen, N. 2010. In vitro antimicrobial activity of gallium maltolate against virulent Rhodococcus equi. Veterinary Microbiology 146(1), 175-178.

Collery, P., Keppler, B., Madoulet, C. and Desoize, B. 2002. Gallium in cancer treatment. Critical Reviews in Oncology/Hematology 42(3), 283-296.

Collery, P., Millart, H., Lamiable, D., Vistelle, R., Rinjard, P., Tran, G., Gourdier, B., Cossart, C., Bouana, J.C., Pechery, C. and et al. 1989. Clinical pharmacology of gallium chloride after oral administration in lung cancer patients. Anticancer Research 9(2), 353-356.

Collins, G.A. and Goldberg, A.L. 2017. The logic of the 26S proteasome. Cell 169(5), 792-806.

Collvin, L. 1985. The effect of copper on growth, food consumption and food conversion of perch *Perca fluviatilis* L. Offered maximal food rations. Aquatic Toxicology 6(2), 105-113.

Cooman, W.D., Blaise, C., Janssen, C.R., Detemmerman, L., Elst, R. and Persoone, G. 2015. History and sensitivity comparison of two standard whole-sediment toxicity tests with crustaceans: the amphipod *Hyalella azteca* and the ostracod *Heterocypris incongruens* microbiotest. Knowledge and Management of Aquatic Ecosystems 416, 15.

Corcé, V., Gouin, S.G., Renaud, S., Gaboriau, F. and Deniaud, D. 2016. Recent advances in cancer treatment by iron chelators. Bioorganic and Medicinal Chemistry Letters 26(2), 251-256.

Correia-Melo, C. and Passos, J.F. 2015. Mitochondria: Are they causal players in cellular senescence? Biochimica et Biophysica Acta (BBA) - Bioenergetics 1847(11), 1373-1379.

Cory, J.G. 1983. Role of ribonucleotide reductase in cell division. Pharmacology and Therapeutics 21(2), 265-276.

Coward, J. and Harding, A. 2014. Size does matter: Why polyploid tumor cells are critical drug targets

in the war on cancer. Frontiers in Oncology 4(123).

Crunkhorn, S. 2018. Gallium fights infection in phase I trial. Nature Reviews Drug Discovery 17(11), 786-786.

Cummings, K.J., Donat, W.E., Ettensohn, D.B., Roggli, V.L., Ingram, P. and Kreiss, K. 2010. Pulmonary alveolar proteinosis in workers at an indium processing facility. American Journal of Respiratory and Critical Care Medicine 181(5), 458-464.

Cummings, K.J., Nakano, M., Omae, K., Takeuchi, K., Chonan, T., Xiao, Y.-l., Harley, R.A., Roggli, V.L., Hebisawa, A., Tallaksen, R.J., Trapnell, B.C., Day, G.A., Saito, R., Stanton, M.L., Suarthana, E. and Kreiss, K. 2012. Indium Lung Disease. Chest 141(6), 1512-1521.

Cummings, K.J., Virji, M.A., Trapnell, B.C., Carey, B., Healey, T. and Kreiss, K. 2014. Early changes in clinical, functional, and laboratory biomarkers in workers at risk of indium lung disease. Annals of the American Thoracic Society 11(9), 1395-1403.

Dörr, J.R., Yu, Y., Milanovic, M., Beuster, G., Zasada, C., Däbritz, J.H.M., Lisec, J., Lenze, D., Gerhardt, A., Schleicher, K., Kratzat, S., Purfürst, B., Walenta, S., Mueller-Klieser, W., Gräler, M., Hummel, M., Keller, U., Buck, A.K., Dörken, B., Willmitzer, L., Reimann, M., Kempa, S., Lee, S. and Schmitt, C.A. 2013. Synthetic lethal metabolic targeting of cellular senescence in cancer therapy. Nature 501(7467), 421-425.

D'Angiolella, V., Donato, V., Forrester, Frances M., Jeong, Y.-T., Pellacani, C., Kudo, Y., Saraf, A., Florens, L., Washburn, Michael P. and Pagano, M. 2012. Cyclin F-mediated degradation of ribonucleotide reductase M2 controls genome integrity and DNA repair. Cell 149(5), 1023-1034.

Dabrowska, M., Uram, L., Zielinski, Z., Rode, W. and Sikora, E. 2018. Oxidative stress and inhibition of nitric oxide generation underlie methotrexate-induced senescence in human colon cancer cells. Mechanisms of Ageing and Development 170, 22-29.

Dahm, C.N. 1981. Pathways and mechanisms for removal of dissolved organic carbon from leaf

leachate in streams. Canadian Journal of Fisheries and Aquatic Sciences 38(1), 68-76.

Dailey, H.A., Dailey, T.A., Gerdes, S., Jahn, D., Jahn, M., O'Brian, M.R. and Warren, M.J. 2017. Prokaryotic heme biosynthesis: multiple pathways to a common essential product. Microbiology and Molecular Biology Reviews 81(1), e00048-00016.

Dailey, H.A., Dailey, T.A., Wu, C.K., Medlock, A.E., Rose, J.P. and Wang, K.F. 2000. Ferrochelatase at the millennium: Structures, mechanisms and [2Fe-2S] clusters. Cellular and Molecular Life Sciences CMLS 57(13), 1909-1926.

Dailey, H.A., Finnegan, M.G. and Johnson, M.K. 1994. Human ferrochelatase is an iron-sulfur protein. Biochemistry 33(2), 403-407.

Dailey, H.A. and Meissner, P.N. 2013. Erythroid heme biosynthesis and its disorders. Cold Spring Harbor Perspectives in Medicine 3(4), a011676-a011676.

De Boeck, G., Vlaeminck, A. and Blust, R. 1997. Effects of sublethal copper exposure on copper accumulation, food consumption, growth, energy stores, and nucleic acid content in common carp. Archives of Environmental Contamination and Toxicology 33(4), 415-422.

Deane, E.E. and Woo, N.Y.S. 2009. Modulation of fish growth hormone levels by salinity, temperature, pollutants and aquaculture related stress: A review. Reviews in Fish Biology and Fisheries 19(1), 97-120.

Debacq-Chainiaux, F., Ben Ameur, R., Bauwens, E., Dumortier, E., Toutfaire, M. and Toussaint, O. 2016. Cellular ageing and replicative senescence. Rattan, S.I.S. and Hayflick, L. (eds), pp. 243-262, Springer International Publishing, Cham.

Decharat, S. 2018. Urinary mercury levels among workers in e-waste shops in Nakhon Si Thammarat Province, Thailand. Journal of Preventive Medicine and Public Health 51(4), 196-204.

Dexter, D.L., Spremulli, E.N., Fligiel, Z., Barbosa, J.A., Vogel, R., VanVoorhees, A. and Calabresi, P. 1981. Heterogeneity of cancer cells from a single human colon carcinoma. The American Journal of Medicine 71(6), 949-956.

Di Micco, R., Fumagalli, M., Cicalese, A., Piccinin, S., Gasparini, P., Luise, C., Schurra, C., Garre', M., Giovanni Nuciforo, P., Bensimon, A., Maestro, R., Giuseppe Pelicci, P. and d'Adda di Fagagna, F. 2006. Oncogene-induced senescence is a DNA damage response triggered by DNA hyper-replication. Nature 444(7119), 638-642.

Diakonov, I.I., Pokrovski, G.S., Bénézeth, P., Schott, J., Dandurand, J.-L. and Escalier, J. 1997. Gallium speciation in aqueous solution. Experimental study and modelling: Part 1. Thermodynamic properties of $Ga(OH)_4^-$ to 300°C. Geochimica et Cosmochimica Acta 61(7), 1333-1343.

Dixon, K.M., Lui, G.Y.L., Kovacevic, Z., Zhang, D., Yao, M., Chen, Z., Dong, Q., Assinder, S.J. and Richardson, D.R. 2013. Dp44mT targets the AKT, TGF-β and ERK pathways via the metastasis suppressor NDRG1 in normal prostate epithelial cells and prostate cancer cells. British Journal of Cancer 108(2), 409-419.

Dominici, S., Pieri, L., Comporti, M. and Pompella, A. 2003. Possible role of membrane gamma-glutamyltransferase activity in the facilitation of transferrin-dependent and -independent iron uptake by cancer cells. Cancer Cell International 3(1), 7.

Dong, Z., Arnold, R.J., Yang, Y., Park, M.H., Hrncirova, P., Mechref, Y., Novotny, M.V. and Zhang, J.-T. 2005. Modulation of differentiation-related gene 1 expression by cell cycle blocker mimosine, revealed by proteomic analysis*. Molecular and Cellular Proteomics 4(7), 993-1001.

Drobyski, W.R., Ul-Haq, R., Majewski, D. and Chitambar, C.R. 1996. Modulation of *in vitro* and *in vivo* T-cell responses by transferrin-gallium and gallium nitrate. Blood 88(8), 3056-3064.

Dussault, È.B., Balakrishnan, V.K., Sverko, E., Solomon, K.R. and Sibley, P.K. 2008. Toxicity of human pharmaceuticals and personal care products to benthic invertebrates. Environmental Toxicology and Chemistry 27(2), 425-432.

Ebrahimpour, M., Alipour, H. and Rakhshah, S. 2010. Influence of water hardness on acute toxicity

of copper and zinc on fish. Toxicology and Industrial Health 26(6), 361-365.

Edwards, C.L. and Hayes, R.L. 1969. Tumor scanning with 67Ga citrate. Journal of Nuclear Medicine 10(2), 103-105.

Einhorn, L. 2003. Gallium nitrate in the treatment of bladder cancer. Seminars in Oncology 30(2 Suppl 5), 34-41.

Elstner, A., Holtkamp, N. and von Deimling, A. 2007. Involvement of Hif-1 in desferrioxamine-induced invasion of glioblastoma cells. Clinical and Experimental Metastasis 24(1), 57-66.

Engström, Y., Eriksson, S., Jildevik, I., Skog, S., Thelander, L. and Tribukait, B. 1985. Cell cycle-dependent expression of mammalian ribonucleotide reductase. Differential regulation of the two subunits. Journal of Biological Chemistry 260(16), 9114-9116.

Enkirch, T., Sauber, S., Anderson, D.E., Gan, E.S., Kenanov, D., Maurer-Stroh, S. and von Messling, V. 2019. Identification and *in vivo* efficacy assessment of approved orally bioavailable human host protein-targeting drugs with broad anti-influenza A activity. Frontiers in Immunology 10, 1097-1097.

Erenpreisa, J., Ivanov, A., Wheatley, S.P., Kosmacek, E.A., Ianzini, F., Anisimov, A.P., Mackey, M., Davis, P.J., Plakhins, G. and Illidge, T.M. 2008. Endopolyploidy in irradiated p53-deficient tumour cell lines: Persistence of cell division activity in giant cells expressing Aurora-B kinase. Cell Biology International 32(9), 1044-1056.

Eriksson, J. 2001. Concentrations of 61 trace elements in sewage sludge, farmyard manure, mineral fertiliser, precipitation and in oil and crops, Swedish Environmental Protection Agency.

Eriksson, S., Gräslund, A., Skog, S., Thelander, L. and Tribukait, B. 1984. Cell cycle-dependent regulation of mammalian ribonucleotide reductase. The S phase-correlated increase in subunit M2 is regulated by de novo protein synthesis. Journal of Biological Chemistry 259(19), 11695-11700.

Ewald, J.A., Desotelle, J.A., Wilding, G. and Jarrard, D.F. 2010. Therapy-induced senescence in

cancer. Journal of the National Cancer Institute 102(20), 1536-1546.

Eychenne, R., Bouvry, C., Bourgeois, M., Loyer, P., Benoist, E. and Lepareur, N. 2020. Overview of radiolabeled somatostatin analogs for cancer imaging and therapy. Molecules 25(17), 4012.

Fani, M., Nicolas, G.P. and Wild, D. 2017. Somatostatin receptor antagonists for imaging and therapy. Journal of Nuclear Medicine 58(Supplement 2), 61S-66S.

Fei, F., Liu, K., Li, C., Du, J., Wei, Z., Li, B., Li, Y., Zhang, Y. and Zhang, S. 2020. Molecular mechanisms by which S100A4 regulates the migration and invasion of PGCCs with their daughter cells in human colorectal cancer. Frontiers in Oncology 10(182), 1-13.

Fei, F., Zhang, D., Yang, Z., Wang, S., Wang, X., Wu, Z., Wu, Q. and Zhang, S. 2015. The number of polyploid giant cancer cells and epithelial-mesenchymal transition-related proteins are associated with invasion and metastasis in human breast cancer. Journal of Experimental & Clinical Cancer Research 34(1), 158.

Ferguson, A.D. and Deisenhofer, J. 2002. TonB-dependent receptors—structural perspectives. Biochimica et Biophysica Acta (BBA) - Biomembranes 1565(2), 318-332.

Fetters, K.J., Costello, D.M., Hammerschmidt, C.R. and Burton Jr., G.A. 2016. Toxicological effects of short-term resuspension of metal-contaminated freshwater and marine sediments. Environmental Toxicology and Chemistry 35(3), 676-686.

Filella, M. and Rodríguez-Murillo, J.C. 2017. Less-studied TCE: Are their environmental concentrations increasing due to their use in new technologies? Chemosphere 182, 605-616.

Finley, D. 2009. Recognition and processing of ubiquitin-protein conjugates by the proteasome. Annual Review of Biochemistry 78(1), 477-513.

Fiorillo, M., Tóth, F., Brindisi, M., Sotgia, F. and Lisanti, M.P. 2020. Deferiprone (DFP) targets cancer stem cell (CSC) propagation by inhibiting mitochondrial metabolism and inducing ROS production. Cells 9(6), 1529.

Flerus, B., Billmann, L., Bokelmann, K., Stauber, R. and Friedrich, B. 2019. Recovery of gallium

from smartphones – Part I: Thermal and mechanical pretreatment, pp. 1-14, Düsseldorf.

Flerus, B. and Friedrich, B. 2020. Recovery of gallium from smartphones-Part II: Oxidative alkaline pressure leaching of gallium from pyrolysis residue. Metals 10(12), 1-19.

Flora, S.J., Kannan, G.M., Pant, B.P. and Jaiswal, D.K. 2002. Combined administration of oxalic acid, succimer and its analogue for the reversal of gallium arsenide-induced oxidative stress in rats. Archives of Toxicology 76(5), 269-276.

Forsythe, B. and Klaine, S. 1994. The interaction of sulfate and selenate (Se^{6+}) effects on brine shrimp, *Artemia* spp. Chemosphere 29, 789-800.

FRANCE, R.L. 1993. Production and turnover of *Hyalella azteca* in central Ontario, Canada compared with other regions. Freshwater Biology 30(3), 343-349.

Fryknäs, M., Zhang, X., Bremberg, U., Senkowski, W., Olofsson, M.H., Brandt, P., Persson, I., D'Arcy, P., Gullbo, J., Nygren, P., Schughart, L.K., Linder, S. and Larsson, R. 2016. Iron chelators target both proliferating and quiescent cancer cells. Scientific Reports 6, 38343-38343.

Fu, D. and Richardson, D.R. 2007. Iron chelation and regulation of the cell cycle: 2 mechanisms of posttranscriptional regulation of the universal cyclin-dependent kinase inhibitor p21CIP1/WAF1 by iron depletion. Blood 110(2), 752-761.

Fukuchi, K., Tomoyasu, S., Watanabe, H., Kaetsu, S., Tsuruoka, N. and Gomi, K. 1995. Iron deprivation results in an increase in p53 expression. Biological Chemistry Hoppe-Seyler 376(10), 627-630.

Fyrestam, J. and Östman, C. 2017. Determination of heme in microorganisms using HPLC-MS/MS and cobalt(III) protoporphyrin IX inhibition of heme acquisition in *Escherichia coli*. Analytical and Bioanalytical Chemistry 409(30), 6999-7010.

Götze, R. and Rotter, V.S. 2012. Challenges for the recovery of critical metals from waste electronic equipment – a case study of indium in LCD panels, pp. 1-8.

Gaillardet, J., Viers, J. and Dupré, B. 2003. Treatise on Geochemistry. Holland, H.D. and Turekian,

K.K. (eds), pp. 225-272, Pergamon, Oxford.

Galluzzi, L., Vitale, I., Aaronson, S.A., Abrams, J.M., Adam, D., Agostinis, P., Alnemri, E.S., Altucci, L., Amelio, I., Andrews, D.W., Annicchiarico-Petruzzelli, M., Antonov, A.V., Arama, E., Baehrecke, E.H., Barlev, N.A., Bazan, N.G., Bernassola, F., Bertrand, M.J.M., Bianchi, K., Blagosklonny, M.V., Blomgren, K., Borner, C., Boya, P., Brenner, C., Campanella, M., Candi, E., Carmona-Gutierrez, D., Cecconi, F., Chan, F.K.M., Chandel, N.S., Cheng, E.H., Chipuk, J.E., Cidlowski, J.A., Ciechanover, A., Cohen, G.M., Conrad, M., Cubillos-Ruiz, J.R., Czabotar, P.E., D'Angiolella, V., Dawson, T.M., Dawson, V.L., De Laurenzi, V., De Maria, R., Debatin, K.-M., DeBerardinis, R.J., Deshmukh, M., Di Daniele, N., Di Virgilio, F., Dixit, V.M., Dixon, S.J., Duckett, C.S., Dynlacht, B.D., El-Deiry, W.S., Elrod, J.W., Fimia, G.M., Fulda, S., García-Sáez, A.J., Garg, A.D., Garrido, C., Gavathiotis, E., Golstein, P., Gottlieb, E., Green, D.R., Greene, L.A., Gronemeyer, H., Gross, A., Hajnoczky, G., Hardwick, J.M., Harris, I.S., Hengartner, M.O., Hetz, C., Ichijo, H., Jäättelä, M., Joseph, B., Jost, P.J., Juin, P.P., Kaiser, W.J., Karin, M., Kaufmann, T., Kepp, O., Kimchi, A., Kitsis, R.N., Klionsky, D.J., Knight, R.A., Kumar, S., Lee, S.W., Lemasters, J.J., Levine, B., Linkermann, A., Lipton, S.A., Lockshin, R.A., López-Otín, C., Lowe, S.W., Luedde, T., Lugli, E., MacFarlane, M., Madeo, F., Malewicz, M., Malorni, W., Manic, G., Marine, J.-C., Martin, S.J., Martinou, J.-C., Medema, J.P., Mehlen, P., Meier, P., Melino, S., Miao, E.A., Molkentin, J.D., Moll, U.M., Muñoz-Pinedo, C., Nagata, S., Nuñez, G., Oberst, A., Oren, M., Overholtzer, M., Pagano, M., Panaretakis, T., Pasparakis, M., Penninger, J.M., Pereira, D.M., Pervaiz, S., Peter, M.E., Piacentini, M., Pinton, P., Prehn, J.H.M., Puthalakath, H., Rabinovich, G.A., Rehm, M., Rizzuto, R., Rodrigues, C.M.P., Rubinsztein, D.C., Rudel, T., Ryan, K.M., Sayan, E., Scorrano, L., Shao, F., Shi, Y., Silke, J., Simon, H.-U., Sistigu, A., Stockwell, B.R., Strasser, A., Szabadkai, G., Tait, S.W.G., Tang, D., Tavernarakis, N., Thorburn, A., Tsujimoto, Y., Turk, B., Vanden Berghe, T., Vandenabeele, P., Vander Heiden, M.G., Villunger, A., Virgin, H.W., Vousden, K.H., Vucic, D., Wagner, E.F., Walczak, H., Wallach, D., Wang, Y., Wells, J.A., Wood,

W., Yuan, J., Zakeri, Z., Zhivotovsky, B., Zitvogel, L., Melino, G. and Kroemer, G. 2018. Molecular mechanisms of cell death: Recommendations of the Nomenclature Committee on Cell Death 2018. Cell Death and Differentiation 25(3), 486-541.

Gao, J. and Richardson, D.R. 2001. The potential of iron chelators of the pyridoxal isonicotinoyl hydrazone class as effective antiproliferative agents, IV: The mechanisms involved in inhibiting cell-cycle progression. Blood 98(3), 842-850.

García-Prat, L., Martínez-Vicente, M., Perdiguero, E., Ortet, L., Rodríguez-Ubreva, J., Rebollo, E., Ruiz-Bonilla, V., Gutarra, S., Ballestar, E., Serrano, A.L., Sandri, M. and Muñoz-Cánoves, P. 2016. Autophagy maintains stemness by preventing senescence. Nature 529(7584), 37-42.

Gatter, K.C., Brown, G., Trowbridge, I.S., Woolston, R.E. and Mason, D.Y. 1983. Transferrin receptors in human tissues: their distribution and possible clinical relevance. Journal of Clinical Pathology 36(5), 539-545.

Gensemer, R.W. and Playle, R.C. 1999. The bioavailability and toxicity of aluminum in aquatic environments. Critical Reviews in Environmental Science & Technology 29(4), 315-450.

Gerding, J., Peters, C., Wegscheider, W., Stranzinger, J., Lessmann, F., Pitzke, K., Harth, V., Eickmann, U. and Nienhaus, A. 2021. Metal exposure of workers during recycling of electronic waste: a cross-sectional study in sheltered workshops in Germany. International Archives of Occupational and Environmental Health 94(5), 935-944.

Gerhardt, A. 1993. Review of impact of heavy metals on stream invertebrates with special emphasis on acid conditions. Water, Air, and Soil Pollution 66(3), 289-314.

GESTIS (GESTIS-Substance Database) 2021. GESTIS substance database. IFA (Institut fur Arbeitsschutz). Available from: https://limitvalue.ifa.dguv.de/, accessed 10 November 2021.

Gill, E.H. 2021. The effect of aqueous aluminium on mortality and respiration in the amphipod *Gammarus lacustris*, Inland Norway University of Applied Sciences, Norway.

Goering, P.L. and Rehm, S. 1990. Inhibition of liver, kidney, and erythrocyte δ-aminolevulinic acid

dehydratase (porphobilinogen synthase) by gallium in the rat. Environmental Research 53(2), 135-151.

Gogvadze, V., Zhukova, A., Ivanov, A., Khassanova, L., Khassanova, Z. and Collery, P. 1996. Metal ions in biology and medicine. Collery, P., Corbella, J., Domingo, J.L., Etienne, J.C. and Llobet, J.M. (eds), pp. 249-252, John Libbey Eurotext, Paris, France.

Goldberg, A.L. 2007. Functions of the proteasome: from protein degradation and immune surveillance to cancer therapy. Biochemical Society Transactions 35(1), 12-17.

Golias, C.H., Charalabopoulos, A. and Charalabopoulos, K. 2004. Cell proliferation and cell cycle control: A mini review. International Journal of Clinical Practice 58(12), 1134-1141.

Gorgoulis, V., Adams, P.D., Alimonti, A., Bennett, D.C., Bischof, O., Bishop, C., Campisi, J., Collado, M., Evangelou, K., Ferbeyre, G., Gil, J., Hara, E., Krizhanovsky, V., Jurk, D., Maier, A.B., Narita, M., Niedernhofer, L., Passos, J.F., Robbins, P.D., Schmitt, C.A., Sedivy, J., Vougas, K., von Zglinicki, T., Zhou, D., Serrano, M. and Demaria, M. 2019. Cellular senescence: Defining a path forward. Cell 179(4), 813-827.

Graedel, T.E., Allwood, J., Birat, J.-P., Buchert, M., Hagelüken, C., Reck, B.K., Sibley, S.F. and Sonnemann, G. 2011. What do we know about metal recycling rates? Journal of Industrial Ecology 15(3), 355-366.

Green, D.A., Antholine, W.E., Wong, S.J., Richardson, D.R. and Chitambar, C.R. 2001. Inhibition of malignant cell growth by 311, a novel iron chelator of the pyridoxal isonicotinoyl hydrazone class: Effect on the R2 subunit of ribonucleotide reductase. Clinical Cancer Research 7(11), 3574-3579.

Guo, R., Zong, S., Wu, M., Gu, J. and Yang, M. 2017. Architecture of human mitochondrial respiratory megacomplex $I_2III_2IV_2$. Cell 170(6), 1247-1257.e1212.

Gwinn, W.M., Qu, W., Bousquet, R.W., Price, H., Shines, C.J., Taylor, G.J., Waalkes, M.P. and Morgan, D.L. 2015. Macrophage solubilization and cytotoxicity of indium-containing

particles as *in vitro* correlates to pulmonary toxicity *in vivo*. Toxicological Sciences 144(1), 17-26.

Gwinn, W.M., Qu, W., Shines, C.J., Bousquet, R.W., Taylor, G.J., Waalkes, M.P. and Morgan, D.L. 2013. Macrophage solubilization and cytotoxicity of indium-containing particles *in vitro*. Toxicological Sciences 135(2), 414-424.

Habashy, H.O., Powe, D.G., Staka, C.M., Rakha, E.A., Ball, G., Green, A.R., Aleskandarany, M., Paish, E.C., Douglas Macmillan, R., Nicholson, R.I., Ellis, I.O. and Gee, J.M.W. 2009. Transferrin receptor (CD71) is a marker of poor prognosis in breast cancer and can predict response to tamoxifen. Breast Cancer Research and Treatment 119(2), 283.

Haga, N., Fujita, N. and Tsuruo, T. 2003. Mitochondrial aggregation precedes cytochrome c release from mitochondria during apoptosis. Oncogene 22(36), 5579-5585.

Hamaguchi, T., Omae, K., Takebayashi, T., Kikuchi, Y., Yoshioka, N., Nishiwaki, Y., Tanaka, A., Hirata, M., Taguchi, O. and Chonan, T. 2008. Exposure to hardly soluble indium compounds in ITO production and recycling plants is a new risk for interstitial lung damage. Occupational and Environmental Medicine 65(1), 51-55.

Hampel, B., Malisan, F., Niederegger, H., Testi, R. and Jansen-Dürr, P. 2004. Differential regulation of apoptotic cell death in senescent human cells. Experimental Gerontology 39(11), 1713-1721.

Hamza, I. and Dailey, H.A. 2012. One ring to rule them all: Trafficking of heme and heme synthesis intermediates in the metazoans. Biochimica et Biophysica Acta (BBA) - Molecular Cell Research 1823(9), 1617-1632.

Hann, H.-W.L., Stahlhut, M.W. and Hann, C.L. 1990. Effect of iron and desferoxamine on cell growth and in vitro ferritin synthesis in human hepatoma cell lines. Hepatology 11(4), 566-569.

Hara, T. 1974. On the binding of gallium to transferrin. International Journal of Nuclear Medicine and Biology 1(3), 152-IN151.

Harford, A.J., Hogan, A.C., Tsang, J.J., Parry, D.L., Negri, A.P., Adams, M.S., Stauber, J.L. and van Dam, R.A. 2011. Effects of alumina refinery wastewater and signature metal constituents at the upper thermal tolerance of: 1. The tropical diatom *Nitzschia closterium*. Marine Pollution Bulletin 62(3), 466-473.

Harris, A.W. and Sephton, R.G. 1977. Transferrin promotion of 67Ga and 59Fe uptake by cultured mouse myeloma cells. Cancer Research 37(10), 3634-3638.

Hartig, S.M. 2013. Basic image analysis and manipulation in ImageJ. Current Protocols in Molecular Biology 102(1), 14.15.11-14.15.12.

Hawley Blackley, B., Cummings, K.J., Stanton, M., Stefaniak, A.B., Gibbs, J.L., Park, J.Y., Harvey, R.R. and Virji, M.A. 2019. Work tasks as determinants of respirable and inhalable indium exposure among workers at an indium–tin oxide production and reclamation facility. Annals of Work Exposures and Health 64(2), 175-184.

Hayflick, L. and Moorhead, P.S. 1961. The serial cultivation of human diploid cell strains. Experimental Cell Research 25(3), 585-621.

He, Y., Ma, E. and Xu, Z. 2014. Recycling indium from waste liquid crystal display panel by vacuum carbon-reduction. Journal of Hazardous Materials 268, 185-190.

Hernandez-Segura, A., Nehme, J. and Demaria, M. 2018. Hallmarks of cellular senescence. Trends in Cell Biology 28(6), 436-453.

Herron, T. and Gossman, W. 2021. 111 Indium white blood cell scan, StatPearls Publishing, Treasure Island (FL).

Higashikubo, I., Arito, H., Eitaki, Y., Ando, K., Araki, A., Shimizu, H. and Sakurai, H. 2019. Evaluation of personal exposure of workers to indium concentrations in total dust and its respirable fraction at three Japanese indium plants. Industrial Health 57(3), 392-397.

Higashikubo, I., Arito, H., Eitaki, Y., Araki, A., Ando, K., Shimizu, H. and Sakurai, H. 2018. Quantitative assessment of occupational exposure to total indium dust in Japanese indium

plants. Industrial Health 56(6), 553-560.

Hijazi, S., Visaggio, D., Pirolo, M., Frangipani, E., Bernstein, L. and Visca, P. 2018. Antimicrobial activity of gallium compounds on ESKAPE pathogens. Frontiers in Cellular and Infection Microbiology 8(316).

Hileti, D., Panayiotidis, P. and Hoffbrand, A.V. 1995. Iron chelators induce apoptosis in proliferating cells. British Journal of Haematology 89(1), 181-187.

Homma, S., Miyamoto, A., Sakamoto, S., Kishi, K., Motoi, N. and Yoshimura, K. 2005. Pulmonary fibrosis in an individual occupationally exposed to inhaled indium-tin oxide. European Respiratory Journal 25(1), 200-204.

Homma, T., Ueno, T., Sekizawa, K., Tanaka, A. and Hirata, M. 2003. Interstitial pneumonia developed in a worker dealing with particles containing indium-tin oxide. Journal of Occupational Health 45(3), 137-139.

Hsieh, S.J., Chen, C.C. and Say, W.C. 2009. Process for recovery of indium from ITO scraps and metallurgic microstructures. Materials Science and Engineering: B 158(1), 82-87.

Hsu, Y.T., Su, T.Y., Chen, C.Y., Liao, H.Y., Kuo, Y.C., Wu, W.T., Li, L.A., Lai, C.H. and Liou, S.H. 2021. Exposure profiles of workers from indium tin oxide target manufacturing and recycling factories in Taiwan. International Journal of Hygiene and Environmental Health 233, 113708.

Huang, E.H., Gabler, D.M., Krecic, M.E., Gerber, N., Ferguson, R.M. and Orosz, C.G. 1994. Differential effects of gallium nitrate on T lymphocyte and endothelial cell activation. Transplantation 58(11), 1216-1222.

Huang, Y., Liu, X., Wang, Y.H., Yeh, S.D., Chen, C.L., Nelson, R.A., Chu, P., Wilson, T. and Yen, Y. 2014. The prognostic value of ribonucleotide reductase small subunit M2 in predicting recurrence for prostate cancers. Urologic Oncology: Seminars and Original Investigations 32(1), 51.e9-51.e19.

Huaux, F., De Gussem, V., Lebrun, A., Yakoub, Y., Palmai-Pallag, M., Ibouraadaten, S.,

Uwambayinema, F. and Lison, D. 2018. New interplay between interstitial and alveolar macrophages explains pulmonary alveolar proteinosis (PAP) induced by indium tin oxide particles. Archives of Toxicology 92(4), 1349-1361.

Hultkvist, U., Westergren, G., Hansson, U.B. and Lewan, L. 1987. Effects of pH on the stability of the indium-113m blood protein complex and the selective binding of indium-113m to transferrin. Research in Experimental Medicine 187(2), 131-137.

Hunter, T. 2000. Signaling-2000 and beyond. Cell 100(1), 113-127.

Hustedt, N. and Durocher, D. 2017. The control of DNA repair by the cell cycle. Nature Cell Biology 19(1), 1-9.

Hydbring, P., Malumbres, M. and Sicinski, P. 2016. Non-canonical functions of cell cycle cyclins and cyclin-dependent kinases. Nature Reviews Molecular Cell Biology 17(5), 280-292.

Ibrahim, O. and O'Sullivan, J. 2020. Iron chelators in cancer therapy. BioMetals 33(4), 201-215.

Illidge, T.M., Cragg, M.S., Fringes, B., Olive, P. and Erenpreisa, J.A. 2000. Polyploid giant cells provide a survival mechanism for p53 mutant cells after DNA damage. Cell Biology International 24(9), 621-633.

Inoue, K., Nishiura, M., Kawakita, H., Ohto, K. and Harada, H. 2008. Recovery of indium from spent panel of liquid crystal display panels. Kagaku Kogaku Ronbunshu 34, 282-286.

Institute of Labor, Occupational Safety and Health, Ministry of Labor (ILOSH). 2015. Follow-up study on indium exposed workers and effectiveness of control measure.

Iwasawa, S., Nakano, M., Miyauchi, H., Tanaka, S., Kawasumi, Y., Higashikubo, I., Tanaka, A., Hirata, M. and Omae, K. 2017. Personal indium exposure concentration in respirable dusts and serum indium level. Industrial Health 55(1), 87-90.

Iwata, S., Lee, J.W., Okada, K., Lee, J.K., Iwata, M., Rasmussen, B., Link, T.A., Ramaswamy, S. and Jap, B.K. 1998. Complete structure of the 11-subunit bovine mitochondrial cytochrome bc1 complex. Science 281(5373), 64-71.

James, R., Sampath, K. and Edward, D.S. 2003. Copper toxicity on growth and reproductive potential in an ornamental fish, *Xiphophorus helleri*. Asian Fisheries Science, 317-326.

Javed, M.A. 2012. Growth responses of fish under chronic exposure of waterborne and dietary metals. International Journal of Agriculture and Biology 14, 281-285.

Jensen, E.C. 2013. Quantitative analysis of histological staining and fluorescence using ImageJ. The Anatomical Record 296(3), 378-381.

Jensen, H., Gaw, S., Lehto, N.J., Hassall, L. and Robinson, B.H. 2018. The mobility and plant uptake of gallium and indium, two emerging contaminants associated with electronic waste and other sources. Chemosphere 209, 675-684.

Jeong, J., Kim, J., Seok, S.H. and Cho, W.S. 2016. Indium oxide (In_2O_3) nanoparticles induce progressive lung injury distinct from lung injuries by copper oxide (CuO) and nickel oxide (NiO) nanoparticles. Archives of Toxicology 90(4), 817-828.

Jiang, W., Wang, X., Osborne, O.J., Du, Y., Chang, C.H., Liao, Y.-P., Sun, B., Jiang, J., Ji, Z., Li, R., Liu, X., Lu, J., Lin, S., Meng, H., Xia, T. and Nel, A.E. 2017. Pro-inflammatory and pro-fibrogenic effects of ionic and particulate arsenide and indium-containing semiconductor materials in the murine lung. ACS Nano 11(2), 1869-1883.

Johnson, D.G. and Walker, C.L. 1999. Cyclins and cell cycle checkpoints. Annual Review of Pharmacology and Toxicology 39(1), 295-312.

Jordan, I. and Kaplan, J. 1994. The mammalian transferrin-independent iron transport system may involve a surface ferrireductase activity. Biochemical Journal 302(3), 875-879.

Julander, A., Lundgren, L., Skare, L., Grandér, M., Palm, B., Vahter, M. and Lidén, C. 2014. Formal recycling of e-waste leads to increased exposure to toxic metals: An occupational exposure study from Sweden. Environment International 73, 243-251.

Juárez-Hernández, R.E., Franzblau, S.G. and Miller, M.J. 2012. Syntheses of mycobactin analogs as potent and selective inhibitors of *Mycobacterium tuberculosis*. Organic and Biomolecular

Chemistry 10(37), 7584-7593.

Kabata-Pendias, A. 2000. Trace elements in soils and plants (3rd Edition), CRC Press, Boca Raton.

Kabata-Pendias, A. and Mukherjee, A.B. 2007. Trace elements from soil to human, pp. 321-350, Springer Berlin Heidelberg, Berlin, Heidelberg.

Kabata-Pendias, A. and Szteke, B. 2015. Trace elements in abiotic and biotic environments, CRC Press.

Kaneko, Y., Thoendel, M., Olakanmi, O., Britigan, B.E. and Singh, P.K. 2007. The transition metal gallium disrupts Pseudomonas aeruginosa iron metabolism and has antimicrobial and antibiofilm activity. Journal of Clinical Investigation 117(4), 877-888.

Kastan, M.B., Canman, C.E. and Leonard, C.J. 1995. P53, cell cycle control and apoptosis: implications for cancer. Cancer and Metastasis Reviews 14(1), 3-15.

Kato, T., Igarashi, S., Ishiwatari, Y., Furukawa, M. and Yamaguchi, H. 2013. Separation and concentration of indium from a liquid crystal display via homogeneous liquid, liquid extraction. Hydrometallurgy 137, 148-155.

Kelly, T.D. and Matos, G.R. 2016. Historical statistics for mineral and material commodities in the United States (2016 version): U.S. Geological Survey Data Series 140, accessed [12/10/2017], at https://minerals.usgs.gov/minerals/pubs/historical-statistics/.

Kelson, A.B., Carnevali, M. and Truong-Le, V. 2013. Gallium-based anti-infectives: targeting microbial iron-uptake mechanisms. Current Opinion in Pharmacology 13(5), 707-716.

Khan, A., Singh, P. and Srivastava, A. 2018. Synthesis, nature and utility of universal iron chelator – Siderophore: A review. Microbiological Research 212-213, 103-111.

Khasheii, B., Mahmoodi, P. and Mohammadzadeh, A. 2021. Siderophores: Importance in bacterial pathogenesis and applications in medicine and industry. Microbiological Research 250, 126790.

Kim, B.M. and Chung, H.W. 2008. Desferrioxamine (DFX) induces apoptosis through the p38-

caspase8-Bid-Bax pathway in PHA-stimulated human lymphocytes. Toxicology and Applied Pharmacology 228(1), 24-31.

Kim, B.S., Yoon, K.-H., Oh, H.-M., Choi, E.Y., Kim, S.W., Han, W.C., Kim, E.A., Choi, S.C., Kim, T.H., Yun, K.J., Kim, E.C., Lyou, J.H., Nah, Y.H., Chung, H.T., Cha, Y.N. and Jun, C.D. 2002. Involvement of p38 MAP kinase during iron chelator-mediated apoptotic cell death. Cellular Immunology 220(2), 96-106.

Kircheva, N. and Dudev, T. 2019. Novel insights into gallium's mechanism of therapeutic action: A DFT/PCM study of the interaction between Ga^{3+} and ribonucleotide reductase substrates. The Journal of Physical Chemistry B 123(26), 5444-5451.

Kircheva, N. and Dudev, T. 2020. Gallium as an antibacterial agent: A DFT/SMD study of the Ga^{3+}/Fe^{3+} competition for binding bacterial siderophores. Inorganic Chemistry 59(9), 6242-6254.

Kircheva, N. and Dudev, T. 2021. Competition between abiogenic and biogenic metal cations in biological systems: Mechanisms of gallium's anticancer and antibacterial effect. Journal of Inorganic Biochemistry 214, 111309.

Kiyani, V., Hosynzadeh, M.H. and Ebrahimpour, M. 2018. Investigation acute toxicity some of the heavy metals at different water hardness. International Journal of Advanced Biological and Biomedical Research 6(4), 225-232.

Koljonen, T. and Elo, S. 1992. Suomen geokemian atlas = The geochemical atlas of Finland. Osa 2 = Part 2, Moreeni = Till, Geologian tutkimuskeskus, Espoo.

Kopp, B., Zalko, D. and Audebert, M. 2018. Genotoxicity of 11 heavy metals detected as food contaminants in two human cell lines. Environmental and Molecular Mutagenesis 59(3), 202-210.

Kovac, S., Anderson, G.J. and Baldwin, G.S. 2011. Gastrins, iron homeostasis and colorectal cancer. Biochim Biophys Acta 1813(5), 889-895.

Kovacevic, Z., Chikhani, S., Lovejoy, D.B. and Richardson, D.R. 2011. Novel thiosemicarbazone iron chelators induce up-regulation and phosphorylation of the metastasis suppressor N-myc down-stream regulated gene 1: A new strategy for the treatment of pancreatic cancer. Molecular Pharmacology 80(4), 598-609.

Krajcovic, M. and Overholtzer, M. 2012. Mechanisms of ploidy increase in human cancers: A new role for cell cannibalism. Cancer Research 72(7), 1596-1601.

Krewulak, K.D. and Vogel, H.J. 2008. Structural biology of bacterial iron uptake. Biochimica et Biophysica Acta (BBA) - Biomembranes 1778(9), 1781-1804.

Krohn, A.J., Wahlbrink, T. and Prehn, J.H. 1999. Mitochondrial depolarization is not required for neuronal apoptosis. The Journal of Neuroscience 19(17), 7394-7404.

Kuang, Y., Guo, W., Ling, J., Xu, D., Liao, Y., Zhao, H., Du, X., Wang, H., Xu, M., Song, H., Wang, T., Jing, B., Li, K., Hu, M., Wu, W., Deng, J. and Wang, Q. 2019. Iron-dependent CDK1 activity promotes lung carcinogenesis via activation of the GP130/STAT3 signaling pathway. Cell Death and Disease 10(4), 297-297.

Kubitz, J.A., Besser, J.M. and P., G.J. 1996. A two-step experimental design for a sediment bioassay using growth of the amphipod *Hyalella azteca* for the test end point. Environmental Toxicology and Chemistry 15(10), 1783-1792.

Kuilman, T., Michaloglou, C., Mooi, W.J. and Peeper, D.S. 2010. The essence of senescence. Genes & Development 24(22), 2463-2479.

Kulp, K.S., Green, S.L. and Vulliet, P.R. 1996. Iron deprivation inhibits cyclin-dependent kinase activity and decreases cyclin D/CDK4 protein levels in asynchronous MDA-MB-453 human breast cancer cells. Experimental Cell Research 229(1), 60-68.

Kumar, V. and Boddeti, D.K. 2013. (68)Ga-radiopharmaceuticals for PET imaging of infection and inflammation. Recent Results in Cancer Research 194, 189-219.

Kumari, R. and Jat, P. 2021. Mechanisms of cellular senescence: cell cycle arrest and senescence

associated secretory phenotype. Frontiers in Cell and Developmental Biology 9(485).

Kuntawee, C., Tantrakarnapa, K., Limpanont, Y., Lawpoolsri, S., Phetrak, A., Mingkhwan, R. and Worakhunpiset, S. 2020. Exposure to heavy metals in electronic waste recycling in Thailand. International Journal of Environmental Research and Public Health 17(9), 2996.

Kuo, L.J. and Yang, L.X. 2008. γ-H2AX - A Novel biomarker for DNA double-strand breaks. In Vivo 22(3), 305-309.

Kyriakou, D., Eliopoulos, A.G., Papadakis, A., Alexandrakis, M. and Eliopoulos, G.D. 1998. Decreased expression of c-myc oncoprotein by peripheral blood mononuclear cells in thalassaemia patients receiving desferrioxamine. European Journal of Haematology 60(1), 21-27.

Løvik, A.N., Restrepo, E. and Müller, D.B. 2015. The global anthropogenic gallium system: determinants of demand, supply and efficiency improvements. Environmental Science & Technology 49(9), 5704-5712.

López-Otín, C., Blasco, M.A., Partridge, L., Serrano, M. and Kroemer, G. 2013. The hallmarks of aging. Cell 153(6), 1194-1217.

L Thelander, a. and Reichard, P. 1979. Reduction of ribonucleotides. Annual Review of Biochemistry 48(1), 133-158.

Labbh , R.F., Vreman, H. and Stevenson, D.K. 1999. Zinc protoporphyrin: A metabolite with a mission. Clinical Chemistry 45 12, 2060-2072.

Lan, L., Wei, W., Zheng, Y., Niu, L., Chen, X., Huang, D., Gao, Y., Mo, S., Lu, J., Guo, M., Liu, Y. and Lu, B. 2018. Deferoxamine suppresses esophageal squamous cell carcinoma cell growth via ERK1/2 mediated mitochondrial dysfunction. Cancer Letters 432, 132-143.

Lavender, J.P., Lowe, J., Barker, J.R., Burn, J.I. and Chaudhri, M.A. 1971. Gallium 67 citrate scanning in neoplastic and inflammatory lesions. The British Journal of Radiology 44(521), 361-366.

Lawrence, S.G. 1981. Manual for the culture of selected freshwater invertebrates, Canadian special

publication of fisheries and aquatic science no. 54, Department of Fisheries and Oceans, Ottawa.

Layer, G., Reichelt, J., Jahn, D. and Heinz, D.W. 2010. Structure and function of enzymes in heme biosynthesis. Protein Science 19(6), 1137-1161.

Le, N.T.V. and Richardson, D.R. 2004. Iron chelators with high antiproliferative activity up-regulate the expression of a growth inhibitory and metastasis suppressor gene: A link between iron metabolism and proliferation. Blood 104(9), 2967-2975.

Lebrun, J.D. and Gismondi, E. 2020. Behavioural and biochemical alterations in gammarids as induced by chronic metallic exposures (Cd, Cu and Pb): Implications for freshwater biomonitoring. Chemosphere 257, 127253.

Leonard, R., Zulfikar, R. and Stansbury, R. 2020. Coal mining and lung disease in the 21st century. Current Opinion in Pulmonary Medicine 26(2), 135-141.

Lewis, S.S., Cox, G.M. and Stout, J.E. 2014. Clinical utility of indium 111-labeled white blood cell scintigraphy for evaluation of suspected infection. Open Forum Infectious Diseases 1(2), 1-8.

Lezaja, A. and Altmeyer, M. 2018. Inherited DNA lesions determine G1 duration in the next cell cycle. Cell Cycle 17(1), 24-32.

Li, B., Deng, A., Li, K., Hu, Y., Li, Z., Xiong, Q., Liu, Z., Guo, Q., Zou, L., Zhang, H., Zhang, M., Ouyang, F., Su, J., Su, W., Xu, J., Lin, H., Sun, J., Peng, J., Jiang, H., Zhou, P., Hu, T., Luo, M., Zhang, Y., Zheng, H., Xiao, J., Liu, T., Che, R., Zeng, H., Zheng, Z., Huang, Y., Yu, J., Yi, L., Wu, J., Chen, J., Zhong, H., Deng, X., Kang, M., Pybus, O.G., Hall, M., Lythgoe, K.A., Li, Y., Yuan, J., He, J. and Lu, J. 2021. Viral infection and transmission in a large well-traced outbreak caused by the Delta SARS-CoV-2 variant. MedRxiv, 2021.2007.2007.21260122.

Li, Y.H., Zhao, Q.L. and Huang, M.H. 2005. Cathodic adsorptive voltammetry of the gallium-alizarin red S complex at a carbon paste electrode. Electroanalysis 17(4), 343-347.

Liang, S.X. and Richardson, D.R. 2003. The effect of potent iron chelators on the regulation of p53:

Examination of the expression, localization and DNA-binding activity of p53 and the transactivation of WAF1. Carcinogenesis 24(10), 1601-1614.

Liao, Y.H., Yu, H.S., Ho, C.K., Wu, M.T., Yang, C.Y., Chen, J.R. and Chang, C.C. 2004. Biological monitoring of exposures to aluminium, gallium, indium, arsenic, and antimony in optoelectronic industry workers. Journal of Occupational and Environmental Medicine 46(9), 931-936.

Liao, Y.H., Hwang, L.C., Kao, J.S., Yiin, S.J., Lin, S.F., Lin, C.H., Lin, Y.C. and Aw, T.C. 2006. Lipid peroxidation in workers exposed to aluminium, gallium, indium, arsenic, and antimony in the optoelectronic industry. Journal of Occupational and Environmental Medicine 48(8), 789-793.

Liber, K., Doig, L.E. and White-Sobey, S.L. 2011. Toxicity of uranium, molybdenum, nickel, and arsenic to *Hyalella azteca* and *Chironomus dilutus* in water-only and spiked-sediment toxicity tests. Ecotoxicology and Environmental Safety 74(5), 1171-1179.

Lin, H.C. and Hwang, P.P. 1998. Acute and chronic effects of gallium chloride ($GaCl_3$) on tilapia (*Oreochromis mossambicus*) larvae. Bulletin of Environmental Contamination and Toxicology 60(6), 931-935.

Liou, S.H., Wu, W.T., Liao, H.Y., Chen, C.Y., Tsai, C.Y., Jung, W.T. and Lee, H.L. 2017. Global DNA methylation and oxidative stress biomarkers in workers exposed to metal oxide nanoparticles. Journal of Hazardous Materials 331, 329-335.

Littenberg, R.L., Taketa, R.M., Alazraki, N.P., Halpern, S.E. and Ashburn, W.L. 1973. Gallium-67 for localization of septic lesions. Annals of Internal Medicine 79(3), 403-406.

Liu, H.H., Chen, C.Y., Chen, G.I., Lee, L.H. and Chen, H.L. 2012a. Relationship between indium exposure and oxidative damage in workers in indium tin oxide production plants. International Archives of Occupational and Environmental Health 85(4), 447-453.

Liu, W., Xing, F., Iiizumi-Gairani, M., Okuda, H., Watabe, M., Pai, S.K., Pandey, P.R., Hirota, S., Kobayashi, A., Mo, Y.-Y., Fukuda, K., Li, Y. and Watabe, K. 2012b. N-myc downstream

regulated gene 1 modulates Wnt-β-catenin signalling and pleiotropically suppresses metastasis. EMBO Molecular Medicine 4(2), 93-108.

Liu, W., Zhang, S., Nekhai, S. and Liu, S. 2020. Depriving iron supply to the virus represents a promising adjuvant therapeutic against viral survival. Current Clinical Microbiology Reports, 1-7.

Liu, Y.H., Shaheen, S.M., Rinklebe, J. and Hseu, Z.Y. 2021. Pedogeochemical distribution of gallium, indium and thallium, their potential availability and associated risk in highly-weathered soil profiles of Taiwan. Environmental Research 197, 110994.

Liu, Y., Cui, Y., Shi, M., Zhang, Q., Wang, Q. and Chen, X. 2014. Deferoxamine promotes MDA-MB-231 cell migration and invasion through increased ROS-dependent HIF-1α accumulation. Cellular Physiology and Biochemistry 33(4), 1036-1046.

Lucas, J.J., Szepesi, A., Domenico, J., Takase, K., Tordai, A., Terada, N. and Gelfand, E.W. 1995. Effects of iron-depletion on cell cycle progression in normal human T lymphocytes: Selective inhibition of the appearance of the cyclin A-associated component of the p33cdk2 kinase. Blood 86(6), 2268-2280.

Lui, G.Y.L., Kovacevic, Z., Richardson, V., Merlot, A.M., Kalinowski, D.S. and Richardson, D.R. 2015a. Targeting cancer by binding iron: Dissecting cellular signaling pathways. Oncotarget 6(22), 18748-18779.

Lui, G.Y.L., Kovacevic, Z., V. Menezes, S., Kalinowski, D.S., Merlot, A.M., Sahni, S. and Richardson, D.R. 2015b. Novel thiosemicarbazones regulate the signal transducer and activator of transcription 3 (STAT3) pathway: Inhibition of constitutive and interleukin 6–induced activation by iron depletion. Molecular Pharmacology 87(3), 543-560.

Lv, H., Shi, Y., Zhang, L., Zhang, D., Liu, G., Yang, Z., Li, Y., Fei, F. and Zhang, S. 2014. Polyploid giant cancer cells with budding and the expression of cyclin E, S-phase kinase-associated protein 2, stathmin associated with the grading and metastasis in serous ovarian tumor. BMC

Cancer 14, 576-576.

Møller, M.B. 2000. p27 in cell cycle control and cancer. Leukemia and Lymphoma 39(1-2), 19-27.

Möllmann, U., Heinisch, L., Bauernfeind, A., Köhler, T. and Ankel-Fuchs, D. 2009. Siderophores as drug delivery agents: application of the “Trojan Horse” strategy. BioMetals 22(4), 615-624.

Ma, E., Lu, R. and Xu, Z. 2012. An efficient rough vacuum-chlorinated separation method for the recovery of indium from waste liquid crystal display panels. Green Chemistry 14(12), 3395-3401.

Madden, E.F., Anderson, C.J. and Goering, P.L. 2004. Elements and their compounds in the environment, pp. 801-809.

Maltby, L. and Naylor, C. 1990. Preliminary observations on the ecological relevance of the Gammarus `Scope for growth' assay: effect of zinc on reproduction. Functional Ecology 4(3), 393-397.

Maltby, L., Naylor, C. and Calow, P. 1990. Effect of stress on a freshwater benthic detritivore: Scope for growth in *Gammarus pulex*. Ecotoxicology and Environmental Safety 19(3), 285-291.

Malumbres, M. 2014. Cyclin-dependent kinases. Genome Biology 15(6), 122-122.

Manyak, M.J. 2008. Indium-111 capromab pendetide in the management of recurrent prostate cancer. Expert Review of Anticancer Therapy 8(2), 175-181.

March, B.G.E.d. 1977. The effects of photoperiod and temperature on the induction and termination of reproductive resting stage in the freshwater amphipod *Hyalella azteca* (Saussure). Canadian Journal of Zoology 55(10), 1595-1600.

Marcotte, R., Lacelle, C. and Wang, E. 2004. Senescent fibroblasts resist apoptosis by downregulating caspase-3. Mechanisms of Ageing and Development 125(10), 777-783.

Marzilli, L.G., De Castro, B., Caradonna, J.P., Stewart, R.C. and Van Vuuren, C.P. 1980. Nucleoside complexing. A Raman and carbon-13 NMR spectroscopic study of the binding of hard and soft metal species. Journal of the American Chemical Society 102(3), 916-924.

Matkovic, V., Balboa, A., Clinchot, D.M., Whitacre, C.C., Zwilling, B.S., Brown, D., Weisbrode, S.E., Apseloff, G. and Gerber, N. 1991. Gallium prevents adjuvant arthritis in rats and interferes with macrophage/T-cell function in the immune response. Current Therapeutic Research-clinical and Experimental 50, 255-267.

Matsuda, S., Matsuda, R., Matsuda, Y., Yanagisawa, S.-y., Ikura, M., Ikura, T. and Matsuda, T. 2014. An easy-to-use genotoxicity assay using EGFP-MDC1-expressing human cells. Genes and Environment 36(1), 17-28.

Matsumoto, A. and Hinkley, T.K. 2001. Trace metal suites in Antarctic pre-industrial ice are consistent with emissions from quiescent degassing of volcanoes worldwide. Earth and Planetary Science Letters 186(1), 33-43.

Matthews, H.K., Bertoli, C. and de Bruin, R.A.M. 2021. Cell cycle control in cancer. Nature Reviews Molecular Cell Biology.

Mazzu, Y.Z., Armenia, J., Chakraborty, G., Yoshikawa, Y., Coggins, S.A.A., Nandakumar, S., Gerke, T.A., Pomerantz, M.M., Qiu, X., Zhao, H., Atiq, M., Khan, N., Komura, K., Lee, G.-S.M., Fine, S.W., Bell, C., O'Connor, E., Long, H.W., Freedman, M.L., Kim, B. and Kantoff, P.W. 2019. A novel mechanism driving poor-prognosis prostate cancer: Overexpression of the DNA repair gene, ribonucleotide reductase small subunit M2 (RRM2). Clinical Cancer Research 25(14), 4480-4492.

Mazzu, Y.Z., Armenia, J., Nandakumar, S., Chakraborty, G., Yoshikawa, Y., Jehane, L.E., Lee, G.-S.M., Atiq, M., Khan, N., Schultz, N. and Kantoff, P.W. 2020. Ribonucleotide reductase small subunit M2 is a master driver of aggressive prostate cancer. Molecular Oncology 14(8), 1881-1897.

McGregor, S.J. and Brock, J.H. 1992. Effect of pH and citrate on binding of iron and gallium by transferrin in serum. Clinical Chemistry 38(9), 1883-1885.

McHard, J.A., Foulk, S.J. and Winefordner, J.D. 1980. A comparison of trace element contents of

Florida and Brazil orange juice. Journal of Agricultural and Food Chemistry 28(5), 1042-1042.

Mendeleev, D. 1871. The periodical regularity of the chemical elements. Annalen der Chemie und Pharmacie 8, 133-229.

Merli, D., Profumo, A., Bloise, N., Risi, G., Momentè, S., Cucca, L. and Visai, L. 2018. Indium/Gallium maltolate effects on human breast carcinoma cells: *In vitro* investigation on cytotoxicity and synergism with mitoxantrone. ACS Omega 3(4), 4631-4640.

Ministry of Health, Labour and Welfare (MHLW), Japan. 2010. The technical guideline for preventing health impairment of workers engaged in the indium tin oxide handling processes. Available at https://www.mhlw.go.jp/bunya/roudoukijun/anzeneisei42/dl/03.pdf (accessed on 10 November 2021).

Ministry of Health, Labour and Welfare (MHLW), Japan. 2013. Amendment to ordinance on industrial safety and health law and to ordinance on prevention of hazards due to specified chemical substances. Available at https://www.mhlw.go.jp/bunya/roudoukijun/anzeneisei48/dl/anzeneisei48-01.pdf (accessed on 10 November 2021).

Mikuła-Pietrasik, J., Niklas, A., Uruski, P., Tykarski, A. and Książek, K. 2020. Mechanisms and significance of therapy-induced and spontaneous senescence of cancer cells. Cellular and Molecular Life Sciences 77(2), 213-229.

Milani, D., Reynoldson, T.B., Borgmann, U. and Kolasa, J. 2003. The relative sensitivity of four benthic invertebrates to metals in spiked-sediment exposures and application to contaminated field sediment. Environmental Toxicology and Chemistry 22(4), 845-854.

Millour, S., Noël, L., Chekri, R., Vastel, C., Kadar, A., Sirot, V., Leblanc, J.-C. and Guérin, T. 2012. Strontium, silver, tin, iron, tellurium, gallium, germanium, barium and vanadium levels in foodstuffs from the Second French Total Diet Study. Journal of Food Composition and Analysis 25(2), 108-129.

Minandri, F., Bonchi, C., Frangipani, E., Imperi, F. and Visca, P. 2014. Promises and failures of

gallium as an antibacterial agent. Future Microbiology 9(3), 379-397.

Mitsuhashi, T. 2020. Effects of indium exposure on respiratory symptoms: A retrospective cohort study in Japanese workers using health checkup data. PeerJ 8, e8413-e8413.

Miwa, S., Jow, H., Baty, K., Johnson, A., Czapiewski, R., Saretzki, G., Treumann, A. and von Zglinicki, T. 2014. Low abundance of the matrix arm of complex I in mitochondria predicts longevity in mice. Nature Communications 5(1), 3837.

Miyazaki, A., Kimura, A. and Tao, H. 2012. Distribution of indium, thallium and bismuth in the environmental water of Japan. Bulletin of Environmental Contamination and Toxicology 89(6), 1211-1215.

Mohsen, A., Collery, P., Garnotel, R., Brassart, B., Etique, N., Mohamed Sabry, G., Elsherif Hassan, R., Jeannesson, P., Desmaële, D. and Morjani, H. 2017. A new gallium complex inhibits tumor cell invasion and matrix metalloproteinase MMP-14 expression and activity†. Metallomics 9(8), 1176-1184.

Moiseeva, O., Bourdeau, V., Roux, A., Deschênes-Simard, X. and Ferbeyre, G. 2009. Mitochondrial dysfunction contributes to oncogene-induced senescence. Molecular and Cellular Biology 29(16), 4495-4507.

Montalto, F.I. and De Amicis, F. 2020. Cyclin D1 in cancer: A molecular connection for cell cycle control, adhesion and invasion in tumor and stroma. Cells 9(12), 2648.

Mora, A.L., Rojas, M., Pardo, A. and Selman, M. 2017. Emerging therapies for idiopathic pulmonary fibrosis, a progressive age-related disease. Nature Reviews Drug Discovery 16(11), 755-772.

Moraes, R., Gerhard, P., Andersson, L., Sturve, J., Rauch, S. and Molander, S. 2003. Establishing causality between exposure to metals and effects on fish. Human and Ecological Risk Assessment: An International Journal 9(1), 149-169.

Moran, P.L. and Seligman, P.A. 1989. Effects of transferrin-indium on cellular proliferation of a human leukemia cell line. Cancer Research 49(15), 4237-4241.

Mosieniak, G., Sliwinska, M.A., Alster, O., Strzeszewska, A., Sunderland, P., Piechota, M., Was, H. and Sikora, E. 2015. Polyploidy formation in doxorubicin-treated cancer cells can favor escape from senescence. Neoplasia 17(12), 882-893.

Nagoba, B. and Vedpathak, D. 2011. Medical applications of siderophores. European Journal of General Medicine 8(3), 229-235.

Nakano, M., Omae, K., Tanaka, A. and Hirata, M. 2019. Possibility of lung cancer risk in indium-exposed workers: An 11-year multicenter cohort study. Journal of Occupational Health 61(3), 251-256.

Nakano, M., Omae, K., Tanaka, A., Hirata, M., Michikawa, T., Kikuchi, Y., Yoshioka, N., Nishiwaki, Y. and Chonan, T. 2009. Causal relationship between indium compound inhalation and effects on the lungs. Journal of Occupational Health 51(6), 513-521.

Narasimhan, J., Antholine, W.E. and Chitambar, C.R. 1992. Effect of gallium on the tyrosyl radical of the iron-dependent M2 subunit of ribonucleotide reductase. Biochemical Pharmacology 44(12), 2403-2408.

Negri, A.P., Harford, A.J., Parry, D.L. and van Dam, R.A. 2011. Effects of alumina refinery wastewater and signature metal constituents at the upper thermal tolerance of: 2. The early life stages of the coral *Acropora tenuis*. Marine Pollution Bulletin 62(3), 474-482.

Nejmeddine, F., Caillat-Vigneron, N., Escaig, F., Moretti, J.L., Raphael, M. and Galle, P. 1998. Mechanism involved in gallium-67 (Ga-67) uptake by human lymphoid cell lines. Cellular and Molecular Biology (Noisy-le-Grand, France) 44(8), 1215-1220.

Neville, C.M. 1985. Physiological response of juvenile rainbow trout, *Salmo gairdneri*, to acid and aluminum - prediction of field responses from laboratory data. Canadian Journal of Fisheries and Aquatic Sciences 42(12), 2004-2019.

Ng, A.M.C., Guo, M.Y., Leung, Y.H., Chan, C.M.N., Wong, S.W.Y., Yung, M.M.N., Ma, A.P.Y., Djurišić, A.B., Leung, F.C.C., Leung, K.M.Y., Chan, W.K. and Lee, H.K. 2015. Metal oxide

nanoparticles with low toxicity. Journal of Photochemistry and Photobiology B: Biology 151, 17-24.

Nicolafrancesco, C., Porcaro, F., Pis, I., Nappini, S., Simonelli, L., Marini, C., Frangipani, E., Visaggio, D., Visca, P., Mobilio, S., Meneghini, C., Fratoddi, I., Iucci, G. and Battocchio, C. 2019. Gallium- and iron-pyoverdine coordination compounds investigated by X-ray photoelectron spectroscopy and X-ray absorption spectroscopy. Inorganic Chemistry 58(8), 4935-4944.

Nierop, K.G.J.J., Jansen, B. and Verstraten, J.M. 2002. Dissolved organic matter, aluminium and iron interactions: Precipitation induced by metal/carbon ratio, pH and competition. Science of The Total Environment 300(1), 201-211.

Nigg, E.A. 1995. Cyclin-dependent protein kinases: Key regulators of the eukaryotic cell cycle. BioEssays 17(6), 471-480.

Nilsson, R., Schultz, I.J., Pierce, E.L., Soltis, K.A., Naranuntarat, A., Ward, D.M., Baughman, J.M., Paradkar, P.N., Kingsley, P.D., Culotta, V.C., Kaplan, J., Palis, J., Paw, B.H. and Mootha, V.K. 2009. Discovery of genes essential for heme biosynthesis through large-scale gene expression analysis. Cell Metabolism 10(2), 119-130.

National Institute for Occupational Safety and Health (NIOSH). 2021. NIOSH pocket guide to chemical hazards. Indium compounds.

Niu, N., Mercado-Uribe, I. and Liu, J. 2017. Dedifferentiation into blastomere-like cancer stem cells via formation of polyploid giant cancer cells. Oncogene 36(34), 4887-4900.

Niu, N., Zhang, J., Zhang, N., Mercado-Uribe, I., Tao, F., Han, Z., Pathak, S., Multani, A.S., Kuang, J., Yao, J., Bast, R.C., Sood, A.K., Hung, M.C. and Liu, J. 2016. Linking genomic reorganization to tumor initiation via the giant cell cycle. Oncogenesis 5(12), e281-e281.

Noguchi, S., Eitoku, M., Kiyosawa, H. and Suganuma, N. 2016. Fibrotic gene expression coexists with alveolar proteinosis in early indium lung. Inhalation Toxicology 28(9), 421-428.

Norberg-King, T.J., Sibley, P.K., Burton, G.A., Ingersoll, C.G., Kemble, N.E., Ireland, S., Mount, D.R. and Rowland, C.D. 2006. Interlaboratory evaluation of *Hyalella azteca* and Chironomus tentans short-term and long-term sediment toxicity tests. Environmental Toxicology and Chemistry 25(10), 2662-2674.

Nordberg, G., Fowler, B. and Nordberg, M. 2014. Handbook on the toxicology of metals, Elsevier Science.

Novak, L. and Taylor, L.N. 2017. Biological test method: Test for survival, growth and reproduction in sediment and water using the freshwater amphipod *Hyalella azteca*, Environmental Science and Technology Centre (Canada). Ottawa.

Nozaki, Y., Lerche, D., Alibo, D.S. and Snidvongs, A. 2000a. The estuarine geochemistry of rare earth elements and indium in the Chao Phraya River, Thailand. Geochimica et Cosmochimica Acta 64(23), 3983-3994.

Nozaki, Y., Lerche, D., Alibo, D.S. and Tsutsumi, M. 2000b. Dissolved indium and rare earth elements in three Japanese rivers and Tokyo Bay: Evidence for anthropogenic Gd and In. Geochimica et Cosmochimica Acta 64(23), 3975-3982.

Nyholm, S., Mann, G.J., Johansson, A.G., Bergeron, R.J., Gräslund, A. and Thelander, L. 1993. Role of ribonucleotide reductase in inhibition of mammalian cell growth by potent iron chelators. Journal of Biological Chemistry 268(35), 26200-26205.

O'Donnell, K.A., Yu, D., Zeller, K.I., Kim, J.-W., Racke, F., Thomas-Tikhonenko, A. and Dang, C.V. 2006. Activation of transferrin receptor 1 by c-Myc enhances cellular proliferation and tumorigenesis. Molecular and Cellular Biology 26(6), 2373-2386.

Obata, H., Alibo, D.S. and Nozaki, Y. 2007. Dissolved aluminum, indium, and cerium in the Sea of Japan and the Sea of Okhotsk: Comparison to the marginal seas of the western North Pacific. Journal of Geophysical Research: Oceans 112(C12).

Ogrodnik, M., Salmonowicz, H., Jurk, D. and Passos, J.F. 2019. Expansion and cell-cycle arrest:

Common denominators of cellular senescence. Trends in Biochemical Sciences 44(12), 996-1008.

Ohyashiki, J.H., Kobayashi, C., Hamamura, R., Okabe, S., Tauchi, T. and Ohyashiki, K. 2009. The oral iron chelator deferasirox represses signaling through the mTOR in myeloid leukemia cells by enhancing expression of REDD1. Cancer Science 100(5), 970-977.

Olakanmi, O., Britigan, B.E. and Schlesinger, L.S. 2000. Gallium disrupts iron metabolism of mycobacteria residing within human macrophages. Infection and Immunity 68(10), 5619-5627.

Olakanmi, O., Gunn, J.S., Su, S., Soni, S., Hassett, D.J. and Britigan, B.E. 2010. Gallium disrupts iron uptake by intracellular and extracellular *Francisella* strains and exhibits therapeutic efficacy in a murine pulmonary infection model. Antimicrobial Agents and Chemotherapy 54(1), 244-253.

Olakanmi, O., Kesavalu, B., Pasula, R., Abdalla, M.Y., Schlesinger, L.S. and Britigan, B.E. 2013. Gallium nitrate is efficacious in murine models of tuberculosis and inhibits key bacterial Fe-dependent enzymes. Antimicrobial Agents and Chemotherapy 57(12), 6074-6080.

Olgun, N.S., Morris, A.M., Barber, T.L., Stefaniak, A.B., Kashon, M.L., Schwegler-Berry, D., Cummings, K.J. and Leonard, S.S. 2017. Comparison of the toxicity of sintered and unsintered indium-tin oxide particles in murine macrophage and epidermal cells. Toxicology and Applied Pharmacology 331(Supplement C), 85-93.

Olivares, C.I., Field, J.A., Simonich, M., Tanguay, R.L. and Sierra-Alvarez, R. 2016. Arsenic (III, V), indium (III), and gallium (III) toxicity to zebrafish embryos using a high-throughput multi-endpoint in vivo developmental and behavioral assay. Chemosphere 148, 361-368.

Oliveira, A.A., Perdigão, G.M.C., Rodrigues, L.E., da Silva, J.G., Souza-Fagundes, E.M., Takahashi, J.A., Rocha, W.R. and Beraldo, H. 2017. Cytotoxic and antimicrobial effects of indium(iii) complexes with 2-acetylpyridine-derived thiosemicarbazones. Dalton Transactions 46(3),

918-932.

Onikura, N., Nakamura, A. and Kishi, K. 2005. Acute toxicity of gallium and effects of salinity on gallium toxicity to brackish and marine organisms. Bulletin of Environmental Contamination and Toxicology 75(2), 356-360.

Onikura, N., Nakamura, A. and Kishi, K. 2008. Acute toxicity of thallium and indium toward brackish-water and marine organisms. Journal of the Faculty of Agriculture, Kyushu University 53(2), 467-469.

Othman, M.S. and Pascoe, D. 2001. Growth, development and reproduction of *Hyalella azteca* (Saussure, 1858) in laboratory culture. Crustaceana 74(2), 171-181.

Oughton, D.H., Salbu, B., Bjørnstad, H.E. and Day, J.P. 1992. Use of an aluminium-26 tracer to study the deposition of aluminium species on fish gills following mixing of limed and acidic waters. Analyst 117(3), 619-621.

Pahl, P.M.B. and Horwitz, L.D. 2005. Cell permeable iron chelators as potential cancer chemotherapeutic agents. Cancer Investigation 23(8), 683-691.

Panagakos, F.S., Kumar, E., Venescar, C. and Guidon, P. 2000. The effect of gallium nitrate on synoviocyte MMP activity. Biochimie 82(2), 147-151.

Panov, V.E. and McQueen, D.J. 1998. Effects of temperature on individual growth rate and body size of a freshwater amphipod. Canadian Journal of Zoology 76(6), 1107-1116.

Pardo, A. and Selman, M. 2016. Lung fibroblasts, aging, and idiopathic pulmonary fibrosis. Annals of the American Thoracic Society 13(Supplement_5), S417-S421.

Parisi, M.T., Otjen, J.P., Stanescu, A.L. and Shulkin, B.L. 2018. Radionuclide imaging of infection and inflammation in children: A review. Seminars in Nuclear Medicine 48(2), 148-165.

Park, J.C. 2011. The recovery of indium metal from ITO-scrap using hydrothermal reaction in alkaline solution. Bulletin of the Korean Chemical Society 32.

Pascoe, D., Evans, S.A. and Woodworth, J. 1986. Heavy metal toxicity to fish and the influence of

water hardness. Archives of Environmental Contamination and Toxicology 15(5), 481-487.

Passos, J.F., Nelson, G., Wang, C., Richter, T., Simillion, C., Proctor, C.J., Miwa, S., Olijslagers, S., Hallinan, J., Wipat, A., Saretzki, G., Rudolph, K.L., Kirkwood, T.B. and von Zglinicki, T. 2010. Feedback between p21 and reactive oxygen production is necessary for cell senescence. Molecular Systems Biology 6, 347.

Pattus, F. and Abdallah, M.A. 2000. Siderophores and iron-transport in microorganisms. Journal of the Chinese Chemical Society 47(1), 1-20.

Paul, B.T., Manz, D.H., Torti, F.M. and Torti, S.V. 2017. Mitochondria and iron: Current questions. Expert Review of Hematology 10(1), 65-79.

Pennesi, C., Amato, A., Occhialini, S., Critchley, A.T., Totti, C., Giorgini, E., Conti, C. and Beolchini, F. 2019. Adsorption of indium by waste biomass of brown alga *Ascophyllum nodosum*. Scientific Reports 9(1), 16763.

Petrova, N.V., Velichko, A.K., Razin, S.V. and Kantidze, O.L. 2016. Small molecule compounds that induce cellular senescence. Aging Cell 15(6), 999-1017.

Pinnix, Z.K., Miller, L.D., Wang, W., D'Agostino, R., Kute, T., Willingham, M.C., Hatcher, H., Tesfay, L., Sui, G., Di, X., Torti, S.V. and Torti, F.M. 2010. Ferroportin and iron regulation in breast cancer progression and prognosis. Science Translational Medicine 2(43), 43ra56-43ra56.

Piomboni, P., Focarelli, R., Stendardi, A., Ferramosca, A. and Zara, V. 2012. The role of mitochondria in energy production for human sperm motility. International Journal of Andrology 35(2), 109-124.

Playle, R., Goss, G. and Wood, C. 1989. Physiological disturbances in rainbow trout (*Salmo gairdneri*) during acid and aluminum exposures in soft water of two calcium concentrations. Canadian Journal of Zoology 67, 314-324.

Poléo, A.B. and Bjerkely, F. 2000. Effect of unstable aluminium chemistry on Arctic char (*Salvelinus alpinus*). Canadian Journal of Fisheries and Aquatic Sciences 57(7), 1423-1433.

Poléo, A.B.S. 1995. Aluminium polymerization - A mechanism of acute toxicity of aqueous aluminium to fish. Aquatic Toxicology 31(4), 347-356.

Poléo, A.B.S., Schjolden, J., Sørensen, J. and Nilsson, G.E. 2017. The high tolerance to aluminium in crucian carp (*Carassius carassius*) is associated with its ability to avoid hypoxia. PLOS ONE 12(6), e0179519.

Połedniok, J., Kita, A. and Zerzucha, P. 2012. Spectrophotometric and inductively coupled plasma–optical emission spectroscopy determination of gallium in natural soils and soils polluted by industry: Relationships between elements. Communications in Soil Science and Plant Analysis 43(8), 1121-1135.

Ponka, P. 1999. Cell biology of heme. The American Journal of the Medical Sciences 318(4), 241-256.

Porcaro, F., Bonchi, C., Ugolini, A., Frangipani, E., Polzonetti, G., Visca, P., Meneghini, C. and Battocchio, C. 2017. Understanding the biomimetic properties of gallium in *Pseudomonas aeruginosa*: An XAS and XPS study. Dalton Transactions 46(21), 7082-7091.

Poynton, H.C., Hasenbein, S., Benoit, J.B., Sepulveda, M.S., Poelchau, M.F., Hughes, D.S.T., Murali, S.C., Chen, S., Glastad, K.M., Goodisman, M.A.D., Werren, J.H., Vineis, J.H., Bowen, J.L., Friedrich, M., Jones, J., Robertson, H.M., Feyereisen, R., Mechler-Hickson, A., Mathers, N., Lee, C.E., Colbourne, J.K., Biales, A., Johnston, J.S., Wellborn, G.A., Rosendale, A.J., Cridge, A.G., Munoz-Torres, M.C., Bain, P.A., Manny, A.R., Major, K.M., Lambert, F.N., Vulpe, C.D., Tuck, P., Blalock, B.J., Lin, Y.-Y., Smith, M.E., Ochoa-Acuña, H., Chen, M.-J.M., Childers, C.P., Qu, J., Dugan, S., Lee, S.L., Chao, H., Dinh, H., Han, Y., Doddapaneni, H., Worley, K.C., Muzny, D.M., Gibbs, R.A. and Richards, S. 2018. The toxicogenome of *Hyalella azteca*: A model for sediment ecotoxicology and evolutionary toxicology. Environmental Science & Technology 52(10), 6009-6022.

Qi, Y., Huang, B. and Darilek, J.L. 2014. Effect of drying on heavy metal fraction distribution in rice

paddy soil. PLOS ONE 9(5), e97327.

Ragaini, R.C., Ralston, H.R. and Roberts, N. 1977. Environmental trace metal contamination in Kellogg, Idaho, near a lead smelting complex. Environmental Science & Technology 11(8), 773-781.

Raghu, G., Collard, H.R., Egan, J.J., Martinez, F.J., Behr, J., Brown, K.K., Colby, T.V., Cordier, J.F., Flaherty, K.R., Lasky, J.A., Lynch, D.A., Ryu, J.H., Swigris, J.J., Wells, A.U., Ancochea, J., Bouros, D., Carvalho, C., Costabel, U., Ebina, M., Hansell, D.M., Johkoh, T., Kim, D.S., King, T.E., Jr., Kondoh, Y., Myers, J., Müller, N.L., Nicholson, A.G., Richeldi, L., Selman, M., Dudden, R.F., Griss, B.S., Protzko, S.L. and Schünemann, H.J. 2011. An official ATS/ERS/JRS/ALAT statement: idiopathic pulmonary fibrosis: evidence-based guidelines for diagnosis and management. American Journal of Respiratory and Critical Care Medicine 183(6), 788-824.

Rathore, R.S. and Khangarot, B.S. 2003. Effects of water hardness and metal concentration on a freshwater *Tubifex tubifex* Muller. Water, Air, and Soil Pollution 142(1), 341-356.

Reed, S.I. 1997. Control of the G1/S transition. Cancer Surveys 29, 7-23.

Reich, F. and Richter, T. 1863. Vorläufige notiz über ein neues metall. Journal für Praktische Chemie 89(1), 441-448.

Renton, F.J. and Jeitner, T.M. 1996. Cell cycle-dependent inhibition of the proliferation of human neural tumor cell lines by iron chelators. Biochemical Pharmacology 51(11), 1553-1561.

Richardson, D.R. 2001. Iron and gallium increase iron uptake from transferrin by human melanoma cells: further examination of the ferric ammonium citrate-activated iron uptake process. Biochimica et Biophysica Acta (BBA) - Molecular Basis of Disease 1536(1), 43-54.

Richter, K., Thomas, N., Zhang, G., Prestidge, C.A., Coenye, T., Wormald, P.-J. and Vreugde, S. 2017. Deferiprone and gallium-protoporphyrin have the capacity to potentiate the activity of antibiotics in Staphylococcus aureus small colony variants. Frontiers in Cellular and Infection

Microbiology 7, 280-280.

Roberts, D.A. 2012. Causes and ecological effects of resuspended contaminated sediments (RCS) in marine environments. Environment International 40, 230-243.

Rodriguez, G.M., Gardner, R., Kaur, N. and Phanstiel, O. 2008. Utilization of Fe^{3+}-acinetoferrin analogs as an iron source by *Mycobacterium tuberculosis*. BioMetals 21(1), 93-103.

Rogers, H.J., Synge, C. and Woods, V.E. 1980. Antibacterial effect of scandium and indium complexes of enterochelin on *Klebsiella pneumoniae*. Antimicrobial agents and chemotherapy 18(1), 63-68.

Rogers, H.J., Woods, V.E. and Synge, C. 1982. Antibacterial effect of the scandium and indium complexes of enterochelin on *Escherichia coli*. Journal of General Microbiology 128(10), 2389-2394.

Rose, M., Baxter, M., Brereton, N. and Baskaran, C. 2010. Dietary exposure to metals and other elements in the 2006 UK Total Diet Study and some trends over the last 30 years. Food Additives & Contaminants: Part A 27(10), 1380-1404.

Ryder, R.A. and Pesendorfer, J. 1992. Food, growth, habitat, and community interactions of young-of-the-year burbot, *Lota lota* L., in a Precambrian Shield lake. Hydrobiologia 243(1), 211-227.

Ryu, S.J., Oh, Y.S. and Park, S.C. 2007. Failure of stress-induced downregulation of Bcl-2 contributes to apoptosis resistance in senescent human diploid fibroblasts. Cell Death and Differentiation 14(5), 1020-1028.

Saitoh, M., Nishitoh, H., Fujii, M., Takeda, K., Tobiume, K., Sawada, Y., Kawabata, M., Miyazono, K. and Ichijo, H. 1998. Mammalian thioredoxin is a direct inhibitor of apoptosis signal-regulating kinase (ASK) 1. EMBO Journal 17(9), 2596-2606.

Salama, R., Sadaie, M., Hoare, M. and Narita, M. 2014. Cellular senescence and its effector programs. Genes and Development 28(2), 99-114.

Saleh, T., Tyutynuk-Massey, L., Cudjoe, E.K., Jr., Idowu, M.O., Landry, J.W. and Gewirtz, D.A. 2018.

Non-cell autonomous effects of the senescence-associated secretory phenotype in cancer therapy. Frontiers in Oncology 8, 164.

Saleh, T., Tyutyunyk-Massey, L. and Gewirtz, D.A. 2019. Tumor cell escape from therapy-Induced senescence as a model of disease recurrence after dormancy. Cancer Research 79(6), 1044-1046.

Salguero, I., Belotserkovskaya, R., Coates, J., Sczaniecka-Clift, M., Demir, M., Jhujh, S., Wilson, M.D. and Jackson, S.P. 2019. MDC1 PST-repeat region promotes histone H2AX-independent chromatin association and DNA damage tolerance. Nature Communications 10(1), 5191.

Salis, O., Bedir, A., Kilinc, V., Alacam, H., Gulten, S. and Okuyucu, A. 2014. The anticancer effects of desferrioxamine on human breast adenocarcinoma and hepatocellular carcinoma cells. Cancer Biomarkers 14, 419-426.

Sanders, Y.Y., Liu, H., Zhang, X., Hecker, L., Bernard, K., Desai, L., Liu, G. and Thannickal, V.J. 2013. Histone modifications in senescence-associated resistance to apoptosis by oxidative stress. Redox Biology 1(1), 8-16.

Sandoval-Acuña, C., Torrealba, N., Tomkova, V., Jadhav, S.B., Blazkova, K., Merta, L., Lettlova, S., Adamcová, M.K., Rosel, D., Brábek, J., Neuzil, J., Stursa, J., Werner, L. and Truksa, J. 2021. Targeting mitochondrial iron metabolism suppresses tumor growth and metastasis by inducing mitochondrial dysfunction and mitophagy. Cancer Research 81(9), 2289-2303.

Sapieha, P. and Mallette, F.A. 2018. Cellular senescence in postmitotic cells: Beyond growth arrest. Trends in Cell Biology 28(8), 595-607.

Sato, R., Abe, S., Yamada, Y., Toyama, D., Ohtake, Y., Sato, N. and Ohkubo, Y. 2004. The entering of indium-111 and iron-59 into the hepatocytes from partially hepatectomized rats differ from that of gallium-67. Biological and Pharmaceutical Bulletin 27(8), 1193-1196.

Satoshi Itoh and Katsuya Maruyama 2011. Recoveries of metallic indium and tin from ITO by means of pyrometallurgy. High Temperature Materials and Processes 30(4), 317-322.

Sayle, B.A., Fawcett, H.D., Wilkey, D.J., Cierny, G. and Mader, J.T. 1985. Indium-111 chloride imaging in chronic osteomyelitis. Journal of Nuclear Medicine 26(3 Part 1), 225-229.

Sayle, B.A., Helmer, R.E., Birdsong, B.A., Balachandran, S. and Gardner, F.H. 1982. Bone-marrow imaging with Indium-111 chloride in aplastic anemia and myelofibrosis: Concise communication. Journal of Nuclear Medicine 23(2), 121-125.

Schneider, J.L., Rowe, J.H., Garcia-de-Alba, C., Kim, C.F., Sharpe, A.H. and Haigis, M.C. 2021. The aging lung: Physiology, disease, and immunity. Cell 184(8), 1990-2019.

Schulz, K.J., DeYoung, J.J.H., Seal Ii, R.R. and Bradley, D.C. 2017. Critical mineral resources of the United States-Economic and environmental geology and prospects for future supply, Reston, VA.

Seligman, P.A., Kovar, J., Schleicher, R.B. and Gelfand, E.W. 1991. Transferrin-independent iron uptake supports B lymphocyte growth. Blood 78(6), 1526-1531.

Selman, M. and Pardo, A. 2014. Revealing the pathogenic and aging-related mechanisms of the enigmatic idiopathic pulmonary fibrosis. An integral model. American Journal of Respiratory and Critical Care Medicine 189(10), 1161-1172.

Seymour, G.J., Walsh, M.D., Lavin, M.F., Strutton, G. and Gardiner, R.A. 1987. Transferrin receptor expression by human bladder transitional cell carcinomas. Urological Research 15(6), 341-344.

Shacklette, H.T. and Boerngen, J.G. 1984. element concentrations in soils and other surficial materials of the conterminous United States, U.S. Geological Survey Professional Paper.

Shah, K.N., Wilson, E.A., Malla, R., Elford, H.L. and Faridi, J.S. 2015. Targeting ribonucleotide reductase M2 and NF-κB activation with didox to circumvent tamoxifen resistance in breast cancer. Molecular Cancer Therapeutics 14(11), 2411-2421.

Shang, C., Zhou, H., Liu, W., Shen, T., Luo, Y. and Huang, S. 2020. Iron chelation inhibits mTORC1 signaling involving activation of AMPK and REDD1/Bnip3 pathways. Oncogene 39(29),

5201-5213.

Sharma, B., Sarkar, A., Singh, P. and Singh, R.P. 2017. Agricultural utilization of biosolids: A review on potential effects on soil and plant grown. Waste Management 64, 117-132.

Sherr, C.J. 1994. G1 phase progression: Cycling on cue. Cell 79(4), 551-555.

Sherr, C.J. and Roberts, J.M. 1999. CDK inhibitors: Positive and negative regulators of G1-phase progression. Genes and Development 13(12), 1501-1512.

Shetty, T. and Corson, T.W. 2020. Mitochondrial heme synthesis enzymes as therapeutic targets in vascular diseases. Frontiers in Pharmacology 11(1015).

Shiller, A.M. 1998. Dissolved gallium in the Atlantic Ocean. Marine Chemistry 61(1), 87-99.

Shiller, A.M. and Frilot, D.M. 1996. The geochemistry of gallium relative to aluminum in Californian streams. Geochimica et Cosmochimica Acta 60(8), 1323-1328.

Shindo, M., Torimoto, Y., Saito, H., Motomura, W., Ikuta, K., Sato, K., Fujimoto, Y. and Kohgo, Y. 2006. Functional role of DMT1 in transferrin-independent iron uptake by human hepatocyte and hepatocellular carcinoma cell, HLF. Hepatology Research 35(3), 152-162.

Shpyleva, S.I., Tryndyak, V.P., Kovalchuk, O., Starlard-Davenport, A., Chekhun, V.F., Beland, F.A. and Pogribny, I.P. 2011. Role of ferritin alterations in human breast cancer cells. Breast Cancer Research and Treatment 126(1), 63-71.

Siu, P.M., Donley, D.A., Bryner, R.W. and Alway, S.E. 2003. Citrate synthase expression and enzyme activity after endurance training in cardiac and skeletal muscles. Journal of Applied Physiology 94(2), 555-560.

Skaar, E.P. 2010. The battle for iron between bacterial pathogens and their vertebrate hosts. PLOS Pathogens 6(8), e1000949.

Smith, D.B., Cannon, W.F., Woodruff, L.G., Garrett, R.G., Klassen, R., Kilburn, J.E., Horton, J.D., King, H.D., Goldhaber, M.B. and Morrison, J.M. 2005. Major- and trace-element concentrations in soils from two continental-scale transects of the United States and Canada,

p. 22, Reston, VA.

Song, Y., Zhao, Y., Deng, Z., Zhao, R. and Huang, Q. 2021. Stress-induced polyploid giant cancer cells: Unique way of formation and non-negligible characteristics. Frontiers in Oncology 11(3390).

Soule, H.D., Vazquez, J., Long, A., Albert, S. and Brennan, M. 1973. A human cell line from a pleural effusion derived from a breast carcinoma. JNCI: Journal of the National Cancer Institute 51(5), 1409-1416.

Spina, R.J., Chi, M.M., Hopkins, M.G., Nemeth, P.M., Lowry, O.H. and Holloszy, J.O. 1996. Mitochondrial enzymes increase in muscle in response to 7-10 days of cycle exercise. Journal of Applied Physiology 80(6), 2250-2254.

Spinazzi, M., Casarin, A., Pertegato, V., Salviati, L. and Angelini, C. 2012. Assessment of mitochondrial respiratory chain enzymatic activities on tissues and cultured cells. Nature Protocols 7(6), 1235-1246.

Stöckl, P., Hütter, E., Zwerschke, W. and Jansen-Dürr, P. 2006. Sustained inhibition of oxidative phosphorylation impairs cell proliferation and induces premature senescence in human fibroblasts. Experimental Gerontology 41(7), 674-682.

Stapleton, J.T., Klinzman, D., Olakanmi, O., Wuenschmann, S., Schlesinger, L.S. and Britigan, B.E. 1993. Gallium nitrate: A potent inhibitor of HIV-1 infection *in vitro*. Abstracts of 39th Interscience Conference on Antimicrobial Agents and Chemotherapy, 319.

Stephenson, M. and Mackie, G.L. 1989. A laboratory study of the effects of waterborne cadmium, calcium, and carbonate concentrations on cadmium concentrations in *Hyalella azteca* (Crustacea: Amphipoda). Aquatic Toxicology 15(1), 53-62.

Stiff, M.J. 1971. Copper/bicarbonate equilibria in solutions of bicarbonate ion at concentrations similar to those found in natural water. Water Research 5(5), 171-176.

Stojiljkovic, I., Evavold, B.D. and Kumar, V. 2001. Antimicrobial properties of porphyrins. Expert

Opinion on Investigational Drugs 10(2), 309-320.

Stojiljkovic, I., Kumar, V. and Srinivasan, N. 1999. Non-iron metalloporphyrins: potent antibacterial compounds that exploit haem/Hb uptake systems of pathogenic bacteria. Molecular Microbiology 31(2), 429-442.

Straus, D.J. 2003. Gallium nitrate in the treatment of lymphoma. Seminars in Oncology 30(2 Suppl 5), 25-33.

Sturm, B., Lassacher, U., Ternes, N., Jallitsch, A., Goldenberg, H. and Scheiber-Mojdehkar, B. 2006. The influence of gallium and other metal ions on the uptake of non-transferrin-bound iron by rat hepatocytes. Biochimie 88(6), 645-650.

Su, J.Y., Syu, C.H. and Lee, D.Y. 2018. Growth inhibition of rice (*Oryza sativa* L.) seedlings in Ga- and In-contaminated acidic soils is respectively caused by Al and Al+In toxicity. Journal of Hazardous Materials 344, 274-282.

Subathra, S. and Karuppasamy, R. 2007. Toxic effects of copper on bioenergetics and growth rates in fingerlings and adult stage of the fish, *Mystus vittatus*. Journal of Fisheries and Aquatic Science 2, 285-293.

Sun, J., Zhang, D., Zheng, Y., Zhao, Q., Zheng, M., Kovacevic, Z. and Richardson, D.R. 2013. Targeting the metastasis suppressor, NDRG1, using novel iron chelators: Regulation of stress fiber-mediated tumor cell migration via modulation of the ROCK1/pMLC2 signaling pathway. Molecular Pharmacology 83(2), 454-469.

Surova, O. and Zhivotovsky, B. 2013. Various modes of cell death induced by DNA damage. Oncogene 32(33), 3789-3797.

Swain, B., Mishra, C., Kang, L., Park, K.-S., Lee, C.G. and Hong, H.S. 2015. Recycling process for recovery of gallium from GaN an e-waste of LED industry through ball milling, annealing and leaching. Environmental Research 138, 401-408.

Syu, C.H., Chen, L.Y. and Lee, D.Y. 2021. The growth and uptake of gallium (Ga) and indium (In)

of wheat seedlings in Ga- and In-contaminated soils. Science of The Total Environment 759, 143943.

Syu, C.H., Chen, P.W., Huang, C.C. and Lee, D.Y. 2020. Accumulation of gallium (Ga) and indium (In) in rice grains in Ga- and In-contaminated paddy soils. Environmental Pollution 261, 114189.

Tabei, Y., Sonoda, A., Nakajima, Y., Biju, V., Makita, Y., Yoshida, Y. and Horie, M. 2016. Intracellular accumulation of indium ions released from nanoparticles induces oxidative stress, proinflammatory response and DNA damage. Journal of Biochemistry 159(2), 225-237.

Taguchi, O. and Chonan, T. 2006. Three cases of indium lung [in Japanese]. The Journal of the Japanese Respiratory Society 44, 532-536.

Takagi, R., Suzuki, Y., Seki, Y., Ikehata, M., Kajihara, C., Shimizu, H. and Yanagisawa, H. 2011. Indium chloride-induced micronuclei in *in vivo* and *in vitro* experimental systems. Journal of Occupational Health 53(2), 102-109.

Takeda, A., Kimura, K. and Yamasaki, S.-i. 2004. Analysis of 57 elements in Japanese soils, with special reference to soil group and agricultural use. Geoderma 119, 291-307.

Takenaka, Y., Inoue, I., Nakano, T., Ikeda, M. and Kakinuma, Y. 2020. Prolonged disturbance of proteostasis induces cellular senescence via temporal mitochondrial dysfunction and enhanced mitochondrial biogenesis in human fibroblasts. BioRxiv, 2020.2001.2022.916221.

Takyi, S.A., Basu, N., Arko-Mensah, J., Dwomoh, D., Houessionon, K.G. and Fobil, J.N. 2021. Biomonitoring of metals in blood and urine of electronic waste (E-waste) recyclers at Agbogbloshie, Ghana. Chemosphere 280, 130677.

Tanaka, A., Hirata, M., Homma, T. and Kiyohara, Y. 2010. Chronic pulmonary toxicity study of indium-tin oxide and indium oxide following intratracheal instillations into the lungs of hamsters. Journal of Occupational Health 52(1), 14-22.

Tanaka, K. 2009. The proteasome: overview of structure and functions. Proceedings of the Japan

Academy, Ser. B, Physical and Biological Sciences 85(1), 12-36.

Taylor, L.N., Novak, L., Rendas, M., Antunes, P.M.C. and Scroggins, R.P. 2016. Validation of a new standardized test method for the freshwater amphipod *Hyalella azteca*: Determining the chronic effects of silver in sediment. Environmental Toxicology and Chemistry 35(10), 2430-2438.

Tchidjou Kuekou, H., Palandri, L., Pouplin, S., LiThiao Te, V., Righi, E., Castelain, S. and Ricard, J. 2021. SARS-COV-2 infection in children and red blood cell distribution width. Cureus 13(9), e17837-e17837.

Terada, N., Lucas, J.J. and Gelfand, E.W. 1991. Differential regulation of the tumor suppressor molecules, retinoblastoma susceptibility gene product (Rb) and p53, during cell cycle progression of normal human T cells. The Journal of Immunology 147(2), 698-704.

Thompson, E.W., Reich, R., Shima, T.B., Albini, A., Graf, J., Martin, G.R., Dickson, R.B. and Lippman, M.E. 1988. Differential regulation of growth and invasiveness of MCF-7 breast cancer cells by antiestrogens. Cancer Research 48(23), 6764-6768.

Thompson, M.G., Truong-Le, V., Alamneh, Y.A., Black, C.C., Anderl, J., Honnold, C.L., Pavlicek, R.L., Abu-Taleb, R., Wise, M.C., Hall, E.R., Wagar, E.J., Patzer, E. and Zurawski, D.V. 2015. Evaluation of gallium citrate formulations against a multidrug-resistant strain of *Klebsiella pneumoniae* in a murine wound model of infection. Antimicrobial Agents and Chemotherapy 59(10), 6484-6493.

Tong, Y. and Guo, M. 2009. Bacterial heme-transport proteins and their heme-coordination modes. Archives of Biochemistry and Biophysics 481(1), 1-15.

Tonks, N.K. 2006. Protein tyrosine phosphatases: from genes, to function, to disease. Nature Reviews Molecular Cell Biology 7(11), 833-846.

Torres, C.A. and Perez, V.I. 2008. Proteasome modulates mitochondrial function during cellular senescence. Free Radical Biology and Medicine 44(3), 403-414.

Toso, A., Revandkar, A., Di Mitri, D., Guccini, I., Proietti, M., Sarti, M., Pinton, S., Zhang, J., Kalathur, M., Civenni, G., Jarrossay, D., Montani, E., Marini, C., Garcia-Escudero, R., Scanziani, E., Grassi, F., Pandolfi, Pier P., Catapano, Carlo V. and Alimonti, A. 2014. Enhancing chemotherapy efficacy in Pten-deficient prostate tumors by activating the senescence-associated antitumor immunity. Cell Reports 9(1), 75-89.

Trenfield, M.A., van Dam, J.W., Harford, A.J., Parry, D., Streten, C., Gibb, K. and van Dam, R.A. 2015. Aluminium, gallium, and molybdenum toxicity to the tropical marine microalga *Isochrysis galbana*. Environmental Toxicology and Chemistry 34(8), 1833-1840.

Trenfield, M.A., van Dam, J.W., Harford, A.J., Parry, D., Streten, C., Gibb, K. and van Dam, R.A. 2016. A chronic toxicity test for the tropical marine snail *Nassarius dorsatus* to assess the toxicity of copper, aluminium, gallium, and molybdenum. Environmental Toxicology and Chemistry 35(7), 1788-1795.

Tsao, Y.C., Fan, H.Y. and Luo, J.C.J. 2021. Case reports of indium lung disease in Taiwan. Journal of the Formosan Medical Association 120(2), 893-898.

Tyler, G. 2004. Vertical distribution of major, minor, and rare elements in a Haplic Podzol. Geoderma 119(3), 277-290.

Uryu, T., Yoshinaga, J. and Yanagisawa, Y. 2003. Environmental fate of gallium arsenide semiconductor disposal. Journal of Industrial Ecology 7(2), 103-112.

United States Geological Survey (USGS). 2021a. Mineral commodity summaries 2021, pp. 62-63, Reston, VA.

United States Geological Survey (USGS). 2021b. Mineral commodity summaries 2021, pp. 78-79, Reston, VA.

van Dam, J.W., Trenfield, M.A., Streten, C., Harford, A.J., Parry, D. and van Dam, R.A. 2018. Assessing chronic toxicity of aluminium, gallium and molybdenum in tropical marine waters using a novel bioassay for larvae of the hermit crab *Coenobita variabilis*. Ecotoxicology and

Environmental Safety 165, 349-356.

Vasileiou, P.V.S., Evangelou, K., Vlasis, K., Fildisis, G., Panayiotidis, M.I., Chronopoulos, E., Passias, P.G., Kouloukoussa, M., Gorgoulis, V.G. and Havaki, S. 2019. Mitochondrial homeostasis and cellular senescence. Cells 8(7).

Viers, J., Dupré, B. and Gaillardet, J. 2009. Chemical composition of suspended sediments in World Rivers: New insights from a new database. Science of The Total Environment 407(2), 853-868.

Vinuesa, V. and McConnell, M.J. 2021. Recent advances in iron chelation and gallium-based therapies for antibiotic resistant bacterial infections. International Journal of Molecular Sciences 22(6), 2876.

Volkoff, H. and Rønnestad, I. 2020. Effects of temperature on feeding and digestive processes in fish. Temperature (Austin) 7(4), 307-320.

Walen, K.H. 2006. Human diploid fibroblast cells in senescence; cycling through polyploidy to mitotic cells. In Vitro Cellular and Developmental Biology - Animal 42(7), 216-224.

Walsh, S., Gosselin, I., Lee, D. and Stuart, M. 2019. The establishment of a new culture of *Hyalella azteca* that would permit toxicity tests to be conducted on low-ionic strength waters. Environmental Toxicology and Chemistry 38(3), 585-590.

Wan, Y., Huang, Q., Camara, A.Y., Wang, Q. and Li, H. 2019. Water management impacts on the solubility of Cd, Pb, As, and Cr and their uptake by rice in two contaminated paddy soils. Chemosphere 228, 360-369.

Wandersman, C. and Delepelaire, P. 2004. Bacterial iron sources: From siderophores to hemophores. Annual Review of Microbiology 58(1), 611-647.

Wang, E. 1995. Senescent Human Fibroblasts Resist Programmed Cell Death, and Failure to Suppress bcl2 Is Involved. Cancer Research 55(11), 2284-2292.

Wang, F., Goulet, R.R. and Chapman, P.M. 2004a. Testing sediment biological effects with the

freshwater amphipod *Hyalella azteca*: the gap between laboratory and nature. Chemosphere 57(11), 1713-1724.

Wang, G., Miskimins, R. and Miskimins, W.K. 2000. Mimosine Arrests Cells in G1 by Enhancing the Levels of p27Kip1. Experimental Cell Research 254(1), 64-71.

Wang, G., Miskimins, R. and Miskimins, W.K. 2004b. Regulation of p27Kip1 by intracellular iron levels. Biometals 17(1), 15-24.

Wang, H., Han, M., Yang, S., Chen, Y., Liu, Q. and Ke, S. 2011. Urinary heavy metal levels and relevant factors among people exposed to e-waste dismantling. Environment International 37(1), 80-85.

Wang, J., Yin, D., Xie, C., Zheng, T., Liang, Y., Hong, X., Lu, Z., Song, X., Song, R., Yang, H., Sun, B., Bhatta, N., Meng, X., Pan, S., Jiang, H. and Liu, L. 2014. The iron chelator Dp44mT inhibits hepatocellular carcinoma metastasis via N-Myc downstream-regulated gene 2 (NDRG2)/gp130/STAT3 pathway. Oncotarget 5(18), 8478-8491.

Wang, N., Ivey, C.D., Brunson, E.L., Cleveland, D., Ingersoll, C.G., Stubblefield, W.A. and Cardwell, A.S. 2018. Acute and chronic toxicity of aluminum to a unionid mussel (*Lampsilis siliquoidea*) and an amphipod (*Hyalella azteca*) in water-only exposures. Environmental Toxicology and Chemistry 37(1), 61-69.

Wang, Q., Wu, P.C., Dong, D.Z., Ivanova, I., Chu, E., Zeliadt, S., Vesselle, H. and Wu, D.Y. 2013. Polyploidy road to therapy-induced cellular senescence and escape. International Journal of Cancer 132(7), 1505-1515.

Wang, W., Yang, X., López de Silanes, I., Carling, D. and Gorospe, M. 2003. Increased AMP:ATP ratio and AMP-activated protein kinase activity during cellular senescence linked to reduced HuR Function *. Journal of Biological Chemistry 278(29), 27016-27023.

Wang, Y., Huang, J., Sun, Y., Stubbs, D., He, J., Li, W., Wang, F., Liu, Z., Ruzicka, J.A., Taylor, E.W., Rayman, M.P., Wan, X. and Zhang, J. 2021. SARS-CoV-2 suppresses mRNA expression of

selenoproteins associated with ferroptosis, endoplasmic reticulum stress and DNA synthesis. Food and Chemical Toxicology 153, 112286.

Was, H., Borkowska, A., Olszewska, A., Klemba, A., Marciniak, M., Synowiec, A. and Kieda, C. 2021. Polyploidy formation in cancer cells: How a Trojan horse is born. Seminars in Cancer Biology.

Weaver, B.A. and Cleveland, D.W. 2008. The aneuploidy paradox in cell growth and tumorigenesis. Cancer Cell 14(6), 431-433.

Webb, D.R., Wilson, S.E. and Carter, D.E. 1986. Comparative pulmonary toxicity of gallium arsenide, gallium(III) oxide, or arsenic(III) oxide intratracheally instilled into rats. Toxicology and Applied Pharmacology 82(3), 405-416.

Weinstein, R.E., Bond, B.H., Silberberg, B., Vaughn, C.B., Subbaiah, P. and Pieper, D.R. 2005. Tissue ferritin concentration and prognosis in carcinoma of the breast. Breast Cancer Research and Treatment 14, 349-353.

Wellborn, G.A. 1994. Size-biased predation and prey life histories: A comparative study of freshwater amphipod populations. Ecology 75(7), 2104-2117.

Welsh, P.G., Skidmore, J.F., Spry, D.J., Dixon, D.G., Hodson, P.V., Hutchinson, N.J. and Hickie, B.E. 1993. Effect of pH and dissolved organic carbon on the toxicity of copper to larval fathead minnow (*Pimephales promelas*) in natural lake waters of low alkalinity. Canadian Journal of Fisheries and Aquatic Sciences 50(7), 1356-1362.

Wheat, J. 1985. Diagnostic strategies in osteomyelitis. American Journal of Medicine 78(6b), 218-224.

White, S.J.O., Keach, C. and Hemond, H.F. 2015. Atmospheric deposition of indium in the Northeastern United States: Flux and historical trends. Environmental Science & Technology 49(21), 12705-12713.

Wijesinghe, T.P., Dharmasivam, M., Dai, C.C. and Richardson, D.R. 2021. Innovative therapies for

neuroblastoma: The surprisingly potent role of iron chelation in up-regulating metastasis and tumor suppressors and down-regulating the key oncogene, N-myc. Pharmacological Research 173, 105889.

Wilks, A. and Burkhard, K.A. 2007. Heme and virulence: How bacterial pathogens regulate, transport and utilize heme. Natural Product Reports 24(3), 511-522.

Witt, J.D. and Hebert, P.D. 2000. Cryptic species diversity and evolution in the amphipod genus *Hyalella* within central glaciated North America: A molecular phylogenetic approach. Canadian Journal of Fisheries and Aquatic Sciences 57(4), 687-698.

Wood, S.A. and Samson, I.M. 2006. The aqueous geochemistry of gallium, germanium, indium and scandium. Ore Geology Reviews 28(1), 57-102.

Wu, Y.H., Wu, T.M., Hong, C.Y., Wang, Y.S. and Yen, J.H. 2014. Screening differentially expressed genes in an amphipod (*Hyalella azteca*) exposed to fungicide vinclozolin by suppression subtractive hybridization. Journal of Environmental Science and Health 49(11), 856-863.

Xiao, Y.L., Cai, H.R., Wang, Y.H., Meng, F.Q. and Zhang, D.P. 2010. Pulmonary alveolar proteinosis in an indium-processing worker. Chinese Medical Journal 123(10), 1347-1350.

Xu, T. and Chen, Y. 2020. Research progress of [68Ga]citrate PET's utility in infection and inflammation imaging: A review. Molecular Imaging and Biology 22(1), 22-32.

Xu, X., Page, J.L., Surtees, J.A., Liu, H., Lagedrost, S., Lu, Y., Bronson, R., Alani, E., Nikitin, A.Y. and Weiss, R.S. 2008. Broad overexpression of ribonucleotide reductase genes in mice specifically induces lung neoplasms. Cancer Research 68(8), 2652-2660.

Xue, D., Zhou, C.X., Shi, Y.B., Lu, H. and He, X.Z. 2015. Decreased expression of ferroportin in prostate cancer. Oncology Letters 10(2), 913-916.

Yang, D.C., Wang, F., Elliott, R.L. and Head, J.F. 2001. Expression of transferrin receptor and ferritin H-chain mRNA are associated with clinical and histopathological prognostic indicators in breast cancer. Anticancer Research 21(1b), 541-549.

Yang, J.L. 2014. Comparative acute toxicity of gallium(III), antimony(III), indium(III), cadmium(II), and copper(II) on freshwater swamp shrimp (*Macrobrachium nipponense*). Biological research 47(1), 13-13.

Yang, J.L. and Chen, H.C. 2003. Effects of gallium on common carp (Cyprinus carpio): acute test, serum biochemistry, and erythrocyte morphology. Chemosphere 53(8), 877-882.

Yang, J.L. and Chen, L.H. 2018. Toxicity of antimony, gallium, and indium toward a teleost model and a native fish species of semiconductor manufacturing districts of Taiwan. Journal of Elementology 23, 191-199.

Yang, M. and Chitambar, C.R. 2008. Role of oxidative stress in the induction of metallothionein-2A and heme oxygenase-1 gene expression by the antineoplastic agent gallium nitrate in human lymphoma cells. Free Radical Biology and Medicine 45(6), 763-772.

Yin, M., Liu, Y. and Chen, Y. 2021. Iron metabolism: An emerging therapeutic target underlying the anti-cancer effect of quercetin. Free Radical Research 55(3), 296-303.

Ylä-Mella, J. and Pongrácz, E. 2016. Drivers and constraints of critical materials recycling: The case of indium. Resources 5(4), 34.

Yoon, Y.S., Byun, H.O., Cho, H., Kim, B.K. and Yoon, G. 2003. Complex II defect via down-regulation of iron-sulfur subunit induces mitochondrial dysfunction and cell cycle delay in iron chelation-induced senescence-associated growth arrest *. Journal of Biological Chemistry 278(51), 51577-51586.

You, J., Pehkonen, S., Weston, D.P. and Lydy, M.J. 2008. Chemical availability and sediment toxicity of pyrethroid insecticides to *Hyalella azteca*: Application to field sediment with unexpectedly low toxicity. Environmental Toxicology and Chemistry 27(10), 2124-2130.

You, S.J. 2014. 霄裡溪環境監測計畫 (第三次工作報告). 中原大學生物環境工程系中原大學環境風險管控研究中心.

Yu, Y., Gutierrez, E., Kovacevic, Z., Saletta, F., Obeidy, P., Suryo Rahmanto, Y. and R. Richardson,

D. 2012. Iron chelators for the treatment of cancer. Current Medicinal Chemistry 19(17), 2689-2702.

Yu, Y., Kalinowski, D.S., Kovacevic, Z., Siafakas, A.R., Jansson, P.J., Stefani, C., Lovejoy, D.B., Sharpe, P.C., Bernhardt, P.V. and Richardson, D.R. 2009. Thiosemicarbazones from the old to new: Iron chelators that are more than just ribonucleotide reductase inhibitors. Journal of Medicinal Chemistry 52(17), 5271-5294.

Yu, Y., Kovacevic, Z. and Richardson, D.R. 2007. Tuning cell cycle regulation with an iron key. Cell Cycle 6(16), 1982-1994.

Yu, Y. and Richardson, D.R. 2011. Cellular iron depletion stimulates the JNK and p38 MAPK signaling transduction pathways, dissociation of ASK1-thioredoxin, and activation of ASK1. Journal of Biological Chemistry 286(17), 15413-15427.

Yuan, B.J., Li, C., Gao, L.C., Wang, D.M. and Cui, J.J. 2018. The significance of serum KL-6 levels in patients with stageI coal worker's pneumoconiosis. Labeled Immunoassays and Clinical Medicine 25(12), 1881-1884.

Yuan, L., Zhang, J., Liu, Y., Zhao, J., Jiang, F. and Liu, Y. 2017. Indium(III) induces isolated mitochondrial permeability transition by inhibiting proton influx and triggering oxidative stress. Journal of Inorganic Biochemistry 177, 17-26.

Zalom, M.L., Waxman, A.D., Yu, R., Lee, J., Ih, G. and Wolin, E.M. 2009. Metabolic and receptor imaging in patients with neuroendocrine tumors: Comparison of fludeoxyglucose-positron emission tomography and computed tomography with indium in 111 pentetreotide. Endocrine Practice 15(6), 521-527.

Zelicoff, J.T. and Thomas, P. 1998. Immunotoxicology of environmental and occupational metals, Taylor & Francis.

Zeng, C., Gonzalez-Alvarez, A., Orenstein, E., Field, J.A., Shadman, F. and Sierra-Alvarez, R. 2017. Ecotoxicity assessment of ionic As(III), As(V), In(III) and Ga(III) species potentially released

from novel III-V semiconductor materials. Ecotoxicology and Environmental Safety 140, 30-36.

Zeng, X., Wang, F., Sun, X. and Li, J. 2015. Recycling indium from scraped glass of liquid crystal display: Process optimizing and mechanism exploring. ACS Sustainable Chemistry & Engineering 3(7), 1306-1312.

Zetterberg, A., Larsson, O. and Wiman, K.G. 1995. What is the restriction point? Current Opinion in Cell Biology 7(6), 835-842.

Zhan, L., Xia, F., Xia, Y. and Xie, B. 2018. Recycle gallium and arsenic from GaAs-based e-wastes via pyrolysis–vacuum metallurgy separation: Theory and feasibility. ACS Sustainable Chemistry & Engineering 6(1), 1336-1342.

Zhan, Y., Jiang, L., Jin, X., Ying, S., Wu, Z., Wang, L., Yu, W., Tong, J., Zhang, L., Lou, Y. and Qiu, Y. 2021. Inhibiting RRM2 to enhance the anticancer activity of chemotherapy. Biomedicine and Pharmacotherapy 133, 110996.

Zhang, C. 2014. Essential functions of iron-requiring proteins in DNA replication, repair and cell cycle control. Protein Cell 5(10), 750-760.

Zhang, J., Hu, W., Ding, C., Yao, G., Zhao, H. and Wu, S. 2019a. Deferoxamine inhibits iron-uptake stimulated osteoclast differentiation by suppressing electron transport chain and MAPKs signaling. Toxicology Letters 313, 50-59.

Zhang, K., Li, B., Wu, Y., Wang, W., Li, R., Zhang, Y.-N. and Zuo, T. 2017. Recycling of indium from waste LCD: A promising non-crushing leaching with the aid of ultrasonic wave. Waste Management 64, 236-243.

Zhang, K., Wu, Y., Wang, W., Li, B., Zhang, Y. and Zuo, T. 2015. Recycling indium from waste LCDs: A review. Resources, Conservation and Recycling 104, 276-290.

Zhang, L., Ding, P., Lv, H., Zhang, D., Liu, G., Yang, Z., Li, Y., Liu, J. and Zhang, S. 2014a. Number of polyploid giant cancer cells and expression of EZH2 are associated with VM formation and

tumor grade in human ovarian tumor. BioMed Research International 2014, 903542-903542.

Zhang, Q., Chen, H., Huang, D., Xu, C., Zhu, H. and Zhu, Q. 2019b. Water managements limit heavy metal accumulation in rice: Dual effects of iron-plaque formation and microbial communities. Science of The Total Environment 687, 790-799.

Zhang, S., Chen, Y., Guo, W., Yuan, L., Zhang, D., Xu, Y., Nemeth, E., Ganz, T. and Liu, S. 2014b. Disordered hepcidin–ferroportin signaling promotes breast cancer growth. Cellular Signalling 26(11), 2539-2550.

Zhang, S., Mercado-Uribe, I., Xing, Z., Sun, B., Kuang, J. and Liu, J. 2014c. Generation of cancer stem-like cells through the formation of polyploid giant cancer cells. Oncogene 33(1), 116-128.

Zhang, S., Zhang, D., Yang, Z. and Zhang, X. 2016. Tumor budding, micropapillary pattern, and polyploidy giant cancer cells in colorectal cancer: Current status and future prospects. Stem Cells International 2016, 4810734.

Zhang, W., Wu, Y., Yan, Q., Ma, F., Shi, X., Zhao, Y., Peng, Y., Wang, J. and Jiang, B. 2014d. Deferoxamine enhances cell migration and invasion through promotion of HIF-1α expression and epithelial-mesenchymal transition in colorectal cancer. Oncology Reports 31(1), 111-116.

Zhang, Z.Y. 2002. Protein tyrosine phosphatases: structure and function, substrate specificity, and inhibitor development. Annual Review of Pharmacology and Toxicology 42(1), 209-234.

Zhao, R.Z., Jiang, S., Zhang, L. and Yu, Z.B. 2019. Mitochondrial electron transport chain, ROS generation and uncoupling (Review). International Journal of Molecular Medicine 44(1), 3-15.

Zhou, B.S., Tsai, P., Ker, R., Tsai, J., Ho, R., Yu, J., Shih, J. and Yen, Y. 1998. Overexpression of transfected human ribonucleotide reductase M2 subunit in human cancer cells enhances their invasive potential. Clinical and Experimental Metastasis 16(1), 43-49.

Zhou, H., Zhou, X., Zeng, M., Liao, B.H., Liu, L., Yang, W.T., Wu, Y.-M., Qiu, Q.Y. and Wang, Y.J.

2014a. Effects of combined amendments on heavy metal accumulation in rice (*Oryza sativa* L.) planted on contaminated paddy soil. Ecotoxicology and Environmental Safety 101, 226-232.

Zhou, W., Lv, T.-F., Chen, Y., Westby, A.P. and Ren, W.-J. 2014b. Soil physicochemical and biological properties of paddy-upland rotation: A review. The Scientific World Journal 2014, 856352.

Zhu, Y., Jin, F., Yang, S., Li, J., Hu, D. and Liao, L. 2013. Pre-treatment with EDTA-gallium prevents the formation of biofilms on surfaces. Experimental and Therapeutic Medicine 5(4), 1001-1004.

Ziegler, T.L., Divine, K.K. and Goering, P.L. 2004. Elements and Their Compounds in the Environment, pp. 775-786.

Zosky, G.R., Hoy, R.F., Silverstone, E.J., Brims, F.J., Miles, S., Johnson, A.R., Gibson, P.G. and Yates, D.H. 2016. Coal workers' pneumoconiosis: An Australian perspective. Medical Journal of Australia 204(11), 414-418.

Zubrod, J.P., Englert, D., Feckler, A., Rosenfeldt, R.R., Pasternack, H., Hollert, H., Seiler, T.-B., Schulz, R. and Bundschuh, M. 2019. Is *Hyalella azteca* a suitable model leaf-shredding benthic crustacean for testing the toxicity of sediment-associated metals in Europe? Bulletin of Environmental Contamination and Toxicology 102(3), 303-309.

Zurita, J.L., Jos, A., del Peso, A., Salguero, M., Cameán, A.M., López-Artíguez, M. and Repetto, G. 2007. Toxicological assessment of indium nitrate on aquatic organisms and investigation of the effects on the PLHC-1 fish cell line. Science of The Total Environment 387(1), 155-165.

Zwerschke, W., Mazurek, S., Stöckl, P., Hütter, E., Eigenbrodt, E. and Jansen-Dürr, P. 2003. Metabolic analysis of senescent human fibroblasts reveals a role for AMP in cellular senescence. Biochemical Journal 376(Pt 2), 403-411.

Acknowledgements

This dissertation would not have been finished without the help from so many people. First and foremost, I would like to thank my advisor, Dr. Yoshihisa Shimizu and Dr. Tomonari Matsuda, for their dedicated support, guidance and encouragement. Under their mentorship, I have grown greatly from a graduate student to an independent scientist. I would also like to extend my gratitude to my dissertation committee members, Dr. Yoshihisa Shimizu, Dr. Minoru Yoneda and Dr. Tomonari Matsuda, for their guidance and fully supports in completion of my dissertation.

People from Shimizu-ken had provided enormous help to make my research possible. I am so grateful to work with Kengo Ikebata and Araki Sou who trained and assisted me on extensive experiments. I would like to thank Wong Yong Jie (Jacky) who made my Ph.D. life much easier. I would like to show my gratefulness to all the staffs and students currently and previously work in Shimizu-ken, Yoshimi Nishio, Ryosuke Homma, Sayoka Hariya, Sho Shin, Khagendra Bharambe, Luksanaree Maneechot, Akinori Kamiya, Yoshino Kaito, Aiko Hiroki, Tetsunobu Anazawa, and Sora Shigeta. I am indebted to Kenji Shiota for the help with ICP-MS experiments as well as sample analysis. I would also like to extend my gratefulness to National Institute for Environmental Studies in Japan for their generosity to share the freshwater amphipod (*Hyalella azteca*).

Last, but not least, my journey in graduate school would not be completed without the love and support from my friends and family. Especially to my parents who have been such a positive influence in my life and given me the greatest support through the years of graduate school.

Dedication

This dissertation is dedicated to my parents, Mei-chu Fan and Chien-pin Tan, and my sister, Shih-hua Tan.